THE UNIVERSITY
of EDINBURGH

The LKB1-AMPK signalling pathway drives the hypoxic ventilatory response by regulating brainstem nuclei but not the carotid body

By

Amira Dia Mahmoud

THE UNIVERSITY *of* EDINBURGH

Thesis submitted for the degree of doctor of philosophy at the University of Edinburgh

2015

Disclaimer

I, Amira Dia Mahmoud, performed all of the experiments presented in this thesis unless otherwise clearly stated in the text. No part of this work has been or is being submitted for any other degree or qualification.

Signed:

Date:

Acknowledgements

First of all I would like to thank my supervisor, Prof. A. Mark Evans, for his continuous guidance, advise, and support and making this PhD a "bobby dazzler" despite the revolutions, government call-ups, stolen laptop, etc. etc. etc. I would also like to thank him for introducing me to his lovey wife Sonny who was impeccable and extremely supportive during my PhD. I would also like to thank my secondary supervisors, Prof. Mike Shipston and Dr. Peter Flatman, for their help throughout the many years. Also, many thanks to Prof. Mayank Dutia for his continuous patience and assistance, which has immensely helped in bringing me closer to that PhD degree.

To the current and former members of my lab, you have been such a remarkable support group whether at 8pm on a weekday or 8am on the weekend while also creating a stimulating environment that has enriched my experience in the lab. I consider myself lucky to have shared my PhD experience with you.

I would also like to thank the very special friends I made during my PhD who made sure I kept laughing both inside and outside the Hugh Robson building: "best friend and sister" Xin (definitely not a nun), "twin" Fabio (brother from another mother… and father), "sister-in-law" Lola (bosa bosa), and "trips on air" Sampurna… you have made the last few years in Edinburgh some of the best years of my life and will always see you as my non-Scottish, Scottish family. I will always cherish our many many wonderful memories together while looking forward to the many more we will have together. Also, to Ryan and Scott thanks for some of the best laughs I have had – they made that very thin line between sanity and insanity appear a bit thicker. Also to my Italian family, Sayora and Zia Maria, thanks for taking care of me and being there for me… and introducing me to the best mozzarella EVER in Italy.

Now, to the major support group in Egypt. Starting with my dearest and most loving parents. Before thanking you, I must apologise for being away from home for so long. It is something I know that was never going to be easy but there is no way I would have followed my dreams or achieved my goals if it was not for your unconditional love and the many sacrifices you made - a lot of who I am and what I have achieved is because of you and I will forever be grateful. To Ramy, Dina,

Heba, Dana, and Karim… it was never easy being the person who always missed the special occassions so thank you for the continuous calls, pictures, messages and making sure I was still a part of it all. Also, thank you for making sure I had a blast whenever I visited and introducing me to Woody. And to the rest of the family who kept me motivated, especially Mimi and Amo, thank you for your continuous thoughts and prayers throughout the PhD. Finally, I would like to thank my amazing friends in Egypt… I know I was only meant to be away for a year… but now, 8 years later, I could still say that you are truly special and mean the world to me.

I think I could say that going through this PhD was the most difficult experience I have encountered thus far. But what kept me going were not only the lessons and support from the people I mentioned above but also people who have influenced me from such a young age and throughout my life. Author T. A. Barron once said that "there is nothing more heroic than the teacher who helps a young person discover those vast reserves inside himself or herself, who gives him hope when all seems hopeless, who shows her dreams in the midst of nightmares, and teaches us all to face fear with strong determination". And I have certainly been lucky with having such teachers. Whether it was my 6th grade biology teacher Mr. Leon Boyler who always knew I would be a scientist or Mr. Sayed Anan my P.E. teacher and track and field coach… whether it was Rima Abushakra who made me realise through Model United Nations that we are all global citizens with responsibilities… or Madame Pascale Igounet my I.B French teacher (oui, c'est vrai). And of course Mr. Christopher Allo, the popular French teacher next door who never actually taught me inside a classroom but still had a massive impact outside of one… and grew to become a great friend who I randomly bumped into Russell Crowe with. I am not sure if my teachers realised just how powerful an impact they had on me as an individual and how it still has an affect today… but I hope this dedication can display how grateful I am for how they helped shape the person I grew to be.

Finally, I would like to make a special dedication to the late James Lay… the many lessons that I learnt from him through our mutual love for sports continues to have a massive impact on my life. You really are one of a kind and I will always be grateful for the crossing of our paths 14 years ago.

Table of Contents

Abstract

Ventilatory drive is mediated by respiratory central pattern generators that are located in the brainstem, which are continuously modulated by specialised peripheral and central chemoreceptors to adjust ventilatory patterns according to changes in arterial PO_2. These specialised oxygen-sensing chemoreceptors are activated in response to acute reductions in arterial PO_2 and ultimately trigger a respiratory response that acts to restore oxygen-levels. However, the molecular mechanism by which mammals are able to regulate their breathing pattern in such a manner during hypoxia remains controversial.

Therefore, the studies performed in this thesis aimed to investigate the possibility that this process may be mediated by the liver kinase B 1 (LKB1)/ AMP-activated protein kinase (AMPK) signalling pathway, which is central to cellular adaptations to metabolic stress. This first involved the development of transgenic mice in which *Lkb1* or *AMPK* were deleted. Global knockout of *Lkb1* (Sakamoto, 2006) or *AMPK* activity (Viollet et al., 2009) are embryonic lethal. Thus, the Cre/loxP system was used to develop transgenic mice that had either *Lkb1* or both isoforms of the *AMPK catalytic α-subunit* (α1 and α2) conditionally knocked out in catecholaminergic cells (including therein hypoxia-activated cells of the brainstem and carotid body) by driving Cre expression through a tyrosine-hydroxylase-specific promoter region.

The consequent effects on the ventilatory response to hypoxia were then examined using unrestrained whole-body plethysmography. This demonstrated that, in contrast to the hyperventilation evoked in controls, increased ventilation was virtually abolished in the *Lkb1* and *AMPK α1* and *α2* double knockouts during hypoxia. Both knockout mice also exhibited periods of hypoventilation with frequent apnoeas during hypoxia. Additionally, studies on single *AMPK α1* and *AMPK α2* knockouts identified that the ventilatory dysfunction in *AMPK* α1 and α2 double knockouts was primarily caused by *AMPK α1* deletion. In contrast, the severe ventilatory abnormalities exhibited during hypoxia following the deletion of *Lkb1* and *AMPK* in catecholaminergic cells were mostly reversed upon exposure of mice to hypoxia with hypercapnia. Also, the

ventilatory response to hypercapnia alone was without any major effect as a result of *Lkb1* deletion or the dual-deletion of *AMPK α1* and *α2* catalytic subunits in catecholaminergic cells.

This thesis therefore demonstrates, for the first time, that the LKB1-AMPK signalling pathway is key to respiratory adaptations during hypoxia, by regulating catecholaminergic oxygen-sensing cells, thus protecting against hypoventilation and apnoeas. The LKB1-AMPK signaling pathway can thereby determine oxygen and energy supply at both a cellular and whole-body level.

List of Abbreviations

A1	A1 noradrenergic cells
A2	A2 noradrenergic cells
A5	A5 noradrenergic cells
A6	A6 noradrenergic cells
ADI	Apnoea-duration index
ADP	Adenosine diphosphate
AICAR	5-aminoimidazole-4-carboxamide ribonucleotide
AKAPs	a-kinase anchoring protein
AMP	Adenosine monophosphate
AMPK	AMPK-activated protein kinase
AMPK-RKs	AMP-activated protein kinase related kinases
AP	Area postrema
ATP	Adenosine triphosphate
BötC	Bötzinger complex
BRSK	Brain specific kinase
CaMKK-β	Ca^{2+}/Calmodulin-dependent protein kinase beta
cNTS	Caudal nucleus tractus solitarius
C1	C1 adrenergic cells
C2	C1 adrenergic cells
CB1 cells	carotid body type I cells
CBS motif	Cystathionine-β-synthase motif
CCHS	Congenital central hypoventilation syndrome
Cre	Causes recombination events
CSB	Cheyne-Stokes Breathing
CSN	Carotid sinus nerve
cVRG	Caudal ventral respiratory group
DBH	Dopamine-β–hydroxylase

DRG	Dorsal respiratory group
GLUT	Glucose transporter
H_2O_2	hydrogen peroxide
HIF	Hypoxia inducible factor
KF	Kölliker-Fuse nucleus
KO	Knockout
LC	Locus coeruleus
LKB1	liver kinase B1
MAH cells	Immortalised adrenomedullary chromaffin cells
MARK	MAP/microtubule affinity-regulating kinase
MECP2	Methyl-CpG-binding protein 2
MO25	Mouse protein 25
mROS	Mitochondrial reactive oxygen species
nAMCs	Neonatal adrenomedullary chromaffin cells
NEC	Non-enzyme control
NTS	Nucleus tractus solitarius
PB	Parabrachial
PCR	Polymerase chain reaction
pFRG	Parafacial respiratory group
pre-BötC	Pre-Bötzinger complex
PRG	Pontine respiratory group
rCPG	Respiratory central pattern generators
REM	Rapid eye movement
rNTS	Rostral nucleus tractus solitarius
ROS	reactive oxygen species
RT	Reverse transcription
RTN	Retrotrapezoid nucleus
rVRG	rostral ventral respiratory group
SD	Standard deviation
SEM	Standard error of the mean

SIK	Salt-inducible kinase
SolC	Commissural nucleus of the nucleus tractus solitarius
SP-SAP	Saporin conjugated to substance P
STRAD	Ste-20-related adaptor
TAO	Thousand and one amino acids
Te	Expiration time
TH	Tyrosine hydroxylase
Thr	Threonine
Ti	Inspiration time
To	Total breath duration
Tv	Tidal Volume
VRC	Ventral respiratory column
WT	Wild-type

List of Figures

List of Tables

Chapter One:
General Introduction

1.1 The AMP-activated Protein Kinase (AMPK)

1.1.1 Structure of AMPK

AMPK is a ubiquitously expressed serine-threonine kinase that is activated during metabolic stress and functions to re-establish energy levels. It is a heterotrimer consisting of one catalytic subunit (α-subunit) and two regulatory subunits (β and γ-subunits), of which there are multiple isoforms (Figure 1.1). There are 2 isoforms each of the catalytic α-subunit (α1 and α2) and regulatory β-subunit (β1 and β2) while there are 3 isoforms of the γ-subunit (γ1, γ2 and γ3). Hence, with a heterotrimeric complex forming with a 1α:1β:1γ ratio, there are at least 12 different complexes of AMPK that can be formed (Stapleton et al., 1997).

Within the N-terminus of the catalytic α-subunits lies the serine-threonine kinase domain (Figure 1.1). This contains an activation loop with a threonine residue at position 172 (Thr-172), which is phosphorylated by upstream kinases to fully activate AMPK (as described further below) (Hawley et al., 1996). The C-terminus region of the α-subunit contains a binding domain that interacts with the binding domain within the C-terminus of the regulatory β-subunit (Crute et al., 1998). This binding domain within the β-subunit also acts as a binding site for the γ-subunit, thereby tethering the three subunits to form a heterotrimeric complex (Iseli et al., 2005). The β-subunit also consists of a glycogen binding site within its N-terminus, although the physiological significance of this remains unclear (McBride et al., 2009; Polekhina et al., 2003). Nevertheless, AMPK also has the capacity to bind to adenine nucleotides via binding sites within the regulatory γ-subunits (Figure 1.1). This is composed of four tandem repeats of cystathionine-β-synthase (CBS) motifs, which are assembled in a pseudosymmetrical manner that forms four clefts where ATP, ADP, and AMP bind (Figure 1.1). One of these clefts (site 4) binds to AMP tightly and does not exchange with ADP or ATP. Two of the other clefts (sites 1 and 3) competitively bind to AMP, ADP, and ATP based on the metabolic status of the cell and accordingly gives AMPK the capacity to monitor metabolic stress (Xiao et al., 2007; 2011).

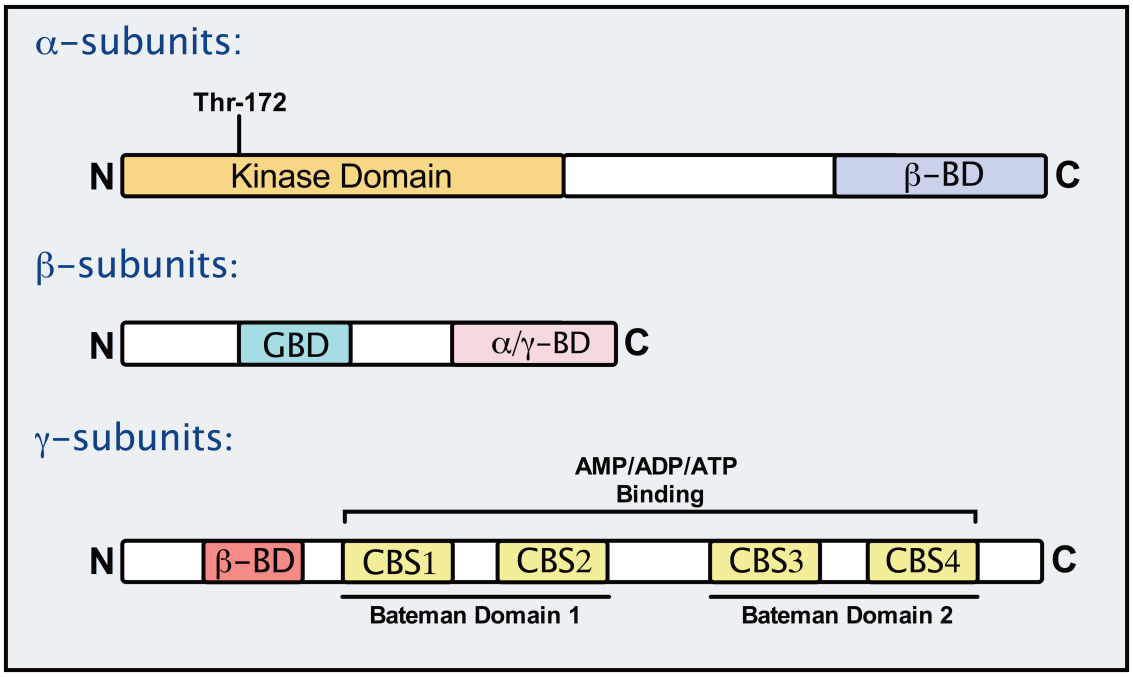

Figure 1.1: Structural domains of the AMPK catalytic and regulatory subunits. The catalytic α-subunit contains a serine/threonine kinase domain within its N-terminus. This contains the threonine residue at position 172 (Thr-172), which is phosphorylated by upstream kinases. The C-terminus of the α-subunit contains a binding domain for the β-subunit (β-BD). The β-subunit contains two conserved binding domains: (1) glycogen binding domain (GBD) in the N-terminus, and (2) a binding domain that links the α-subunit with the γ-subunit **(**α/γ-BD). The γ-subunit's corresponding binding domain lies within its N-terminus (β-BD). The γ-subunit also contains four tandem repeats of cystathionine-β-synthase (CBS) motifs that act in pairs (Bateman Domain 1 and 2) to form the binding sites for the adenine nucleotides. Figure adapted from (Hardie and Ashford, 2014).

1.1.2 Regulation of AMPK by upstream kinases and adenine nucleotides

AMPK is regulated in a manner that gives it the capacity to sense and respond to metabolic stress in order to reestablish energy levels. As briefly mentioned above, the full activation of AMPK is dependent on the phosphorylation of Thr-172 within the activation loop of the catalytic α-subunit (Hawley et al., 1996). This is primarily driven by the tumor suppressor kinase, LKB1. LKB1 is part of a heterotrimeric complex that also contains Ste20-related adaptor (STRAD) and mouse protein 25 (MO25), which are required for allosteric activation of the kinase; LKB1 activation is independent of phosphorylation (Zeqiraj et al., 2009). The extent of which AMPK is phosphorylated and activated is closely associated with the activity of LKB1 and requires the presence of LKB1 and its accessory subunits, STRAD and MO25 (Hawley et al., 2003). However, the Ca^{2+}/calmodulin-dependent protein kinase beta (CaMKK-β) has been identified as an alternative upstream kinase that can directly phosphorylate and activate AMPK in a Ca^{2+} dependent manner (Hawley et al., 2005)(Figure 1.2). Nevertheless, the binding of AMP, ADP, and ATP to the γ-subunit may also directly modulate AMPK activity (Figure 1.2).

Under resting conditions, AMPK is constitutively phosphorylated by LKB1. However, sustained activation of AMPK by LKB1 is not maintained as under metabolic/energy homeostasis, ATP is bound to sites 1 and 3 of the γ-subunit and promotes the continuous dephosphorylation of AMPK by phosphatases, namely PP2A and PP2C (Davies et al., 1995)(Figure 1.2). By contrast, during metabolic stress ATP is depleted within the cell with a subsequent increase in the AMP:ATP ratio. ATP is consequently displaced by AMP on the γ-subunit of AMPK, which increases AMPK activity by up to 10-fold via direct allosteric activation (Suter et al., 2006). Nevertheless, AMP further increases AMPK activity by >200-fold by causing a conformational change that protects AMPK from dephosphorylation by phosphatases (Davies et al., 1995; Suter et al., 2006) (Figure 1.2). Hence, AMP can collectively increase AMPK activation by up to >2000-fold during metabolic stress.

Recent studies have further demonstrated that in addition to AMP, ADP can also displace ATP during metabolic stress and activate AMPK by >200-fold by protecting

against dephosphorylation by phosphatases (Xiao et al., 2007; 2011) (Figure 1.2). However, unlike AMP, ADP does not have the capacity to mediate direct allosteric activation of AMPK (Xiao et al., 2007). Hence, the ability of AMPK to monitor the ADP:ATP and AMP:ATP ratio as an index of metabolic stress gives it the capacity to appropriately respond to a range of metabolic stress and energy deficits. That is, under relatively mild conditions of metabolic stress, AMPK would respond to fluctuations in the ADP:ATP ratio whereas under relatively more severe conditions, when the levels of AMP increases further, additional allosteric activation by AMP can increase overall activity to >2000-fold. Accordingly, AMPK then acts to reestablish energy levels by activating ATP-producing processes and/or inhibiting non-essential ATP-consuming processes (Hardie, 2007).

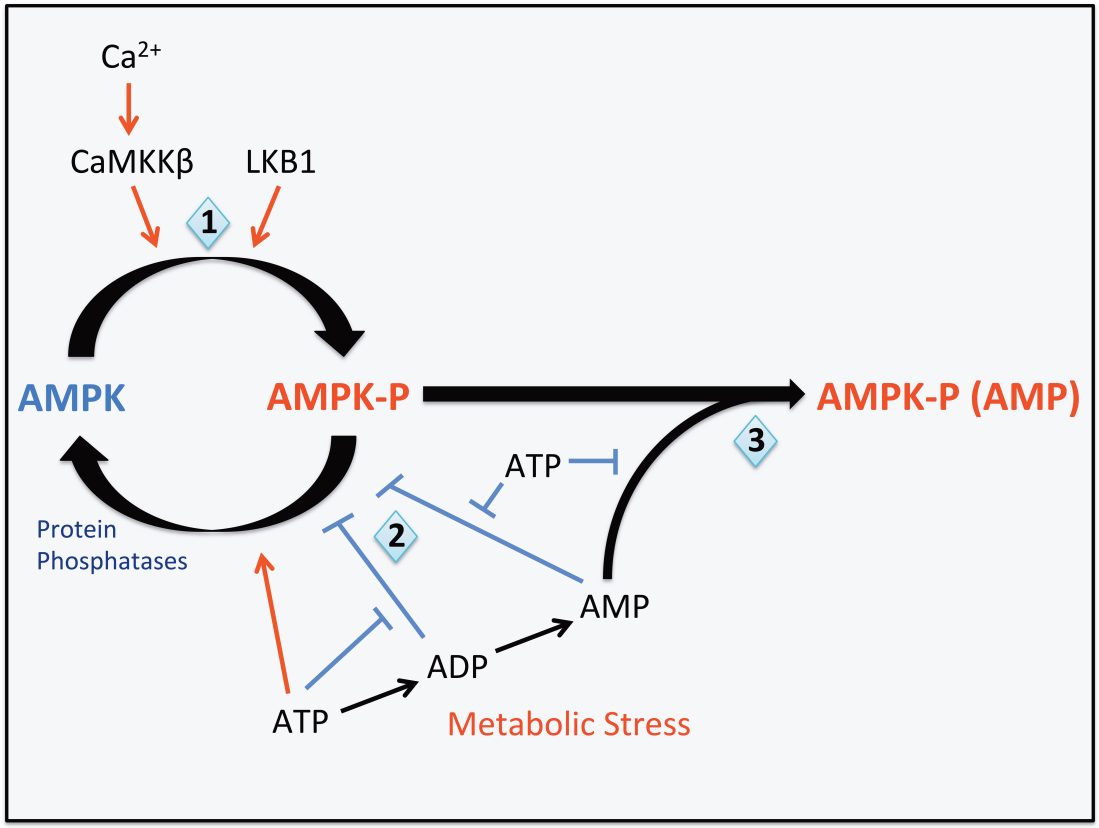

Figure 1.2: Regulation of AMPK by upstream kinases and adenine nucleotides. **(1)** AMPK is phosphorylated by upstream kinases, namely by LKB1 and by the Ca^{2+}-dependent CaMKKβ. (2) Metabolic stress depletes ATP, which results in an increase in the ADP:ATP and AMP:ATP ratio. ADP and AMP then displace ATP and bind to AMPK. This promotes AMPK activation by inhibiting dephosphorylation by protein phosphatases. (3) AMP can further increase AMPK activity by additional allosteric activation. Figure adapted from (Hardie and Ashford, 2014).

1.1.3 The Ancestral role of AMPK

AMPK has been found to exist universally. Well conserved genes encoding its catalytic α-subunit and regulatory β and γ-subunits can be found in essentially all eukaryotes, including plants, fungi, protists, and animals. Consistent with its role as a metabolic gauge, its ancestral role is believed to involve the response and adaptation to nutrient deprivation as shown by work on the budding yeast (*Saccharomyces cerevisiae*).

In *S. cerevisiae*, the genes encoding the AMPK catalytic α-subunit and regulatory γ-subunit are referred to as *SNF1* and *SNF4*, respectively. Yeast cells rapidly proliferate in a growth medium containing a high concentration of glucose (~2% glucose) by using fermentation, such as producing ethanol, to generate ATP. However, as glucose runs out in the medium, this cannot be sustained and growth decelerates until a switch is made to generate ATP by oxidative phosphorylation, which is more efficient. Interestingly, a SNF1 complex is required to decelerate growth in the absence of glucose as well as to switch to oxidative phosphorylation to generate ATP (Erecinska and D. F. Wilson, 1981; Hedbacker and Carlson, 2008). Furthermore, in *snf1*-null mutants, yeast are unable to detect glucose starvation and continue to grow rapidly and maintain fermentation until becoming nonviable (Carlson, 1999; Carlson et al., 1981; W. A. Wilson et al., 1996). This demonstrates an ancestral function of AMPK that involves restraining growth with glucose deprivation and appropriately triggering a switch to oxidative phosphorylation to maintain energy supply during metabolic stress.

Interestingly, an ancestral role for AMPK in response to starvation is also evident in plants. For plants, periods of starvation coincide with periods of darkness. In the moss (*Physcomitrella patens*), plants lacking both catalytic subunit orthologs of AMPK (SnRK1) are only able to survive under constant illumination as they fail to grow under more physiological conditions, i.e. light:dark cycles (Thelander et al., 2004). Furthermore, in the *Arabidopsis thaliana*, the down regulation of the SnRK1 catalytic subunit restricted growth while the overexpression of the catalytic subunit causes resistance to carbohydrate starvation generation under low light levels (Baena-González et al., 2007). All together, this strongly indicates that AMPK's role as a metabolic gauge

may have developed at the early stages of eukaryotic evolution to monitor nutrient deprivation, and hence energy supply, and to trigger an appropriate response that allows for survival and adaptation to metabolic stress.

Nevertheless, the early stages of eukaryotic evolution also significantly involved the engulfment of oxidative prokaryotes that, through evolution, developed into the ATP-producing mitochondria. This allowed eukaryotes to efficiently use oxygen for oxidative metabolism to generate energy in the form of ATP. Cellular aerobic respiration was extremely advantageous as it provided 20 times more free metabolic energy than that derived from anaerobic pathways (Maina, 2002). However, unlike carbohydrates and fats that can be strategically stored as metabolic substrates, oxygen has to be continuously acquired and processed. Hence, the evolution of gas exchangers and respiratory and circulatory organs/systems were equally important as it provided a continuous supply and delivery of oxygen for oxidative phosphorylation at a cellular and whole-body level (Maina, 2002). This paved way for the development and maintenance of large, diverse, and complex animals as respiration and mitochondrial oxidative phosphorylation sufficiently and consistently provided enough energy to sustain life while sufficient O_2 is present. However, with molecular oxygen becoming the preferred and main source of energy and the mitochondria the main cellular power source, an additional evolutionary event was required. That is, to develop a mechanism that has the capacity to monitor changes in oxygen supply and to accordingly respond in a manner that maintains oxygen homeostasis, and thus mitochondrial function and energy supply, at a cellular and whole-body level.

In this regard, specialised chemoreceptors evolved with the capacity to sense acute reductions in oxygen and trigger a respiratory response that acts to re-establish oxygen-levels. However, the molecular mechanism by which these specialised oxygen-sensing cells are activated during hypoxia to trigger respiratory adjustments remains controversial. Given its ability to monitor and respond to metabolic stress and energy in the form of nutrient deprivation (such as glucose deprivation in yeast or light deprivation in plants), could AMPK have adapted to mediate the activation of specialised oxygen-

sensing cells during oxygen-deprivation, namely hypoxia, thereby regulating energy supply as a whole body level?

1.1.4 AMPK's proposed role as the hypoxia-response coupler

Mammals are able to deliver oxygen to tissues at a whole body level by respiratory and circulatory systems. Atmospheric air, rich in O_2 (21% O_2), is inhaled into the lungs and diffuses into the blood where it binds to hemoglobin and is then carried throughout the body via the circulatory system. Despite the wide range of oxygen demand (during exercise versus during sleep), the partial pressure of oxygen (PO_2) and carbon dioxide (PCO_2) are regulated to remain within close limits in arterial blood (Spengler et al., 2001). This strict and elegant regulation of gas exchange is accomplished by the respiratory system, which finely controls the level of ventilation. This includes peripheral and central specialised chemoreceptors which were able to detect minor changes in PO_2, as well as increases in PCO_2 and/or [H^-], and subsequently send a signal to the respiratory centres in the brainstem to adjust ventilation in a manner that would appropriately meet oxygen-demand and consequently CO_2 output (Mulligan et al., 1981; Spengler et al., 2001) (Figure 1.3).

However, as mentioned above, discrepancies arise with regards to the molecular mechanism within the specialised oxygen-sensing cells that allows for cell activation and ultimately the ventilatory response to hypoxia. Nevertheless, several studies have strongly suggested that the mitochondrion is the primary site for O_2-sensing (Mills and Jöbsis, 1972; Duchen and Biscoe, 1992a; Buttigieg et al., 2008; Buckler and Turner, 2013) with the inhibition of mithocondrial ATP synthesis being the primary event that triggers the hypoxia chemotransduction cascade (Wyatt and Buckler, 2004), as described further in chapter 3. Research has hence been directed at elucidating the identity of the hypoxia-response coupler downstream to hypoxic-inhibition of the mitochondria in oxygen-sensing cells. Given the ability of the LKB1-AMPK pathway to monitor and respond to the ADP:ATP and AMP:ATP ratios as an index of metabolic stress, linked with previous findings showing AMPK's ability to directly regulate ion channels (Ikematsu et al., 2011; Ross et al., 2011; Wyatt et al., 2007) and mimic the hypoxic

response in specialised oxygen sensing cells (as described further in chapter 3), has put it in prime position for coupling hypoxic inhibition of mitochondrial ATP-synthesis with ion channel regulation and hence the subsequent activation of specialised oxygen-sensing cells (Figure 1.4). Accordingly, the LKB1-AMPK signalling pathway may act to re-establish oxygen-supply, and thus acting as a metabolic gauge, at both a cellular and whole-body level.

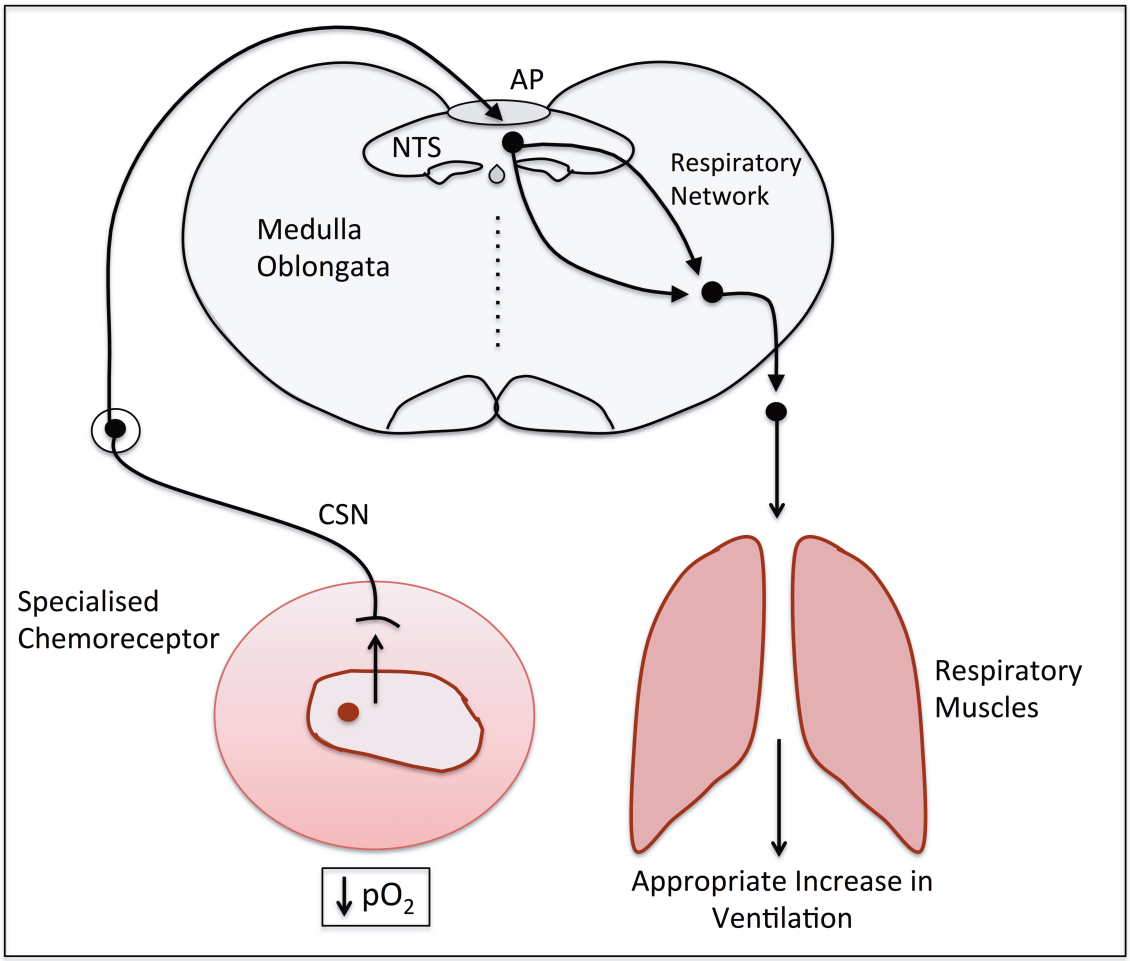

Figure 1.3: Chemosensory regulation of breathing. Peripheral specialised oxygen-sensing cells, namely the type I cells of the carotid body, are activated during acute hypoxia. This increases afferent fibre discharge along the carotid sinus nerve (CSN) to the dorsomedial medulla, which includes the area-postrema (AP) and the nucleus tractus solitarius (NTS). These signals are integrated with input from central chemosensitive neurons within the dorsomedial region and then relayed to the ventrolateral medulla, which consists of the respiratory central pattern generators that accordingly modulate the respiratory muscles to promote an increase in ventilation. Adapted from (Gourine, 2005)

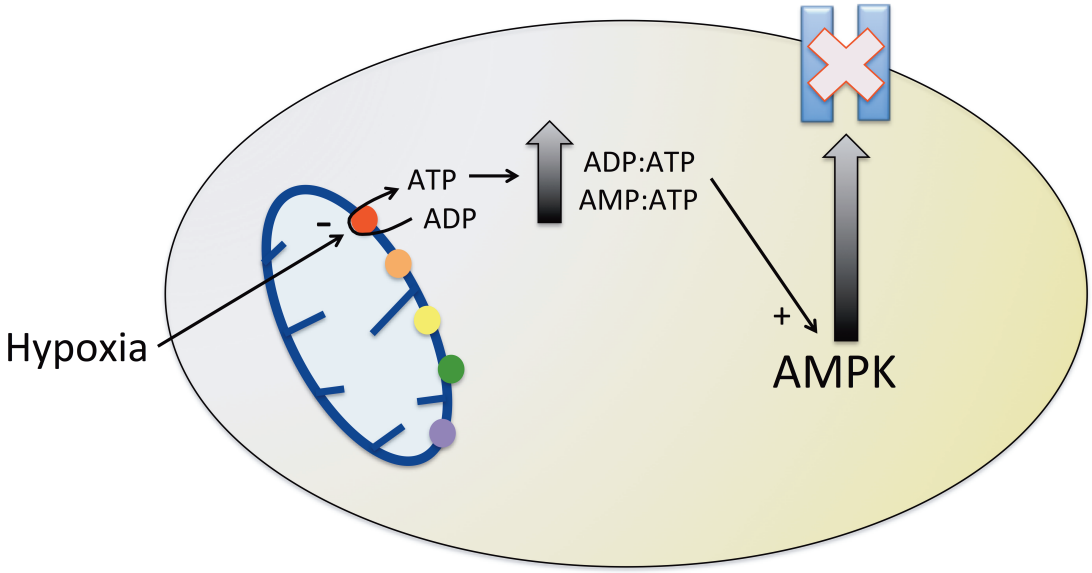

Figure 1.4: Proposed role for AMPK as the hypoxia-response coupler in specialised oxygen-sensing cells. Upon hypoxic inhibition of the mitochondrial oxidative phosphorylation, and hence ATP synthesis, activation of AMPK is initiated by subsequent increases in the ADP:ATP and AMP:ATP ratio. AMPK then responds by regulating ion channels, thereby promoting cell activation, and ultimately an appropriate ventilatory response to hypoxia.

1.2 The respiratory network

1.2.1 Historical perspectives of respiratory physiology

By the 1600s, the understanding of respiration was had largely been drawn from the findings and descriptions of the ancient Greek physician, Claudius Galenus (129-201 A.D.). His first medical post was to treat gladiators, which gave him the opportunity to observe and evaluate injuries to the respiratory system. He was able to describe in significant detail how to perform noteworthy surgeries and experiments to study the anatomy and apparent function of the respiratory muscles (Derenne et al., 1995). This included a series of muscle denervations and sections along the spinal cord that demonstrated the actions of the diaphragm and how it moves the ribcage. He was also able to identify the movement of lungs during expiration through an exposed pleural space and further described the connection between the lungs and chest wall. He hypothesised that the ribcage and abdominal muscles interacted in a manner that would maintain the position of the diaphragm, demonstrating his awareness and understanding that the diaphragm can move upward as long as the ribcage is allowed to expand (Derenne et al., 1995). However, although Galen was able to identify and describe respiratory muscles, he fell short of deducing their function.

Galen's considerations on respiratory function was a reformation of concepts made nearly 400 years earlier by the Alexandrian physiologist, Erasistratus (Galen et al., 1984). Galen agreed with Erasistratus's abstract and complex description of 'innate heat' and the presence of 'pneuma' within living creatures; innate heat was defined as a source of heat or warmth that is closely associated with life itself while pneuma was a vital presence within living creatures that was somehow connected with air. Galen considered both were somehow linked suggesting that Galen may have possibly anticipated the similarities between respiration and combustion, which was demonstrated and described nearly 1500 years later (as further described below). However, Galen had admitted he was oblivious as to why living organisms and flames are quickly diminished in the absence of air (Galen et al., 1984; Derenne et al., 1995). Nevertheless, he thought inspired air (or pneuma) infiltrated through the pulmonary vein

and merged with blood before entering the left ventricle of the heart. From there he believed a proportion of the blood with 'vital spirit' would go to the brain where it was transformed into 'animal spirit' which promotes sensory and motor functions while the rest of the 'vital spirit' was delivered to the rest of the body through arteries with 'pneumatised' blood (Siegel, 1968; Galen et al., 1984; Derenne et al., 1995).

Galen had also considered the lung tissue to be comparable to the liver or pancreas with the exception of being lighter and more porous. He thought that the light and porous nature of the lung tissue was a result of the foam of a light vaporous blood as it solidified, unlike the thick heavy blood that would solidify to form the liver (L. G. Wilson, 1960). With respect, it is clear from this assumption that Galen was completely unaware of the lungs acting as a system of air sacs linked to the branches of the trachea. Nevertheless, this misassumption of structure of the lungs persisted until the 17th century. It was not until 1661, that the misunderstandings of the lungs' structure were revolutionised with the advancements in microscopes alongside the mind and observations of Marcello Malpighi. In a letter written to his friend, Alfonso Borelli, Malpighi described the lungs as a dense collection of thin fine membranes and, when stretched and folded, form a vast number of 'orbicular bladders' that resemble the honeycomb cells of beehives (Malpighius, 1686; L. G. Wilson, 1960). He further described how these 'orbicular bladders' were positioned in a manner that allowed a connection with the trachea. However, even though his accurate observations revolutionised our understandings of the structure of the lungs, his interpretation of the function of the lungs was also incorrect. Similar to Galen and his other scientific predecessors, Malpighi believed the expanding and contracting nature of the lungs (as occurs during inspiration and expiration, respectively) was to press and squeeze blood through the blood vessels and capillary network within the lungs (Malpighius, 1686; L. G. Wilson, 1960).

It was shortly after Malpighi's revolutionary observations on the structure of the lungs that Robert Hooke was able to deduce the role of the lungs as a respiratory organ. Hooke used a vivisection technique, surgery on a live animal, in order to observe the function of the lung *in vivo*. This involved opening the chest and cutting through the ribs

and then separating them, as well as the breastbone, from the diaphragm. This allows the entire ventral wall of the chest to be lifted, such that the whole chest cavity is exposed. Hooke then pricked holes in the lungs and quickly provided a continuous current of air by using bellows before the animal suffocated. This meant that air was continuously supplied to the lungs and accordingly the lungs would remain 'motionless' as it remained expanded. With this ingenious technique, Hooke was able to demonstrate that blood was still able to flow through the lungs even though they remained still. He further demonstrated that it was not the motionless lung or the stopping of circulation of the blood through the lungs that would be the immediate cause of death, but the lack of a sufficient supply of air into the lungs (Hooke, 1667; L. G. Wilson, 1960).

Hooke's series of experiments were not only crucial for the development of our understanding of the functional role of lungs, but also because it guided Richard Lower to observe the change in colour of blood as it passed through the lungs. Before Hooke's setup, Lower struggled to draw blood from the pulmonary vein. The reason why was that his technique involved the opening of the chest very widely, which subsequently led to lungs collapsing as soon as the pleural cavities were opened (L. G. Wilson, 1960). It is with Hooke's setup that Lower was able to draw blood from the pulmonary vein while the lungs remained ventilated with air and the heart remained viably functional. He also demonstrated that blood would turn scarlet red when forced through lungs that contained fresh air, even when the animal is dead and the heart is no longer moving. All together, this gave Lower the capacity to observe the colour change of blood that takes place in lungs when they are ventilated with air and how it does not involve mixing or stirring of the blood in the capillary network as previously presumed by Galen and Malpighi, amongst the other scientists of their times. He concluded that the purpose of the flow of blood through the lungs was to receive something from the air, or what he referred to at the time as a 'nitrous spirit' (L. G. Wilson, 1960).

It was not until 80 years later, in 1774, that the British scientist, Joseph Priestley, discovered this 'nitrous spirit'. Priestley called his discovery "dephlogisticated air" before being renamed to oxygen by Antoine Lavoisier. Priestley's choice of nomenclature was derived from the phlogiston theory, which was widely accepted at the

time. According to this theory, fires released their 'phlogiston', or combustible components, into the atmosphere. Using a burning lens with focused sunlight emitting through, Priestley moderately heated mercuric oxide in an inverted glass container placed in a pool of mercury. He recognised that the gas emitted during this process intensified the flame of a candle and extended the lifespan of mice by about four times as much as a similar volume of atmospheric air would (Priestley, 1775; Grainge, 2004). Priestley believed he was introducing phlogiston into the mercury from the atmosphere, thereby purifying the air; hence, the term 'dephlogisticated air' (Grainge, 2004; Priestley, 1775). Fortunately, records of Priestley's description of inhaling dephlogisticated air have been conserved:

> The feeling of it to my lungs was not sensibly different from that of common air; but I fancied that my breast felt peculiarly light and easy for some time afterwards. Who can tell but that, in time, this pure air may become a fashionable article in luxury. Hitherto, only two mice and myself have had the privilege of breathing it. (Priestley, 1775)

The dephlogisticated or pure air inhaled by Priestley and his two experimental mice was oxygen released from the previously burnt mercury. Although Priestley failed to accurately interpret his findings, it nevertheless provided Antoine Lavoisier with a clue. As luck would have it, Priestley met Antoine Lavoisier during a trip to France and described his findings of dephlogisticated air. From their encounter, Lavoisier was able to develop his theory of chemical reactions in 1778 and argued against the phlogiston theory. Lavoisier argued that flames or burning substances did not release phlogiston, but instead reacted with Priestley's gas, which Lavoisier called oxygen – the Greek word for 'acid-maker' (Grainge, 2004; Karamanou and Androutsos, 2013).

A few years later, Lavoisier grew more interested in the connection between combustion and respiration. He believed that they were both one and the same and that combustion occurs with every breath during respiration (Karamanou and Androutsos, 2013; Grainge, 2004; Shectman, 2003). Accordingly, Lavoisier and his friend, Pierre-Simon Laplace, designed a setup to measure and compare the amount of heat that was emitted during combustion and respiration. The setup consisted of a 3 chambered

apparatus: (1) an inside chamber that contained a source of heat, which was either a living guinea pig or a piece of burning charcoal; (2) the middle chamber that contained a specific amount of ice for the source of heat to melt; and (3) the outside chamber that contained packed snow for insulation. Furthermore, they collected the air that was given off during combustion from the charcoal or respiration from the guinea pig by connecting a sleeve to the apparatus. They were able to then measure the amount of caloric and air produced during respiration and concluded that respiration is combustion. He further noted that this enables the guinea pig to maintain its body temperature above its surrounding (Karamanou and Androutsos, 2013; Shectman, 2003). Lavoisier's scientific observations on respiration provided a fundamental pillar for the development of respiratory physiology. However, his research unfortunately came to an abrupt and violent end as he, who is now commonly referred to as one of the 'fathers of modern chemistry', was executed on the guillotine during the French revolution (Karamanou and Androutsos, 2013; Shectman, 2003).

1.2.2 The structure of the central respiratory network

Respiration is driven by respiratory networks and neuromodulatory nuclei, which are distributed bilaterally within the neuraxis of the brainstem. Each side of the pons and medulla oblongata contains a ventral respiratory column (VRC) that incorporates neuronal networks that generate the motor patterns that are observed during rhythmic breathing (Figure 1.5). These pontine-medullary respiratory circuits are hierarchically arranged and include, from rostral to caudal, the retrotrapezoid nucleus/parafacial respiratory group complex (RTN/pFRG), the Bötzinger complex (BötC), the pre-Bötzinger complex (Pre-BötC), the rostral ventral respiratory group (rVRG), and the caudal ventral respiratory group (cVRG, (Alheid and McCrimmon, 2008; Feldman and Del Negro, 2006; McCrimmon et al., 2004; Feldman and J. C. Smith, 1989). The respiratory network also contains the Kölliker-Fuse nucleus (KF) and the parabrachial complex (PB), located in the dorsal pons, as well as the nucleus tractus solitarius (NTS) within the dorsomedial medulla (Figure 1.5).

The histological and functional characteristics of the individual circuits and nuclei in the respiratory networks are quite distinct (Gray et al., 1999; Janczewski and Feldman, 2006; McCrimmon et al., 2004). Inspiratory interneurons are predominately populated in the pre-BötC and rVRG. By contrast, the expiratory neurons are predominately populated in the BötC and cVRG, many of which are bulbospinal (meaning they originate in the medulla and project and terminate in the spinal cord) as well as propriobulbar (those that project and terminate within the medulla) (Figure 1.6, (Onimaru and Homma, 2003; Thoby-Brisson and Ramirez, 2001; Janczewski and Feldman, 2006)). It has also been suggested that the BötC, KF, and PB play an important role within the respiratory network and during the transition between inspiratory and expiratory activity (Cohen, 1971; Mörschel and Dutschmann, 2009).

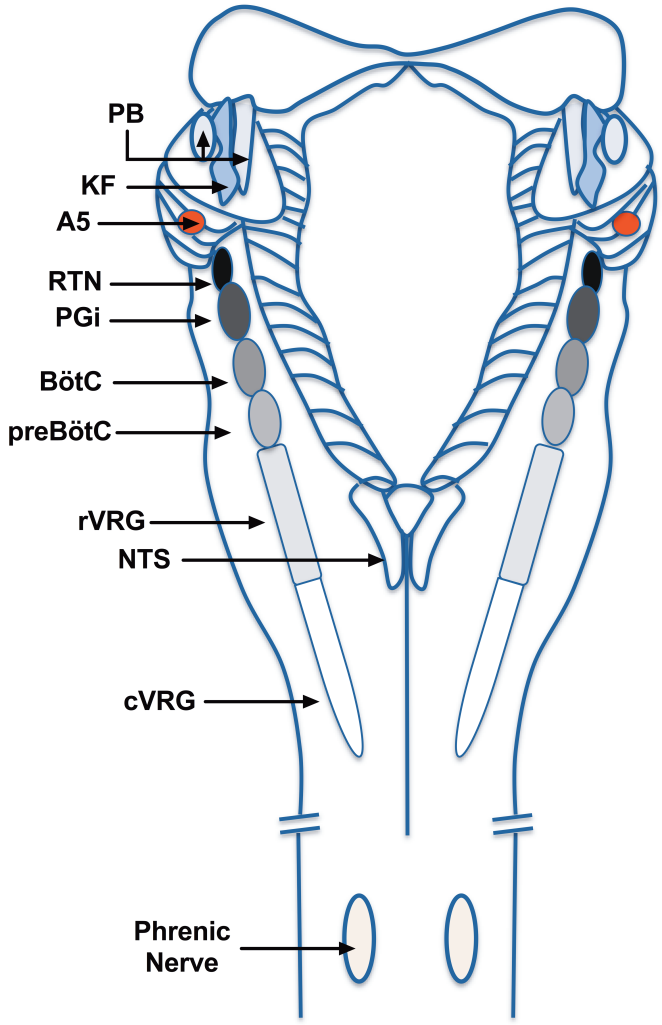

Figure 1.5: Functional compartments of the ventilatory respiratory columns. Dorsal view of the brainstem illustrating the functional compartments within the ventilatory respiratory column. KF, Kölliker-Fuse nucleus; PB, parabrachial nuclei; noradrenergic A5 area; RTN, retrotrapezoid nucleus; PGi, paragigantocellular reticular nucleus; BötC, Bötzinger complex; preBotC, preBötzinger complex; rVRG, rostral ventral respiratory group; cVRG, caudal ventral respiratory group. Image adapted from (Rekling and Feldman, 1998).

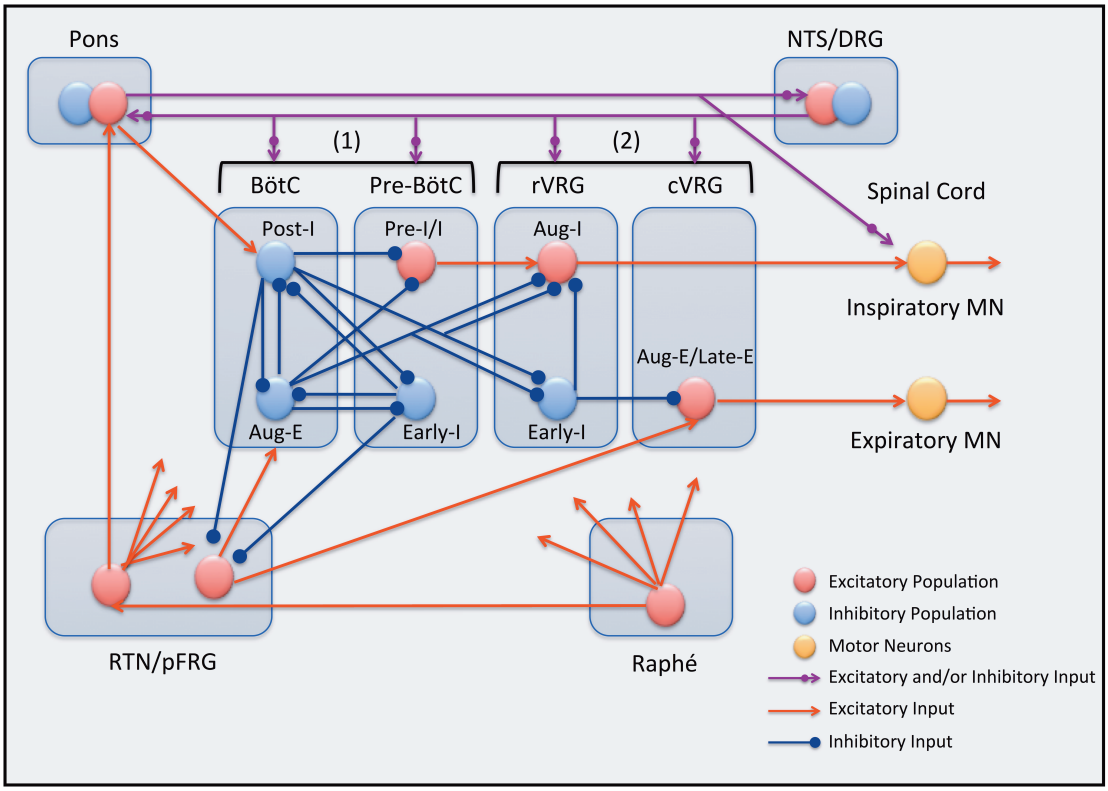

Figure 1.6: Microcircuits involved in respiratory rhythm and pattern generation. The Bötzinger (BötC) and pre-BötC (pre-BötC) have been suggested to act as (1) rhythmogenic microcircuits. These circuits involve a population of excitatory pre-inspiratory-inspiratory (Pre-I/I, red) neurons and 3 inhibitory populations (blue). The inhibitory populations not only project inhibitory connections to the excitatory population within the Pre-BötC, but also mutually inhibit each other via an 'inhibitory ring' between the post-inspiratory (Post-I), augmenting-expiratory (Aug-E), and early inspiratory (Early-I) populations. Projections are also made from the (1) rhythmogenic microcircuits to the (2) transmission circuits which contains the rostral and caudal ventral respiratory group (rVRG and cVRG, respectively). The Pre-I/I population of excitatory neurons within the pre-BötC project to an excitatory population of augmenting inspiratory (Aug-I) premotor neurons within the rVRG. These premotor neurons then project to inspiratory motorneurons (Mn) within the spinal cord. An excitatory population within the cVRG also project to the spinal cord but to expiratory motorneurons. Furthermore, all four compartments receive tonic, phasic, or rhythmic input from the pontine, nucleus solitarius tract/dorsal respiratory group (NTS/DRG), retrotrapezoid nucleus, parafacial respiratory group (RTN/pFRG), and the Raphé. Figure adapted from (J. C. Smith et al., 2013).

1.2.3 Functional compartments of the respiratory network

Pre-Bötzinger complex

The pre-BötC complex sits rostral to the BötC and plays an important role in triggering respiratory activity; this was suggested by experiments on brainstem slices from neonatal rats. With the pre-BötC intact, the neuronal circuits therein were able to generate rhythmic activity *in vitro*. However, localised bilateral lesions of NK1R-expressing neurons sitting within the pre-BötC resulted in disordered breathing; even unilateral lesions eliminated the ability to stimulate respiration when glutamate was injected into the pre-BötC (H. Wang et al., 2002; Gray et al., 2001; Stornetta et al., 2002). Moreover, targeted ablation of NK1R-expressing neurons with the use of the toxin saporin conjugated to substance P (SP-SAP) resulted in disordered breathing which was observed during rapid eye movement (REM) sleep as early as day 4 post-injection, and increased in severity with time. Disturbances in the respiration included central apnoeas (as indicated by a cessation of airflow accompanied by a loss of thoracic activity). Furthermore, around 9-10 days post-injection disturbances in breathing began to occur during wakefulness and involved severe ataxic breathing with irregular high frequency of breathing and sighs with scattered appearances of many hypopneas and apnoeas. In some cases, such ataxic respiratory patterns were intermingled with a periodic Cheyne-Stokes-like breathing normally observed in subjects with congestive heart failure (McKay et al., 2005; Eckert et al., 2007) and is characterised by a sinusoidal ventilatory pattern that cycles from progressively deeper and faster breathes to a gradual decrease which ultimately reaches an apnoeic event (Eckert et al., 2007).

This progressive disruption in rhythmic breathing is likely to have occurred as neurons within the pre-BötC progressively continued to be ablated after initial SP-SAP injection but also from further neuronal death occurring within the pre-BötC in non-NK1R-expressing neurons (McKay et al., 2005; Gray et al., 2001). That is, within 3-6 days, pre-BötC lesions resulted in disordered breathing which only occurred during REM sleep and that included apnoeas. These prolonged and frequent apnoeic events would lead to intermittent hypoxia and it was proposed that the cumulative effect may possibly have resulted in further neuronal death that is no longer restricted to NK1R-

expressing neurons. Namely, other neurons present near the pre-BötC that are involved in stimulating breathing and modulating respiratory rhythm, i.e. chemosensitive catecholaminergic C1 neurons. It was therefore suggested that progressive disturbances in breathing during wakefulness was likely driven by loss of chemosensing neurons (McKay et al., 2005; Guyenet et al., 2013).

Ventral respiratory groups

Within the spinal cord lie inspiratory and expiratory motor neurons that are innervated by premotor neurons located within the VRG; subdivided into rVRG and cVRG. Both inspiratory and expiratory premotor neurons innervate spinal inspiratory and expiratory motor neurons, respectively (Figure 1.6). The pre-inspiratory motor neurons are bilaterally clustered within the rVRG and are bulpospinal. They are activated by the excitatory pre-BötC neurons and inhibited by the expiratory neurons within the BötC (Figure 1.6). Collectively, these inputs influence the ramping pattern of inspiratory rVRG neuronal activity which subsequently affects the inspiratory drive to the spinal motor neurons and their motor output pattern (i.e. to the phrenic motorneurons that innervate the diaphragm) (Bianchi et al., 1995; J. C. Smith et al., 2013). In contrast, the cVRG contains bulbospinal expiratory neurons that receive inputs from the BötC and the RTN/pFRG. Based on the converging inputs, they accordingly shape the activity of spinal expiratory motorneurons, whose axons terminate at the intercostal nerves as well as abdominal muscles (J. C. Smith et al., 2013; Richter, 1996). However, the spatial separation of rVRG and cVRG is not exclusive with some overlap of inspiratory and expiratory neurons and their activity. For instance, the expiratory neurons within the cVRG receive inhibitory inputs from the inspiratory neurons within the rVRG (Figure 1.6, (J. C. Smith et al., 2013; Alheid and McCrimmon, 2008)). Nevertheless, the rVRG is predominately key for the modulation of the inspiratory phase of respiration while cVRG is for the expiratory phase.

Retrotrapezoid nucleus and the parafacial respiratory group

Rostral to the pre-BötC lies the RTN/pFRG which contain excitatory glutamatergic neurons that express the transcription factor PHOX2B and has been implicated with congenital central hypoventilation syndrome as will be described below (Dubreuil et al., 2009; Mulkey et al., 2004; Stornetta et al., 2006). In perinatal rodents, many of these neurons have an intrinsic rhythmic activity; which are normally referred to as pFRG (Thoby-Brisson et al., 2009). In adults, the pFRG are then referred to as the RTN as they change and become tonically active (Abbott et al., 2009; Mulkey et al., 2004) due to a developmental transformation (Guyenet and Mulkey, 2010). The neurons nevertheless are chemosensitive and are regulated by changes in CO_2 or pH. They are also modulated by arterial changes in O_2 as it receives inputs from peripheral and central oxygen-sensing cells/neurons, i.e. type I cells of the carotid body and noradrenergic neurons within the NTS (Stornetta et al., 2006; Guyenet et al., 2010; King et al., 2012).

Nucleus tractus solitarius

The dorsomedial region of the medulla contains the NTS, which receives converging inputs; centrally from the pons region (King et al., 2012) and from peripheral chemoreceptors, such as the carotid body (Mifflin, 1992). Accordingly the caudal nucleus tractus solitarius (cNTS) and the associated dorsal respiratory group (DRG) within the NTS mediate afferent modulation of respiration via their projections back to pontine and the VRC compartments (i.e. Pre-BötC, BötC, and VRG, Figure 1.6). The neurons within the NTS appear to play a critical role in modulating the respiratory pattern and the ventilatory response to hypoxia, as opposed to the generation of respiratory rhythm itself (Song et al., 2011; King et al., 2012).

Kölliker-Fuse and parabrachial nuceli

The pontine respiratory group (PRG) contains the Kölliker-Fuse (KF) and parabrachial (PB) nuclei and regulates the transition between the inspiratory and expiratory phases of respiration (Dutschmann and Herbert, 2006). In addition, *in situ* studies on perfused working heart-brainstem preparation demonstrated that the

introduction of glutamate by injections into the intermediate KF would result in a transient post-inspiratory apneoa while injections in the surrounding margin of the KF area results in bradypnea and enhanced post-inspiratory activity (Stettner et al., 2007). This suggests that PRG may modulate the post-inspiratory activity through their projections to the VRC compartments (Stettner et al., 2007; Dutschmann and Herbert, 2006). Also, the transection of the pons regions has been found to promote increased phrenic activity, suggesting that the pontine regions may also play an inhibitory role with respect to respiratory rhythm (Hilaire et al., 1989).

1.3 The regulation of ventilation during hypoxia by catecholaminergic oxygen-sensing cells

As described above, the evolution of a respiratory system that was able to provide a continuous supply and delivery of oxygen paved way for the development and maintenance of large, diverse, and complex animals as respiration and mitochondrial oxidative phosphorylation sufficiently and consistently provided enough oxygen and energy, respectively, to sustain life while sufficient O_2 is present. Nevertheless, with molecular oxygen becoming the preferred and main source of energy and the mitochondria the main cellular power source, an additional evolutionary event was required. That is, to develop a mechanism that has the capacity to monitor changes in oxygen-supply and to accordingly respond in a manner that maintains oxygen homeostasis, and thus mitochondrial function and energy supply, at a whole-body level (Maina, 2002). In this regard, specialised chemoreceptors evolved with the capacity to sense acute reductions in oxygen and trigger a respiratory response that acts to re-establish oxygen-levels. Identification of respiratory diseases, such as CCHS and Rett syndrome, highlights the importance of such chemoreceptors, namely catecholaminergic chemoreceptors, to the regulation of the respiratory network to protect against disordered breathing.

1.3.1 Type I cells of the carotid body

Albrecht von Haller was the first to describe the carotid body in 1762. His anatomical studies had exposed a mass of tissue situated at the bifurcation of the common carotid artery into the internal and external carotid arteries. Then referred to as the ganglion exiguum, due to its resemblance to a ganglion-like structure, the proposition was that this tissue had a glandular function under the control of motor input. However, the first direct evidence of a sensory function, rather than motor, for the carotid body came from the work of Fernando de Castro who identified using anatomical and histological studies the afferent innervation of the carotid body by the IXth cranial nerve, the glossopharyngeal nerve (Kumar and Prabhakar, 2012). He then astutely suggested that, due to the anatomical characteristics of the carotid body along with its location at the bifurcation of the common carotid artery, the carotid body is able to detect changes in blood composition and provide feedback that would modulate the activity of other organs. It was shortly after this that such a sensory role was first validated, by Jean Francois Heymans and his son, Corneille.

Using vascularly isolated carotid bifurcations from dogs, Heymans and his son performed cross perfusion experiments and demonstrated that the carotid body was involved in cardiorespiratory homeostasis, which earned them the Nobel Prize in 1938. Their studies were the first to show that the carotid bodies were primary peripheral arterial chemoreceptors, as their activation triggered hyperventilation in response to decreases in arterial PO_2 (Kumar and Prabhakar, 2012). Subsequent to these pivotal discoveries of the sensory nature of the carotid body, interest and research into the carotid body advanced into the 20^{th} century with several ultra structural studies and stimulus-response measurements being performed at the whole organ level. Such *in vitro* studies helped identify the catecholaminergic type I cells, which synapses with the carotid sinus nerve (CSN), as being responsible for the specialised oxygen-sensing ability within the carotid body (Verna et al., 1975). It has been well established that upon exposure to acute hypoxia, CB1 cells are rapidly activated subsequent to ion channel regulation, thereby triggering neurotransmitter release and an increase in afferent fibre discharge along the CSN to the respiratory centres in the brainstem, which

ultimately elicits an increase in ventilation (Biscoe et al., 1989; Biscoe and Duchen, 1990) (Figure 1.3). Furthermore, studies also helped demonstrate that the carotid body not only has the largest blood flow/unit weight relative to any other organ but also a high O_2 consumption and metabolic rate (Biscoe et al., 1989).

1.3.2 Neonatal adrenomedullary chromaffin dells

The catecholaminergic neonatal adrenomedullary chromaffin cells (nAMCs) play a critical role perinatally as they trigger a surge of catecholamine release in response to hypoxic stress that is experienced during birth. The burst of catecholamines helps develop the lungs into an air-breathing organ to prepare newborns for extra-uterine life but plays a significant role in the postnatal maturation of the brain and carotid body (Jiang and Haddad, 1994; Liu et al., 1999). In utero, the sensitivity of CB1 cells is established in a relatively hypoxic atmosphere when compared to the higher PO_2 experienced in the atmosphere after birth. As a result, at birth the carotid body is silent as it experiences a relatively hyperoxic environment. It has been suggested that the surge of adrenaline release by the nAMCs at birth resets the carotid body, in order to aid the adaptation to the new environment (Wasicko et al., 1999; Donnelly, 2005).

Despite the non-neurogenic nature of the nAMCs at birth, the nAMCs are able to detect and respond to hypoxia before they are innervated by the sympathetic splanchnic nerve. Briefly, the oxygen-sensing ability of nAMCs disappears postnatally at a time coincident with the maturation of sympathetic innervation (Seidler and Slotkin, 1985; Slotkin and Seidler, 1988). Similar to the CB1 cells (which are also derived from the neural crest), the hypoxic response of nAMCs involves the regulation of ion channels and subsequent depolarisation and voltage-dependent Ca^{2+} influx and neurotransmitter release. Recent studies on immortalised adrenomedullary chromaffin cells (MAH cells) further indicate that hypoxic chemotransduction requires functional mitochondria as its absence prevents K^+ channel regulation and subsequent adrenaline release during hypoxia (Buttigieg et al., 2008). This suggests that oxygen-sensing in nAMCs and subsequent K^+ channel regulation and neurotransmitter release during hypoxia relies on an upstream effector that is dependent on functional mitochondria.

1.3.3 Central neurons of the brainstem

A single neuromodulator can differentially act within the respiratory network on a series of receptor subtypes, thereby exerting distinct and often diverging effects. Several studies on catecholaminergic neurons within the brainstem, namely clusters of noradrenergic (A1, A2, A5, and A6) and adrenergic (C1, C2) nuclei, have attempted to identify their neuromodulatory effects on the neuronal control of breathing during hypoxia.

A5 and A6 nuclei

In the pons region, the A6 containing locus coeruleus neurons are regulated by hypoxia. Both *in vitro* and *in vivo* studies on the activity of A6 during hypoxia have demonstrated that a number of these neurons are excited while others are inhibited; nevertheless, they stimulate breathing overall (Guyenet et al., 1993). This is consistent with the increase in breathing frequency observed upon electrical stimulation of the locus coeruleus (Doi and Ramirez, 2010) as well as the decrease in respiratory activity in mice deficient of A6 neurons (Viemari et al., 2004). Similar to the A6 nucleus, hypoxia appears to have an excitatory effect *in vitro* on A5 neurons but instead inhibits breathing (Guyenet et al., 1993). This is supported by lesion studies that demonstrated that targeting the A5 neurons increases breathing frequency (Guyenet et al., 1993). All together, this demonstrates that even when modulated under similar conditions, the example being hypoxia, both noradrenergic A5 and A6 neurons are able to distinctly modulate respiratory network activity.

A1/C1 and A2/C2 neurons

Besides the A5 and A6 neurons, endogenous release of noradrenaline and adrenaline has been demonstrated *in vitro* from the dorsomedial medullary A1 and C1 neurons, respectively, which increases respiratory rhythm (Viemari, 2008). Noradrenaline also has a stimulating effect on the respiratory network when

exogenously applied to medullary slices by directly affecting inspiratory neurons (Zanella et al., 2006). It appears that neurons within the A1/C1 and A2/C2 regions are stimulated during hypoxia as low oxygen levels appear to increase TH expression and Fos-like immunoreactivity (Peyronnet et al., 2003; Roux et al., 2003; Erickson and Millhorn, 1994; Teppema et al., 1997). As will be discussed later in this thesis, the decrease in the number of TH-positive neurons and catecholamine content in A1/C1 and A2/C2 regions has also been associated with the progressive increase in breathing irregularities in certain syndromes, such as Rett syndrome, (Viemari et al., 2005) including prolonged and frequent apnoeas and unstable breathing pattern. The A1/C1 and A2/C2 regions have also been found associated with mediating the hypoxic ventilatory response in the absence of a functional input from the carotid body (Roux et al., 2000).

1.4 Hypothesis:

Taken together, ventilatory drive is mediated by respiratory central pattern generators (rCPGs), which are continuously modulated by specialised catecholaminergic peripheral and central chemoreceptors to adjust ventilatory patterns according to changes in arterial PO_2, PCO_2, and pH levels. In response to hypoxia, these specialised oxygen-sensing chemoreceptors, primarily the carotid body type I cells but also including the catecholaminergic cells of the brain stem, are necessarily activated to ultimately trigger an increase in ventilation to restore oxygen-levels. However, the molecular mechanism by which mammals are able to regulate their breathing pattern in such a manner during hypoxia remains controversial.

Given the ability of the LKB1-AMPK pathway to (1) monitor and respond to the ADP:ATP and AMP:ATP ratios as an index of metabolic stress, linked with (2) evidence demonstrating AMPK's ability to directly regulate ion channels and mimic the hypoxic response (i.e. promoting depolarisation, calcium influx, neurotransmitter release, and subsequent increases in afferent fibre discharge to the respiratory centres of the brainstem in the primary specialised oxygen-sensor, namely the carotid body type I

cells (Ikematsu et al., 2011; Ross et al., 2011; Wyatt et al., 2007), I therefore hypothesise that the LKB1-AMPK signalling pathway is essential in carotid body type I cells and respiratory centres in the brainstem to promote an appropriate ventilatory response to hypoxia at the whole body-level.

1.5 Aims of Thesis

Therefore, the studies performed in this thesis aimed to investigate the possibility that the hypoxic ventilatory response may be driven by the LKB1/AMPK signalling pathway, which is central to cellular adaptations to metabolic stress. This involved:

(1) The development of transgenic mice in which *Lkb1* or both *AMPK α1* and α2 catalytic subunits are conditionally deleted in catecholaminergic cells.

(2) Examine the consequent effects of conditional *Lkb1* and *AMPK α1* and *α2* deletion in catecholaminergic cells on the ventilatory response to hypoxia using unrestrained whole-body plethysmography, and whether the effects are reversed under hypoxia with hypercapnia

(3) To further distinguish the relative contributions of the AMPK α1 and AMPK α2 isoforms in mediating the ventilatory response to hypoxia.

Chapter Two:
Materials and Methods

2.1 Introduction

2.1.1 The Cre/loxP system

The biological role of a specific gene is quite difficult to discern by simply recognising amino acid motifs in the corresponding protein or by examining closely related proteins (Iredale, 1999). As a result, gene targeting through homologous recombination has increasingly been utilised as an essential tool in scientific research since its development in the early 1980s (Thomas and Capecchi, 1987; 1986). It has provided a means to manipulate a designated gene to help better understand its biological role. Gene targeting has been commonly used to develop 'knockout' mice as homologous recombination is engineered to introduce a 'loss of function' mutation in a gene of interest (Hall et al., 2009). The consequent inactivation of the gene delineates the biological role of the protein and the resulting phenotype allows a more detailed study of the importance of that gene. So it might not be so surprising that, to date, over 11,000 out of the 25,000 genes in mice have been genetically targeted and knocked out (Hall et al., 2009). Nevertheless, general or global knockouts of certain genes have been found in many cases to be lethal, or in instances result in misleading unaltered phenotypes due to compensatory gene expression. As a result, an alternative gene targeting strategy was developed to control where (and in certain cases when) designated genes would be knocked out.

Such 'conditional knockout' involves the Cre/loxP system derived from P1 bacteriophage. The Cre (Causes recombination events) recombinase excises (and in effect deletes) genomic sequences that are flanked by a specific 34bp loxP site (Nagy, 2000). It was first suggested that this system would maintain its functionality in eukaryotic cells in the late 80s and early 90s in *in-vitro* cell culture experiments (Sauer and Henderson, 1989; 1988). These were then followed by exciting studies which showed, when expressed from a transgene, that Cre recombinase maintained its function in a mouse (Lakso et al., 1992; Orban et al., 1992). The potential of this new tool was quickly recognised leading to gene targeting being used in mice to flank vital exons of designated genes with the 34bp loxP sites. The result being a floxed allele containing an

exon flanked by loxP sites in all tissues, but that is otherwise phenotypically wildtype. It is only when these mice are bred with transgenic animals that have had Cre introduced into their genome that the floxed exon is excised, and in effect, the gene function knocked out (Gu et al., 1994). And this can be done conditionally by using a lineage/cell type-specific promoter region to drive the expression of Cre (Gu et al., 1994; Nagy, 2000).

2.1.2 Aims

In order to study the role of the LKB1-AMPK dependent pathways in regulating ventilation in response to hypoxia *in vivo*, I sought to develop transgenic mice in which LKB1 or AMPK were deleted. With global knockout of *Lkb1* (Sakamoto, 2006) or both isoforms of the *AMPK* catalytic α-subunits (Viollet et al., 2009) being embryonic lethal, the Cre/loxP system was used to develop transgenic mice that had either *Lkb1* or *AMPK catalytic α1* and/or *α2 subunits* conditionally knocked out. Conditional knockout of these genes was generated by driving Cre expression through a tyrosine hydroxylase-specific promoter region; the result being the loss of *Lkb1* or the *catalytic α-subunits* of *AMPK* in tyrosine hydroxylase expressing cells, and hence catecholaminergic cells. Deletion in catecholaminergic cells therefore includes but is not limited to the specialised oxygen-sensing type I cells of the carotid body, neonatal adrenomedullary chromaffin cells, and catecholaminergic regions in the respiratory centres of the brain stem (i.e. A1/C1 and A2/C2 cell groups), which have all been shown to modulate the ventilatory response to hypoxia (King et al., 2012; Song et al., 2011; Heymans et al., 1931; Biscoe and Duchen, 1990; Slotkin and Seidler, 1988; Seidler and Slotkin, 1985).

2.2 Results

2.2.1 Mouse model development and colony management

2.2.1.1 Expression of Cre recombinase in tyrosine hydroxylase expressing cells

Tyrosine hydroxylase (TH) acts as the first and rate-limiting enzyme during catecholamine biosynthesis (Karobath, 1971). Accordingly, in order to limit the knockout of *Lkb1* and *AMPK catalytic* α *-subunits* in catecholaminergic cells, transgenic mice expressing Cre recombinase under the control of a tyrosine hydroxylase promoter was used (TH-Cre mice). Such TH-Cre mice have been previously developed using a knock-in strategy that involved the introduction of *Cre* preceded with an encephalomyocarditis virus internal ribosome entry site (IRES) into the 3'untranslated region (3'UTR) of the *TH* gene (Figure 2.1A, Lindeberg et al., 2004). This allows the simultaneous expression of the bicistronic mRNA encoding both TH and Cre.

Previous studies have demonstrated the co-expression of TH and Cre by co-immunofluorescence in the catecholaminergic ventral mesencephalon and adrenal gland of adult mice (Lindeberg et al., 2004). Nevertheless, further studies were importantly performed to determine the expression pattern of Cre and its functional capacity to mediate genomic recombination (as required to mediate the excision of loxP sites). This involved the crossing of the TH-Cre mice with transgenic mice that contain a Cre-dependent reporter gene that promotes the expression of β-galactosidase (LacZ). Accordingly, LacZ should, and was indeed, found in cells that express Cre. However, LacZ was scarcely found in tissue that does not express TH, i.e. the larynx, taste buds, salivary glands, and cardiomyocytes in the right atrium (Lindeberg et al., 2004). Nevertheless, Dr. Marta Jeltai performed experiments on the brain of TH-Cre mice (used for the current studies) and importantly demonstrated that Cre-induced YFP expression was limited to tyrosine hydroxylase expressing regions (Appendix 2A).

2.2.1.1a Breeding scheme and colony management

In order to develop and maintain a TH-Cre mouse colony, heterozygous expressing mice (TH-Cre$^{+/-}$, EM:00254; Th-IRES-Cre; supplied by the European Mutant Mouse Archive) were crossed with wild-type C57/Bl6 mice (Figure 2.1 – Panel A). Brother/sister mating was avoided and no restrictions, i.e. infertility, were met when setting up breeding pairs with regards to using male or females of either the transgenic TH-Cre$^{+/-}$ or control C57/Bl6 mouse. Nevertheless, the preferred breeding pair included a male TH-Cre$^{+/-}$ mouse and multiple C57/Bl6 female mice to optimize output of litters, and hence number of desired transgenic animals, per breeding cage while also using the minimum number of transgenic animals for breeding. Two weeks after birth, pups were weaned and ear notched for identification and to provide tissue for genotype analysis (Figure 2.1- Panel B). Details of genotype analysis of TH-Cre mice will be discussed in Section 2.2.2.

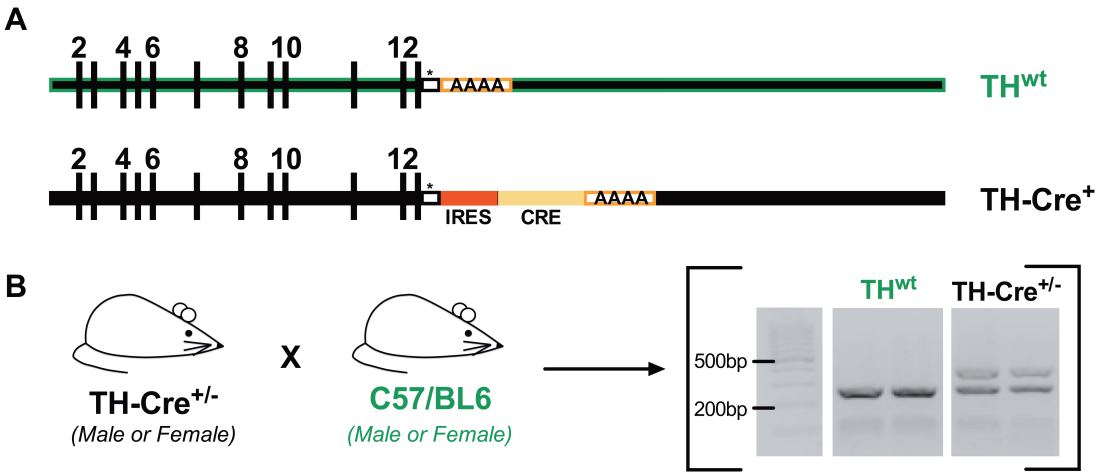

Figure 2.1: Generation of mice expressing Cre-recombinase in tyrosine hydroxylase expressing cells. (A) Schematic diagram (not to scale) illustrating the genomic structure of the tyrosine hydroxylase wild-type allele (TH^{wt}, *top*) and that including Cre-recombinase ($TH\text{-}Cre^{+}$, *bottom*). The stop codon is indicated with an asterisk (*). **(B)** The breeding scheme used to maintain mice expressing Cre in tyrosine hydroxylase expressing cells with possible genotype outcomes (Expected band lengths: 290bp for WT, 430bp for Cre).

2.2.1.2 Conditional deletion of *Lkb1* in tyrosine hydroxylase expressing cells

2.2.1.2a *Lkb1* homozygous floxed mice

Lkb1 floxed mice (*Lkb1*^{fl}), that have been previously developed (Sakamoto et al., 2005), were used to generate conditional knockouts for these studies. The *Lkb1* gene in this transgenic line has a cDNA cassette in exchange for exons 5-7 but nevertheless homogeneously encodes the *Lkb1* sequence being replaced (Figure 2.2 – Panel A). The 34bp loxP sites flank the exon 4 and the end of the cDNA cassette (Figure 2.2 – Panel A, *bottom*). As a result, this promotes the maintained expression of a full-length wild-type LKB1 transcript, even though the gene is flanked with the loxP sites in the absence of Cre. Similar to previous studies (Sakamoto et al., 2005), litter size and genotype outcomes were lower than expected by Mendelian frequency. Also, male *Lkb1* homozygous floxed mice (*Lkb1*$^{fl/fl}$ mice) were found to be infertile while the females were not (Figure 2.2 – Panel Bi). As a result, in order to develop and maintain the *Lkb1* floxed mouse colony, female *Lkb1*$^{fl/fl}$ mice were initially crossed with control C57/Bl6 male mice to produce heterozygous *Lkb1* floxed mice (*Lkb1*$^{fl/+}$, Figure 3.2 – Panel Bii, *upper panel*). Male *Lkb1*$^{fl/+}$ mice, which are fertile, were then backcrossed with female *Lkb1*$^{fl/fl}$ mice (Figure 2.2 – Panel B, *lower panel*).

The lower than expected birthrate is believed to be a result of the hypomorphic phenotype observed in these transgenic mice. Previous studies on various tissues were performed to quantify the amount and activity of LKB1 in the homozygous *Lkb1* floxed mice. When compared to *Lkb1*$^{+/+}$ littermates, LKB1 expression and activity in *Lkb1*$^{fl/fl}$ mice was found to be up to 5-10 fold lower in the testis, skeletal muscle, heart, liver and kidney. Contrary to this finding, levels in the brain of *Lkb1*$^{fl/fl}$ were less severely compromised with a reduction by ~1 fold. (Sakamoto et al., 2005). It is also important to note that AMP-activated protein kinase (AMPK) activity was found to be significantly attenuated in a manner dependent on the degree of LKB1 deficiency; AMPK activity was more severely attenuated after complete loss of LKB1 expression compared to the hypomorphic phenotype (Sakamoto et al., 2005).

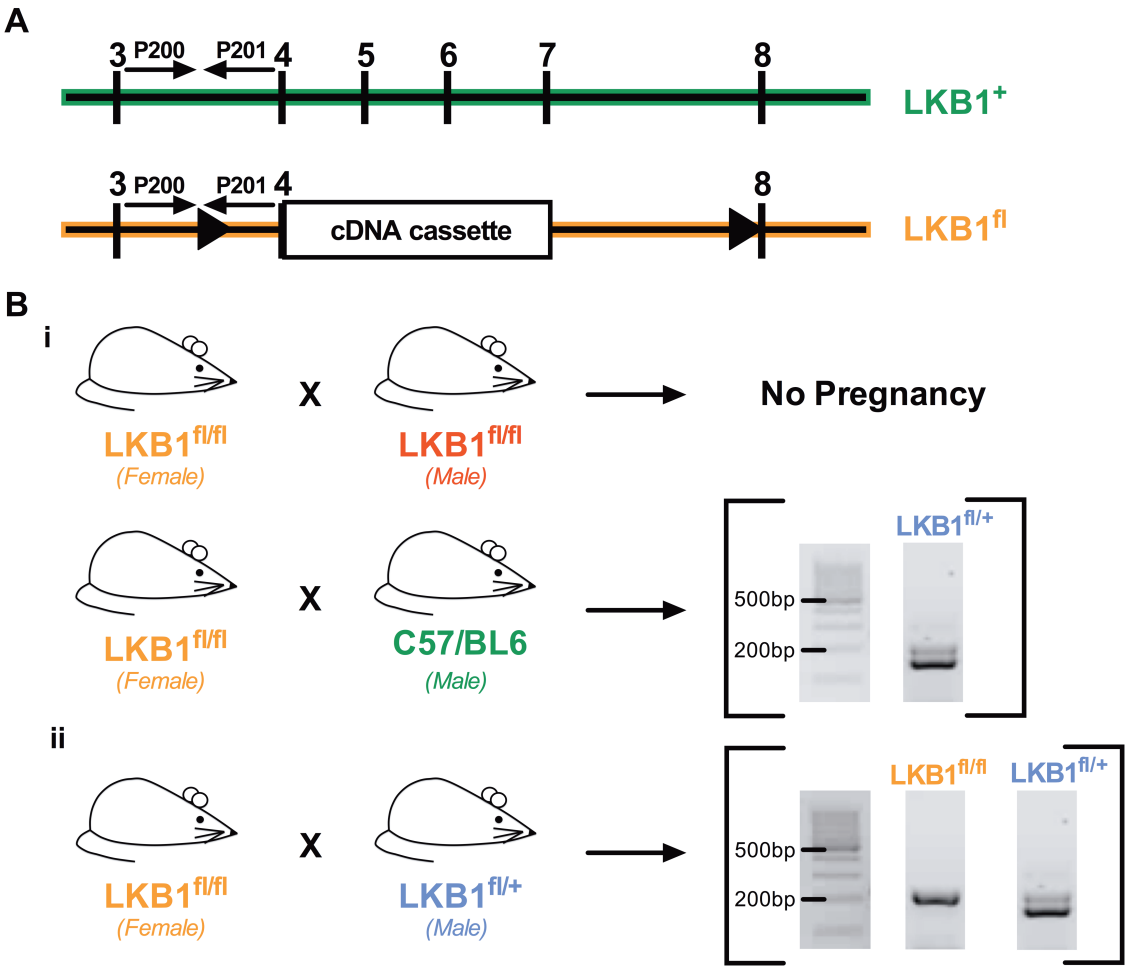

Figure 2.2: Generation and maintenance of *Lkb1* homozygous floxed mice. (A) Schematic diagram (not to scale) illustrating the positions of exons 3-8 (black boxes) in the *Lkb1* wild-type allele ($LKB1^{+}$, *top*) and that floxed with loxP sites (triangles) in an *Lkb1* floxed allele ($LKB1^{fl}$, *bottom*). The diagram also shows the placement of the primers P200 and P201 that are used to genotype the mice. **(B)** The breeding plan used to obtain *Lkb1* homozygous floxed mice ($LKB1^{fl/fl}$) along with genotyping confirmation (Expected band length: 196bp for WT and 240bp for $LKB1^{fl}$). Male $LKB1^{fl/fl}$ mice are infertile **(i).** As a result, female $LKB1^{fl/fl}$ mice were crossed with C57/Bl6 mice to obtain male *Lkb1* heterozygous mice ($LKB1^{fl/+}$, **Bii -** *upper panel*). These heterozygous mice were then backcrossed with female $LKB1^{fl/fl}$ mice to maintain the $LKB1^{fl/fl}$ mouse line **(Bii -** *lower panel*).

2.2.1.2b Conditional *Lkb1* knockout mice

Conditional deletion of *Lkb1* in tyrosine-hydroxylase expressing cells was accomplished by crossing the $Lkb1^{fl/fl}$ mice with TH-Cre mice. Upon the breeding of these two transgenic lines, the targeted expression of Cre to tyrosine hydroxylase cells will conditionally excise the *Lkb1* gene at the loxP sites flanking exon 4-7 and the cDNA cassette only in catecholaminergic cells (Figure 2.3 – Panel A). As mentioned above, male $Lkb1^{fl/fl}$ mice are infertile. To overcome this issue female $Lkb1^{fl/fl}$ mice were crossed with male TH-Cre mice (TH-$Cre^{+/-}$), giving two possible genotypes for further breeding (Figure 2.3 Panel Bi): (1) *Lkb1* heterozygous floxed mice without Cre ($Lkb1^{fl/+}Cre^{-/-}$) and (2) the desired *Lkb1* heterozygous floxed mice with Cre expression ($Lkb1^{fl/+}Cre^{+/-}$, *Lkb1* heterozygous knockouts). Heterozygous males of the $Lkb1^{fl/+}Cre^{+/-}$ genotype were then backcrossed with female homozygous $Lkb1^{fl/fl}$ mice. From this crossing, there are four possible outcomes (Figure 2.3 – Panel Bii): (1) heterozygous floxed: $Lkb1^{fl/+}Cre^{-/-}$ mice, (2) heterozygous knockout: $Lkb1^{fl/+}Cre^{+/-}$ mice, (3) homozygous floxed: $Lkb1^{fl/lf}Cre^{-/-}$ mice, and (4) homozygous knockout: $Lkb1^{fl/lf}Cre^{+/-}$ mice. Accordingly, there is a 25% chance of obtaining the desired *Lkb1* homozygous knockouts.

Even though other breeding schemes can be used with greater probability of obtaining the desired *Lkb1* homozygous knockout mice (i.e. female $Lkb1^{fl/fl}Cre^{+/-}$ crossed with male $Lkb1^{fl/+}Cre^{+/-}$ gives 33% chance of obtaining a *Lkb1* homozygous knockout mouse), the described breeding scheme used was preferred as in addition to the desired $Lkb1^{fl/fl}Cre^{+/-}$ experimental knockout mice, the three other genotype outcomes can be used for either breeding scheme used to maintain the transgenic colonies or for experimental use. That is, with outcome: (1) male $Lkb1^{fl/+}Cre^{-/-}$ mice can be used in the breeding scheme used to maintain $Lkb1^{fl/fl}$ mice as described in Section 2.2.1.2; (2) male $Lkb1^{fl/+}Cre^{+/-}$ mice and (3) female $Lkb1^{fl/lf}Cre^{-/-}$ can be used for the breeding scheme described here to generate conditional *Lkb1* knockout mice. Furthermore, female or male $Lkb1^{fl/lf}Cre^{-/-}$ were also used for experiments to importantly observe the possible underlying effects of *Lkb1* hypomorphism on the ventilatory response to hypoxia and/or hypercapnia.

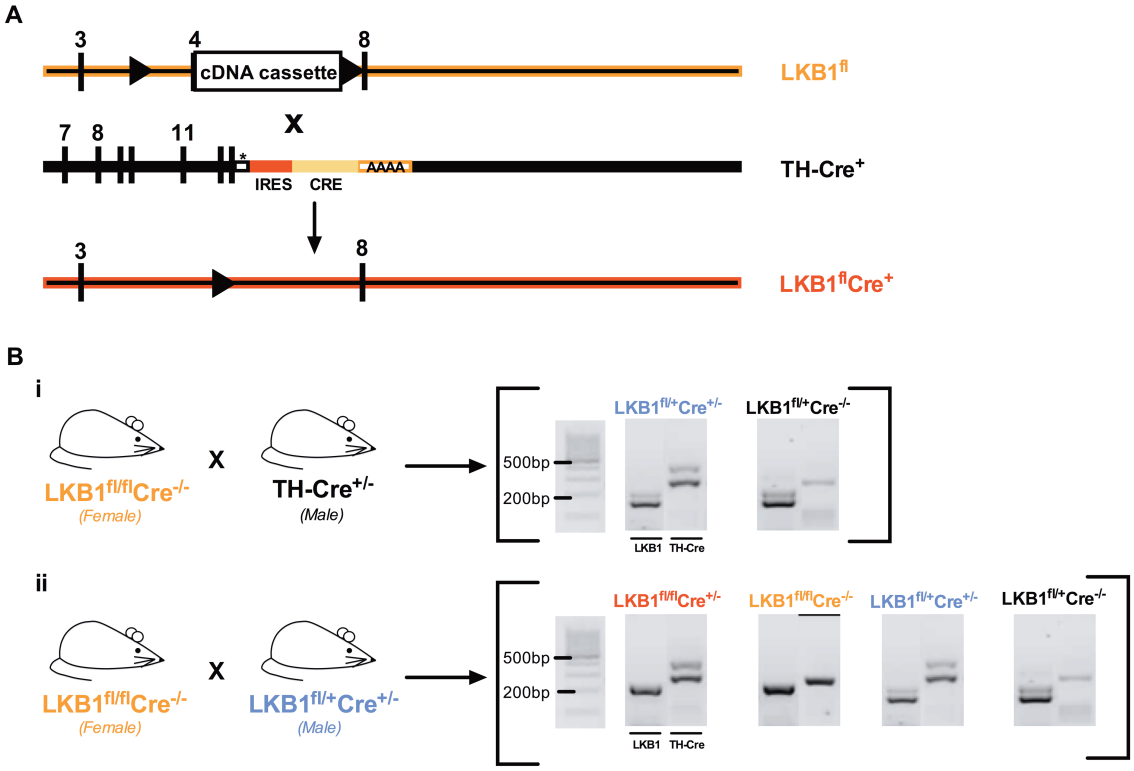

Figure 2.3: Generation and maintenance of conditional *Lkb1* homozygous knockout mice. (A) Schematic diagram (not to scale) illustrating the crossing of the *Lkb1* floxed allele (*Lkb1*^{fl}) with a Cre-allele under a tyrosine hydroxylase promoter (TH-Cre^{+}). The result, LKB1^{fl}Cre^{+}, results in the active Cre recombinase excising the *Lkb1* gene at the loxP sites and accordingly exons 4-7. **(B)** The breeding plan used to obtain conditional *Lkb1* homozygous knockout mice (LKB1$^{fl/fl}$Cre$^{+/-}$) along with genotyping confirmation (Expected band length: 196bp for WT and 240bp for LKB1^{fl}).

2.2.1.3 Conditional deletion of *AMPK* catalytic α-subunits in tyrosine hydroxylase expressing cells

Similar methods to those described above were used in order to develop mice with conditional deletion of the catalytic *α-subunits* of *AMPK* in tyrosine hydroxylase expressing cells (Figure 2.4). This was accomplished with the use of transgenic mice with the catalytic domains of the *AMPK α1* or *α2* subunit flanked with loxP sites (Lantier et al., 2014). In order to generate *AMPK α1* and *α2* double floxed mice, the single *AMPK α1* floxed (*AMPK* $\alpha1^{fl/fl}\alpha2^{+/+}$) and single *AMPK α2* floxed mice (*AMPK* $\alpha1^{+/+}\alpha2^{fl/fl}$) were crossed together (Figure 2.4 – Panel Bi). This would generate a litter with all the pups having both catalytic α-*subunit* heterozygous floxed (*AMPK* $\alpha1^{fl/+}\alpha2^{fl/+}$). These *AMPK* $\alpha1^{fl/+}\alpha2^{fl/+}$ mice were then backcrossed with either single *AMPK α1* floxed or single *AMPK α2* floxed mice to generate the desired *AMPK* $\alpha1^{fl/fl}\alpha2^{fl/+}$ and *AMPK* $\alpha1^{fl/+}\alpha2^{fl/fl}$, respectively (Figure 2.4 – Panel Bii). Finally, these mice were then crossed with mice with the identical genotype (while avoiding brother/sister mating) to generate *AMPK α1* and *α2* double floxed mice (*AMPK* $\alpha1^{fl/fl}\alpha2^{fl/fl}$, Figure 2.4 – Panel Biii). Unlike the *Lkb1* homozygous floxed mice, neither the single or double *AMPK α1* and *α2* floxed mice were infertile. Hence, to maintain the development of these lines, there was no need to backcross and instead the single or double knockouts where crossed with mice with the same genotype (Figure 2.4 – Panel Biv).

Similar to that discussed with *Lkb1* homozygous knockouts, single *AMPK α1* or *α2* floxed mice and the *AMPK α1* and *α2* double floxed mice were crossed with the TH-Cre mice to generate single or double knockouts of the *AMPK catalytic α-subunits*; the result being the catalytic domain of the *α-subunit* deleted in catecholaminergic cells (Figure 2.5 – Panel A). The breeding scheme used as well as the genotype outcomes can be found in Figure 2.5 – Panel B.

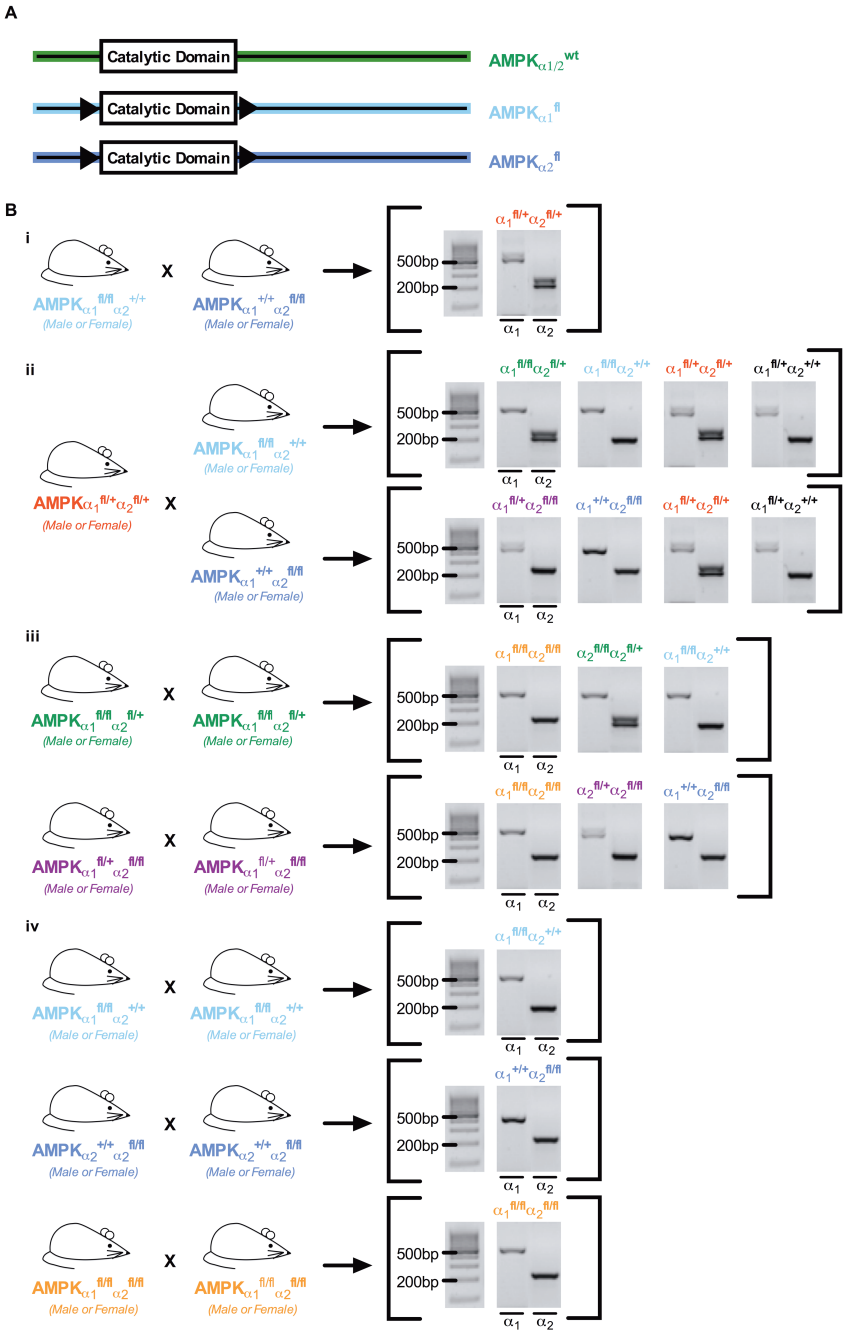

Figure 2.4: Generation and maintenance of *AMPK α1* and/or *α 2* floxed mice. (A) Schematic diagram (not to scale) illustrating *AMPK* wild-type alleles for both catalytic α-subunits ($AMPK_{\alpha1/\alpha2}^{wt}$, *top*) and that with catalytic domains floxed with loxP sites (triangles) (AMPK $\alpha1^{fl}$ and AMPK $\alpha2^{fl}$ - *middle and bottom, respectively*). **(B)** The breeding plan used to obtain mice where both catalytic α-subunits were homozygous floxed ($AMPK_{\alpha1}^{fl/fl}{}_{\alpha2}^{fl/fl}$) along with genotype confirmation (Expected Band Length: α1 WT: 588bp, α1 floxed: 682 bp, α2 WT: 204bp, α2 floxed: 250bp).

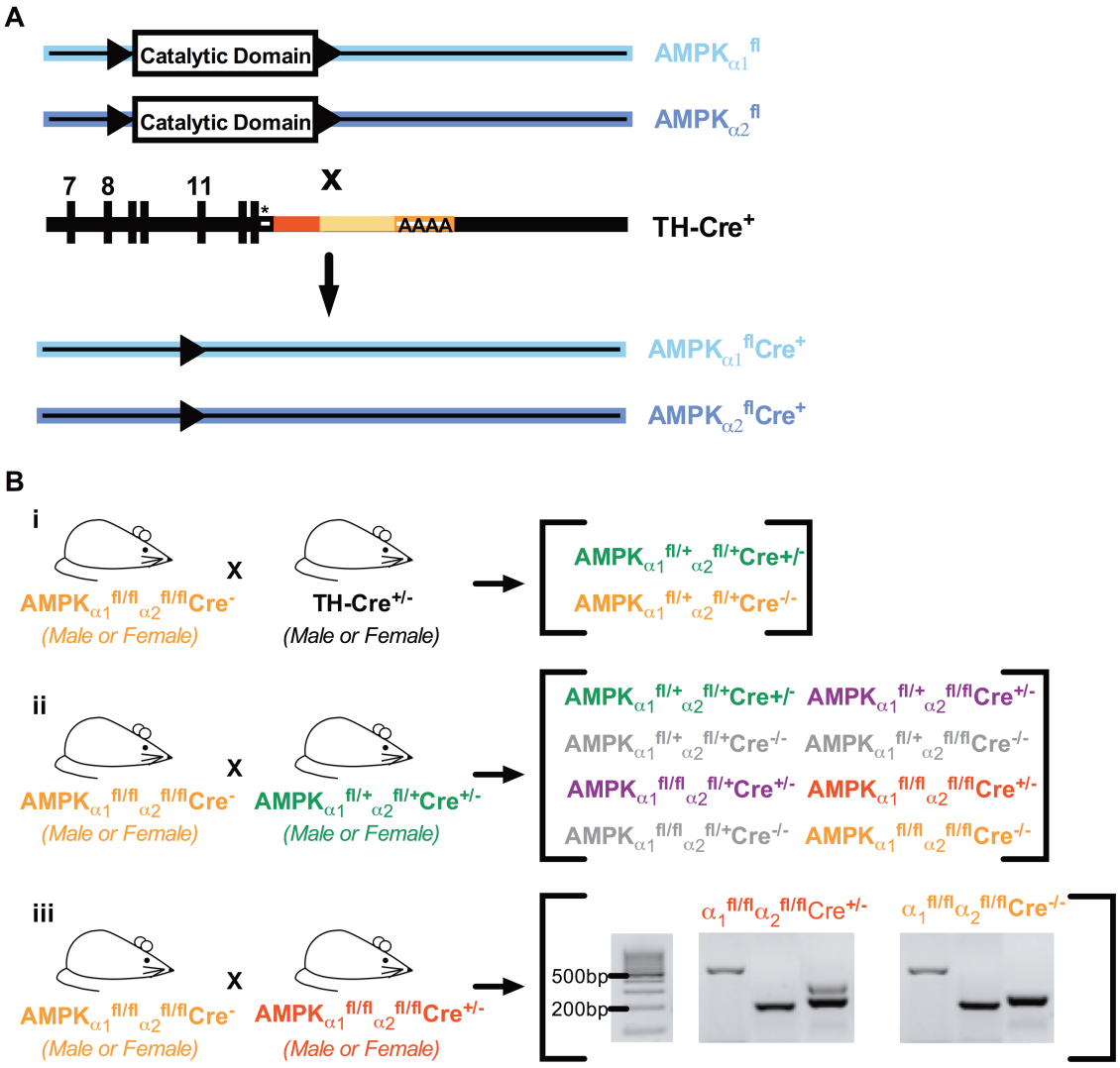

Figure 2.5: Generation and maintenance of conditional *AMPK α1* and *α2* double knockout mice. (A) Schematic diagram (not to scale) illustrating the crossing of the *AMPK* double floxed alleles (AMPK $\alpha1^{fl}$ and AMPK $\alpha2^{fl}$) with a Cre-allele under a tyrosine hydroxylase promoter (TH-Cre^{+}). The result, AMPK $\alpha1^{fl}Cre^{+}$ and AMPK $\alpha2^{fl}Cre^{+}$, results in the active Cre recombinase in tyrosine hydroxylase expressing cells excising the genes at the loxP sites and accordingly the catalytic domains of the α-subunits. **(B)** The breeding plan used to obtain conditional *AMPK α1* and *α2* double knockout mice (AMPK $\alpha 1^{fl/fl}$ $\alpha 2^{fl/fl}Cre^{+/-}$) along with genotyping confirmation (Expected Band Length: α1 WT: 588bp, α1 floxed: 682 bp, α2 WT: 204bp, α2 floxed: 250bp, Cre: WT: 290bp, Cre: 430bp).

2.2.2 Genotype analysis

Approximately 0.5cm of ear or tail clips were submerged in 300µl of Direct PCR lysis reagent (Viagen Biotech, Inc.) containing 0.2-0.4mg/ml Proteinase K (Fermentas Life Sciences) in 0.75ml tubes. Samples were then placed in a rotating hybridisation oven (Thermo Hybrid) at 55ºC for 5 hours or until tissue appeared dissociated. Subsequently samples were moved into a water bath that was preheated to 85ºC for 45min. This step is critical as it inactivates Proteinase K which would otherwise compromise the activity of Taq Polymerase used for further PCR experiments.

2µl of the sample lysate was then used in a 24µl PCR reaction. The PCR reaction includes the 2xGoTaq® Polymerase Green Master Mix, forward and reverse primers for the gene of interest (purchased from Sigma), and nuclease free water. The list of primers and PCR protocol used for genotype analysis is shown in Table 2.1. A GeneAmp® PCR System 9700 (Applied Biosystems) was used for the PCR reaction and 15µl of the resulting samples along with a 100bp DNA Ladder (GeneRulerTM, Fermentas) were run on a 1.5% agarose gel made with SYBR®Safe DNA gel stain (Invitrogen). Gels were then imaged using a Genius Bio Imaging System and GeneSnap Software (Syngene).

Table 2.1 Primers used for genotype analysis

Genotype	Primer Sequence	Expected Band Length
TH-Cre	TH-FWD: 5' CACCCTGACCCAAGCACT 3' TH-REV: 5' CTTTCCTTCCTTTATTGAGAT 3' Cre-UD: 5' GATACCTGGCCTGGTCTCG 3'	WT: 290bp Cre: 430bp
STK11 (Lkb1)	P200: 5' CCAGCCTTCTGACTCTCAGG 3' P201: 5' GTAGGTA TTCCAGGCCGTCA 3'	WT: 196bp Floxed: 240bp
PRKAA-1 (AMPK α1)	α1-FWD: 5' TATTGCTGCCATTAGGCTAC 3' α1-REV: 5' GACCTGACAGAATAGGATAT GCCCAACCTC 3'	WT: 588bp Floxed: 682bp
PRKAA-2 (AMPK α2)	α2-FWD: 5' GCTTAGCACGTTACCCTGGATGG 3' α2-REV: 5' GTTATCAGCCCAACTAATTACAC 3'	WT: 204bp Floxed: 250bp

The PCR protocol used for all genotype primers was: 92ºC for 5min, 92ºC for 45sec, 56ºC for 45sec, 72ºC for 60sec, and 72ºC for 7min for 35 cycles and then 4ºC as the holding temperature.

2.2.3 Carotid body type I cell isolation

Mice ranging from 4-12 months of age were terminally anesthetised using Isoflurane-Vet 100% w/w Inhalation Vapour (Merial). Carotid artery bifurcations were immediately removed and quickly placed in ice-cold dissection medium consisting low Ca^{2+}/low Mg^{2+} PBS with 10mM glucose. The carotid bodies and the surrounding region of the artery were enzymatically digested with isolation medium made up of low Ca^{2+}/low Mg^{2+} HBSS containing 0.125mg/ml Trypsin (Sigma) and 2.5mg/ml Collagenase Type I (Worthington). Once the carotid bodies are dissociated from the surrounding patch of the artery, they were placed in a low $Ca^{2+/}$low Mg^{2+} HBSS medium containing 0.5mg/ml of a trypsin inhibitor (Sigma) for 5min at room temperature. The carotid bodies were then placed in a growth medium constituted with F-12 Ham nutrient mix, 10% fetal bovine serum, and 1% penicillin/streptomycin and pre-equilibrated in an incubator (95% air, 5% CO_2, 37ºC). They were then centrifuged and the resulting pellet was re-suspended in 100µl of growth medium and triturated using a fire polished Pasteur pipette. The isolated cells were then plated onto poly-l-lysine coated coverslips and left for at least 2 hours with growth medium being replenished. Collection of single cells for further single cell RT-PCR experiments was performed within 24 hours and will be discussed in section 2.2.6.

2.2.4 Dissection and isolation of adrenomedullary chromaffin cells

Wild type mice were culled by gross dislocation of the upper cervical spinal column and adrenal glands were quickly dissected and placed in ice-cold PBS. The adrenal cortex and medulla were carefully separated to obtain samples rich in adrenomedullary chromaffin cells and to prevent contamination from the adrenal cortex, which does not express tyrosine hydroxylase. RNA extraction and cDNA synthesis was then performed on the samples and lysates were used for PCR experiments as a positive control for LKB1 and AMPK catalytic α-subunit expression.

2.2.5 RNA extraction and cDNA synthesis in acutely isolated carotid body type I cells and adrenomedullary chromaffin cells

2.2.5.1 Acutely isolated carotid body type I cells

The cover slips containing the isolated carotid body type I cells (CB1 cells) were transferred to the recording chamber on the stage of a Zeiss Aziovert 200M inverted microscope. With the use of a PatchStar Micromanipulator (Scientifica), single CB1 cells were suctioned into autoclaved and sterilized RNAase-free borosilicate patch pipettes filled with RNase-free water and then immediately transferred into a microcentrifuge tube for cDNa synthesis. With the help of Dr. Helene Widmer, this involved the use of Sensiscript® reverse transcriptase (Qiagen), ribonuclease inhibitor (RNasin®, Promega), and a mix of random and poly(dT) nucleotide in a final volume of 20µl at 37ºC for 1 hour.

2.2.5.2 Adrenomedullary chromaffin cells

Following the manufacturer's guidelines, RNA was extracted using the High Pure RNA Tissue Kit (Roche). Firstly, the adrenal medulla was placed in lysis buffer (4,5 M guanidine-HCl, 100mM sodium phosphate, pH 6.6) and homogenised using a syringe. The samples were then incubated for 15min with 10kU DNase and an incubation buffer (1M NaCl, 20mM Tris-HCl, 10mM $MnCl_2$, pH 7.0) to eliminate any genomic DNA contamination; this may result in false positives. Next, the samples were washed with a buffer containing 5M guanidine-HCL, 20mM Tris-HCl, pH 6.6 then centrifuged at 8,000 x *g* for 15 seconds. The samples were then washed with a second buffer containing 20mM NaCl, 2mM Tris-HCl, pH 7.5 and again centrifuged at 8,000 x *g* for 15s. The samples were then washed for the final time using the second buffer again and centrifuged at 13,000 x *g* for 2min. Finally, the RNA was eluted using an elution buffer (PCR grade water: purified, double-distilled, deionized, and autoclaved water) followed by a centrifuge at 8,000 x *g* for 1min. The RNA yield was then measured using a Nanodrop 1000 spectrophotometer (ThermoScientific).

cDNA synthesis was then performed using the transcriptor high fidelity cDNA synthesis Kit (Roche) following the manufacture's instructions. This involved taking the total RNA (of up to 4μg) and adding 1μl of anchored-oligo(DT) primers or 2μl of random hexamer primers to a final volume of 11.4μl, the remainder of the final volume was made up with PCR-grade water. The samples are then incubated for 10min at 65ºC to allow the template-primer mix (and importantly, RNA secondary structures) to denature. Next, the following were added to the samples: reverse transcriptase reaction buffer (5x concentration: 250mM Tris-HCl, 150mM KCl, 40mM $MgCl_2$, pH ~ 8.5), protector RNase inhibitor, deoxynucleotide mix (10mM each of dATP, dCTP, dGTP, and dTTP), 0.1M DTT, and reverse transcriptase (storage buffer: 200mM potassium phosphate, 2mM dithiothreitol, 0.2% Triton X-100 (v/v), 50% glycerol (v/v), pH ~7.2). The samples were then incubated for at least 30min at 50ºC followed by an incubation period of 5min at 85ºC to inactivate the reverse transcriptase.

2.2.6. Reverse transcription-polymerase chain reaction (RT-PCR)

To confirm the success of the conditional knockout of *Lkb1* (Figure 2.6) and both catalytic subunits of *AMPK* in tyrosine hydroxylase expressing cells (Figure 2.7), single cell and endpoint RT-PCR was performed on isolated carotid body type I cells and adrenomedullary chromaffin cells, respectively.

2.2.6.1 Primer design and validation

Primers pre-designed by Qiagen for *Lkb1* and both catalytic α-subunits of *AMPK* were not used as they detect areas of the genes that are not within the floxed targeted gene sites. This may result in false positives appearing if mRNA transcript is still produced regardless of whether the targeted exons have been excised. As a result, primers were designed by using Primer-BLAST (NCBI) to detect the regions that is known to be excised; that is the targeted exons 4-7 within the *Lkb1* gene and

the catalytic domains of the *AMPK catalytic α1* and *α2 subunits* (as described above).

When designing primers, not only do considerations need to be made with respect to the targeted region and specificity of primers, but also the thermodynamic properties of the primers themselves. Primers should typically be between 15 and 20bp long with a G/C content of approximately 50-60% to suppress the formation of secondary structure (hairpins, loops etc.). Nevertheless, the primers should ideally be anchored with a G/C at the 5'end of the sequence. Also, the melting temperature of the designed primers should be approximately 5C higher than the annealing temperature used for the PCR protocol(Robertson and Walsh-Weller, 1998). With these guidelines, primers were designed that target exons 3-4 of the *Lkb1* gene, exons 4-7 of the *AMPK α1* gene, and exons 5-7 of the *AMPK α2* gene. Details of the primers designed, their GC content, and melting temperatures can be found in Table 2.2. The validity and specificity of the primers were tested against the cDNA of adrenomedullary chromaffin cells from C57/Bl6 wild type mice to ensure only single amplicons with the expected band length were produced.

2.2.6.2 Single cell and endpoint PCR

Amplification of single cell cDNA was performed with the help of Professor Mike Shipston and performed blind. Negative controls included a non-enzyme control and aspirants of extracellular solution used during the collection of the cells. Positive controls included the wildtype adrenomedullary chromaffin cells.

For single cell amplification, GoTaq DNA Polymerase (Promega) was added to 2-5µl of cDNA obtained from each single CB1 cell from wildtype and transgenic mice as well as the wildtype adrenomedullary chromaffin cells. To ensure the validity that the collected cells were indeed CB1 cells and adrenomedullary chromaffin cells, primers obtained from Qiagen were used to detect the expression of tyrosine hydroxylase (QuantiTect Primer Assay, QT00101962) with an expected band length of 92bp. The only cells considered for the expression studies were those that positively expressed tyrosine hydroxylase and where the negative controls were

clean. Primers designed by Qiagen for *Lkb1* and both catalytic α-subunits of *AMPK* were not used as they detect area of the genes that are not within the floxed loxP sites, which may result in false positives appearing if mRNA transcript is still produced regardless of whether the catalytic domains have been excised. Accordingly primers were designed by using Primer-BLAST (NCBI) to detect a region that is known to be excised. See Table 2.2 for information on all primers and the PCR protocol used for Single Cell and End Point PCR.

15µl samples along with a 100bp DNA Ladder (GeneRulerTM, Fermentas) were run on a 2% agarose gel made with SYBR®Safe DNA gel stain (Invitrogen). Gels were then imaged using a Genius Bio Imaging System and GeneSnap Software (Syngene).

Table 2.2 Primers used for single cell and endpoint PCR

Gene	Primer Sequence	Melting Temperature (°C)	GC Content (%)	Exons Targeted	Expected Band Length
Lkb1	FWD: 5'GCTCATGGGTACTTCCGCCAGC 3'	65.74	63.64	3-4	92bp
	REV: 5'AGCAGGTTGCCCGGCTTGATG 3'	64.90	61.90		
AMPK α 1	FWD: 5'GCAAAGATACCGACTTTGGTC 3'	59.90	50.00	4-7	604bp
	REV: 5'GGTCGTCCAGGAAAGAGTCAG 3'	60.07	57.14		
AMPK α 2	FWD: 5'GGTCATCTCAGGAAGGCTGTA 3'	58.89	52.38	4-7	483bp
	REV: 5'GAGGCGAGGAGAACTCACTG 3'	59.87	57.14		

The PCR protocol used for all primers involved two steps: (1) 94ºC for 5min, 94ºC for 30sec, 60ºC for 45sec, 72ºC for 1min, and 72ºC for 7min for 15 cycles and then (2) 94ºC for 5min, 94ºC for 30sec, 60ºC for 45sec, 72ºC for 1min, and 72ºC for 7min for 38 cycles**.**

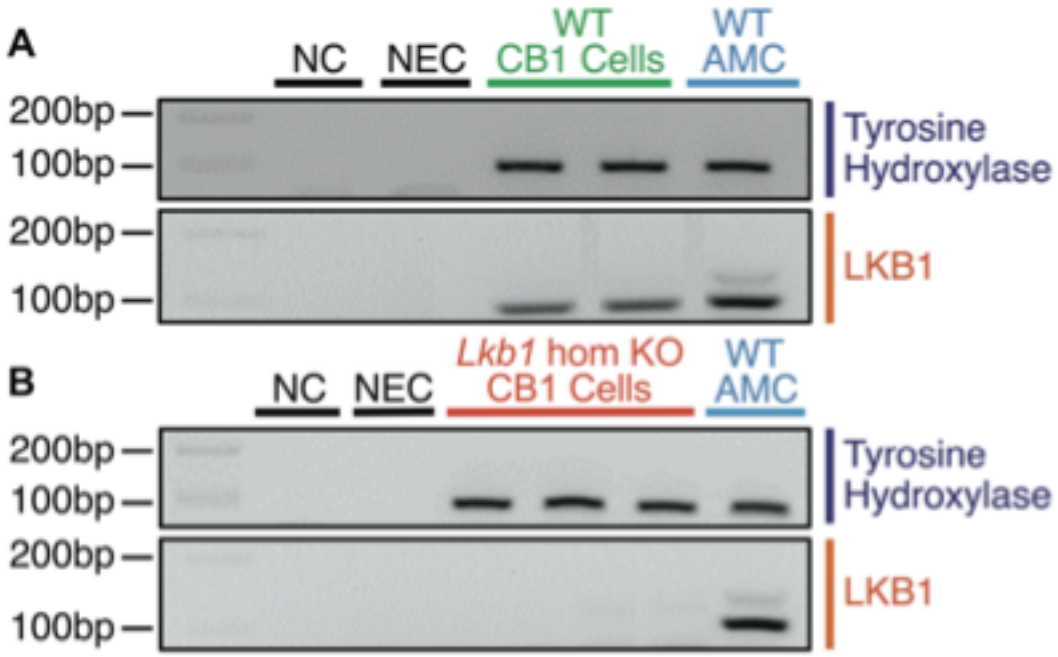

Figure 2.6: Conditional deletion of *Lkb1* in tyrosine hydroxylase expressing cells. Single cell end point RT-PCR amplicons for tyrosine hydroxylase and LKB1 from acutely isolated carotid body type I cells of wild type mice **(A,** WT CB1 Cells**)** and *Lkb1* homozygous knockout mice **(B,** *Lkb1* hom KO CB1 Cells**)**. Positive controls = WT adrenal medulla (WT AMC); Negative controls (NC; aspirant of extracellular fluid) and non-enzyme controls (NEC; cell aspirants with no reverse transcriptase enzyme). ***Isolation of CB1 cells was performed by Dr. Mark Dallas. The collection of CB1 Cells was performed independently. Reverse transcription was performed alongside Dr. Helene Widmer. Primers were designed independently while RT-PCR was performed by Professor Mike Shipston. Finally, the running of the gels was performed independently.***

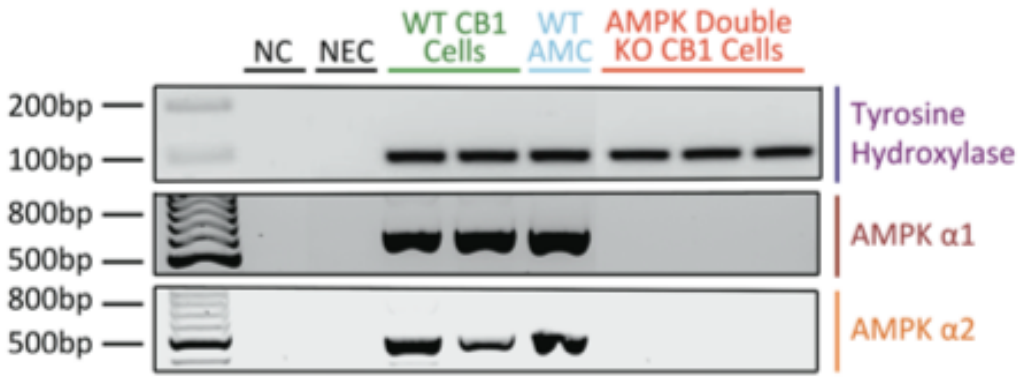

Figure 2.7: Conditional deletion of *AMPK catalytic α -subunits* in tyrosine hydroxylase expressing cells. Single cell end point RT-PCR amplicons for tyrosine hydroxylase and the catalytic α1 and α2 subunits for AMPK from acutely isolated carotid body type I cells of wild type mice **(**WT CB1 Cells**)** and *AMPK α1* and *α2* double knockout mice **(***AMPK* Double KO CB1 Cells**)**. Positive controls = WT adrenal medulla (WT AMC); Negative controls (NC; aspirant of extracellular fluid) and non-enzyme controls (NEC; cell aspirants with no reverse transcriptase enzyme). ***Isolation of CB1 cells was performed with Dr. Mark Dallas. The collection of CB1 Cells was performed independently. Reverse transcription was performed alongside Dr. Helene Widmer. Primers were designed independently while RT-PCR was performed by Professor Mike Shipston. Finally, the running of the gels was performed independently.***

2.2.7 Biological and chemical parameters

The phenotype of the transgenic mice was importantly studied under normoxic conditions to ensure the deletion of *Lkb1* and *AMPK catalytic* α*-subunits* had no underlying effects that may misleadingly affect the ventilatory response to hypoxia and hypercapnia. Such studies included blood gas analysis and the monitoring of weight versus age. This importantly demonstrated the conditional deletion of *Lkb1* or *AMPK* activity in catecholaminergic cells had no effect on weight again with age (Figure 2.8) and that under normoxia, baseline recordings of body temperature, venous blood gas composition, and blood pH are comparable between control and knockout mice (Table 2.3).

For blood gas analysis, mice were terminally anesthetised using Isoflurane-Vet 100% w/w Inhalation Vapour (Merial) and both core body temperature and blood collection was immediately performed using a microprobe thermometer (phyistemp Model BAT-12) and 1ml syringe, respectively. With the help of Dr. Matthew Bailey, the blood was then placed in a sealed eppendorf and blood gas and pH analysis was immediately performed on the samples using a pH/Blood gas analyser (Ciba Corning Diagnostics Corp., Medfield, MA).

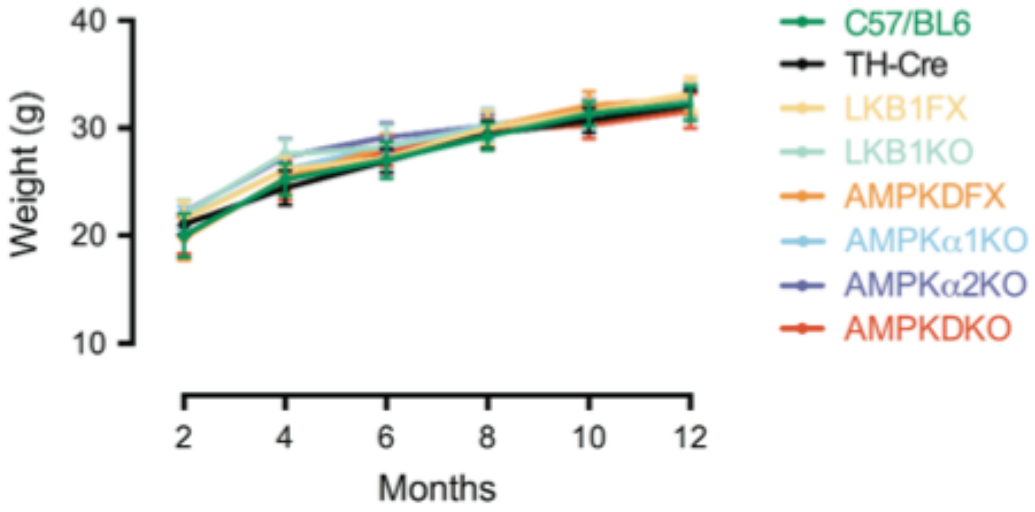

Figure 2.8: Body weight versus age of control and knockout mice. Values shown are mean ± SEM of body weight (g) versus age from 2 months to 12 months in 2 months intervals in control and transgenic knockout mice.

Table 2.3. Core body temperature, Venous Blood Gas, and blood pH analysis								
	C57/Bl6	TH-Cre	*Lkb1* hom KO	*AMPK* Double FX	*AMPK* α 1KO	*AMPK* α2 KO	*AMPK* Double KO	P value
Temperature (ºC)	35.4±0.3	34.9±0.5	34.7±0.3	35.8±0.4	35.6±0.4	36.4±0.4	35.6±0.4	NS
PO_2 (mmHg)	43.7±8.9	60.7±10.5	34.7±2.6	52.2±2.5	53.8±9.4	47.0±6.8	57.3±8.9	NS
PCO_2 (mmHg)	64.2±3.6	80.7±7.0	71.2±7.1	52.5±5.5	54.3±10.0	57.5±2.1	64.8±6.7	NS
pH	7.1±0.03	7.1±0.03	7.1±0.03	7.2±0.02	7.2±0.09	7.2±0.01	7.1±0.02	NS
	n=4	n=3	n=3	n=5	n=4	n=4	n=4	

Values shown as mean ± SEM

Significance tested by one-way ANOVA

2.2.8 Unrestrained whole-body plethysmography

2.2.8.1 Plethysmography system

Unrestrained whole body plethysmography has been widely used for measuring ventilation with the beneficial exclusion of masks and anesthesia. It was as early as the 19th century when Bert observed that pressure changes would occur within an enclosed chamber as a result of an animal inhaling and exhaling (Bert, 1868). Our understanding of these pressure changes developed when Chapin associated the increase in pressure as a subject exhales in an enclosed chamber as a result of the expansion of inspired air, which would likely occur after being subjected to the higher core temperature and humidity within the subject's body (Chapin, 1954). This exchange of air between the body and enclosed chamber induces alterations in air volume, and in effect pressure changes. Such pressure changes develop a respiratory waveform that can be analysed to study ventilation. However, one disadvantage that was noted by Chapin that the respiratory waveform recorded during these pressure changes were unreliable and erratic when the subject was moving or active (Chapin, 1954). As a result, it has become common practice to omit the analysis of the respiratory waveform recorded during gross body movement (Motto et al., 2004; Brown et al., 2008). Accordingly, during the current studies, the inclusion of such unreliable ventilatory recordings made during gross un-ventilatory related body movements, i.e. sniffing and grooming, were avoided. Additionally, a rejection algorithm that was built into the plethysmography system (Buxco Electronics Inc.) helped indicate periods of motion-induced-artefacts.

An unrestrained barometric whole body plethysmography chamber (Buxco Research Systems apparatus) was used to study the ventilatory response to hypoxia and/or hypercapnia in conscious control and transgenic mice. The plethysmography chamber contained a patented Halycon^{TM} low noise pneumotachograph (Buxco Electronics Inc.) that reduces disturbances caused by air currents from outside the chambers (i.e. fans, door slams, air conditioners, etc.), which can disrupt or overwhelm the ventilatory airflows within the chamber. The plethysmography

apparatus (illustrated in Figure 2.9) was used to monitor the respiratory phenotype of both male and female control mice, namely C57/Bl6 wildtype, TH-Cre, and *AMPK* $\alpha 1$ and $\alpha 2$ double floxed mice, and conditional knockout mice, namely *Lkb1* knockouts, *AMPK* $\alpha 1$ knockouts, *AMPK* $\alpha 2$ knockouts, and *AMPK* $\alpha 1$ and $\alpha 2$ double knockouts.

The plethysmograph consists of two superimposed Plexiglas chambers, with a capacity of 450ml and 100ml. The larger one is the mouse chamber while the smaller chamber serves as a reference for pressure measurements (Figure. 2.9). A differential pressure transducer that is connected to a preamplifier is linked to both the reference and mouse chamber and accordingly is able to measure fluctuations in pressure, in relation to the respiratory activity of the mice in the mouse chamber. During the inspiratory phase of breathing, the air inhaled from within the mouse chamber is heated and humidified in the lungs. Hence, the volume of air inside of the thorax is larger than the volume of air initially drawn in by the mouse from the plethysmography mouse chamber. This larger volume of air inside the thorax thereby produces an increase in pressure in the mouse chamber relative to the reference chamber that continuously maintains a constant pressure. Conversely, pressure decreases following expiration because of the condensation of water vapor and the cooling of the expired gas. All together, the transducer measures the differential pressure signal as it increases and decreases during the inspiratory and expiratory phases of ventilation, respectively. This flow, referred to as 'box flow', is then recorded and analysed using the FinePointe Acquisition and Analysis Software with a sampling frequency of 1kHz (Figure 2.9).

Inspiration and expiration are defined or recognised by the system when the box flow pressure/respiratory waveform crosses the zero point, which is the point where there is no change in pressure in the mouse chamber relative to the reference chamber as the mouse is either not ventilating or in between the inspiratory and expiratory phases of ventilation (Figure 2.9). The start of inspiration occurs as the box flow crosses the zero point into negative pressure and ends as it returns back to

zero. Expiration then commences as the waveform crosses the zero point into positive box pressure and ends as it returns to zero. Hence, the total breath duration (To) can be measured from the starting point of inspiration to the end point of expiration (Figure 2.9). From this, breathing frequency per minute can be calculated as 60/To. Furthermore, the tidal volume can be derived by the FinePointe software from the pressure changes and corresponding box flow amplitudes by applying the formula of Fenn and Drorbaugh which takes into account the pressure changes that occurs during ventilation, the core temperature of the mouse, the chamber temperature, and the corresponding vapor pressures (Figure 2.9, (Drorbaug and Fenn, 1955).

$$Tidal\ Volume = \frac{\Delta\ Pressure\ within\ the\ box}{\begin{matrix} Pressure\ change\ per\ unit\ of\ volume \\ change\ within\ the\ box \end{matrix}} \times \frac{1}{\frac{1-(Pa-47)}{(Pa-Pvc)} \times \frac{Tc}{310}}$$

Pa is atmospheric pressure and 47 mmHg is the vapor pressure at body temperature. Pvc is the pressure at chamber temperature. Tc is the chamber temperature in kelvin (K), and 310 is the body temperature in K.

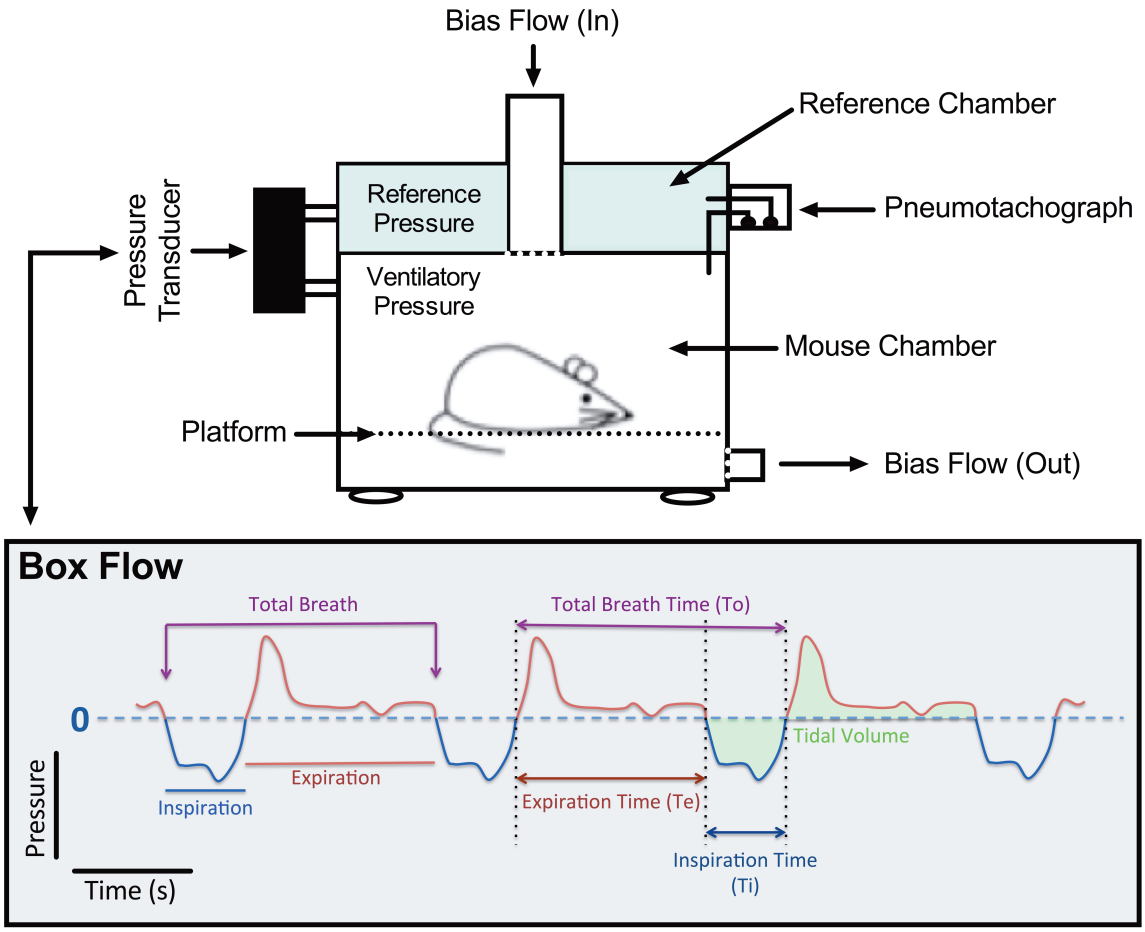

Figure 2.9: Illustration of the plethysmography apparatus and the measured respiratory waveform. Gas is introduced into the mouse chamber via a bias flow on the top of the apparatus. The resulting pressure changes occurring as the mouse ventilates is measured relative to the constant reference chamber by the pressure transducer. This provides a box flow or respiratory waveform from which the FinePointe software is able to calculate the durations of inspiration, expiration and total breath duration as well as tidal volume. Inspiration is measured from the point where the pressure/volume waveform negatively crosses zero and returns back to zero (blue). Subsequently, an expiratory event occurs as the waveform positively crosses zero and ends as the waveform returns back to zero (red). Accordingly, a total breath is measured from the point the waveform crosses zero at the start of inspiration until the point where the waveform returns to zero at the end of expiration. Tidal volume is measured as the total volume of air inhaled and exhaled during a single breath (green).

2.2.8.2 Experimental protocol

Mice, ranging from 3-12 months of age, were handled daily and habituated to the plethysmography chamber for a week before recordings commenced. Subsequently, at the start of each experimental recording day, the plethysmography system was calibrated according to the manufacturer's instructions (User manual for Whole Body Unrestrained Plethysmographs PLY2311). This involved adjusting the preamplifier to zero before a known volume of 1ml of air is injected into the mouse chamber within 2 seconds using a 1ml syringe. Mice were then placed in the mouse chamber where they were given an acclimation period of 10min under normoxic conditions (21% O_2 with 0.05% CO_2, balanced with N_2). Afterwards, normoxic conditions were maintained until a period of quiet and reliable breathing was reached to determine the baseline-ventilation levels (this is also indicated by a measured rejection index of 0 by the FinePointe Acquisition and Analysis Software). If the mouse does not reach such a state by 20min, then the experiment does not continue and the mouse is not used for further experiments under hypoxic or hypercapnic stimuli. If however, such a quiet state of breathing is reached during normoxia and baseline ventilation was successfully recorded, then the mouse was exposed to hypoxia (12% or 8% O_2), hypercapnia (5% CO_2), or hypoxia with hypercapnia (8% O_2 + 5% CO_2) at a constant flow rate of 3L/min for 5min (Figure 2.10). Subsequently, the mice were reintroduced to normoxia and the recovery of ventilation monitored for at least 10min or until mouse ventilation returned to baseline. Given that no progressive changes in the ventilatory response to hypoxia and/or hypercapnia were observed with repeated exposures and/or age, mice were reused for multiple experiments. However, no single mouse across all genotypes used was used more than 7 times per condition and was only placed in the chamber every other day. Also, when referring to numbers used to calculate the mean responses, "n" refers to the number of exposures included in calculating the mean while "N" refers to the number of mice used.

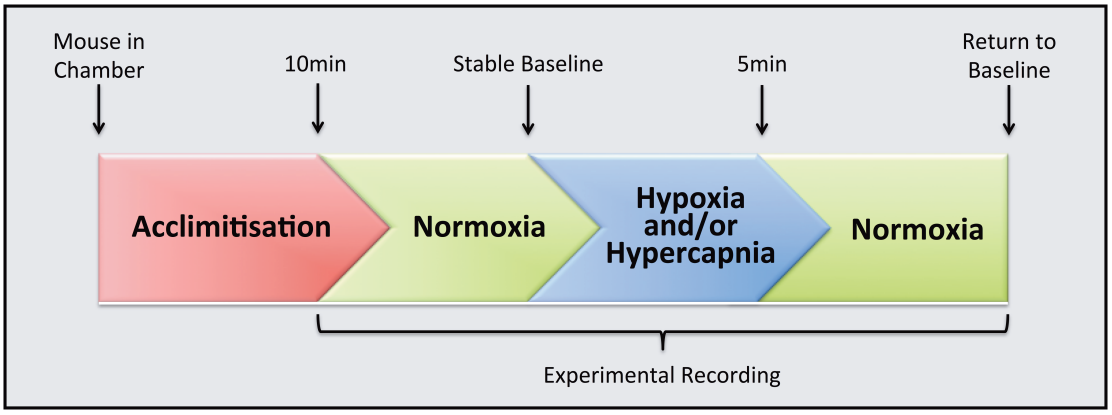

Figure 2.10. Experimental protocol for ventilatory recordings. After a 10min acclimation period under normoxia, recordings commence as mice are maintained under normoxic conditions for a further 10min or at least until a stable baseline is reached before hypoxia and/or Hypercapnia is introduced.

2.2.8.3 Respiratory analysis

The effects of conditional *Lkb1* or *AMPK catalytic α-subunit* deletion on the regularity of breathing patterns was studied graphically by generating Poincaré plots. This was perfomed with the help of Professor Mayank Dutia, who developed a software that was able to provide values for the inter-breath interval (as well as apnoeic events) of the ventilatory records obtained using whole-body unrestrained plethysmography. The Poincaré plots were then developed independently using GraphPad Prism and displayed the distribution and variability of the durations of breath-to-breath interval along the x-axis (BB_n) versus the duration of the subsequent breathing interval along the y-axis (BB_{n+1}) (Figure 2.11). The standard deviation of the distribution of the inter-breath intervals along the y-axis (SD_{BBn+1}) and x-axis (SD_{BBn}) was then calculated and compared in between control and knockout mice to observe the effects of *Lkb1* or *AMPK catalytic α-subunit* deletion on the regularity of breathing patterns and the stability of inter-breath interval.

The breathing frequency, tidal volume, and minute ventilation as derived by the FinePointe Software were also analysed for control and knockout mice. These parameters were measured as mean values taken over a 2s breathing period and *not* on a breath-to-breath basis. Nevertheless, comparisons of these three parameters under normoxic conditions importantly demonstrate that baseline recordings of breathing frequency, tidal volume, and hence minute ventilation are comparable between control and knockouts (Figure 2.12). Accordingly, the changes in breathing frequency, tidal volume, and minute ventilation during hypoxia and/or hypercapnia were analysed as the percentage change from normoxia rather than the absolute values for each parameter.

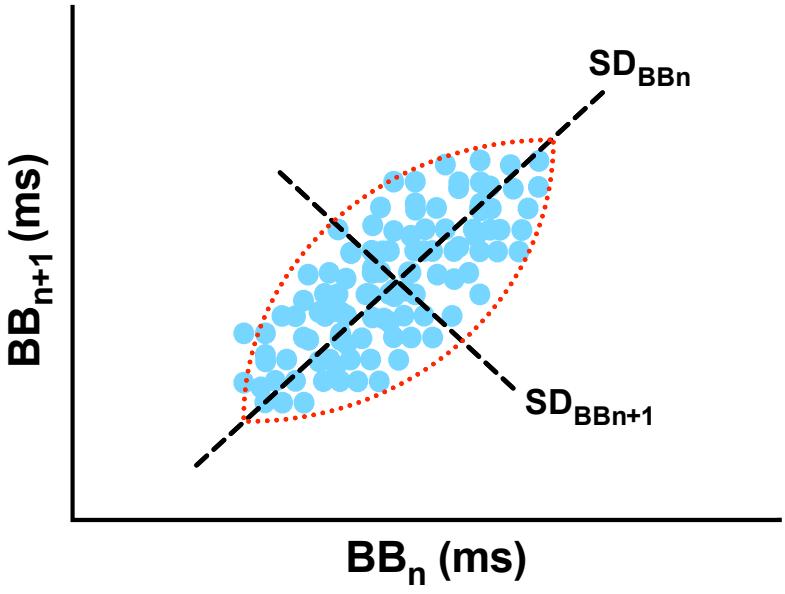

Figure 2.11: Illustration of a Poincaré plot with the analysis of distribution. The distribution of the inter-breath interval (ms) as well as the measurement of regularity/stability via calculating the standard deviation along the y-axis (SD_{BBn+1}) and x-axis (SD_{BBn}).

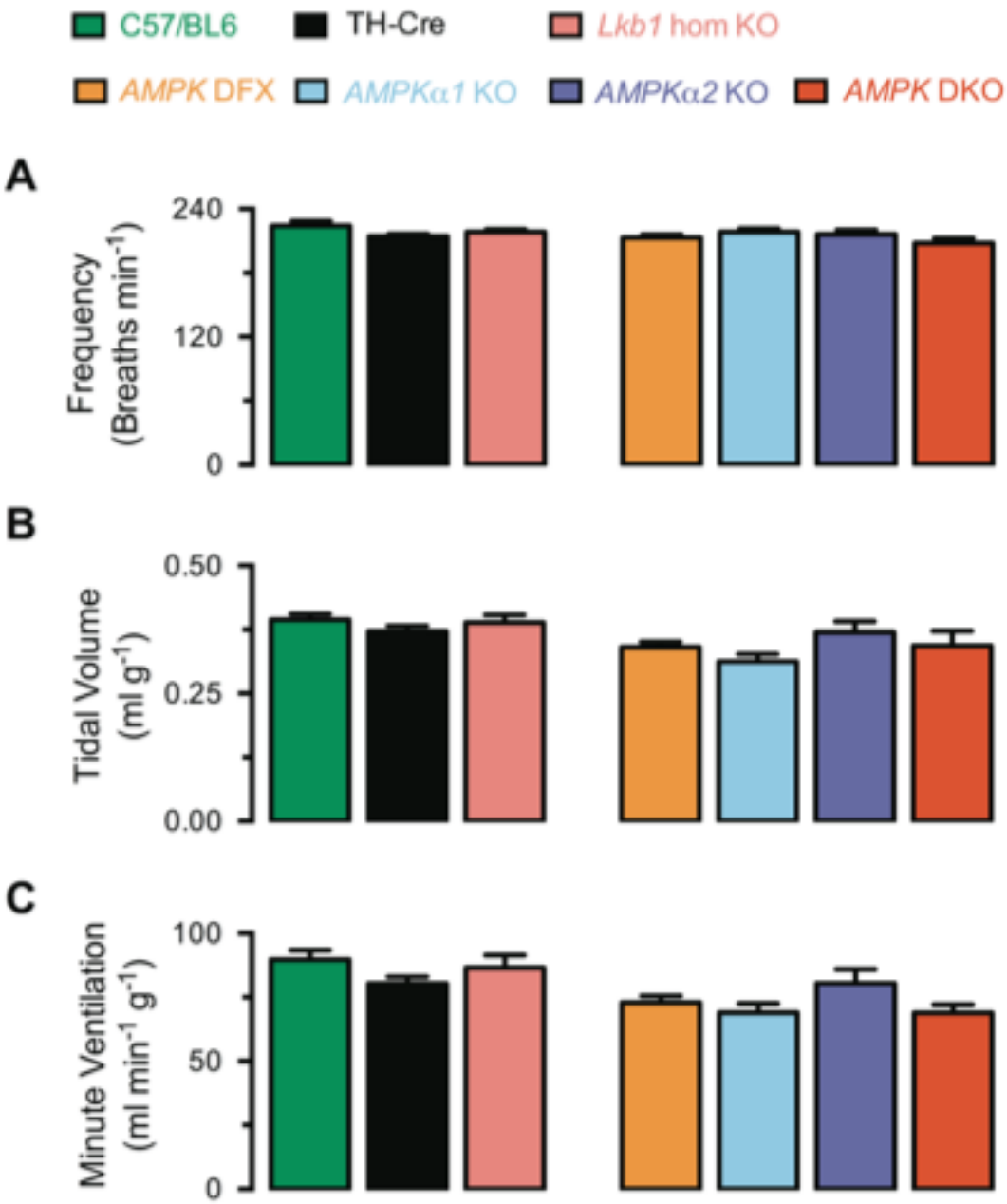

Figure 2.12: Basal breathing frequency, tidal volume and minute ventilation of experimental mice. Bar charts show mean ± SEM of the absolute values for **(A)** breathing frequency (min^{-1}) **(B)** tidal volume (ml g^{-1}) and **(C)** minute ventilation (ml min^{-1} g^{-1}) under normoxia for C57/Bl6 (green, n = 9), TH-Cre (black, n = 11), *Lkb1* homozygous knockout (*Lkb1* hom KO, pink; n = 12), *AMPK α1* and *α2* double floxed (*AMPK* DFX, orange, n = 17), *AMPK α1-subunit* knockout (*AMPKα1* KO, blue, n = 8), *AMPK α2-subunit* knockout (*AMPKα2* KO, purple, n = 19) and *AMPK AMPK α1* and *α2* double knockout mice (*AMPK* DKO, red, n = 11).

2.3 Discussion

2.3.1 Summary

In order to study the role of the LKB1-AMPK dependent pathways in regulating ventilation in response to hypoxia and/or hypercapnia, transgenic mice were developed in a manner by which LKB1 or AMPK were conditionally deleted in tyrosine hydroxylase (TH) expressing cells; global knockouts of LKB1 (Sakamoto, 2006) or both isoforms of the AMPK catalytic α-subunit (Viollet et al., 2009) are embryonic lethal. Deletion in TH-positive, and hence catecholaminergic cells, includes but is not limited to the specialised oxygen-sensing cells of the carotid body, neonatal adrenomedullary chromaffin cells, and catecholaminergic regions in the respiratory centres of the brain stem (i.e. A1/C1 and A2/C2 cell groups), which have all been shown to modulate the ventilatory response to hypoxia (King et al., 2012; Song et al., 2011; Heymans et al., 1931; Biscoe and Duchen, 1990; Slotkin and Seidler, 1988; Seidler and Slotkin, 1985). This, for the first time, gives the capacity to study the role of LKB1 and AMPK at the whole-body level with respect to mediating the ventilatory response to hypoxia and/or hypercapnia.

2.3.2 Specificity of conditional knockouts

The deletion of *Lkb1* and *AMPK α1* and *α2* catalytic subunits in TH-expressing cells was confirmed by performing single cell end point RT-PCR in acutely isolated carotid body type I cells. However, the *Lkb1* strain contains a hypomorphic mutation that significantly decreases LKB1 expression in the absence of Cre recombinase (Sakamoto, 2006). Hence, in additional to the complete deletion of *Lkb1* in catecholaminergic cells, LKB1 activity is reduced in other TH-negative tissue. Previous studies on the same *Lkb1* strain, which targets exons 4-7 of LKB1, have demonstrated that significant reductions in LKB1 expression and activity is found in the heart, liver, and skeletal muscle with only marginal reductions in the brain. Even though these hypomorphic TH-negative tissue are not specialised oxygen-sensing cells involved with mediating the ventilatory response to hypoxia and/or hypercapnia, it is important to

establish the possible underlying effects of *Lkb1* hypomorphism on ventilation during hypoxia and/or hypercapnia. In contrast, the *AMPK* strain are not hypomorphic and will provide further and more precise evidence with regards to the possible role for LKB1- and AMPK-dependent pathways in mediating the ventilatory response to hypoxia and/or hypercapnia.

2.3.2.1 Alternative genetic approaches

In addition to controlling spatial excision of *Lkb1* and *AMPK α1* and *α2-subunits* within catecholaminergic neurons as demonstrated in this chapter, Cre-mediated deletion of the floxed alleles can also be controlled temporally (Feil et al., 1997; Hall et al., 2009). Temporal regulation of excision can be mediated by the use of a tamoxifen-inducible Cre. With this strategy, Cre would be under control of a modified ligand-binding domain of the estrogen receptor that prevents transcription unless tamoxifen is introduced (Feil et al., 1997; Hall et al., 2009). Therefore, in addition to restricting Cre expression in catecholaminergic cells by ligating it to a tyrosine hydroxylase promoter, the time at which the *Lkb1* and *AMPK α1* and *α2-subunits* are deleted can be controlled based on when tamoxifen is applied (i.e. through injection or through feeding).

Although the conditional deletion of *Lkb1* and *AMPK α1* and *α2-subunits* in catecholaminergic cells as performed in this chapter appeared to have had no underlying effects on the development of normoxic phenotype (i.e. baseline breathing and weight gain versus age, as discussed below in 2.3.3), using an adult-onset inducible knockout would be advantageous. One reason is that the catecholaminergic neonatal adrenomedullary chromaffin cells (nAMCs) play a critical role perinatally as they trigger a surge of catecholamine release in response to hypoxic stress that is experienced during birth. The burst of catecholamines helps develop the lungs into an air-breathing organ to prepare newborns for extra-uterine life but plays a significant role in the postnatal maturation of the brain and carotid body (Jiang and Haddad, 1994; Liu et al.,

1999). Hence, with the ability to induce gene knockout, one can time the deletion of *Lkb1* and *AMPK α1* and *α2-subunits* to after this crucial perinatal stage to ensure that catecholaminergic nAMCs and subsequent maturation of the carotid body and central regions in the brain are unaffected during development in the *Lkb1* and *AMPK α1-* and *α2-* double knockouts.

Another reason why temporally controlling deletion may be beneficial is it allows one to observe they hypoxic-response within a mouse both before and after deletion has been induced. That is, prior to inducing deletion by administrating tamoxifen, one can observe the complete hypoxic ventilatory respone within a mouse and observe the changes that occur subsequent to *Lkb1* or *AMPK α1* and *α2-subunits* deletion. That way we can calculate the percentage change in the hypoxic response, i.e. whether the response has been stimulated or blunted by deletion, within each mouse. Having such an 'internal control' would perhaps be more informative when observing the effects of *Lkb1* and *AMPK α1* and *α2-subunit* deletion on the hypoxic ventilatory response than simply comparing the mean hypoxic response between control mice and the knockout mice as performed in this thesis.

2.3.3 Control and knockout mice are indistinguishable under normoxic and normocapnic conditions

Regular control of breathing is crucial to maintain CO_2 and O_2 arterial pressures at a constant level. Abnormal embryogenic development of this regulatory system may impair peripheral and central chemosensitivity at the early stages of life as observed in congenital central hypoventilation syndrome (CCHS) (Spengler et al., 2001). As a result, it was important to demonstrate that the deletion of *Lkb1* and *AMPK* activity in catecholaminergic cells had no underlying effect on the development of normoxic phenotype. Baseline recordings of body temperature, venous blood gas composition and blood pH were comparable between C57/Bl6, TH-Cre, *Lkb1* knockouts, AMPK *α1* and *α2* floxed and *AMPK α1* and *α2* double knockout mice. Furthermore, weight-age relationships for all five groups were similar. Most importantly, baseline breathing frequency, tidal volume, and hence minute ventilation were comparable across all

groups during normoxia. This importantly demonstrates that (1) the introduction of Cre recombinase in tyrosine hydroxylase expressing cells and (2) the deletion of *Lkb1* and *AMPK α1* and *α2* subunits in catecholaminergic cells has no effect on the appropriate control of breathing under normoxic levels to maintain CO_2 and O_2 arterial pressure at a constant level. Hence, any ventilatory abnormalities observed during hypoxia and/or hypercapnia in the knockout mice is likely to be a result of the specific requirement of LKB1 and/or AMPK in catecholaminergic cells to appropriately modulate the ventilatory response.

2.3.4 The plethysmographic measurements

Whole-body plethysmography is the only method available to measure breathing in unrestrained awake mice. Whereas the absolute values for breathing frequency and total breath duration are reliably derived, the absolute values for tidal volume, and accordingly minute ventilation, should be considered with caution. The plethysmography software uses the formula of Fenn and Drorbaugh to derive tidal volume values. Accordingly, the main sources of error come from alveolar temperature and humidity, which are not directly measured but are still used in computing the calibration constant/algorithm used to calculate tidal volume. Therefore, the absolute values of tidal volume, and hence minute ventilation, may be biased and usually underestimated by errors induced by these estimated parameters. Nevertheless, this technique of calculating tidal volume has been validated with a systemic error of <7% (Bonora, 2004; Onodera, 1997; Ramanantsoa et al., 2007). In addition, the same plethysmography system was used for all genotypes used for experiments and hence all measurements were subjected to the same calculation and calibration constant. Still, to overcome the possible system errors due to calibration inaccuracy, all ventilatory parameters were analysed as a percentage change from normoxia.

2.3.5 Conclusion

Previous studies attempting to establish the role of the LKB1-AMPK signaling pathway in mediating hypoxia-response coupling in specialised oxygen-sensing cells

have been largely pharmacological and *in vitro*. These included electrophysiological studies on the CB1 cells that demonstrated the ability of AMPK to directly regulate ion channels as necessarily occurs during hypoxia to lead to cell activation (Ross et al., 2011; Wyatt et al., 2007). However, these studies fall short from demonstrating whether this is sufficient or required to then trigger the ventilatory response to hypoxia at the whole-body level. Hence, with global knockout of *Lkb1* (Sakamoto, 2006) or both isoforms of the *AMPK* catalytic α-subunits (Viollet et al., 2009) being embryonic lethal, the development of conditional *Lkb1* and *AMPK α1* and *α2* knockouts in catecholaminergic cells (including the CB1 cells and respiratory centres in the brainstem) provides, for the first time, the capacity to study the role of LKB1 and AMPK in mediating the ventilatory response to hypoxia at the whole-body level.

Appendix

Appendix 2A

Viral injections

At the start of surgical procedures, 4 month old TH-Cre mice were anesthetized with ketamine/domitor anesthesia (75 and 1 mg/kg, i.p., respectively) and placed on a small animal stereotaxic frame (Stoelting). Recombinant Cre inducible AAV1/2 vector carrying a double-floxed inverted open reading frame encoding a reporter gene (EF1a:YFP) in antisense orientation (final concentration of 3.41 x 10^{-4} GC/ml), was laterally injected adjacent to the locus coeruleus [anteroposterior (AP), 4.122 mm; mediolateral (ML), +/– 1.28 mm; dorsoventral (DV) 3.65 mm] through an internal cannula at a rate of 100 nl/min for 2.5 min (250nl total volume). After surgical procedures, animals were allowed to recover for at least one week. The mice were then perfused and brain extracted and sagittally sectioned (60µm thick) using a vibratome. For co-localization experiments, brain sections from eYFP-transduced mice were incubated in mouse anti-tyrosine hydroxylase (1:1000, Millipore, MAB-318). Sections were then incubated in goat anti-rabbit IgG secondary antibody (1:750, Invitogen, A594). Localised flurorscence of the Cre-inducible AAV2 – YFP within the injected site is illustrated in the figure below.

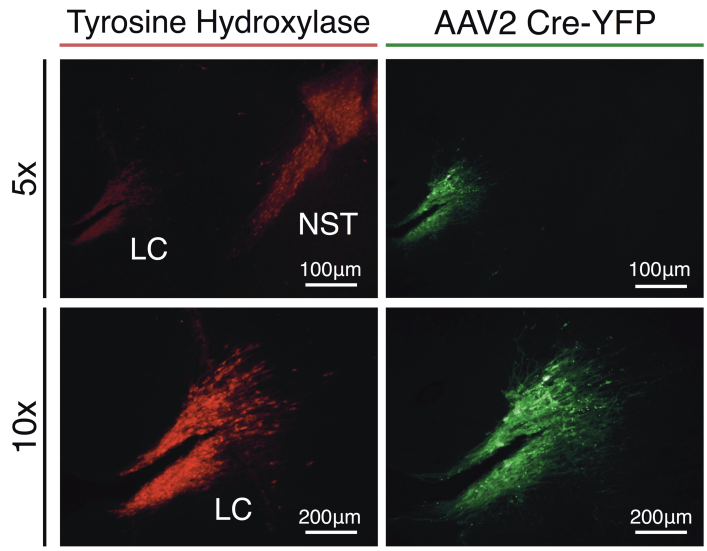

Supplementary Figure 2A. Specificity of Cre expression in tyrosine hydroxylase expressing cells. Images of sagittal sections from the brain of a TH-Cre mouse after injection of AAV1/2 Cre-induced YFP virus into the locus coeruleus (LC) but not the nigrostriatal region (NST), *left panels* show immunostaining depicting tyrosine hydroxylase immunoreactivity (red) and *right panels* show Cre-induced YFP expression (green). *Upper panels* show 5x magnification, *lower panels* show 10x magnification. ***Experiment performed by Dr. Marta Jeltai.***

Chapter Three:
The role of LKB1 in the ventilatory response to hypoxia and hypercapnia

3.1 Introduction

3.1.1 The mitochondria and acute oxygen-sensing

There are at least two distinct cellular pathways involved with respiratory adjustments during hypoxia. One is slow and ubiquitous and involves the modulation of gene expression via the hypoxia inducible factor (HIF) in response to sustained hypoxia, with the point of activation being cell-type-dependent (G. L. Wang et al., 1995; Iyer et al., 1998); HIF targets genes that promote cellular adaptation to hypoxia, including those that increase glucose uptake (GLUT1) and oxygen transport by promoting red blood cell maturation (Epo, transferrin, (Y.-J. Peng et al., 2011; Yuan et al., 2011). The other pathway involves rapid cellular activation via ion channel regulation in response to acute hypoxia and occurs selectively in specialised oxygen-sensing cells. These cells are acutely sensitive to changes in PO_2 within the physiological range and include the catecholaminergic type I cells of the carotid body (CB1 cells), neonatal adrenomedullary chromaffin cells, and may also incorporate subgroups of neurons within the respiratory centres of the brainstem (King et al., 2012; Song et al., 2011; Heymans et al., 1931; Biscoe and Duchen, 1990; Slotkin and Seidler, 1988; Seidler and Slotkin, 1985). In response to acute hypoxia, at levels that have no effect on cells that do not function to monitor O_2 supply, these specialised oxygen-sensing cells are activated and importantly trigger an appropriate ventilatory response to maintain arterial PO_2 levels within physiological limits. However, discrepancies arise with regards to the identity of the primary site or primary O_2 sensor of the hypoxic chemotransduction pathway that leads to cell activation. Nevertheless, several studies have strongly suggested that the mitochondrion is the primary site for O_2-sensing and the origin of the hypoxic chemotransduction pathway in oxygen-sensing cells (Mills and Jöbsis, 1972; Duchen and Biscoe, 1992a; Buttigieg et al., 2008; Buckler and Turner, 2013).

In fact, one of the initial suggestions was that acute O_2-sensing in the specialised oxygen-sensing cells is coupled to mitochondrial oxidative phosphorylation (the metabolic hypothesis). The first direct evidence demonstrating a role for mitochondria in O_2-sensing came from the works of Mills and Jöbsis in 1972. With the use of

fluorometric measurements, they were able to demonstrate in CB1 cells that mitochondrial NADH:NAD^+ ratio increases in a manner inversely related to PO_2. Furthermore, the increase in mitochondrial NADH correlated with increases in afferent fibre discharge over the physiological range of O_2-levels. This led to the hypothesis that mitochondria in CB1 cells contain a specialised cytochrome a3 that, unlike the non-specialised O_2-sensing cells, have a low affinity for O_2 and hence a surprisingly high sensitivity to hypoxia (Mills and Jöbsis, 1972). Consistent with these studies, hypoxia has been found to increase mitochondrial NADH and inhibit the electron transport chain and cytochrome oxidase activity at relatively high PO_2 levels in CB1 cells (Duchen and Biscoe, 1992a; 1992b; Buckler and Turner, 2013); no such effects were observed in sympathetic neurons from the superior cervical ganglia that do not have a specialised oxygen-sensing role (Buckler and Turner, 2013).

Strong evidence in favour of a functional role for mitochondria in O_2-sensing also comes from studies in immortalised neonatal adrenomedullary chromaffin cells (MAH cells). Of these cells, those deficient in functional mitochondria failed to respond to mitochondrial inhibitors and hypoxia, but not hypercapnia, (Buttigieg et al., 2008). All together, these studies strongly suggest that the modulation of the mitochondrial electron transport chain plays an essential part of the hypoxia transduction cascade in specialised oxygen-sensing cells. However, differences arise with regards to the mechanism by which cells are able to further couple the mitochondria with ion channel regulation and cell activation during hypoxia. Nevertheless, studies using a variety of mitochondrial inhibitors, e.g. the ATP synthase inhibitor oligomycin, have indicated that the inhibition of ATP synthesis is the primary event that triggers the hypoxia transduction cascade (Wyatt and Buckler, 2004).

3.1.2 Coupling the mitochondria to cell activation

3.1.2.1 Lkb1 and AMPK

As mentioned previously**,** the AMP-activated protein kinase (AMPK) is a ubiquitously expressed heterotrimer consisting of a catalytic α-subunit and regulatory

β- and γ-subunits. AMPK is activated during metabolic stress as the ADP:ATP and AMP:ATP ratios increase, but requires phosphorylation of the threonine 172 residue (Thr-172) within the catalytic α-subunit by upstream kinases, namely the tumor suppressor kinase LKB1 (Hawley et al., 2003; Woods et al., 2003). AMPK can also be phosphorylated in a Ca^{2+}-dependent manner via the Ca^{2+}/calmodulin-dependent protein kinase kinase β (CaMKK-β) (Hawley et al., 2005; Woods et al., 2005).

Under resting conditions AMPK is constitutively phosphorylated by LKB1, but sustained activation is prevented as ATP is bound to the γ-subunit of AMPK and promotes dephosphorylation by phosphatases, namely PP2C and PP2A (Suter et al., 2006; Davies et al., 1995). As the ADP:ATP and AMP:ATP ratios increase during metabolic stress, such as hypoxia, ATP is displaced by ADP or AMP. This causes a conformational change that protects the phosphorylation of the catalytic subunit by LKB1, thereby increasing AMPK activity by >200-fold. The binding of AMP, but not ADP, can further cause allosteric activation of up to 10-fold (overall allowing a >2000-fold increase in AMPK activity) (Xiao et al., 2007; 2011). Once activated, AMPK responds to re-establish ATP levels by up-regulating catabolic pathways and/or suppressing non-essential anabolic pathways (Hardie, 2007).

The ability of the LKB1-AMPK pathway to monitor and respond to the ADP:ATP and AMP:ATP ratios as an index of metabolic stress, linked with findings showing AMPK's ability to directly regulate ion channels (Ikematsu et al., 2011; Ross et al., 2011; Wyatt et al., 2007), and to mimic the hypoxic response in CB1 cells has put it in prime position for coupling hypoxic inhibition of the mitochondria with ion channel regulation and the subsequent activation of specialised oxygen-sensing cells. This has been demonstrated with the use of *in vitro* and pharmacological studies in acutely isolated CB1 cells. AMPK activation by administration of 5-aminoimidazole-4-carboxamide riboside (AICAR), which is metabolised to the AMP mimetic ZMP, was found to inhibit O_2-sensitive K^+ currents as necessarily occurs during hypoxia to promote depolarisation (Wyatt et al., 2007). The activation of AMPK also mimicked the hypoxic response in CB1 cells by subsequently promoting Ca^{2+} influx and an increase in afferent fibre discharge. Conversely inhibition of

AMPK activation by the antagonist compound C reversed the effects of AICAR and prevented activation of CB1 cell activation during hypoxia. Electrophysiological studies further demonstrated the ability of AMPK to regulate K^+ channels, namely the large conductance Ca^{2+}-activated (BK_{Ca}) channels (Wyatt et al., 2007; Ross et al., 2011), which mediates in part carotid body type I cell activation during hypoxia.

Accordingly, the LKB1-AMPK signalling pathway may maintain energy levels not only at a cellular level but also the whole-body level by regulating the ventilatory response to changes in O_2-supply. CaMKK-β may also play a role and act synergistically to activate AMPK, but only secondary to cell activation as it is dependent on increases in calcium levels. However, alternative suggestions have been made with regards to the manner by which AMPK is activated during hypoxia, namely by mitochondrial reactive oxygen species (mROS) and not increases in the ADP:ATP and AMP:ATP ratios (Emerling et al., 2009).

3.1.2.2 Mitochondrial reactive oxygen species and AMPK

Studies on embryonic fibroblasts and osteosarcoma cells have demonstrated that hypoxia necessarily activates AMPK via increases in mitochondrial reactive oxygen species (mROS) and not in an AMP-dependent manner (Emerling et al., 2009). However, it is important to note that these cell types are not specialised oxygen-sensing cells and so the response observed may be a ubiquitous cellular response to severe hypoxia (Evans et al., 2011) and not for specialised acute oxygen-sensing. Nevertheless, these studies indicated that AMPK was only activated by LKB1 in the presence of functional mitochondria, with no detectable changes in the AMP:ATP ratio, and that activation was blocked by an antioxidant (Emerling et al., 2009; Chandel, 2010). Also, in cells deficient of mitochondrial cytochrome b, which allows for mROS production at complex III during hypoxia but not oxidative phosphorylation, AMPK was still activated by hypoxia; this thereby suggesting that inhibition of mitochondrial oxidative phosphorylation and consequent decreases in ATP synthesis is not required for AMPK-dependent oxygen-sensing but that the production of mROS is. AMPK was also activated by exogenous H_2O_2 in cells

lacking mitochondria. However, this required LKB1 as cells deficient in the upstream kinase resulted in an attenuated response to H_2O_2 (Chandel, 2010; Emerling et al., 2009). Therefore, this would suggest that, similar to AMP, H_2O_2 must necessarily cause a conformational change that protects the phosphorylation by LKB1 of the catalytic subunit of AMPK from dephosphorylation by phosphatases.

Several studies have provided evidence that strongly opposes such an AMP-independent and mROS-dependent activation of AMPK during hypoxia. Using AMP-insensitive AMPK heterotrimers, have shown that H_2O_2 can no longer activate AMPK directly and that H_2O_2 promotes AMPK activation in an LKB1-dependent manner by inhibiting mitochondrial function and subsequently increasing the AMP:ATP ratio (Hawley et al., 2010; Auciello et al., 2014). Therefore, if H_2O_2 or mROS were to effect AMPK activation during hypoxia, this would likely involve the facilitation of mitochondrial inhibition (Evans et al., 2011; Auciello et al., 2014). Also, exogenous H_2O_2 was found to have no effect on the specialised oxygen-sensing CB1 cells (Wyatt and Buckler, 2004) and even suppressed the hypoxic response in neonatal adrenomedullary chromaffin cells (Thompson et al., 2007). All together, this strongly indicates that direct activation of AMPK by mROS during hypoxia, in an AMP-independent manner, is highly unlikely.

3.1.3 The hypoxic ventilatory response in mice

Similar to humans, the hypoxic ventilatory response is biphasic in mice which is characterized by an initial augmentation phase lasting up to 2min followed by a secondary "roll-off" phase as ventilation decreases until reaching a steady-state (Robinson et al., 2000; Bissonnette and Knopp, 2001). Furthermore, the hypoxic ventilatory response remains biphasic regardless of the degree of hypoxia or the age of mice (and other mammals). However, there is developmental variability in the magnitude of the roll-off phase. In neonates, the percentage change from the augmentation phase to the roll-off phase is more severe when compared to the difference observed in juvenile and adult mice; i.e. the secondary roll-off phase is more severe in neonates (Robinson et al., 2000; Bissonnette and Knopp, 2001).

The breathing pattern during hypoxia is also variable developmentally in mice. Although in both neonates and adults the stimulation of ventilation is primarily driven by increases in breathing frequency, in neonates this increase is a result of reductions in the durations of both inspiration and expiration while in adults it is only a result of a reduction of the later. Also, the depressed ventilation observed during the secondary roll-off phase is primarily driven in neonates by reductions in tidal volume while in adults this also involves reductions in breathing frequency (Robinson et al., 2000). As all experimental mice used during the thesis were at least 3 months of age, the effects of LKB1 and AMPK deletion in catecholaminergic cells were only examined with regards to the hypoxic ventilatory response during adulthood and not perinatally.

3.1.4 Aims

Given the above, I sought to test the hypothesis that LKB1 is required to couple mitochondrial inhibition by hypoxia to catecholaminergic cell activation by hypoxia and thus to the ventilatory response to hypoxia at a whole-body level. Accordingly, the aims of the current chapter were to determine the role of the upstream kinase LKB1 in regulating the ventilatory response to hypoxia (and/or hypercapnia) in adult mice. This involved the use of mice of at least 3 months of age with conditional deletion of *Lkb1* in catecholaminergic cells (as described in Chapter 2). Studies were also performed on the hypomorphic *Lkb1* floxed mice to examine any possible underlying effects of the non-specific deficiencies in LKB1 expression in TH-negative cells.

3.2 Results

3.2.1 The effects of *Lkb1* deletion on the ventilatory response to hypoxia

Under normoxia, baseline recordings of body temperature, venous blood gas composition, blood pH, breathing frequency, tidal volume, and minute ventilation after conditional *Lkb1* deletion in catecholaminergic cells were consistent with measures taken from control mice, including TH-Cre mice and C57/Bl6 mice (as discussed in Chapter 2: Table 2.1 and Figure 2.12). Moreover, there was no significant difference in weight gain with age between 2 and 12 months (Chapter 2: Figure 2.8). However, conditional deletion of *Lkb1* in catecholaminergic cells, driven by Cre-expression under the control of a tyrosine hydroxylase (TH) promoter, resulted in irregular breathing and precipitated apnoeas during hypoxia.

3.2.1.1 *Lkb1* deletion increases the frequency and duration of apnoeas in a PO_2-dependent manner

Ventilatory traces obtained using unrestrained whole-body plethysmography revealed that conditional deletion of *Lkb1* in catecholaminergic cells in mice (*Lkb1* knockout mice) induced more frequent and prolonged apnoeas in a PO_2-dependent manner when compared with control TH-Cre mice. Apnoeas were identified as a cessation of breathing for a duration that is at least equivalent to the duration of two regular breaths (i.e. two respiratory cycles have been missed) (Y.-J. Peng et al., 2011; Nakamura and Kuwaki, 2004; Voituron et al., 2009), which equated to a cessation ≥500ms in our experimental mice. Importantly, the ventilatory abnormalities observed in the *Lkb1* knockouts were more severe than the hypomorphic *Lkb1* floxed mice, thereby suggesting that the effects observed is due to deficiencies of LKB1 expression in catecholaminergic cells rather than non-specific deficiencies due to hypmorphism (this will be discussed further in Section 3.2.2).

Figure 3.1 shows example ventilatory traces of TH-Cre and *Lkb1* knockout mice during normoxia (21% O_2), mild hypoxia (12% O_2) and severe hypoxia (8% O_2) and the calculated means ± SEM for the apnoeic index (apnoeas/min), apnoea duration,

and apnoea duration index (product of the apnoeic index and duration) under each condition (data is also summarised in table 3.1). Consistent with studies on wild-type C56/Bl6 mice (Stettner et al., 2008), hypoxia induced brief and infrequent apnoeas in control TH-Cre mice. Apnoeas observed in TH-Cre mice appeared marginally PO_2-dependent, as the mean apnoeic index significantly increased from 0.23 ± 0.08 apnoeas min^{-1} (n = 19 from 5 mice) during 12% O_2 to 1 ± 0.2 apnoeas min^{-1} (n = 24 from 5 mice) during 8% O_2 ($p < 0.001$, by one-way ANOVA). The mean duration of apneoas, however, exhibited no pO_2-dependence, as it was comparable at 577 ± 20ms and 629 ± 15ms during exposures to 12% O_2 and 8% O_2, respectively (Figure 3.1 – Panel Bii). By contrast, in *Lkb1* knockouts both the frequency and duration of apnoeas increased markedly in a manner that was not only inversely related to PO_2 but also significantly greater than control TH-Cre mice during 12% O_2 and 8% O_2. This is clear from cross comparison of the mean apnoeic index (12% O_2: 0.7 ± 0.2 min^{-1}, n = 17 from 4 mice, $p < 0.05$; 8% O_2: 5.9 ± 0.7 min^{-1}; n = 29 from 4 mice, $p < 0.0001$) and apnoea duration (12% O_2: 746 ± 23 ms, $p < 0.0001$; 8% O_2 895 ± 11 ms; $p < 0.0001$).

Overall, this translates to a PO_2-dependent increase in the apnoea duration index, which is significantly greater for *Lkb1* knockouts (12% O_2: 3 ± 0.8, $p < 0.05$; 8% O_2: 5.4 ± 0.6, $p < 0.0001$) than for TH-Cre mice (12% O_2: 0.3 ± 0.1; 8% O_2: 0.7 ± 0.1) irrespective of the degree of hypoxia (Figure 3.1 – Panel Biii).

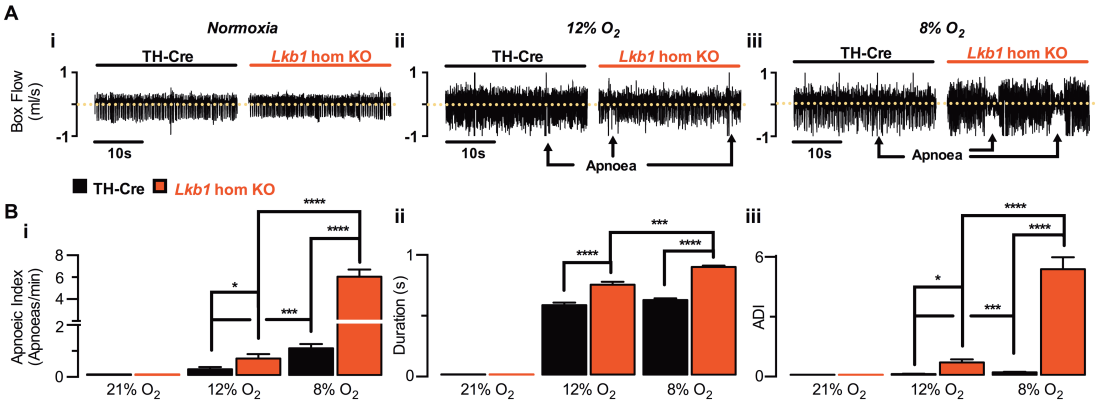

Figure 3.1: *Lkb1* deletion precipitates apnoeas in a PO_2-dependent manner. (A) Records of ventilatory activity from TH-Cre (*left panel*) and *Lkb1* homozygous knockout mice (*Lkb1* hom KO; *right panel*) during **(i)** normoxia (21% O_2 + 0.05% CO_2), **(ii)** mild hypoxia (12% O_2 + 0.05% CO_2) and **(iii)** severe hypoxia (8% O_2 + 0.05% CO_2). **(B)** Mean ± SEM for **(i)** apnoeic index (AI, apnoeas per minute), **(ii)** apnoea duration (s) and **(iii)** the apnoea-duration index (ADI) (TH-Cre - 12% O_2: n = 19 exposures from 5 mice, 8% O_2: n = 24 exposures from 5 mice, black; *Lkb1* hom KO - 12% O_2: n = 17 exposures from 4 mice, 8% O_2: n = 29 exposures from 4 mice, red). * = $p < 0.05$, *** = $P< 0.001$, **** = $p < 0.0001$. Significance tested by one-way ANOVA with Bonferroni multiple comparisons.

Table 3.1: The affects of *AMPK* deletion on the frequency and duration of apnoeas

	TH-Cre			*Lkb1* floxed			*Lkb1* knockouts			Related Figure
	21% O_2	12% O_2	8% O_2	21% O_2	12% O_2	8% O_2	21% O_2	12% O_2	8% O_2	
Apnoeic Index (Apnoeas/min)	NA	0.2 ± 0.1 n = 19	1.0 ± 0.2 n = 24	NA	0.1 ± 0.1 n = 16	3.5 ± 0.6 n = 15	NA	0.7 ± 0.2 n = 17	5.9 ± 0.7 n = 29	3.1 & 3.11
Apnoea Duration (ms)	NA	587 ± 21 n = 19	620 ± 21 n = 24	NA	650 ± 32 n = 16	769 ± 18 n = 15	NA	746 ± 23 n = 17	895 ± 11 n = 29	
Apnoea Duration Index	NA	0.3 ± 0.1 n = 19	0.7 ± 0.1 n = 24	NA	0.7 ± 0.2 n = 16	2.7 ± 0.5 n = 15	NA	3.0 ± 0.8 n = 17	5.4 ± 0.6 n = 29	

NA = not applicable

Breathing irregularities of *Lkb1* knockout mice appeared even more complex when examined on an expanded time scale as illustrated in Figure 3.2. Under mild hypoxia, apnoeas appeared only slightly prolonged (maximum apnoea was ~1s) when compared to TH-Cre (maximum was ~830ms). Also, the apnoeas observed in both control TH-Cre and *Lkb1* knockout mice were often preceded by a sigh, which was identified as an exaggerated breath with an inspiratory and expiratory amplitude, i.e. tidal volume, at least twice as large as the inspiratory and expiratory amplitude of the three previous breaths (Voituron et al., 2009). However, under severe hypoxia the apnoeas were not only more frequent and prolonged, with a maximum apnoea duration of ~4s in *Lkb1* knockout mice (~ 900ms in TH-Cre), but the ventilatory pattern varied extensively in the *Lkb1* knockouts. Periodic breathing was occasionally evident as prolonged post-sigh apnoeas would occur at regular intervals of ~0.1Hz (Appendix 3A illustrates this on a longer time-course). This was occasionally associated with Cheyne-Stokes-like breathing (CSB), which is characterised by a sinusoidal ventilatory pattern that cycles from progressively deeper and faster breathes to a gradual decrease in frequency and tidal volume which ultimately reaches an apnoeic event (Eckert et al., 2007)(as shown in Figure 3.2 – Panel Bii, *record 1*). Paradoxically, severe hypoxia also induced periods of hypoventilation in the *Lkb1* knockout mice with prolonged apnoeas that were either preceded by a sigh or occurred spontaneously (Figure 3.2 – Panel Bii, *records 2-4*). The likelihood that this results from the hypomorphic expression of *Lkb1* in non-catecholaminergic cells seems unlikely as the *Lkb1* floxed mice show milder ventilatory abnormalities that do not include CSB (this will be addressed further in Section 3.2.2).

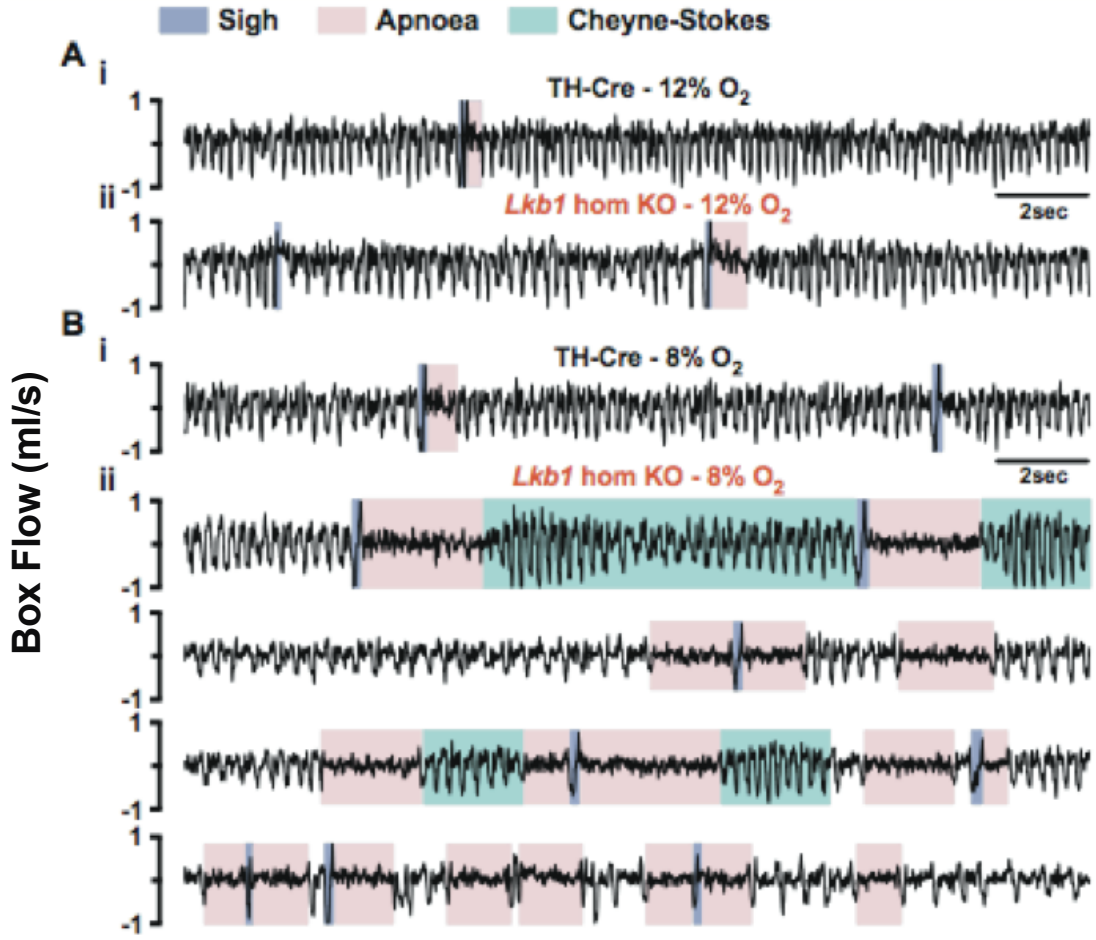

Figure 3.2: *Lkb1* deletion precipitates abnormalities in ventilatory pattern that includes apnoeas, hypoventilation, and Cheyne-Stokes-like breathing in a manner that is PO_2-dependent. Typical ventilatory records on an expanded time scale during **(A)** mild hypoxia (12% O_2) and **(B)** severe hypoxia (8% O_2) from **(i)** TH-Cre and **(ii)** *Lkb1* homozygous knockout mice (*Lkb1* hom KO). **(Bii)** Different *Lkb1* hom KO mice during severe hypoxia (8% O_2) which exhibit (top to bottom) Cheyne-Stokes-like breathing with post-sigh apnoeas, sinusoidal breathing with spontaneous and post-sigh apnoeas, mild sinusoidal breathing with spontaneous and post-sigh apnoeas, hypoventilation with spontaneous and post-sigh apnoeas.

Further analysis strongly indicates that central rather than obstructive apnoeas are induced by *Lkb1* deletion in catecholaminergic cells. Central apnoeas are characterised by the lack of central drive to breath and a lack of respiratory effort during the cessation of breathing. In contrast, obstructive apnoea results from an obstruction of the airway and is associated with ongoing respiratory efforts during the period over which ventilation ceases (Eckert et al., 2007). In order to determine whether central or obstructive apneoas were induced by hypoxia following complete loss of *Lkb1* function in catecholaminergic neurons, thoracic activity was monitored during each apneoic event. To this end, and with the support of Dr. Paolo Puggioni, computational video-analysis of thoracic movement was studied in parallel with measurements of inspiration and expiration by plethysmography. This revealed that in control TH-Cre mice, thoracic movement continuously oscillated in parallel with inspiratory and expiratory events from corresponding ventilatory records obtained during severe hypoxia (Figure 3.3 - Panel A). This was also apparent in the *Lkb1* knockouts as thoracic movement oscillated correspondingly with inspiratory and expiratory events, with robust movements also recorded during exaggerated breaths, e.g. sighs (Figure 3.3 – Panel B, *purple*). However, during apnoeic events there is little or no evidence of thoracic activity, which suggests that there is a lack of thoracic movement and accordingly a lack of respiratory effort (Figure 3.3 – Panel B, *pink*). Hence, the deletion of *Lkb1* in catecholaminergic cells appears to precipitate central and not obstructive apnoeas.

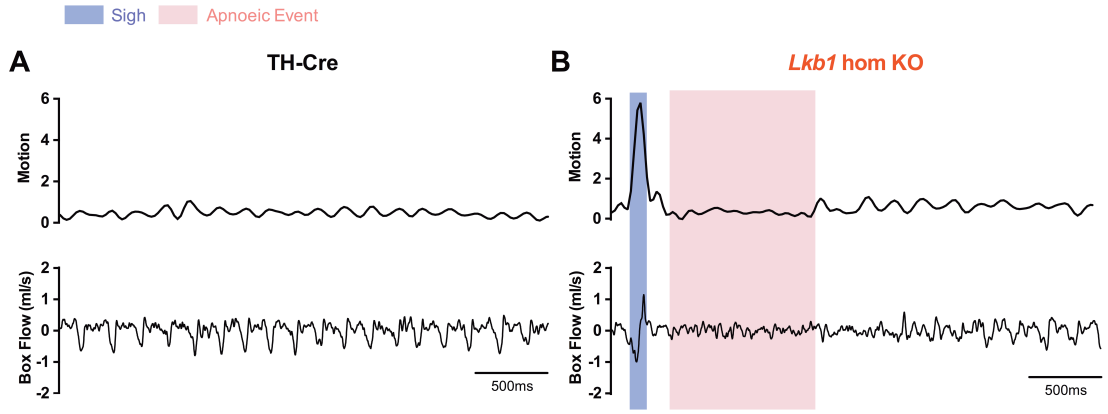

Figure 3.3: Computational video analysis of thoracic movement during ventilation. Computational video analysis of thoracic movement (*upper panel*) with corresponding ventilatory traces obtained using unrestrained whole body plethysmography (8% O_2 + 0.05% CO_2, *lower panel*) in a **(A)** TH-Cre mouse and **(B)** *Lkb1* homozygous knockout mouse (*Lkb1* hom KO). Sighs are highlighted in purple; apnoeas highlighted in pink.

3.2.1.2 Poincaré analysis reveals the PO_2-dependence of disordered breathing in *Lkb1* homozygous knockout mice

Whether considering the periods of hypoventilation, post-sigh apnoeas, or spontaneous apnoeas, the deletion of *Lkb1* in catecholaminergic neurones led to breathing irregularities that increased in severity from mild to severe hypoxia. This was confirmed by plotting the inter-breath interval (BBn) versus the subsequent inter-breath interval (BBn+1) to generate Poincaré plots. Example Poincaré plots of 500 breaths from a single exposure period are shown in Figure 3.4, which compares the breathing patterns of TH-Cre with *Lkb1* knockouts during normoxia (21% O_2), mild hypoxia (12% O_2) and severe hypoxia (8% O_2).

Clearly the variability in the interbreath interval is comparable in both TH-Cre and *Lkb1* knockouts under normoxic conditions (Figure 3.4 – Panel A). Also, as described above, a marginal increase in breathing irregularity is observed in TH-Cre mice from 12% O_2 to 8% O_2; this is entirely consistent with previous studies on wild-type C57/Bl6 mice as brief and infrequent apnoeas are generated by hypoxia in these mice (Stettner et al., 2008). In marked contrast, *Lkb1* knockouts exhibited not only marked but clearly PO_2-dependent increases in breathing irregularities (Figure 3.4 – Panels A-C). From these plots, long interbreath intervals were apparent in *Lkb1* knockouts, ranging from 0.6s to an upper limit of ~4s; corresponding to long apnoeic events. Strikingly, the number of the long interbreath intervals observed within this range increased markedly during 8% O_2. Consistent with the observations made above, this suggests that the loss of *Lkb1* in catecholaminergic cells leads to marked increases in interbreath interval and thus precipitates hypoventilation.

Clearly, the increase in breathing irregularity in *Lkb1* knockout mice increased in a manner proportional to the severity of hypoxia, and was markedly greater than observed in control TH-Cre mice under all conditions studied. This was confirmed by comparison of the variability by standard deviation (SD) of the BBn and BBn+1 as shown in Figure 3.4 – Panels A-C, *lower panels*. The SD in *Lkb1* knockout mice significantly increased from 12% O_2 at 85 ± 3ms (n = 17 exposures from 4 mice) to 8% O_2 at 153 ± 6ms (n = 28 exposures from 4 mice, $p < 0.0001$), and was significantly

greater than the PO_2-dependent change observed in control TH-Cre mice at 12% O_2 (47 ± 5ms, n = 20 exposures from 4 mice, $p < 0.0001$) and 8% O_2 (65 ± 5ms, n = 24 exposures from 5 mice, $p < 0.0001$).

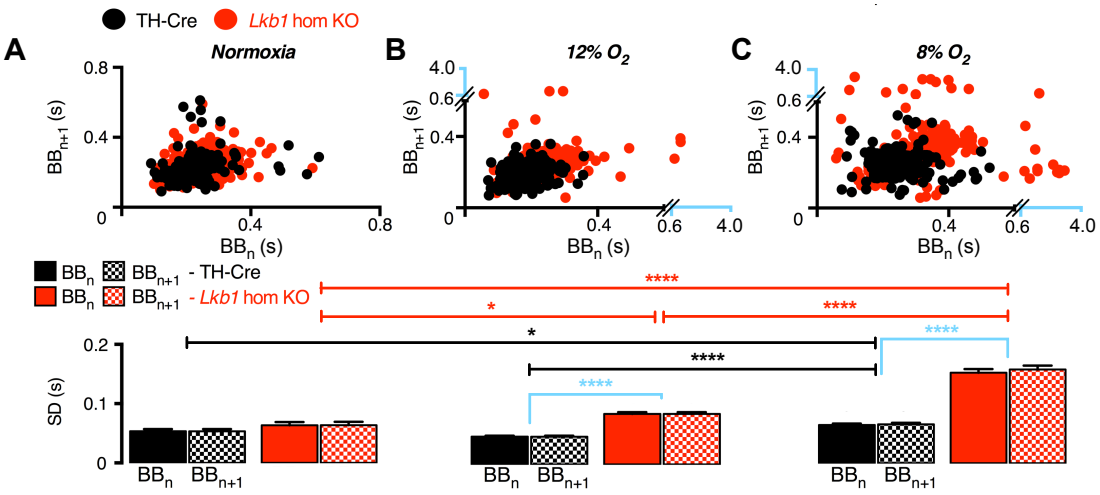

Figure 3.4: *Lkb1* deletion affects the regularity of breathing in a PO_2-dependent manner. *Upper panels* show Poincaré plots of the inter-breath interval (BB_n) versus subsequent interval (BB_{n+1}) of TH-Cre (black) and *Lkb1* homozygous knockout mice (*Lkb1* hom KO, red) during **(A)** normoxia (21% O_2 + 0.05% CO_2), **(B)** mild hypoxia (12% O_2 + 0.05% CO_2), and **(C)** severe hypoxia (8% O_2 + 0.05% CO_2). The corresponding *lower panels*, show the mean ± SEM for the standard deviation (SD) of BB_n and BB_{n+1} of each genotype under normoxia (TH-Cre: n = 25; *Lkb1* hom KO: n = 14), mild hypoxia (TH-Cre n = 20 from 4 mice, *Lkb1* hom KO: n = 17 from 4 mice) and severe hypoxia (TH-Cre: n = 24 from 5 mice, *Lkb1* hom KO: n = 28 from 4 mice). * = $p < 0.05$, ** = $p < 0.01$, *** = $p < 0.001$, and **** = $p < 0.0001$. Significance tested by one-way ANOVA with Bonferroni multiple comparisons.

3.2.1.3 Deletion of *Lkb1* in catecholaminergic cells attenuates the hypoxic ventilatory response

Importantly, the deletion of *Lkb1* in TH-positive catecholaminergic cells markedly attenuated the average increase in ventilation during mild and severe hypoxia. Figure 3.5 shows example records for the change in frequency, tidal volume, and minute ventilation (product of frequency and tidal volume) over the 5min exposure to 12% O_2 and 8% O_2 in both control TH-Cre and *Lkb1* knockout mice (2s sampling period). TH-Cre exhibited a robust increase in these parameters to levels comparable to wild-type C57/Bl6 mice (Appendix 3B); this importantly demonstrates that the introduction of Cre recombinase into tyrosine hydroxylase expressing cells has no underlying affect on the ventilatory response to hypoxia. However, measures of the hypoxic ventilatory response were markedly attenuated in *Lkb1* knockouts. Moreover, as might be expected given the above, these effects were PO_2-dependent.

Breathing frequency As illustrated by the example records, when compared to control TH-Cre mice, *Lkb1* knockouts exhibited an attenuation in the mean ventilatory response to hypoxia across 3 different time points during 12% O_2 (Figure 3.6 – Panel Ai). Initially, the breathing frequency in the control TH-Cre mice increased relative to normoxia at 30s by 51 ± 3% (n = 25 from 5 mice) before decreasing to 34 ± 2% at 100s due to respiratory depression (Bissonnette, 2000). Thereafter, TH-Cre mice breathing frequency slightly decreased to 31 ± 2% of normoxia by the end of the exposure at 300s. In marked contrast, in *Lkb1* knockouts the initial increase in breathing frequency after 30s was significantly less at 3 ± 2% of that observed during normoxia (n = 22 from 4 mice, $p < 0.0001$) (Figure 3.6 – Panel Ai). Strikingly, respiratory depression, assessed after 100s, resulted in a further decrease in frequency that resulted in marked hypoventilation of -2 ± 1% (n = 22 from 4 mice, $p < 0.0001$) relative to normoxia. Thereafter, the percentage change in the frequency remained below normoxic levels in the *Lkb1* knockouts at -3 ± 1% (n = 22 from 4 mice, $p < 0.0001$) for the remainder of the 5min exposure (Figure 3.6 – Panel Ai and Table 3.2).

During severe hypoxia, 8% O_2, the impact of *Lkb1* deletion on the average increase in breathing frequency was greater still but also time-dependent (Figure 3.6 –

Panel Bi and Table 3.2). Similar to 12% O_2, here it was notable that there was an initial robust increase in breathing frequency in TH-Cre control mice at 55 ± 3% (n = 37 exposures from 5 mice) before reducing to 2 ± 2% at 100s before it gradually increased thereafter and peaked at 31 ± 3% by the end of the hypoxia (300s) (Figure 3.6 – Panel Bi). A significant decrease was observed in the *Lkb1* knockouts across all three different time points when compared to the control TH-Cre mice at 8% O_2. Consistent with the PO_2-dependent increases in apnoea-duration index and inter-breath interval, the degree to which *Lkb1* deletion attenuated the ventilatory response to hypoxia was found to be inversely related to PO_2. At 30s following the onset of hypoxia, the percentage change in frequency during 8% O_2 measured only 1 ± 3% (n = 30 exposures from 4 mice). Thereafter, measures taken at 100s demonstrated that respiratory depression reduced breathing frequency further in the *Lkb1* knockouts to -27 ± 2% of that observed during normoxia. Despite marginal recovery to -8 ± 3% of that observed under normoxia, breathing frequency remained below baseline levels until the end of the 5min exposure (Figure 3.6 – Panel Bi).

Tidal volume In marked contrast to the time-dependence of the adjustments in breathing frequency, hypoxia induced a sustained increase in mean tidal volume in TH-Cre mice throughout the 5min exposure to 12% O_2 (30s: 23 ± 3%; 100s: 23 ± 2%; 300s: 24 ± 2%) and 8% O_2 (30s: 31 ± 4%; 100s: 35 ± 4%; 300s: 31 ± 2%) (Figure 3.6 – Panel A,B ii and Table 3.3). A sustained increase in tidal volume was also observed in the *Lkb1* knockouts during 12% O_2. However, this was marginally greater in magnitude to that of TH-Cre mice after 30s (34 ± 5%), 100s (38 ± 5%) and 300s (28 ± 6%), although this did not reach significance using a one-way ANOVA (Figure 3.6 – Panel Aii). In contrast, at 8% O_2 the increase in tidal volume was initially comparable to TH-Cre mice at 30s (38 ± 5%), but was significantly greater than that observed for TH-Cre mice after 100s (53 ± 5%, $p < 0.01$) and 300s (51 ± 4%, $p < 0.01$; Figure 3.6 – Panel Bii and Table 3.3).

Minute ventilation Adjustments in minute ventilation were robust in TH-Cre mice throughout the 5min exposure to 12% O_2 (30s: 86 ± 5%; 100s: 63 ± 4%; 300s: 61 ± 5%) and 8% O_2 (30s: 92 ± 6%; 100s: 29 ± 5%; 300s: 65 ± 5; Figure 3.6 – Panel A,B iii

and Table 3.4). As would be expected given the above, however, deletion of *Lkb1* in catecholaminergic cells led to significant attenuation of minute ventilation during hypoxia. The degree of attenuation increased with the severity of hypoxia, between 12% O_2 (30s: 41 ± 7%; 100s: 33 ± 6%; 300s: 23 ± 6%, $p < 0.0001$) and 8% O_2 (30s: 42 ± 6%; 100s: 13 ± 6%; 300s: 36 ± 6%, $p < 0.0001$; Figure 3.6 – Panel A,B iii and Table 3.4).

Collectively, these data strongly suggest that the tumor suppressor kinase *Lkb1* is required for the modulation by hypoxia of catecholaminergic oxygen-sensing cells and thereby underpins the ventilatory response to hypoxia. Interestingly, preliminary studies I performed demonstrated that the alternative AMPK upstream kinase, Ca^{2+}-dependent CaMKK-β, is without effect on the ventilatory response to hypoxia (Appendix 3C). That aside, it was notable that *Lkb1* knockout mice would lie down and barely move during all exposures to 8% O_2, but not 12% O_2, and this was never observed for TH-Cre or C57/Bl6 mice (Appendix 3D). Therefore it is possible that these mice adjust behaviours in order to reduce O_2 requirements when unable to compensate for a fall in PO_2 supply by increased ventilation.

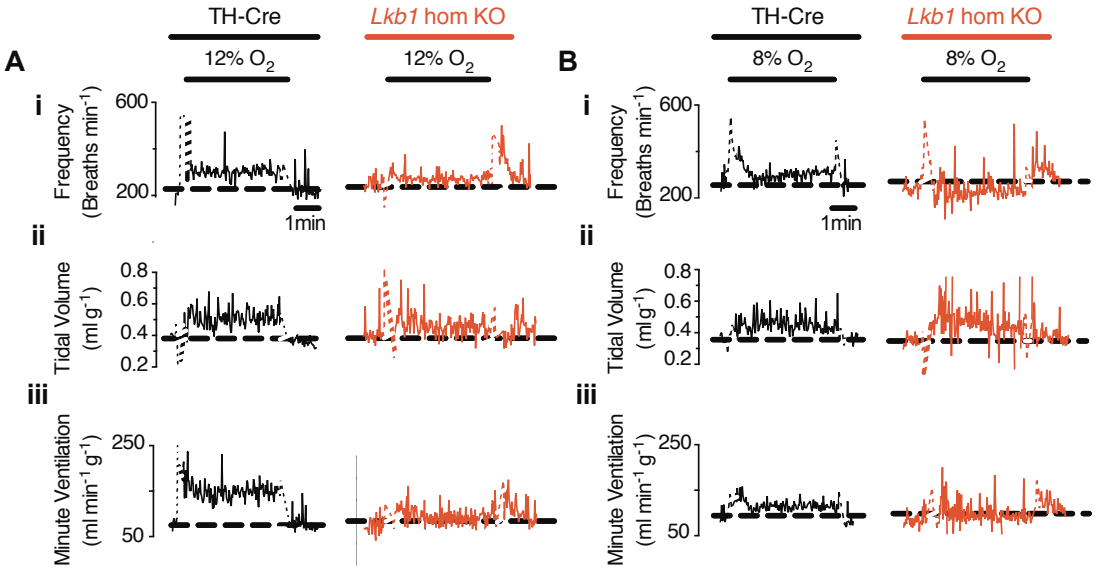

Figure 3.5: *Lkb1* deletion attenuates the ventilatory response in a manner that is PO_2-dependent. The effect over a 5min period of exposure to **(A)** mild hypoxia (12% O_2) and **(B)** severe hypoxia (8% O_2) on **(i)** breathing frequency (min^{-1}), **(ii)** tidal volume (ml g^{-1}) and **(iii)** minute ventilation (ml min^{-1} g^{-1}) in TH-Cre (black) and *Lkb1* homozygous knockout mice (*Lkb1* hom KO, red) with 2s sampling periods. Dashed black line indicating basal level, white line breaks indicate artefact of gas exchange.

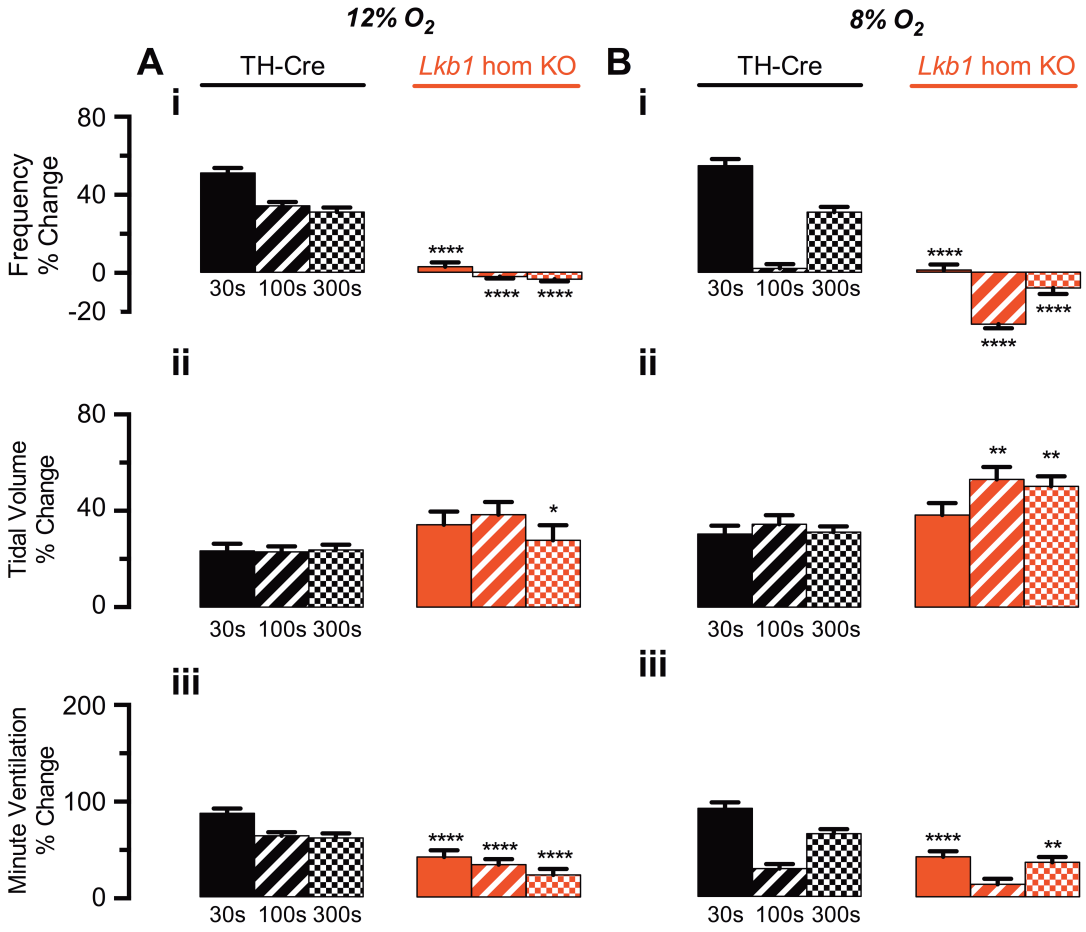

Figure 3.6: The mean ventilatory response to hypoxia is attenuated in *Lkb1* homozygous knockout mice. Mean ± SEM for percent change during **(A)** mild hypoxia (12% O_2) and **(B)** severe hypoxia (8% O_2) in **(i)** breathing frequency (min^{-1}), **(ii)** tidal volume (ml g^{-1}) and **(iii)** minute ventilation (ml min^{-1} g^{-1}) of mice at 3 time points during the 5min hypoxic exposure in TH-Cre (12% O_2: n = 25 exposures from 5 mice; 8% O_2: n = 37 exposures from 4 mice, black) and *Lkb1* homozygous knockout mice (*Lkb1* hom KO; 12% O_2: n = 22 exposures from 4 mice; 8% O_2: n = 30 exposures from 4 mice, red). * = $p < 0.05$, ** = $p < 0.01$, **** = $p < 0.0001$. Significance tested by one-way ANOVA with Bonferroni multiple comparisons.

Table 3.2: Mean percentage change in breathing frequency during hypoxia

	Breathing Frequency (% Change)						Related Figure
	12% O_2			8% O_2			
	30s	100s	300s	30s	100s	300s	
TH-Cre	51 ± 3	34 ± 2	31 ± 2	55 ± 3	2 ± 2	31 ± 3	3.6 & 3.14
	n = 25 exposures from 5 mice			n = 37 exposures from 5 mice			
Lkb1 floxed	40 ± 3	20 ± 2	16 ± 2	25 ± 5	-14 ± 4	-1 ± 4	
	n = 14 exposures from 4 mice			n = 15 exposures from 4 mice			
Lkb1 knockouts	3 ± 2	-2 ± 1	-3 ± 1	1 ± 3	-27 ± 2	-8 ± 3	
	n = 22 exposures from 4 mice			n = 30 exposures from 4 mice			

Table 3.3: Mean percentage change in tidal volume during hypoxia

	Tidal Volume (% Change)						Related Figure
	12% O_2			8% O_2			
	30s	100s	300s	30s	100s	300s	
TH-Cre	23 ± 3	23 ± 2	24 ± 2	31 ± 4	35 ± 4	31 ± 2	3.6 & 3.14
	n = 25 exposures from 5 mice			n = 37 exposures from 5 mice			
Lkb1 floxed	33 ± 4	25 ± 3	22 ± 3	36 ± 5	27 ± 4	26 ± 3	
	n = 14 exposures from 4 mice			n = 15 exposures from 4 mice			
Lkb1 knockouts	34 ± 5	38 ± 5	28 ± 6	38 ± 5	53 ± 5	51 ± 4	
	n = 22 exposures from 4 mice			n = 30 exposures from 4 mice			

Table 3.4: Mean percentage change in minute ventilation during hypoxia

	Minute Ventilation (% Change)						Related Figure
	12% O_2			8% O_2			
	30s	100s	300s	30s	100s	300s	
TH-Cre	86 ± 5	63 ± 4	61 ± 5	92 ± 6	29 ± 5	65 ± 5	3.6 & 3.14
	n = 25 exposures from 5 mice			n = 37 exposures from 5 mice			
Lkb1 Floxed	87 ± 7	50 ± 5	42 ± 5	70 ± 9	9 ± 7	25 ± 6	
	n = 14 exposures from 5 mice			n = 15 exposures from 5 mice			
Lkb1 Knockout	41 ± 7	33 ± 6	23 ± 6	42 ± 6	13 ± 6	36 ± 6	
	n = 22 exposures from 4 mice			n = 30 exposures from 4 mice			

3.2.1.3a The effects of *Lkb1* deletion on breathing frequency are driven by changes to the duration of inspiration and expiration

Given the above it seemed likely that further insight might be obtained from analyses of inspiration time, expiration time, and total breath duration, as this would allow us to determine whether or not the adjustments in the duration(s) of inspiratory and/or expiratory phases of ventilation are compromised in *Lkb1* knockouts. Figures 3.7 and 3.8 show example and averaged (mean ± SEM) records, respectively, of the ratiometric change (Hypoxia/Normoxia) in inspiration time (Ti), expiration time (Te), and total breath time (To) during mild (12% O_2) and severe hypoxia (8% O_2) in control TH-Cre and *Lkb1* knockout mice.

Inspiration Time (Ti) Upon exposure to 12% O_2 and 8% O_2, control TH-Cre mice exhibited a time dependent change in Ti. This involved a reduction in Ti duration relative to normoxia at the start of the 5min exposure to hypoxia at 30s before a gradual prolongation is observed which plateaus by 2min and remains stable for the remainder of the 5min exposure. This is demonstrated by the measured mean ± SEM of Ti at 30s as well as the overall mean ± SEM of Ti during the final 2min of the hypoxic exposure from 3 – 5min (using the formula for error of propagation to calculate the SEM). In the control TH-Cre mice, mean Ti at 30s slightly decreases relative to normoxia to 0.92 ± 0.08 (n = 12 exposures from 4 mice) and 0.90 ± 0.06 (n = 18 exposures from 4 mice) during 12% O_2 and 8% O_2, respectively; this therefore equates to a faster inspiration phase during mild and severe hypoxia when compared to normoxia (Figure 3.8 – Panel A). Thereafter, Ti progressively lengthened in a time-dependent manner until Ti under hypoxia was similar in duration to Ti under normoxia. This is indicated by the overall mean ratio observed during the plateaued final 2min of the hypoxic exposure, which was 1.08 ± 0.02 under 12% O_2 and 1.07 ± 0.02 under 8% O_2 in control TH-Cre mice (Figure 3.8 – Panel A).

In the *Lkb1* knockouts, a time-dependent change in Ti was also observed during hypoxia. Once more an initial shortening of Ti was observed at 12% and 8% O_2. However, relative to the TH-Cre mice the reduction in inspiration time at 30s slightly greater as indicated by the mean ratio of 0.76 ± 0.04 (n = 11 exposures from 4 mice) and

0.83 ± 0.09 (n = 9 exposures from 4 mice) at 12% and 8% O_2, respectively, not significantly different by unpaired student's t-test). A PO_2-dependent lengthening of Ti was also observed to a level that exceeded Ti during normoxia during the final 2min under 12% O_2 (1.16 ± 0.03) and 8% O_2 (1.26 ± 0.04), and was significantly longer than mean Ti observed in control TH-Cre mice during the final 2min of the hypoxic exposures to 12% O_2 ($p < 0.05$) and 8% O_2 ($p < 0.0001$) (Figure 3.8A). Therefore, in response to hypoxia, both control TH-Cre mice and *Lkb1* knockouts exhibit an initial shortening of inspiration time relative to normoxia. Thereafter, the inspiratory phase in TH-Cre recovers during hypoxia back to values equivalent to those observed under normoxia, in contrast, the duration of inspiration in *Lkb1* knockouts overshoots the inspiration time observed under normoxia.

Expiration time (Te) Unlike Ti, Te of TH-Cre mice decreased relative to normoxia in a manner that was maintained throughout the 5min exposure to 12% O_2 and 8% O_2. Therefore, these mice exhibited a shortening of expiration time during hypoxia (Figure 3.8 – Panel B). Reductions in Te exhibited time-dependent characteristics but, similar to Ti, plateaus by 2min of the hypoxic exposure. Initially, there was a marked reduction in Te relative to normoxia at 30s during 12% O_2 (0.64 ± 0.07) and 8% O_2 (0.52 ± 0.05). Thereafter, mean ratio of Te lengthened slightly during the final 2min of 12% O_2 (0.71 ± 0.02) and 8% O_2 (0.82 ± 0.02). Surprisingly, *Lkb1* knockouts exhibited a greater reduction in Te at 30s relative to controls during 12% O_2 (0.53 ± 0.06, not significantly different). However, virtually no change in Te was observed relative to normoxia at 30s upon exposure to 8% O_2 (0.96 ± 0.24), and was significantly longer than TH-Cre mice ($p < 0.0001$). The mean ratio of Te then progressively increased in a PO_2-dependent manner, with a mean of 0.90 ± 0.03 measured during the final 2min with 12% O_2 and 1.0 ± 0.04 with 8% O_2 (Figure 3.8 – Panel B). Overall, this suggests that deletion of *Lkb1* in catecholaminergic cells not only attenuates reductions in Te but also, paradoxically, results in a time-dependent prolongation of Te to levels comparable to those observed during normoxia.

Total breath Duration (To) In controls, outcomes for Ti and Te translated into reductions in *To* during 12% and 8% O_2; consistent with observed increases in breathing

frequency (3.2.1.3). Initially *To*, relative to normoxia, fell at 30s to 0.70 ± 0.05 during 12% O_2 and 0.56 ± 0.01 during 8% O_2, before slightly lengthening to 0.79 ± 0.01 and 0.77 ± 0.02, respectively, during the final 2min of the hypoxic exposure in TH-Cre mice (Figure 3.8 – Panel C). Surprisingly, at the start of 12% O_2 at 30s, *Lkb1* deletion was with an enhanced initial reduction in *To* at 12% O_2 (0.60 ± 0.01), although not significantly different when compared to TH-Cre mice. In contrast*, Lkb1* deletion was with an attenuated reduation in *To* at 30s under 8% O_2 (0.91 ± 0.19), however again not significantly different when compared to TH-Cre mice (Figure 3.8 – Panel C). Thereafter, *To* significantly lengthened relative to controls and approached *To* durations observed during normoxia at both 12% O_2 (0.98 ± 0.03, $p < 0.0001$) and 8% O_2 (1.10 ± 0.04, $p < 0.0001$) (Figure 3.8 – Panel C).

Therefore, reductions in expiration time drives a fall in overall *To*, and hence an increase in breathing frequency, during hypoxia in a manner that likely requires Lkb1-dependent modulation of cateholaminergic inputs to the respiratory central pattern generators (rCPGs).

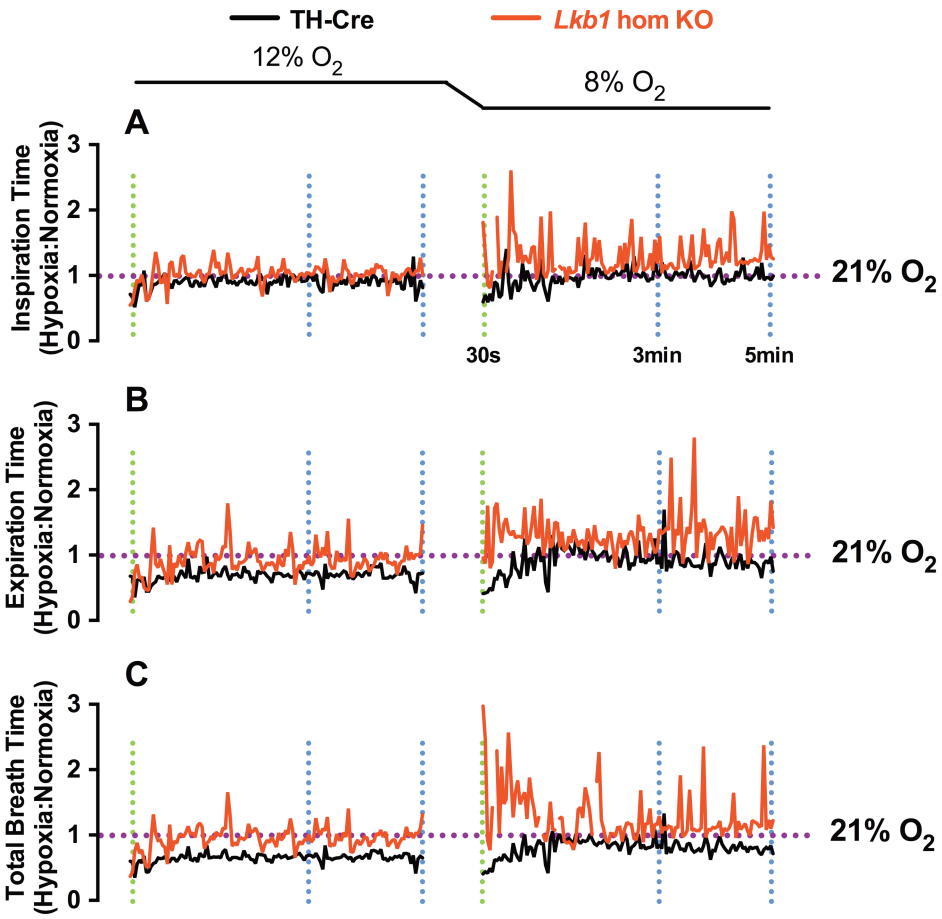

Figure 3.7: The effect of *Lkb1* deletion on the durations of inspiration, expiration and total breath during hypoxia. Example records of the ratiometric changes (relative to normoxia as indicated by dotted line at 1.0, 21% O_2) in the duration (s) of **(A)** inspiration (Ti), **(B)** expiration (Te) and **(C)** total breath (To) over a 5min exposure with 2s sampling periods during mild hypoxia (12% O_2, *left panels*) and **(B)** severe hypoxia (8% O_2, *right panels*) in TH-Cre (black) and *Lkb1* homozygous knockout (*Lkb1* hom KO, red). 30s following the onset of hypoxia indicated by green vertical dotted line; 3-5min indicated by blue vertical dotted lines.

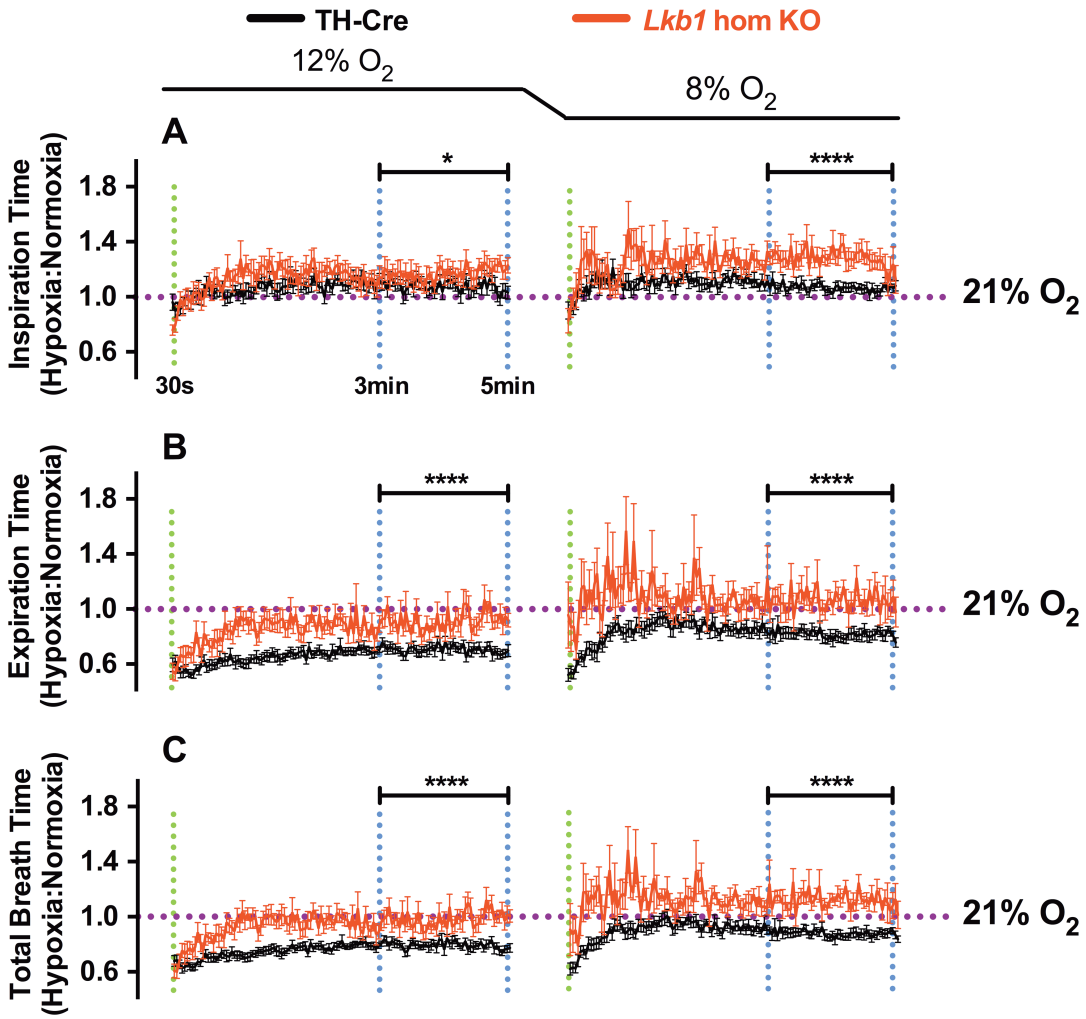

Figure 3.8: The effect of *Lkb1* deletion on the mean duration of inspiration, expiration and total breath time during hypoxia. The mean ± SEM of the ratiometric change (relative to normoxia as indicated by purple dotted line at 1.0, 21% O_2) in **(A)** inspiration time (Ti), **(B)** expiration time (Te), and **(C)** total breath time (To) over a 5min exposure with 2s sampling periods to mild hypoxia (12% O_2) and severe hypoxia (8% O_2) in TH-Cre (black) and *Lkb1* homozygous knockout (*Lkb1* hom KO, red) mice. (TH-Cre - 12% O_2: n = 12 exposures from 4 mice, 8% O_2: n = 18 exposures from 4 mice; *Lkb1* hom KO - 12% O_2: n = 11 exposures from 4 mice, 8% O_2: n = 9 exposures from 4 mice), * = $p < 0.05$, **** = $p < 0.0001$. Unpaired student's t-test was used to test for significance at 30s following the onset of hypoxia (indicated by green vertical dotted line) and from 3-5min (as indicated by blue vertical dotted lines).

3.2.1.3b The effects of *Lkb1* deletion on tidal volume during hypoxia are driven by changes in the duration of inspiration and expiration

When analysing tidal volume during hypoxia as a percentage change from normoxia, *Lkb1* knockouts exhibited greater increases relative to control mice during hypoxia (Section 3.2.1.3). There are two possible explanations for this phenomenon: (1) an increase in the volume of air moved per unit time, or (2) prolonged total breath time relative to normoxia. To determine the relative contribution of these two processes, a different method of ratiometric analysis was performed. Here tidal volume was divided by inspiration (Tv/Ti), expiration (Tv/Te), and total breath time (Tv/To). Figures 3.9 and 3.10 show example and averaged (mean ± SEM) records against time for each of the ratiometric indices relative to values observed during normoxia.

Tv/Ti In both TH-Cre and *Lkb1* knockout mice, time-dependent changes in Tv/Ti were observed. During 12% O_2, Tv/Ti increased at 30s to 1.43 ± 0.11 in controls and comparably to 1.43 ± 0.16 in the *Lkb1* knockouts. Thereafter Tv/Te similarly returned to levels similar to Tv/Te normoxia in TH-Cre mice (1.10 ± 0.03) and *Lkb1* knockouts (1.09 ± 0.03) during the final 2min of the 5min hypoxic exposure (Figure 3.10 – Panel A). Upon exposure to 8% O_2, a comparable, initial increase was also observed in controls (1.54 ± 0.11) and *Lkb1* knockouts (1.63 ± 1.16). However, while controls were able to maintain a Tv/Ti greater than that observed under normoxia during the final 2min of the exposure (1.19 ± 0.02), *Lkb1* knockouts could not (1.05 ± 0.03, $p < 0.001$).

Tv/Te Time-dependent adjustments were also observed in Tv/Te in both control and knockout mice during hypoxia (Figure 3.10 – Panel B). Under 12% O_2, the initial increase at 30s was comparable at 2.09 ± 0.21 and 2.29 ± 0.40 in control and *Lkb1* knockouts, respectively. Thereafter, the change in Tv/Te declined to a level still markedly greater than that observed under normoxia in controls from 3-5min (1.69 ± 0.05). This was also apparent in the *Lkb1* knockouts as Tv/Te declined to 1.44 ± 0.05. However, when compared to TH-Cre mice the decline was significantly enhanced, and accordingly Tv/Te in the *Lkb1* knockouts was significantly lower ($p < 0.01$).

Under 8% O_2, Tv/Te also increased to a comparable level at 30s in TH-Cre (2.70 ± 0.21) and *Lkb1* knockouts (2.22 ± 0.49). However, differences between the controls

and knockouts were apparent of Tv/Te from 3-5min of the hypoxic exposure. In TH-Cre mice, Tv/Te declined to 1.60 ± 0.05 while this decline was more enhanced in the *Lkb1* knockouts as it further declined to 1.32 ± 0.05 ($p < 0.001$, Figure 3.10 – Panel B).

Tv/To Overall, the above translated into a time-dependent change of Tv/To during 12% and 8% O_2 in TH-Cre and *Lkb1* knockout mice. At the start of both exposures, Tv/To at 30s of *Lkb1* knockout mice (12% O_2: 1.91 ± 0.29; 8% O_2: 2.00 ± 0.33) was comparable to control (12% O_2: 1.80 ± 0.15; 8% O_2: 2.22 ± 0.17). Thereafter, however, while Tv/To only marginally decreased in TH-Cre mice to 1.44 ± 0.04 during 12% O_2 and 1.46 ± 0.04 during 8% O_2, a pronounced fall in Tv/To was observed in *Lkb1* knockouts during both 12% O_2 (1.31 ± 0.04, $p < 0.01$) and 8% O_2, (1.20 ± 0.04, $p < 0.0001$) (Figure 3.10 – Panel C). Given that inspiration time is significantly longer in the *Lkb1* knockouts compared to controls, this suggests that the increase in tidal volume relative to control mice results from a prolongation of breath duration and not a compensatory increase in the volume of air moved per unit time.

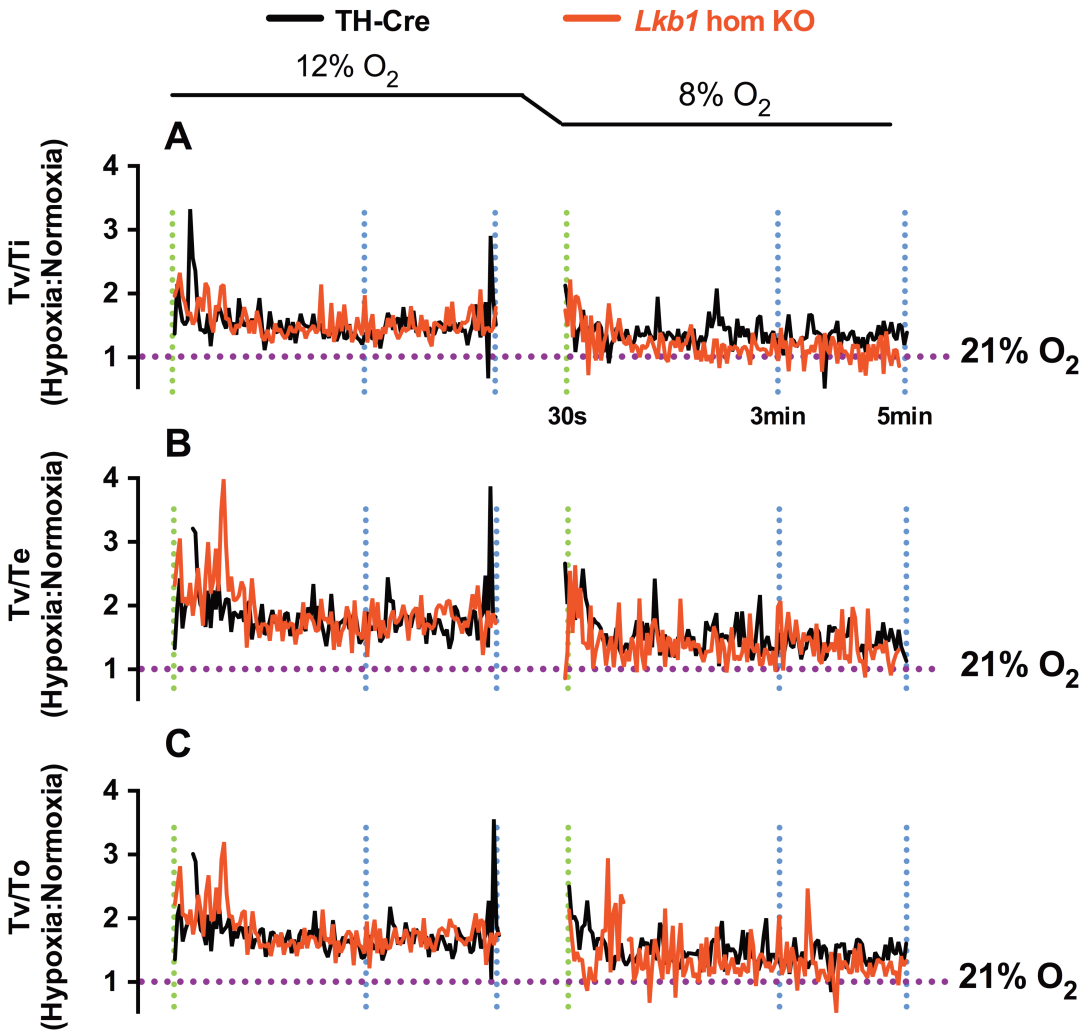

Figure 3.9: Example records of tidal volume relative to the duration of inspiration, expiration and total breath duration. Example records of the ratiometric changes (relative to normoxia as indicated by dotted line at 1.0, 21% O_2) in tidal volume (Tv) relative to the duration of **(A)** inspiration (Tv/Ti), **(B)** expiration (Tv/Te), and **(C)** total breath duration (Tv/To) over a 5min exposure during mild hypoxia (12% O_2, *left panels*) and severe hypoxia (8% O_2, *right panels*) in TH-Cre (black) and *Lkb1* homozygous knockout (*Lkb1* hom KO, red) mice. 30s following the onset of hypoxia indicated by green vertical dotted line; 3-5min indicated by blue vertical dotted lines.

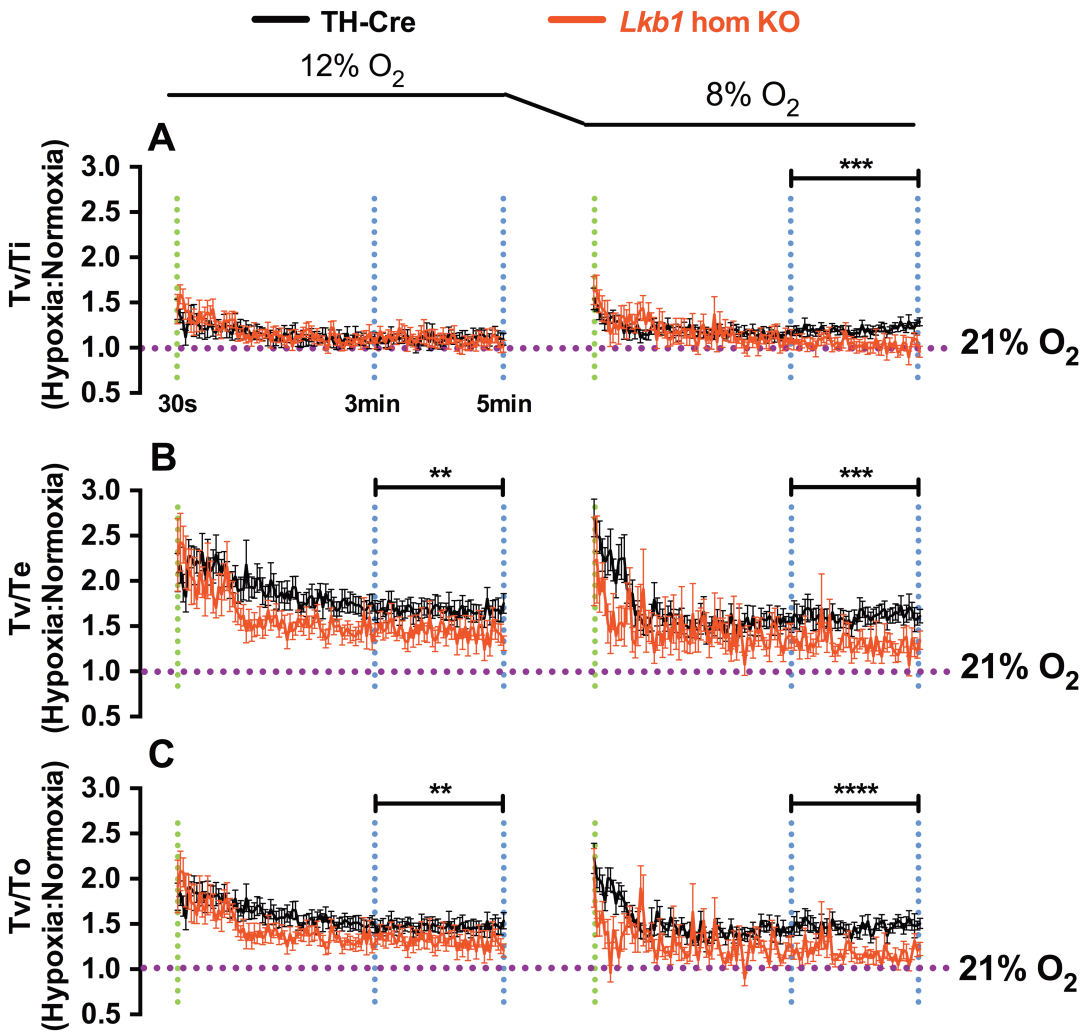

Figure 3.10: The effects of *Lkb1* deletion on tidal volume is driven by changes in inspiration, expiration, and total breath duration during hypoxia. The mean ± SEM of the ratiometric change in tidal volume (Tv) relative to the duration of **(A)** inspiration (Tv/Ti), **(B)** expiration (Tv/Te), and **(C)** total breath duration (Tv/To) over a 5min exposure during mild hypoxia (12% O_2, *left panels*) and severe hypoxia (8% O_2, *right panels*) in TH-Cre (black) and *Lkb1* homozygous knockout (*Lkb1* hom KO, red) mice. (TH-Cre - 12% O_2: n = 12 exposures from 4 mice, 8% O_2: n = 18 exposures from 4 mice; *Lkb1* hom KO - 12% O_2: n = 11 exposures from 4 mice, 8% O_2: n = 9 exposures from 4 mice). ** = $p < 0.01$, *** = $p < 0.001$, **** = $p < 0.0001$. Unpaired student's t-test was used to test for significance at 30s following the onset of hypoxia (indicated by green vertical dotted line) and from 3-5min (as indicated by blue vertical dotted lines).

3.2.2 Hypoxia-induced ventilatory abnormalities are more severe in the *Lkb1* knockouts than in the hypomorphic *Lkb1* floxed mice

As mentioned before, previous studies on *Lkb1* floxed mice have identified that LKB1 protein expression and activity were markedly reduced by up to 10-fold in the testis, skeletal muscle, heart, liver and kidney. In contrast, expression and activity of LKB1 in the brain was only slightly reduced by ~ 1-fold (Sakamoto et al., 2005). This therefore raises the possibility that the hypomorphic nature of the *Lkb1* floxed mice may contribute to the overall ventilatory phenotype observed in the *Lkb1* knockouts. That is, the hypoxia-induced ventilatory abnormalities observed in the *Lkb1* knockouts may not entirely be a result of the complete deletion of *Lkb1* in catecholaminergic cells, but possibly due to *Lkb1* hypomorphism in TH-negative cells. Hence, it was vital to determine the underlying effects of *Lkb1* hypomorphism on the ventilatory response to hypoxia. This was accomplished by studying the ventilatory response to 12% O_2 and 8% O_2 of *Lkb1* homozygous floxed mice (as described in Chapter 2).

3.2.2.1 The effects of *Lkb1* hypomorphism on the apnoea-duration index

Ventilatory traces obtained using unrestrained whole body plethysmography revealed that, when compared to control TH-Cre mice, the hypomorphic nature of the *Lkb1* floxed mice induced more frequent and prolonged apnoeas in a manner inversely related to PO_2. However, this increase was significantly less than that exhibited following the complete deletion of *Lkb1* in catecholaminergic cells in the *Lkb1* knockouts.

As described above, apnoeas were identified as a cessation of breathing for a duration that is at least equivalent to the duration of two regular breaths (i.e. two respiratory cycles have been missed, (Y.-J. Peng et al., 2011; Nakamura and Kuwaki, 2004; Voituron et al., 2009), which equated to a cessation ≥500ms in our experimental mice. Figure 3.11 and table 3.1 show the calculated means ± SEM for the apnoeic index (apnoeas/min), apnoea duration, and apnoea duration index (product of apnoeic index and duration) during normoxia (21% O_2 + 0.05% CO_2), mild hypoxia (12% O_2 + 0.05% CO_2), and severe hypoxia (8% O_2 + 0.05% CO_2) for the control TH-Cre mice,

hypomorphic *Lkb1* floxed mice, and the conditional *Lkb1* knockouts. As described above, the increase in apnoea frequency observed in TH-Cre mice appeared marginally PO_2-dependent, as it significantly increased from 0.23 ± 0.08 apnoeas min^{-1} (n = 19 from 5 mice) during 12% O_2 to 1 ± 0.2 apnoeas min^{-1} (n = 24 from 5 mice) during 8% O_2 ($p < 0.001$, by one-way ANOVA). The mean duration of apneoas, however, exhibited no PO_2-dependence, as it was comparable at 577 ± 20ms and 629 ± 15ms during exposures to 12% O_2 and 8% O_2, respectively (Table 3.1). The *Lkb1* floxed mice exhibited an increase in the frequency and duration of apnoeas which was comparable to TH-Cre mice during 12% O_2 (apnoea index: 0.14 ± 0.05 min^{-1}; apnoea duration: 650 ± 32ms; n = 16 from 4 mice) but significantly greater under 8% O_2, (apnoeic index: 3.47 ± 0.57 min^{-1}, $p < 0.05$; apnoea duration: 769 ± 18 ms, $p < 0.0001$; n = 15 from 4 mice). Importantly, the PO_2-dependent increases in the apnoea frequency and duration observed in the *Lkb1* floxed mice were significantly less than that observed in the *Lkb1* knockouts under both 12% O_2 and 8% O_2 (Figure 3.11 and Table 3.1).

Overall, this translated to a PO_2-dependent increase in the apnoea-duration index, which is significantly greater for *Lkb1* floxed mice at 8% O_2 but not 12% O_2 (12% O_2: 0.7 ± 0.2; 8% O_2: 2.7 ± 0.5; $p < 0.0001$) than for TH-Cre mice (12% O_2: 0.3 ± 0.1; 8% O_2: 0.7 ± 0.1; Figure 3.11 – Panel Biii). However, the increase is greater still with complete deletion of *Lkb1* in catecholaminergic cells as the *Lkb1* knockouts exhibit a PO_2-dependent increase in the apnoea duration index that is significantly greater than TH-Cre and *Lkb1* floxed mice under 12% O_2 (3.0 ± 0.8; $p < 0.001$ when compared to TH-Cre and *Lkb1* floxed mice) and 8% O_2 (5.4 ± 0.6; $p < 0.0001$ when compared to TH-Cre and $p < 0.01$ when compared to *Lkb1* floxed mice).

That *Lkb1* floxed mice exhibited similar PO_2-dependent increases in the apnoeic index, apnoea duration, and apnoea-duration index although milder than the conditional *Lkb1* knockouts suggests that the effects observed in the *Lkb1* floxed mice is a result of deficiencies in LKB1 expression in a similar cell-type or common circuit, i.e. in catecholaminergic cells.

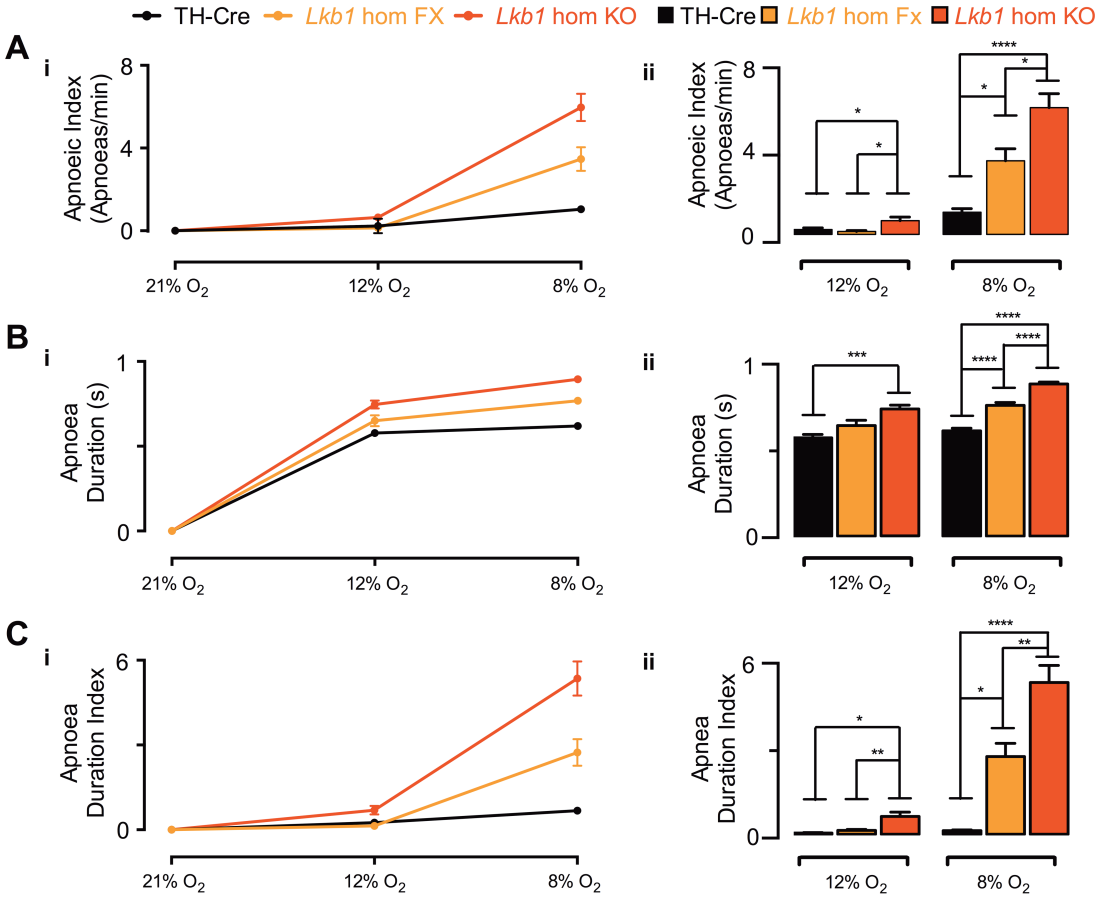

Figure 3.11: The increased effects from *Lkb1* hypomorphism to complete deletion of *Lkb1* in catecholaminergic cells on the apnoea-duration index. The mean ± SEM of the **(A)** apnoeic index (apnoeas/min), **(B)** apnoea duration (s), and **(C)** apnoea duration index during nomoxia (21% O_2), mild hypoxia (12% O_2), and severe hypoxia (8% O_2) in control TH-cre mice (black), hypomorphic *Lkb1* homozygous floxed mice (*Lkb1* hom FX, orange), and conditional *Lkb1* homozygous knockout (*Lkb1* hom KO, red). The line graphs are re-illustrated as bar charts **(A-C, ii)** to display significant differences tested using one-way ANOVA with Bonferroni multiple comparisons. * = $p < 0.05$, ** = $p < 0.01$, *** = $p < 0.001$, **** = $p < 0.0001$. (TH-Cre - 21% O_2: n = 20 from 5 mic3; 12% O_2: n = 19 from 5 mice; 8% O_2: n = 24 from 5 mice) (*Lkb1* hom FX: 21% O_2: n = 20 from 4 mice; 12% O_2: n = 16 from 4 mice; 8% O_2: n = 15 from 4 mice) (*Lkb1* hom KO: 21% O_2: n = 20 from 4 mice; 12% O_2: n = 17 from 4 mice; 8% O_2: n = 29 from 4 mice).

Consistent with the milder increase in the apnoea-duration index in the *Lkb1* floxed mice at 12% O_2 and 8% O_2, ventilatory abnormalities also appeared less severe when compared to the *Lkb1* knockout mice on an expanded time scale (Figure 3.12). Under 12% O_2, the maximum apnoea duration observed was ~840ms in *Lkb1* floxed mice, which is similar to the maximum duration observed in the TH-Cre mice at ~830ms. By contrast, the maximum apnoea duration observed under 12% O_2 in the *Lkb1* knockouts was ~1.0s. The difference in the maximum apnoea duration is more apparent however under 8% O_2, which was lowest at ~900s in the TH-Cre mice, then ~2.5s in the hypomorphic *Lkb1* floxed mice, and longest at ~4.0s in the *Lkb1* knockouts.

Nevertheless, while the apnoeas appeared slightly prolonged in the *Lkb1* floxed mice when compared to the TH-Cre mice, the nature of the apnoeas observed in both control TH-Cre and *Lkb1* floxed mice were similar as they preceded with a sigh (an exaggerated breath with an inspiratory and expiratory amplitude, i.e. tidal volume, at least twice as large as the inspiratory and expiratory amplitude of the three previous breaths (Voituron et al., 2009). In contrast, the *Lkb1* knockouts exhibit severely disordered breathing which did not simply include more frequent and prolonged apnoeas, but additionally periods of hypoventilation, spontaneous apnoeas, and Cheyne-Stokes-like breathing (Figure 3.12).

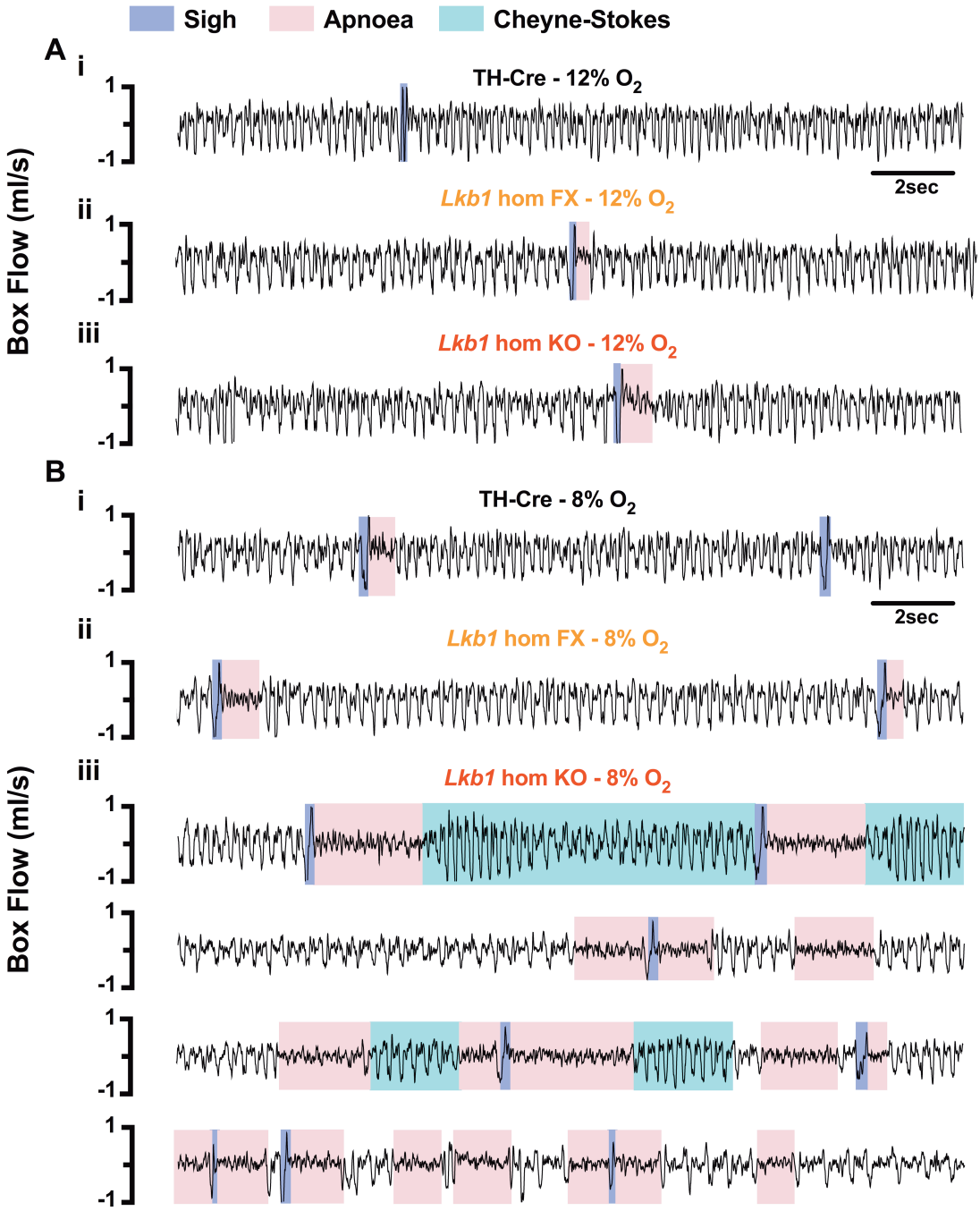

Figure 3.12: *Lkb1* hypomorphism precipitates abnormalities in ventilatory pattern that are milder than the *Lkb1* knockouts. Typical ventilatory records on an expanded time scale during **(A)** mild hypoxia (12% O_2) and **(B)** severe hypoxia (8% O_2) from **(i)** TH-Cre and **(ii)** *Lkb1* homozygous floxed mice (*Lkb1* hom FX).

3.2.2.2 Poincaré analysis reveals the increase in disordered breathing from *Lkb1* floxed mice to conditional *Lkb1* knockouts

Whether considering the reduced breathing frequency or post-sigh apnoeas, *Lkb1* hypomorphism led to breathing irregularities that increased in severity in a PO_2-dependent manner but to a significantly less extent than with complete deletion of *Lkb1* in catecholaminergic cells. This was confirmed by plotting the interbreath interval (BBn) versus the subsequent interbreath interval (BBn+1) to generate Poincaré plots. Example Poincaré plots of 500 breaths from a single exposure period are shown in Figure 3.3, which compares the regularity of breathing between TH-Cre, *Lkb1* floxed mice, and *Lkb1* knockouts during normoxia (21% O_2), mild hypoxia (12% O_2) and severe hypoxia (8% O_2).

Clearly the variability in the interbreath interval is comparable in TH-Cre, *Lkb1* floxed mice, and *Lkb1* knockouts under normoxic (21% O_2) conditions (Figure 3.13 – Panel A). In control TH-Cre mice, the regularity of breathing remained comparable when switching from 21% O_2 to 12% O_2 but marginally increased upon switching form 21% O_2 to 8% O_2. Similarly, in *Lkb1* floxed mice the regularity of breathing appeared comparable to TH-Cre mice when switching from 21% O_2 to 12% O_2, but markedly increased when switching from 21% O_2 to 8% O_2 (Figure 3.13 – Panels A-C).

The fact that the increase in breathing irregularity in *Lkb1* floxed mice appeared markedly greater than that observed in control TH-Cre mice under 8% O_2 and not 12% O_2 was confirmed by comparison of the variability by standard deviation (SD) of the BBn and BBn+1 (Figure 3.13 – Panels A-C, *lower panels*). Under 12% O_2, the SD in TH-Cre and *Lkb1* floxed mice were comparable as it reached 47 ± 2ms (n = 20 exposures from 4 mice) and 49 ± 4ms (n = 16 exposures from 4 mice), respectively. By contrast, while the SD further increased in TH-Cre mice under 8% O_2 to 65 ± 2ms (n = 24 exposures from 5 mice), the increase was greater still in the *Lkb1* floxed mice as it reached 98 ± 8ms (n = 15 exposures from 4 mice, $p < 0.01$). However, the effects of *Lkb1* hypomorphism on the regularity of breathing was significantly less severe than that observed in *Lkb1* knockouts with complete deletion of *Lkb1* in catecholaminergic cells

during 12% O_2 (85 ± 3ms, n = 17 exposures from 4 mice, $p < 0.0001$) and 8% O_2 (153 ± 6ms, n = 28 exposures from 4 mice, $p < 0.0001$).

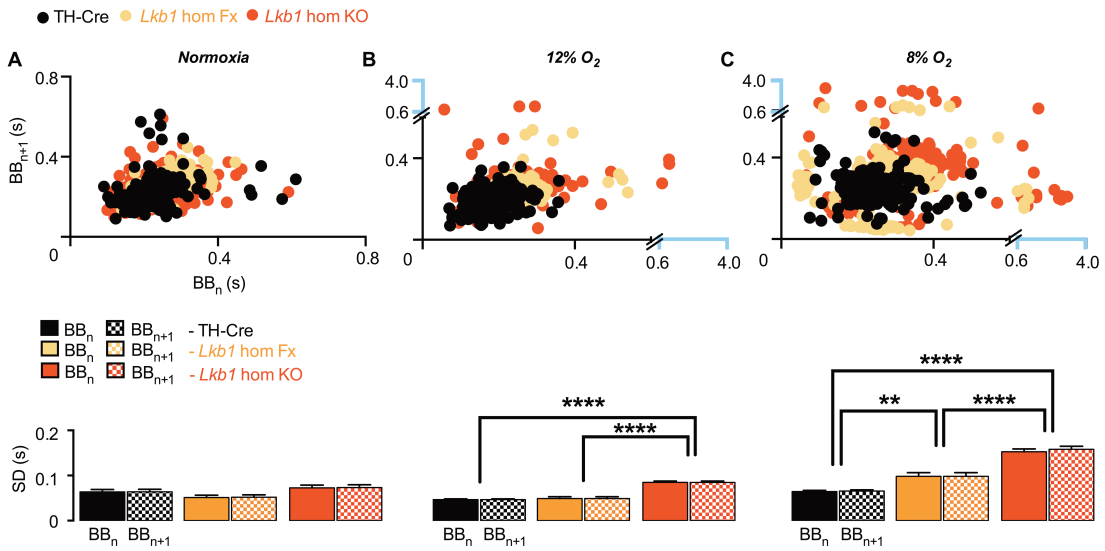

Figure 3.13: The increased effects of *Lkb1* hypomorphism to complete deletion of *Lkb1* in catecholaminergic cells on the regularity of breathing. *Upper panels* show Poincaré plots of the inter-breath interval (BB_n) versus subsequent interval (BB_{n+1}) of TH-Cre (black), *Lkb1* homozygous floxed mice (*Lkb1* hom FX, orange), and *Lkb1* homozygous knockout mice (*Lkb1* hom KO, red) during **(A)** normoxia (21% O_2 + 0.05% CO_2), **(B)** mild hypoxia (12% O_2 + 0.05% CO_2), and **(C)** severe hypoxia (8% O_2 + 0.05% CO_2). The corresponding *lower panels*, show the mean ± SEM for the standard deviation (SD) of BB_n and BB_{n+1} of each genotype under normoxia (TH-Cre: n = 25; *Lkb1* hom FX: n = 16; *Lkb1* hom KO: n = 14), mild hypoxia (TH-Cre n = 20, *Lkb1* hom FX: n = 16; *Lkb1* hom KO: n = 17) and severe hypoxia (TH-Cre: n = 24, *Lkb1* hom FX: n = 15; *Lkb1* hom KO: n = 28). ** = $p < 0.01$, **** = $p < 0.0001$. Significance tested by one-way ANOVA with Bonferroni multiple comparisons.

3.2.2.3 The effects of *Lkb1* hypomorphism on the hypoxic increase in breathing frequency, tidal volume, and minute ventilation

Figure 3.14 shows mean records for the changes in frequency, tidal volume, and minute ventilation (2s sampling period) over the 5min exposure to 12% O_2 and 8% O_2 in control TH-Cre, hypomorphic *Lkb1* floxed mice, and conditional *Lkb1* knockouts (this is also summarised in table 3.1). Consistent with the above, the degree of attenuation on the hypoxic increase in ventilation was more severe in the *Lkb1* knockouts than in the hypomorphic *Lkb1* floxed mice.

Breathing frequency As illustrated by the example records, when compared to control TH-Cre mice, *Lkb1* floxed mice exhibit an attenuated increase of breathing frequency during hypoxia across 3 different time points during 12% O_2. Initially, the breathing frequency in the control TH-Cre mice increased relative to normoxia at 30s by 51 ± 3% (n = 25 from 5 mice) before decreasing to 34 ± 2% at 100s and 31 ± 2% of normoxia by the end of the exposure at 300s (Figure 3.14 – Panel Ai). In marked contrast, in *Lkb1* floxed mice the initial increase in breathing frequency after 30s was significantly less at 40 ± 3% of that observed during normoxia (n = 14 from 4 mice, $p < 0.0001$) (Figure 3.14 – Panel Ai). Strikingly, respiratory depression, assessed after 100s, resulted in a further decrease in frequency until reaching 20 ± 2% ($p < 0.01$) relative to normoxia. Thereafter, the percentage change in the frequency remained significantly attenuated at 16 ± 2% ($p < 0.001$) for the remainder of the 5min exposure (Figure 3.14 – Panel Ai).

During severe hypoxia, 8% O_2, the impact of *Lkb1* hypomorphism on the average increase in breathing frequency was greater still but also time-dependent (Figure 3.14 – Panel Bi). Similar to 12% O_2, here it was notable that there was an initial robust increase in breathing frequency in TH-Cre control mice at 55 ± 3% (n = 37 exposures from 5 mice) before reducing to 2 ± 2% at 100s and then gradually increasing thereafter to 28 ± 4% by the end of the hypoxia (300s) (Figure 3.14 – Panel Bi). In contrast, a significant decrease was observed in the *Lkb1* floxed mice across all three different time points when compared to the control TH-Cre mice at 8% O_2. At 30s following the onset of hypoxia, the percentage change in frequency during 8% O_2 measured only 25 ± 3% (n =

15 exposures from 4 mice). Thereafter, measures taken at 100s demonstrated that respiratory depression reduced breathing frequency further in the *Lkb1* floxed mice to -14 ± 4% of that observed during normoxia, thereby indicating these mice are hypoventilating. Despite marginal recovery to -1 ± 4% of that observed under normoxia, breathing frequency remained below baseline levels until the end of the 5min exposure (Figure 3.14 – Panel Bi).

Consistent with the more severe effects of complete *Lkb1* deletion in catecholaminergic cells on the regularity of breathing during hypoxia, *Lkb1* knockouts exhibited an increase in breathing frequency that was markedly less than *Lkb1* floxed mice throughout the 5min exposure to 12% O_2 (30s: 3 ± 2%, $p < 0.0001$; 100s: -2 ± 1%, $p < 0.0001$; 300s: -3 ± 1%, $p < 0.0001$) and 8% O_2 (30s: 1 ± 3%, $p < 0.001$; 100s: -27 ± 2%, $p < 0.05$; 300s: -8 ± 1%)

Tidal volume As described above (section 3.2.1.3), in marked contrast to the time-dependence of the adjustments in breathing frequency, hypoxia induced a sustained increase in mean tidal volume in TH-Cre mice throughout the 5min exposure to 12% O_2 (30s: 23 ± 3%; 100s: 23 ± 2%; 300s: 24 ± 2%) and 8% O_2 (30s: 31 ± 4%; 100s: 35 ± 4%; 300s: 31 ± 2%) (Figure 3.14 – Panel A,Bii). A sustained increase in tidal volume was also observed in the *Lkb1* floxed mice to levels comparable in magnitude to that of TH-Cre throughout the 5min exposure to 12% O_2 (30s: 33 ± 4%; 100s: 25 ± 3%; 300s: 22 ± 3%; Figure 3.14 – Panel Aii) and 8% O_2 (30s: 36 ± 5%; 100s: 27 ± 4%; 300s: 26 ± 3% Figure 3.14 – Panel Bii).

Minute ventilation Overall, this translates to an increase in minute ventilation that is less attenuated in *Lkb1* floxed mice than in the *Lkb1* knockouts. As would be expected given the above, compared to the robust increase in minute ventilation in the TH-Cre mice throughout the 5min exposure to 12% O_2 (30s: 86 ± 5%; 100s: 63 ± 4%; 300s: 61 ± 5%) and 8% O_2 (30s: 92 ± 6%; 100s: 29 ± 5%; 300s: 65 ± 5%), *Lkb1* floxed mice exhibited a marginal attenuation of minute ventilation. However, the decrease in minute ventilation during 12% O_2 (30s: 87 ± 7%; 100s: 50 ± 5%; 300s: 42 ± 5%), did not reach significance when compared to TH-Cre mice when using a one-way ANOVA. Under 8% O_2, the decrease in minute ventilation also did not reach levels that were

significantly less when compared to TH-Cre at 30s (70 ± 9%) and (100s: 9 ± 7%). However, the attenuation reached significance at 300s as minute ventilation fell to 25 ± 6% (Figure 3.14 – Panel A,Biii, table 3.4).

In marked contrast, the attenuation in minute ventilation was more severe following complete deletion of *Lkb1* in catecholaminergic cells when compared to TH-Cre mice during both 12% O_2 and 8% O_2, as previously described in section 3.2.1.3 (Figure 3.14 and table 3.4). Collectively, these data indicate that the hypomorphic nature of the *Lkb1* floxed mice has underlying affects on the ventilatory response to hypoxia, in a PO_2-dependent manner. Whether this is a result of *Lkb1* hypomorphism within the cells of interest, namely the catecholaminergic cells, or from off target effects from LKB1 deficiencies in TH-negative cells is something that cannot be deduced from these experiments alone. However, that *Lkb1* floxed mice exhibit similar PO_2-dependent increases in the apnoeic index, apnoea duration, and apnoea-duration index, although milder than the conditional *Lkb1* knockouts, strongly suggests that the effects observed in the *Lkb1* floxed mice is a result of deficiencies in LKB1 expression in a similar cell-type or common circuit, i.e. in catecholaminergic cells and/or oxygen-sensing network. However, one cannot completely exclude a possible additive contribution of *Lkb1* hypomorphism in TH-negative cells with complete deletion of *Lkb1* in TH-positive cells to the disordered breathing observed in the *Lkb1* knockouts.

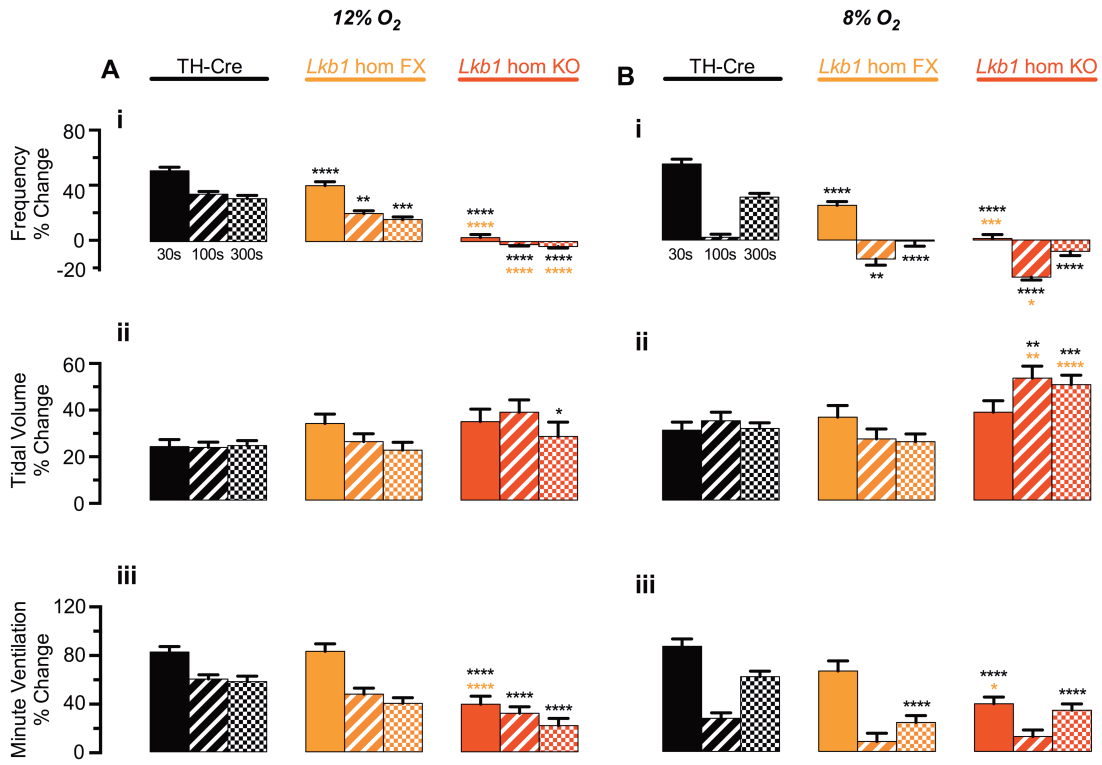

Figure 3.14: The effects of *Lkb1* hypomorphism on the hypoxic increase in breathing frequency, tidal volume, and minute ventilation. Mean ± SEM for percent change during **(A)** mild hypoxia (12% O_2) and **(B)** severe hypoxia (8% O_2) in **(i)** breathing frequency (min^{-1}), **(ii)** tidal volume (ml g^{-1}) and **(iii)** minute ventilation (ml min^{-1} g^{-1}) of mice at 3 time points during the 5min hypoxic exposure in TH-Cre (12% O_2: n = 25 exposures from 5 mice; 8% O_2: n = 37 exposures from 4 mice, black), hypomorphic *Lkb1* floxed mice (*Lkb1* hom FX; 12% O_2: n = 14 exposures from 4 mice; 8% O_2: n = 15 exposures from 4 mice, orange) and *Lkb1* knockout mice (*Lkb1* hom KO; 12% O_2: n = 22 exposures from 4 mice; 8% O_2: n = 30 exposures from 4 mice, red). * = $p < 0.05$, ** = $p < 0.01$, *** = $p < 0.001$, **** = $p < 0.0001$. Significance tested by one-way ANOVA with Bonferroni multiple comparisons.

3.2.3 The effects of *Lkb1* deletion on the ventilatory response to hypercapnia

3.2.3.1 Hypercapnia reverses the effects of *Lkb1* deletion on the frequency and duration of apnoeas during hypoxia

The deletion of *Lkb1* in catecholaminergic cells was found to attenuate the ventilatory response to hypoxia and result in disordered breathing that included more frequent and prolonged apnoeas, as described above. However, unlike the profound effects observed during severe hypoxia (8% O_2), *Lkb1* deletion appeared to have very little effect on the ventilatory response to hypercapnia alone (21% O_2 + 5% CO_2). Moreover, exposure of mice to hypercapnia with severe hypoxia (8% O_2 + 5% CO_2) reversed entirely the disordered breathing precipitated in these mice by hypoxia alone.

5% CO_2 alone induced a pronounced ventilatory response in both controls and *Lkb1* knockouts, with no evidence of apnoeas or periods of hypoventilation. Figure 3.15 shows the ventilatory activity from TH-Cre mice and *Lkb1* knockout mice during 8% O_2 alone, 8% O_2 + 5% CO_2, and 5% CO_2 alone. As described above, TH-Cre mice exhibited short and infrequent apnoeas during severe hypoxia while conditional *Lkb1* deletion in catecholaminergic cells precipitated significantly more frequent and prolonged apnoeas during hypoxia (Figure 3.15 – Panel Ai). Surprisingly, the inclusion of 5% CO_2 with 8% O_2 reversed entirely the disordered breathing observed in *Lkb1* knockout mice, with no evidence of apnoeas or periods of hypoventilation. Additionally, this was comparable with the response to 5% CO_2 alone (Figure 3.15 – Panel Aii). This is further highlighted by cross-comparison of the mean ± SEM of the apnoeic index, apnoea duration, and apnoea duration index in Figure 3.15 as well as examining the ventilatory activity on an expanded time scale in Figure 3.16.

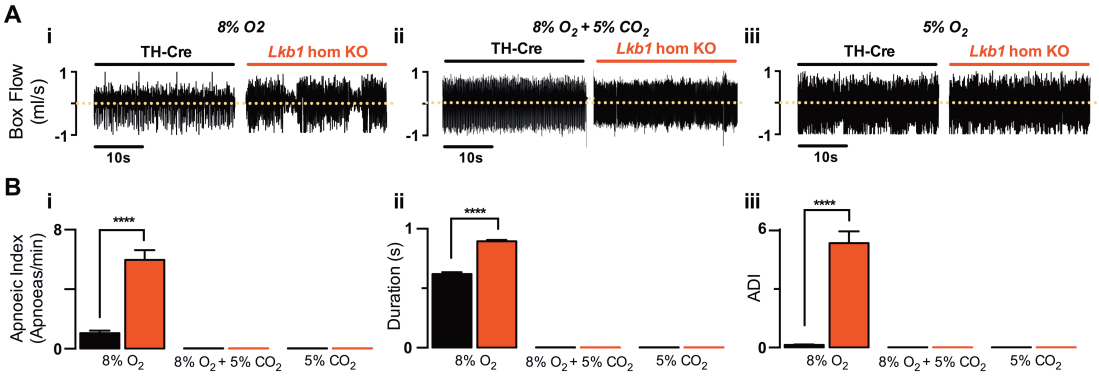

Figure 3.15: *Lkb1* deletion precipitates apnoeas during hypoxia in a manner that is reversed with the inclusion of hypercapnia. (A) Records of ventilatory activity from TH-Cre (*left panel*) and *Lkb1* homozygous knockout mice (*Lkb1* hom KO; *right panel*) during **(i)** severe hypoxia (8% O_2) **(ii)** severe hypoxia with hypercapnia (8% O_2 + 5% CO_2) and **(iii)** hypercapnia alone (5% CO_2). **(B)** Mean ± SEM for **(i)** apnoeic index (apnoeas per minute), **(ii)** apnoea duration (s) and **(iii)** the apnoea-duration index (ADI) (TH-Cre - 8% O_2: n = 24 exposures from 5 mice, 8% O_2 + 5% CO_2: n = 17 exposures from 5 mice, 5% CO_2: n = 20 exposures from 5 mice, black; *Lkb1* hom KO - 8% O_2: n = 22 exposures from 4 mice, 8% O_2 + 5% CO_2: n = 27 exposures from 4 mice, 5% CO_2: n = 20 exposures from 4 mice, N = 4 mice, red). **** = $p < 0.0001$. Significance tested using unpaired student's t-test.

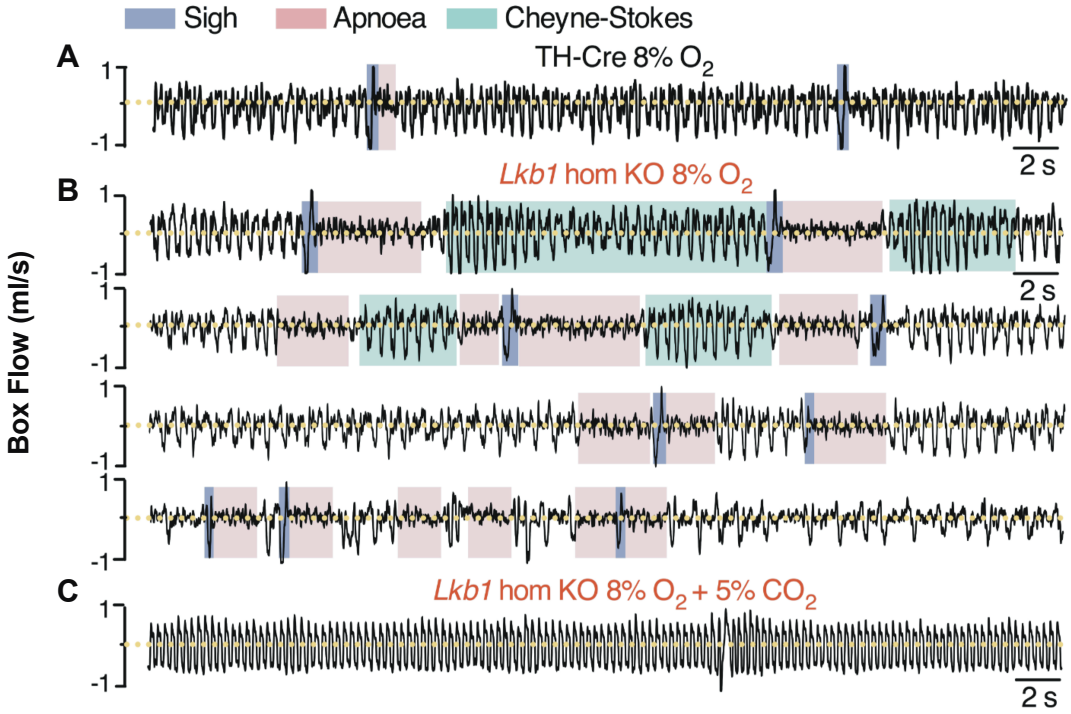

Figure 3.16: *Lkb1* deletion precipitates complex abnormalities in ventilatory pattern during hypoxia and is reversed with the inclusion of hypercapnia. (A) Typical ventilatory records on an expanded time scale from **(A)** a TH-Cre mouse under severe hypoxia (8% O_2), **(B)** different *Lkb1* homozygous knockout (*Lkb1* hom KO) mice during hypoxia (8% O_2) which exhibit (top to bottom) Cheyne-Stokes-like breathing with post-sigh apnoeas, sinusoidal breathing with spontaneous and post-sigh apnoeas, mild sinusoidal breathing with spontaneous and post-sigh apnoeas, hypoventilation with spontaneous and post-sigh apneas and **(C)** a typical ventilatory record from an *Lkb1* hom KO demonstrating the reversal of hypoxia-induced disordered breathing with the co-exposure with hypercapnia (8% O_2 + 5% CO_2).

3.2.3.2 Poincaré analysis reveals that the PO_2-dependent disordered breathing in *Lkb1* knockout mice is reversed by hypercapnia

That inclusion of 5% CO_2 reverses the irregularity of breathing evoked by hypoxia in *Lkb1* knockouts was confirmed by Poincaré plots of interbreath intervals (BBn) versus the subsequent interbreath interval (BBn+1). These are shown in Figure 3.17, which compares TH-Cre with *Lkb1* knockouts during 8% O_2, 8% O_2 + 5% CO_2 and 5% CO_2 alone. These clearly show that the significant increases in irregularity of breathing observed at 8% O_2 in the *Lkb1* knockouts are reversed by the addition of 5% CO_2, and are not observed in the presence of 5% CO_2 alone. In fact the regularity of breathing was restored to levels comparable to that observed in the control TH-Cre mice under the same conditions (Figure 3.17 – Panel A-C, *upper panels*); an observed increase in the irregularity of breathing observed in TH-Cre mice under hypoxia was also reversed by inclusion of 5% CO_2. This is consistent with the findings mentioned above, which demonstrate that apnoeas induced by hypoxia are no longer observed with combined exposure to a hypercapnic stimulus. This is confirmed in Figure 3.17, which shows that the SD for TH-Cre mice is reduced from 65 ± 2ms (n = 24 exposures from 5 mice) at 8% O_2 to 20 ± 1ms (n = 17 exposures from 5 mice) during 8% O_2 + 5% CO_2 and 33 ± 2ms (n = 20 exposures from 5 mice) under 5% CO_2. By contrast, although exposure of *Lkb1* knockouts to 8% O_2 markedly increased the SD to 153 ± 6ms (n = 28 exposures from 4 mice), the SD decreased to 26 ± 2ms (n = 27 exposures from 4 mice) with 8% O_2 + 5% CO_2 and similarly to to 33 ± 2 (n = 20 exposures from 4 mice) during 5% CO_2 alone, which were comparable to the measurements made in the TH-Cre mice.

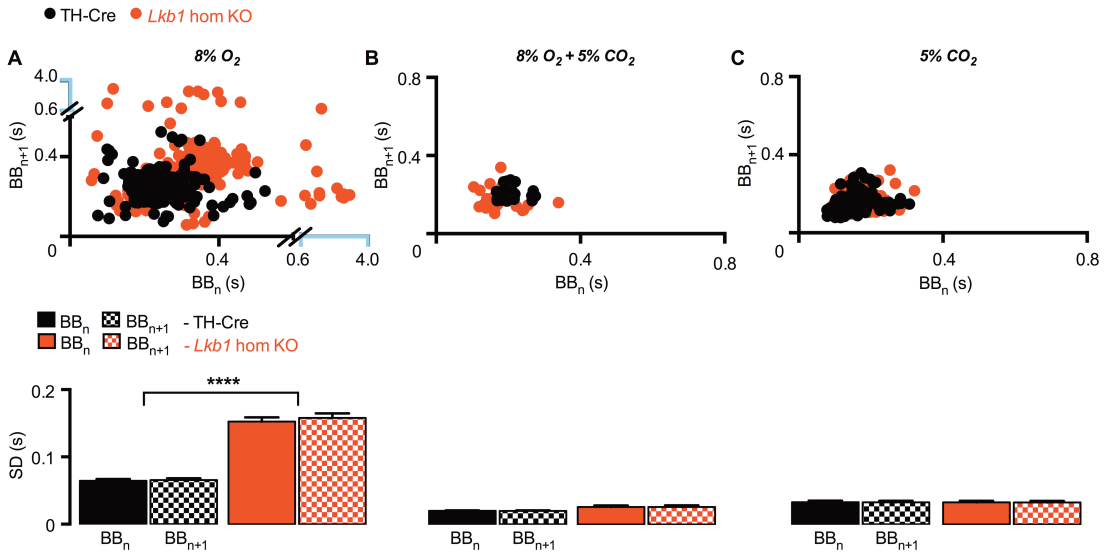

Figure 3.17: *Lkb1* deletion affects the regularity of breathing during hypoxia in a manner that is reversed with the inclusion of hypercapnia. *Upper panels* show Poincaré plots of the inter-breath interval (BB_n) versus subsequent interval (BB_{n+1}) during **(A)** 8% O_2, **(B)** 8% O_2 + 5% CO_2, and (**C**) 5% CO_2. Corresponding *lower panels* show mean ± SEM for the standard deviation (SD) of BB_n and BB_{n+1} of each genotype during **(A)** 8% O_2 (TH-Cre: n = 24 exposures from 5 mice; *Lkb1* hom KO: n = 28 exposures from 4 mice), **(B)** 8% O_2 + 5% CO_2 (TH-Cre: n = 17 exposures from 5 mice, *Lkb1* hom KO: n = 27 exposures from 4 mice) **(C)** 5% CO_2 (TH-Cre: n = 20 exposures from 5 mice, *Lkb1* hom KO: n = 20 exposures from 4 mice). **** = $p < 0.0001$. Significance tested by unpaired student's t-test.

3.2.3.3 Hypercapnia overcomes the effects of *Lkb1* deletion on the ventilatory response to hypoxia whether we consider breathing frequency, tidal volume or minute ventilation

Next the impact of the hypercapnic stimulus, in the presence and absence of 8% O_2, on breathing frequency, tidal volume and minute ventilation was assessed. Figure 3.18 shows example records for the changes in these parameters (2s sampling period) over the 5min exposure of mice to 8% O_2, 8% O_2 + 5% CO2 and 5% CO_2. In contrast to the severe attenuation observed during 8% O_2 in *Lkb1* knockouts, robust increases in breathing frequency, tidal volume, and minute ventilation were observed with 5% CO_2 in addition to 8% O_2 and with 5% CO_2 alone.

Breathing Frequency In TH-Cre mice, a robust increase in breathing frequency was observed and this was sustained throughout the 5min exposure to 8% O_2 + 5% CO_2 (30s: 78 ± 3%, 100s: 73 ± 2%, 300s: 60 ± 2%, n = 17 exposures from 5 mice) and 5% CO_2 (30s: 75 ± 1%, 100s: 75 ± 3%, 300s: 72 ± 3%, n = 20 exposures from 4 mice) (Figure 3.19). A robust and sustained increase in breathing frequency was also observed in *Lkb1* knockouts. It was notable, however, that the response of *Lkb1* knockouts to 8% O_2 + 5% CO_2 was less than TH-Cre at the start of the exposure, but reached a comparable magnitude to that of TH-Cre mice towards the end of the 5 min exposure; Initially at 30s (62 ± 3%, $p < 0.0001$) and 100s (100s: 64 ± 3%, $p < 0.05$) the increase in breathing frequency in the *Lkb1* knockouts was significantly attenuated relative to control, but was comparable at 300s (59 ± 3%, ns; n = 15 exposures from 4 mice; Figure 3.19 – Panel A). Surprisingly, however, although 5% CO_2 alone evoked a robust and sustained increase in breathing frequency in *Lkb1* knockouts, this was significantly attenuated relative to TH-Cre mice throughout the 5min exposure (30s: 61 ± 3%, $p < 0.01$; 100s: 54 ± 2%, $p < 0.0001$; 300s: 59 ± 2%, $p < 0.01$; n = 20 exposures from 4 mice; Figure 3.19 – Panel A).

Tidal volume Tidal volume increases in response to 8% O_2 + 5% CO_2 and 5% CO_2 alone were time-dependent in both TH-Cre and *Lkb1* knockout mice. Initially in TH-Cre mice at 30s following the introduction of 8% O_2 + 5% CO_2, tidal volume increased to 39 ± 4% of that observed under normoxia + normocapnia and peaked at 48

± 4% after 100s, before declining slightly to 34 ± 3% at 300s. By contrast, upon exposure to 5% CO_2 alone tidal volume increased by 46 ± 7% at 30s relative to normoxia + normocapnia, before increasing to a stable level of 65 ± 6% after 100s which was maintained for the remainder of the exposure period (300s, 66 ± 6%) (Figure 3.19 – Panel B).

The increase in tidal volume evoked by to 8% O_2 + 5% CO_2 in *Lkb1* knockouts occurred with a measurable delay when compared to TH-Cre. This was apparent because the increase in tidal volume was significantly smaller at 21 ± 6% ($p < 0.05$) after 30s. However, tidal volume increased thereafter to levels comparable to controls as it reached 42 ± 4% at 100s and 36 ± 3% after 300s. By contrast the response to hypercapnia alone (5% CO_2) was comparable to TH-Cre throughout the 5min exposure (30s: 30 ± 5%; 100s: 55 ± 5; 300s: 60 ± 5%)(Figure 3.19 – Panel B). This suggests that *Lkb1* deletion in catecholaminergic cells delays increases in tidal volume in response to hypoxia with hypercapnia, but not in response to either hypoxia or hypercapnia alone.

Minute ventilation Minute ventilation increased markedly in control TH-Cre mice throughout the 5min exposure to 8% O_2 + 5% CO_2, increasing to 140 ± 7% at 30s and then peaking at 148 ± 7% after 100s, before declining to 114 ± 6% at 300s. This was noticeably smaller than the response to 5% CO_2 alone, which increased to 155 ± 14 after 30s, before peaking at 188 ± 10% after 100s in a manner that was sustained for the remainder of the 5min exposure (300s: 185 ± 11%)(Figure 3.19 – Panel C).

Under 8% O_2 + 5% CO_2 increases in minute ventilation of the *Lkb1* knockouts appeared to be delayed as apparent for tidal volume. At 30s the increase in minute ventilation relative to normoxia + normocapnia was attenuated when compared to TH-Cre mice, measuring only 95 ± 12 ($p < 0.001$). Thereafter, minute ventilation peaked at 100s to 131 ± 8% before slightly declining to 114 ± 6% after 300s, which was comparable to TH-Cre mice. Surprisingly the response to 5% CO_2 was also delayed when compared to the controls. Minute ventilation, measuring relative to normoxia + normocapnia, increased to only 107 ± 9% ($p < 0.05$) at 30s and 142 ± 10% ($p < 0.05$) after 100s, before peaking at 153 ± 8 (similar to control TH-Cre mice) after 300s (Figure 3.19 – Panel C).

These findings indicate that, unlike its effects during hypoxia, *Lkb1* deletion has little effect on the ventilatory response in the presence of a hypercapnic stimulus. Furthermore, this is only apparent up to 100s following the onset of the hypercapnic exposures as by 300s the ventilatory response is at a level comparable in magnitude to controls during both 8% O_2 + 5% CO_2 and 5% CO_2 alone.

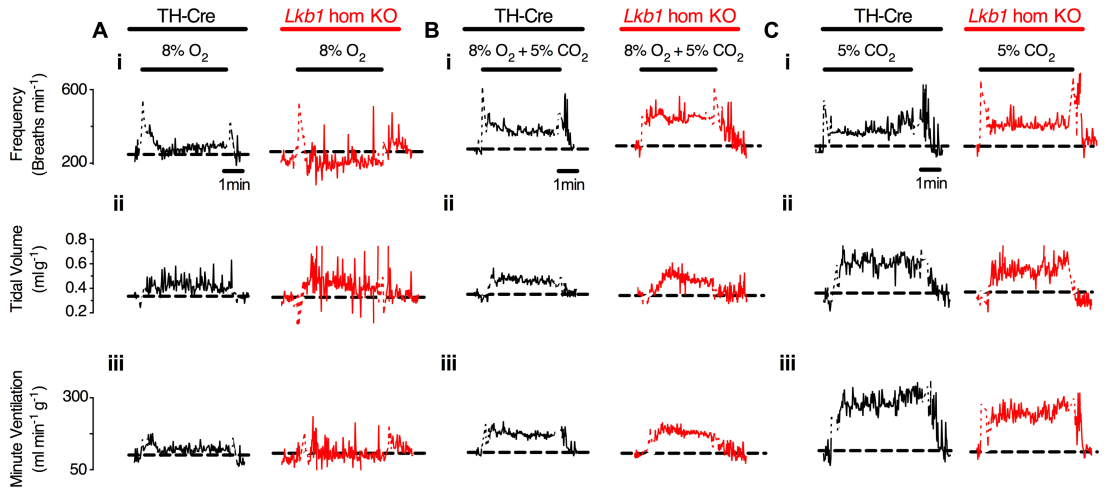

Figure 3.18: *Lkb1* deletion attenuates the ventilatory response to hypoxia in a manner that is reversed by hypercapnia. Example records of the effect over a 5min period of exposure to **(A)** severe hypoxia (8% O_2) **(B)** hypercapnia with severe hypoxia (8% O_2 + 5% CO_2), and **(C)** hypercapnia (5% CO_2) on **(i)** breathing frequency (min^{-1}), **(ii)** tidal volume (ml g^{-1}) and **(iii)** minute ventilation (ml min^{-1} g^{-1}) in TH-Cre (black) and *Lkb1* homozygous knockout mice (*Lkb1* hom KO, red) with 2s sampling periods. Dashed black line indicating basal level, white line breaks indicate artefact of gas exchange.

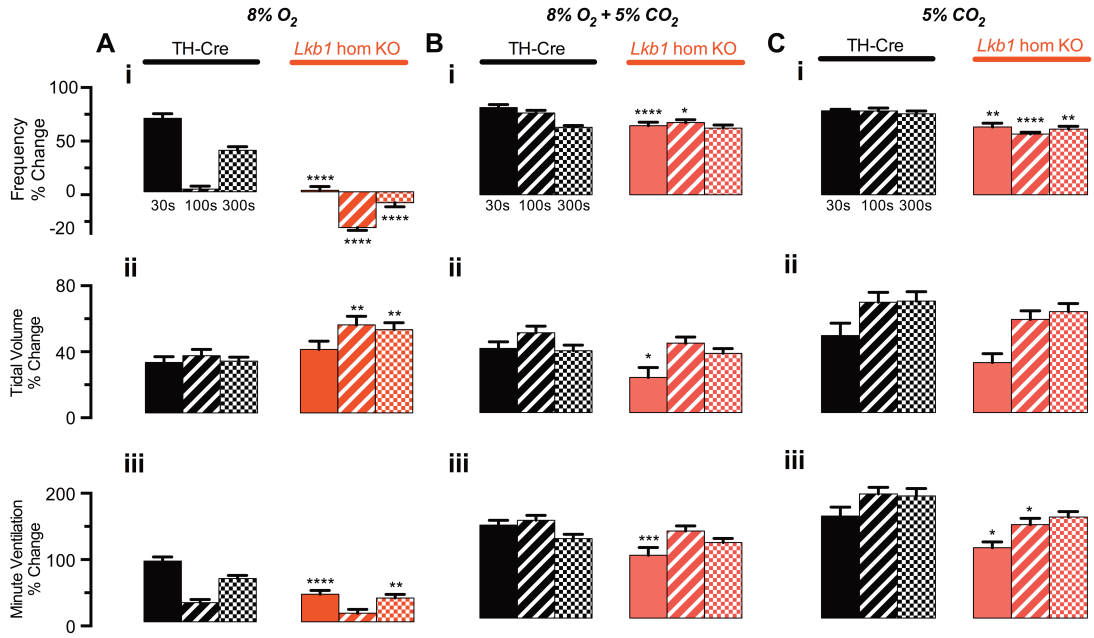

Figure 3.19: The mean ventilatory response to hypoxia is attenuated in *Lkb1* homozygous knockout mice. Mean ± SEM for percent change during **(A)** 8% O_2 **(B)** 8% O_2 + 5% CO_2, and **(C)** 5% CO_2 in **(i)** breathing frequency (min^{-1}), **(ii)** tidal volume (ml g^{-1}) and **(iii)** minute ventilation (ml min^{-1} g^{-1}) at 3 time points during the 5min hypoxic exposure in TH-Cre (8% O_2: n = 27 exposures; 8% O_2 + 5% CO_2: n = 17 exposures; 5% CO_2: n = 20 exposures; black) and *Lkb1* homozygous knockout (*Lkb1* hom KO; 8% O_2: n = 30 exposures; 8% O_2 + 5% CO_2: n = 15 exposures; 5% CO_2: n = 20 exposures; red). * = $p < 0.05$, ** = $p < 0.01$, *** = $p < 0.001$, **** = $p < 0.0001$. Significance tested by one-way ANOVA with Bonferroni multiple comparisons.

3.2.3.2a The effects of *Lkb1* deletion on breathing frequency during hypoxia and/or hypercapnia are driven by changes to the duration of inspiration and expiration

Given the above it seemed likely that further insight might be obtained from analyses of inspiration time, expiration time, and total breath duration, as this would allow us to determine whether or not the inspiratory and/or expiratory phases of ventilation are compromised in *Lkb1* knockouts in the presence of a hypercapnic stimulus, as observed during hypoxia alone. Figures 3.20 and 3.21 display example and average records, respectively, of the ratiometric changes (relative to normoxia + normocapnia) to the duration of inspiration (Ti), expiration (Te), and total breath duration (To) during 8% O_2, 8% O_2 + 5% CO_2, and 5% CO_2 alone in control TH-Cre and *Lkb1* knockout mice.

Inspiration Time (Ti) Similar to that observed during 8% O_2 alone, a time-dependent change in Ti was observed in TH-Cre and *Lkb1* knockout mice during 8% O_2 + 5% CO_2 and 5% CO_2 alone. This involved an initial marked reduction in Ti relative to normoxia at 30s before a gradual increase is observed which plateaus by 2min and remains stable for the remainder of the 5min exposure. This is demonstrated by the measured mean ± SEM of Ti at 30s and the overall mean ± SEM of Ti during the final 2min of the hypercapnia ± hypoxia exposure from 3 – 5min (using the formula for error of propagation). In the control TH-Cre mice, Ti decreases relative to normoxia to 0.90 ± 0.08 (n = 5 exposures from 5 mice) upon being exposed to 8% O_2 + 5% CO_2 at 30s, before gradually prolonging and reaching an averaged 1.08 ± 0.01 during the final 2min of the exposure (Figure 3.21 – Panel A). Under 5% CO_2 alone, TH-Cre mice exhibited an even greater reduction in Ti at 30s with a ratio of 0.85 ± 0.07. Ti prolonged thereafter, but unlike in the presence of hypoxia, Ti remained lower at 0.78 ± 0.01 during the final 2min (Figure 3.21 – Panel A). This suggests that under 8% O_2 + 5% CO_2, inspiration phase prolongs to durations similar to that maintained during normoxia but that under 5% CO_2 alone the inspiration phase remains shorter, and hence quicker, than normoxia + normocapnia throughout the 5min exposure.

In the *Lkb1* knockouts, a time-dependent change in Ti was also observed during 8% O_2 + 5% CO_2 and 5% CO_2 alone. Once more, the ratio of Ti initially decreased at

30s to 0.71 ± 0.13 during 8% O_2 + 5% CO_2, which was a reduction greater (though not statistically significant using an unpaired student's t-test) than the reduction in Ti observed at 30s in TH-Cre mice (Figure 3.21 – Panel A). Subsequently, Ti prolongs in the *Lkb1* knockouts to levels close to Ti during normoxia + normocapnia at 0.97 ± 0.02, which was significantly shorter than Ti in control TH-Cre mice during the final 2min exposure to 8% O_2 + 5% CO_2 ($p < 0.001$). In contrast, Ti reduced relative to normoxia + normocapnia at 30s under 5% CO_2 to 0.86 ± 0.07, which was comparable to the relative shortening observed in TH-Cre mice. Furthermore, by the end of the 5min exposure, Ti remained quicker than during normoxia at 0.83 ± 0.07 in the *Lkb1* knockouts, but was significantly prolonged when compared to the Ti maintained by TH-Cre mice from 3-5min ($p < 0.0001$) (Figure 3.21 – Panel A).

Therefore, and similar to hypoxia alone, in response to hypercapnia with hypoxia and hypercapnia alone, both control TH-Cre mice and *Lkb1* knockouts exhibit an initial shortening of inspiration time relative to normoxia + normocapnia. Moreover, during hypercapnia with hypoxia the inspiration time of both TH-Cre and *Lkb1* knockouts recovers back to values close to those observed under normoxia + normocapnia, though Ti is longer from 3-5min in TH-Cre mice. This is contrary to the adjustments made during hypercapnia alone, which is a shortening of inspiration time relative to normoxia + normocapnia, throughout the 5min exposure. Nevertheless, even though the *Lkb1* knockouts exhibit a Ti that remains quicker relative to normoxia + normocapnia throughout the 5min exposure to 5% CO_2 alone, this appeared significantly attenuated when compared to the TH-Cre mice from 3-5min ($p < 0.0001$).

Expiration Time (Te) A robust and sustained reduction in Te relative to normoxia + normocapnia was evident in both TH-Cre and *Lkb1* knockouts during 8% O_2 + 5% CO_2 and 5% CO_2 alone. In the TH-Cre mice, the expiratory phase significantly shortened at the start of the 5min exposure to 8% O_2 + 5% CO_2 and 5% CO_2 as indicated by the mean ± SEM of Te at 30s which was 0.58 ± 0.11 and 0.55 ± 0.10, respectively. Thereafter, the expiratory phase further shortens as the ratio of Te relative to normoxia + normocapnia reaches 0.48 ± 0.01 and 0.40 ± 0.01 during 8% O_2 + 5% CO_2 and 5% CO_2 alone, respectively, in the final 2min of the exposures (Figure 3.21 – Panel B).

The *Lkb1* knockouts also exhibited a marked reduction in the expiratory phase during 8% O_2 + 5% CO_2 and 5% CO_2 alone. However, the knockouts exhibited a greater reduction in Te at 30s relative to controls during 8% O_2 + 5% CO_2 (0.43 ± 0.04 and 5% CO_2 (0.34 ± 0.05, $p < 0.01$), although not statistically significant when using an unpaired student t-test. However, thereafter Te prolongs in the *Lkb1* knockouts to levels that remained quicker than normoxia but significantly longer than that observed in TH-Cre mice during 8% O_2 + 5% CO_2 as the mean ratio during the final 2min reached 0.67 ± 0.01 ($p < 0.0001$). In contrast, the prolongation observed in Te from 3-5min during 5% CO_2 (0.44 ± 0.002) in *Lkb1* knockouts was comparable to that observed in TH-Cre mice (Figure 3.21 – Panel B).

Total Breath Duration (To) In controls, outcomes for Ti and Te translated into robust reductions in *To* throughout the 5min exposure to 8% O_2 + 5% CO_2 and 5% CO_2 alone; consistent with observed increases in breathing frequency (Section 3.2.3.1). Initially *To*, relative to normoxia + normocapnia, fell at 30s to 0.67 ± 0.08 during 8% O_2 + 5% CO_2 and 0.63 ± 0.09 during 5% CO_2. Subsequently, *To* gradually shortened further until plateauing and maintaining a mean ratio of 0.50 ± 0.01 and 0.54 ± 0.01 during the final 2min of the exposures to 8% O_2 + 5% CO_2 and 5% CO_2 alone, respectively (Figure 3.21 – Panel C).

Surprisingly, the deletion of *Lkb1* enhanced reduction of *To* at 30s in response to 8% O_2 + 5% CO_2 (0.52 ± 0.06) and 5% CO_2 (0.41 ± 0.04), although not significantly different than controls. Thereafter, *To* prolongs to levels significantly longer than controls during the final 2min of the 8% O_2 + 5% CO_2 exposure (0.66 ± 0.01, $p < 0.0001$), but to levels comparable in magnitude to controls during the final 2min of 5% CO_2 (0.54 ± 0.02) (Figure 3.21 – Panel C).

Therefore, the overall reduction in *To* during hypercapnia with hypoxia is primarily driven by reductions in Te relative to normoxia + normocapnia as Ti predominantly remains close to baseline levels throughout the 5min exposure. In contrast, during hypercapnia alone, the reduction in *To* is driven by reductions in both the inspiratory and expiratory durations. This perhaps is not surprising, as in the

presence of hypoxia, it would be paradoxical to reduce the time available for O_2-intake during inspiration.

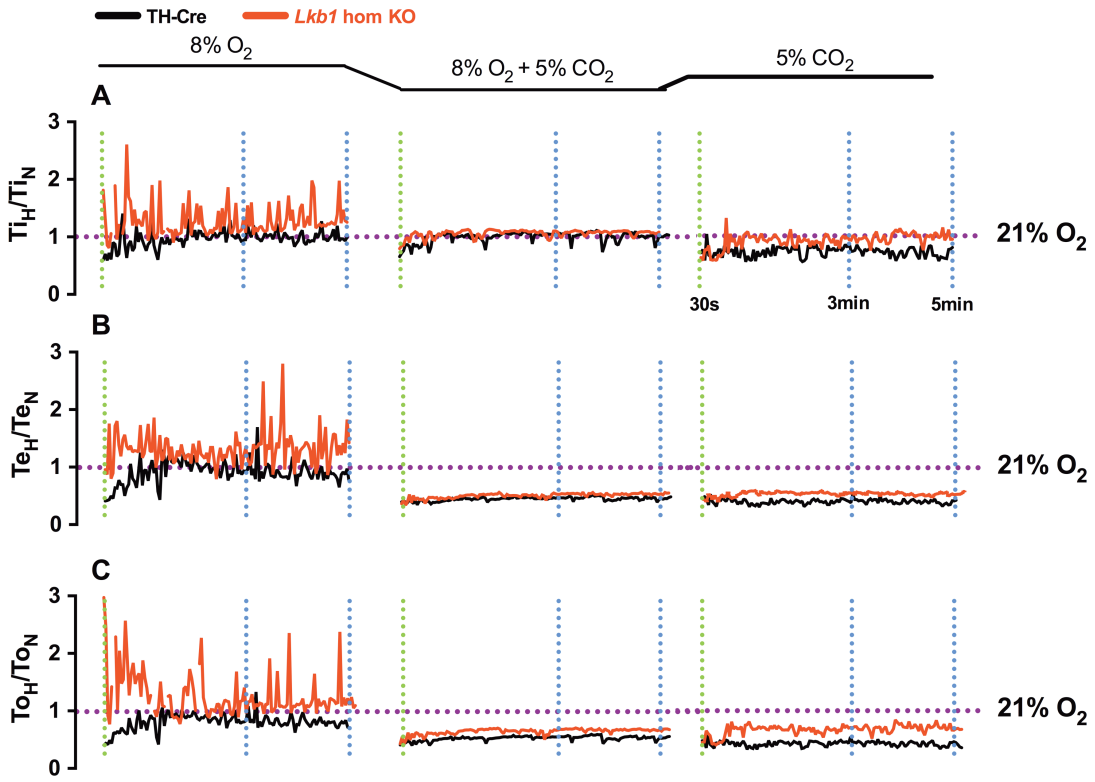

Figure 3.20: Hypercapnia reverses the effects of *Lkb1* deletion on the hypoxic duration(s) of inspiration, expiration and total breath duration. Example records of the ratiometric changes (relative to normoxia as indicated by dotted line at 1.0, 21% O_2) in the duration(s) of **(A)** inspiration (Ti), **(B)** expiration (Te) and **(C)** total breath (To) over a 5min exposure during severe hypoxia 8% O_2, 8% O_2 + 5% CO_2, and 5% CO_2, with 2s sampling periods, in TH-Cre mice (black) and *Lkb1* homozygous knockouts (*Lkb1* hom KO, red). 30s following the onset of hypoxia ± hypercapnia indicated by green vertical dotted line; 3-5min indicated by blue vertical dotted lines.

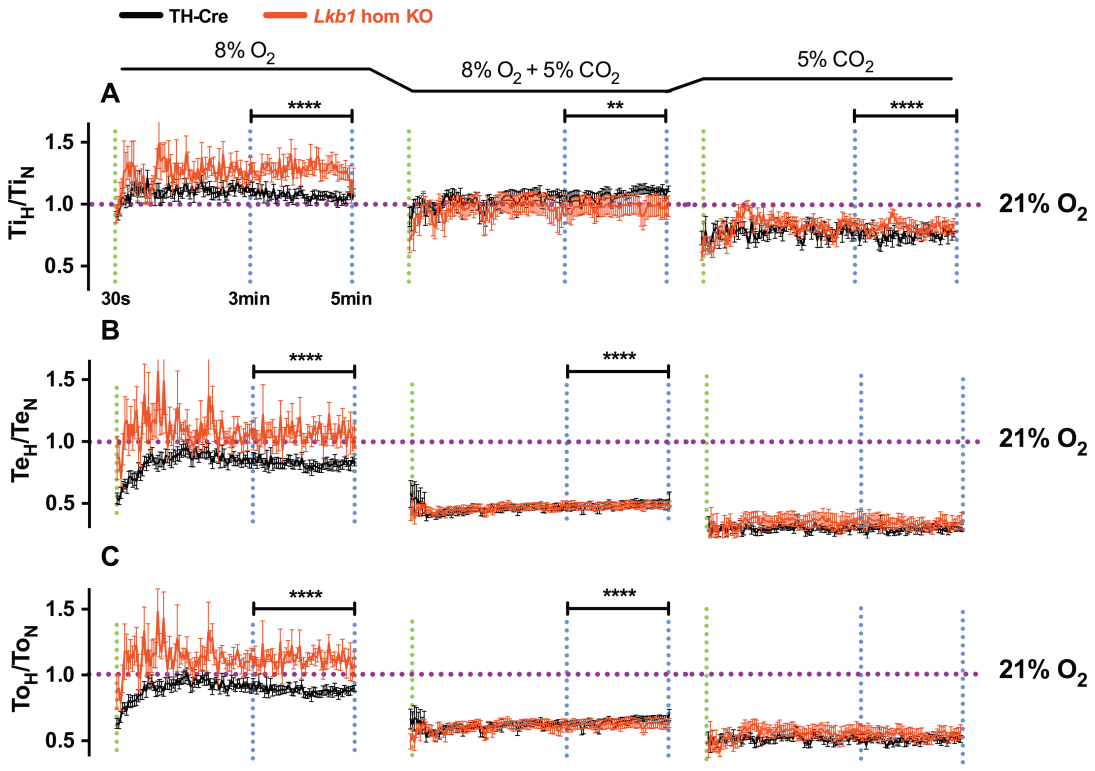

Figure 3.21: Hypercapnia reverses the effects of *Lkb1* deletion on the mean duration of inspiration, expiration and total breath duration during severe hypoxia. Mean ± SEM of the ratiometric changes (relative to normoxia as indicated by dotted line at 1.0, 21% O_2) in the duration (s) of **(A)** inspiration (Ti), **(B)** expiration (Te) and **(C)** total breath (To) over a 5min exposure during 8% O_2 (*left panels*), 8% CO_2 + 5% CO_2 (*middle panels*), and 5% CO_2 (*right panels*) in TH-Cre (black) and *Lkb1* homozygous knockouts (*Lkb1* hom KO, red) mice, with 2s sampling periods. (TH-Cre - 8% O_2: n = 18 exposures from 4 mice, 8% O_2 + 5% CO_2: n = 5 exposures from 5 mice, 5% CO_2: n = 5 exposures from 5 mice; *Lkb1* hom KO - 8% O_2: n = 9 exposures from 4 mice, 8% O_2 + 5% CO_2: n = 5 exposures from 4 mice, 5% CO_2: n = 8 exposures from 4 mice). * = $p < 0.05$, ** = 0.01, **** = $p < 0.0001$.. Unpaired student's t-test was used to test for significance at 30s following the onset of hypoxia ± hypercapnia (indicated by green vertical dotted line) and from 3-5min (as indicated by blue vertical dotted lines).

3.3 Discussion

3.3.1 Summary of findings

Chapter 3 shows that LKB1-dependent signalling pathways are critical for appropriate modulation of ventilation in response to hypoxia. The loss of LKB1 activity in catecholaminergic cells precipitates irregular breathing patterns during hypoxia and attenuates the hypoxic ventilatory response. In instances, these irregular breathing patterns mirror a variety of breathing disorders such as Cheyne-Stokes-like breathing during congestive heart failure (Eckert et al., 2007) and hypoxia-evoked periodic breathing in pre-term infants (Rigatto and Brady, 1972). Nevertheless, the hypomorphic *Lkb1* floxed mice exhibited similar PO_2-dependent ventilatory abnormalities but significantly milder. This suggests that in each case, the ventilatory dysfunction likely results from loss of LKB1 activity within common cell types (i.e. catecholaminergic cells) or a common cell circuit. By contrast, *Lkb1* deletion had very little effect on the ventilatory response to hypercapnia. Additionally, ventilatory defects observed during hypoxia were mostly reversed upon exposure of mice to hypoxia with hypercapnia.

Therefore, LKB1 activity is key to the regulation of ventilation during hypoxia and is accordingly required to maintain oxygen-supply and energy homeostasis at the whole-body level.

3.3.2 The increase in ventilation in response to hypoxia requires LKB1 activity in catecholaminergic cells

Importantly, the deletion of *Lkb1* in catecholaminergic cells had no effect on normoxic ventilation. Also, the *Lkb1* knockouts were still able to hyperventilate in the presence of a hypercapnic stimulus; although it was notable that the initial phase of the hypercapnic ventilatory response (first 30s) was marginally attenuated relative to controls. In marked contrast, increases in minute ventilation during hypoxia were markedly attenuated in *Lkb1* knockouts and in a PO_2-dependent manner. This suggests that the blunted ventilatory response to hypoxia, particularly the period associated with hypoventilating under 8% O_2, is secondary to a primary abnormality of respiratory

control by oxygen-sensing catecholaminergic cells, and hence hypoxic drive, rather than an impairment in respiratory apparatus/muscles.

Several studies have demonstrated that the ventilatory response to hypoxia is biphasic in mice. Initially, there is a relatively rapid increase in ventilation in response to acute hypoxia, designated as the augmentation phase, before respiratory depression occurs (Ramirez, et al., 1998; Bissonnette, 2000). It was proposed that the augmentation phase was driven by rapid afferent input to the respiratory centres of the brainstem following rapid activation of the carotid body during acute hypoxia. By contrast, the depressive phase of ventilation is thought to be due to the depressive effects of hypoxia and a resultant, time-dependent reduction in the stimulation of the carotid body and central respiratory neurons. However, it is interesting to note that the biphasic nature of the hypoxic ventilatory response is retained *in vitro* in rhythmically active preparations from which input from peripheral chemoreceptors are removed (Ramirez et al., 1998). This suggests that central chemoreceptors can also contribute to the initial augmentation phase observed during acute hypoxia and that neither the carotid body nor other peripheral chemoreceptors, e.g. aortic bodies, are necessarily required for the initial onset and subsequent depressive phase of hypoxia-induced ventilation.

The *Lkb1* knockouts fail to exhibit a biphasic response with respect to breathing frequency. This was demonstrated by the mean percentage change ± SEM from normoxia of breathing frequency at 30s following the onset of hypoxia, which was only 3 ± 2% during 12% O_2 and 1 ± 3% during 8% O_2. Hence, when considering the above, this would suggest that *Lkb1* deletion affected the rapid activation of the catecholaminergic carotid type I cells (CB1 cells) and, hence, the subsequent afferent input to the respiratory centres of the brainstem to trigger an increase in breathing frequency during the augmentation phase. However, a possible effect on central catecholaminergic chemosensitive neurons cannot be excluded since, as mentioned above, biphasic ventilatory responses have been found to be retained *in vitro* in preparations lacking input from peripheral chemoreceptors (Ramirez et al., 1998); further studies will be required to directly examine the effects of *Lkb1* deletion in these catecholaminergic cells (and will be discussed in chapter 6).

Additionally, respiratory depression further led to breathing frequency to fall to levels below normoxia, i.e. hypoventilation, in *Lkb1* knockouts. Hence, the overall hypoxic ventilatory response in *Lkb1* knockouts appears to mirror that observed in neonatal mammals, including mice. In neonates, the hypoxic ventilatory response consists of a smaller augmentation phase relative to adults with the secondary depression phase rapidly resulting in hypoventilation (Eden and Hanson, 1987; Teppema and Dahan, 2010). This occurs in neonates as they opt to reduce their metabolism, and hence O_2 demand, to cope with hypoxia rather than increase ventilation as observed during adulthood. This is primarily a result of the time-course of maturity of the oxygen-sensing network, including the catecholaminergic CB1 cells and regions in the nucleus tractus solitarii (NTS), which do not have their specialised oxygen-sensing ability at birth (Teppema and Dahan, 2010; Bissonnette, 2000). Given that *Lkb1* deletion has been targeted to all catecholaminergic neurons, and that *Lkb1* knockouts exhibit a hypoxic ventilatory response (and possibly reduced metabolism as observed with their behaviour during hypoxia, Appendix 3C) in a manner similar to neonates that do not have a matured specialised oxygen-sensing network, provides strong support for the view that the activity of LKB1 is key to the appropriate regulation of ventilation in response to hypoxia, and to the maintenance of oxygen supply, and hence energy homeostasis, at the whole-body level.

3.3.3 The modulation of the durations of inspiratory and expiratory phases of breathing during hypoxia is dependent on LKB1 activity in catecholaminergic cells

Interestingly, the effects of *Lkb1* deletion on the augmentation and depressive phases of the hypoxic ventilatory response appeared to be a result of attenuation in increases in breathing frequency and tidal volume (Figure 3.8 and 3.10). This was demonstrated by studies on the duration of inspiration (*Ti*), expiration (*Te)*, and total breath duration (*To*) as well as the change in tidal volume (*Tv*) relative to *Ti* (Tv/Ti), *Te* (*Tv/Te*), and *To* (*Tv/To*).

To significantly increased when compared to controls as a result of marked prolongation of *Te* and *Ti* in the *Lkb1* knockouts. This suggests that the appropriate

modulation of the inspiratory and/or expiratory phases to accommodate reduced total breath duration, and hence increased breathing frequency, is dependent on LKB1 activity in catecholaminergic cells. The respiratory central pattern generators (rCPGs) contain inspiratory and expiratory neurons that receive inputs from peripheral and central chemoreceptors and accordingly adjust ventilation, to meet metabolic demands. It seems likely, therefore, that the rCPGs are unable to appropriately modulate the inspiratory and expiratory phases of respiration in a manner that promotes an increase in ventilation in response to hypoxia. This is unlikely to be a result of defects in the rCPGs themselves, but instead a likely result of inadequate signalling from either the afferent inputs from peripheral chemoreceptors and/or inputs from central catecholaminergic chemoreceptors to the rCPGs during hypoxia. This is supported by the ability of the rCPGs to generate rhythmic breathing and a complete reduction in *To* in *Lkb1* knockouts when exposed to hypercapnia.

Nevertheless, control TH-Cre mice demonstrate that the overall reduction in *To* observed during hypoxia is primarily driven by shortening of *Te* relative to normoxia and not *Ti*. The duration of the expiratory phase of respiration has been found to be modulated by the retrotrapezoid nucleus (RTN) during hypoxia. It is considered that the RTN drives reductions in *Te* by promoting active expiration during hypoxia and hypercapnia by transforming, through a shortening, the biphasic nature of expiratory pattern to a monophasic event (Abbott et al., 2011). This indicates that the appropriate shortening of the *Te* by the RTN during hypoxia may depend on *Lkb1* expression in catecholamienrgic cells. However, this process involves non-catecholaminergic neurons of the RTN, which are unlikely to be intrinsically affected in the conditional *Lkb1* knockouts used here. It also seems unlikely that the hypomorphic nature of the *Lkb1* knockouts affects these TH-negative neurons of the RTN as the *Lkb1* knockouts still exhibit active expiration in response to hypoxia and/or hypercapnia; this suggests that the RTN is fully functional in this regard in the *Lkb1* knockouts. Hence, it seems likely that the modulation of the expiration phase is disturbed specifically during hypoxia as a result of reduced inputs from catecholaminergic oxygen-sensing cells to the RTN following *Lkb1* deletion.

The RTN receives noradrenergic inputs from the area postrema and the commissural NTS (SolC) as well as the hypoxia-sensitive catecholaminergic C1 neurons, which lie within the RTN itself, and these in turn receive afferent inputs from the carotid body (Washburn et al., 2003; McCrimmon et al., 2004; Alheid et al., 2011). Taken together, the inability of these catecholaminergic neurons to mediate hypoxia-response coupling and hence send signals to the rCPGs following *Lkb1* deletion could possibly be the reason why the inspiratory and expiratory phases are prolonged relative to control, and that the ventilatory response to hypoxia is blunted.

3.3.4 LKB1 is required in catecholaminergic cells to protect against hypoventilation and apnoeas during hypoxia

Given the blunted hypoxic ventilatory response described above, perhaps it is not surprising that the deletion of *Lkb1* in catecholaminergic cells precipitates the number and duration of apnoeas during hypoxia. The increase was PO_2-dependent as the apnoea-duration index significantly increased from 12% O_2 to 8% O_2 in the *Lkb1* knockout mice. In contrast to previous findings, this strongly suggests that PO_2 levels play a prominent role in determining the apnoeic threshold in *Lkb1* knockouts, and cannot therefore be solely governed by PCO_2 (Dempsey, 2005). The apnoeic threshold has previously been defined as a reduced PCO_2, relative to baseline PCO_2, at which apnoeas begin to occur. However, in the *Lkb1* knockouts, the apnoea-duration index increased in a PO_2-dependent manner even though there was a continuous supply of normocapnia (0.05% CO_2) *and* the mice paradoxically hypoventilated, i.e. they did not blow off CO_2 excessively as did controls. Taken together, this strongly indicates that while PO_2 decreases during hypoxia in the *Lkb1* knockouts, PCO_2 levels probably do not and may be increased relative to controls and even eupneic PCO_2. The suggestion that PO_2 also contributes in setting the apnoeic threshold is supported by studies demonstrating that supplying PO_2 can resolve or eliminate the occurrence of apnoeas (Lahiri et al., 1983), that mice with blunted hypoxic ventilatory responses are more susceptible to breathing irregularities and apnoeas (Adachi et al., 2004), and that hypoxia has the capacity to alter the degree of hypocapnia required to trigger apnoeas (Xie et al., 2001).

Lkb1 knockouts exhibited extended periods of hypoventilation with post-sigh and spontaneous apnoeas during hypoxia. This is quite similar to the disordered breathing manifested with Rett syndrome, which exhibited progressive increases in the apnoea-duration index with the progression of the disease (discussed further in chapter 6). This has been associated with progressive degeneration of the catecholaminergic neuromodulatory systems, namely noradrenergic, in the brain (Ide et al., 2005). This includes the noradrenergic A6 neurons of the locus coeruleus as well as the hypoxia-sensitive A1 and A2 groups which also receive afferent inputs from the carotid body (Viemari et al., 2005; Ide et al., 2005; King et al., 2012). Nevertheless, progressive reductions in adrenergic C1 and C2 neurons has also been implicated with Rett syndrome (Viemari et al., 2005). Hence, given that *Lkb1* deletion has been targeted to all catecholaminergic cells and that the *Lkb1* knockouts consequently manifest breathing irregularities that are similar with Rett syndrome, strongly supports the view that the central catecholaminergic cells are crucial for the ventilatory response during hypoxia, that they protect against hypoventilation and apnoea, and that their capacity to do it is depending on LKB1 activity.

3.3.5 Conclusion

In conclusion, LKB1-dependent modulation in catecholaminergic cells is required for modulation of ventilation during hypoxia. The catecholaminergic circuit involved may possibly include both the primary peripheral chemoreceptors, namely the carotid body, as well as the central oxygen-sensitive chemoreceptors in the brainstem, both of which project to the rCPGs. This supports the hypothesis that, the LKB1-AMPK signalling pathway may couple mitochondrial inhibition to ion channel regulation, and hence cell activation, in the specialised oxygen-sensitive cells to regulate oxygen-supply, and thus energy supply at the whole body. However, whether the effects of Lkb1 deletion is a result of corresponding decreases in AMPK activity cannot be determined based on the findings of the current chapter and will require further experiments.

Appendix

APPENDIX 3A

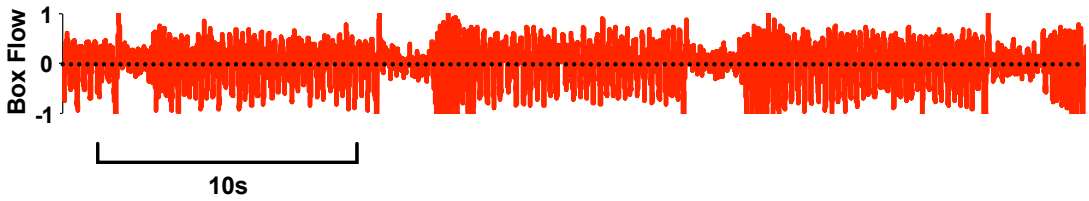

Supplementary Figure 3A: Periodic breathing observed during 8% O_2 in *Lkb1* knockouts with prolonged post-sigh apnoeas occuring at regular intervals of ~0.1Hz.

Appendix 3B

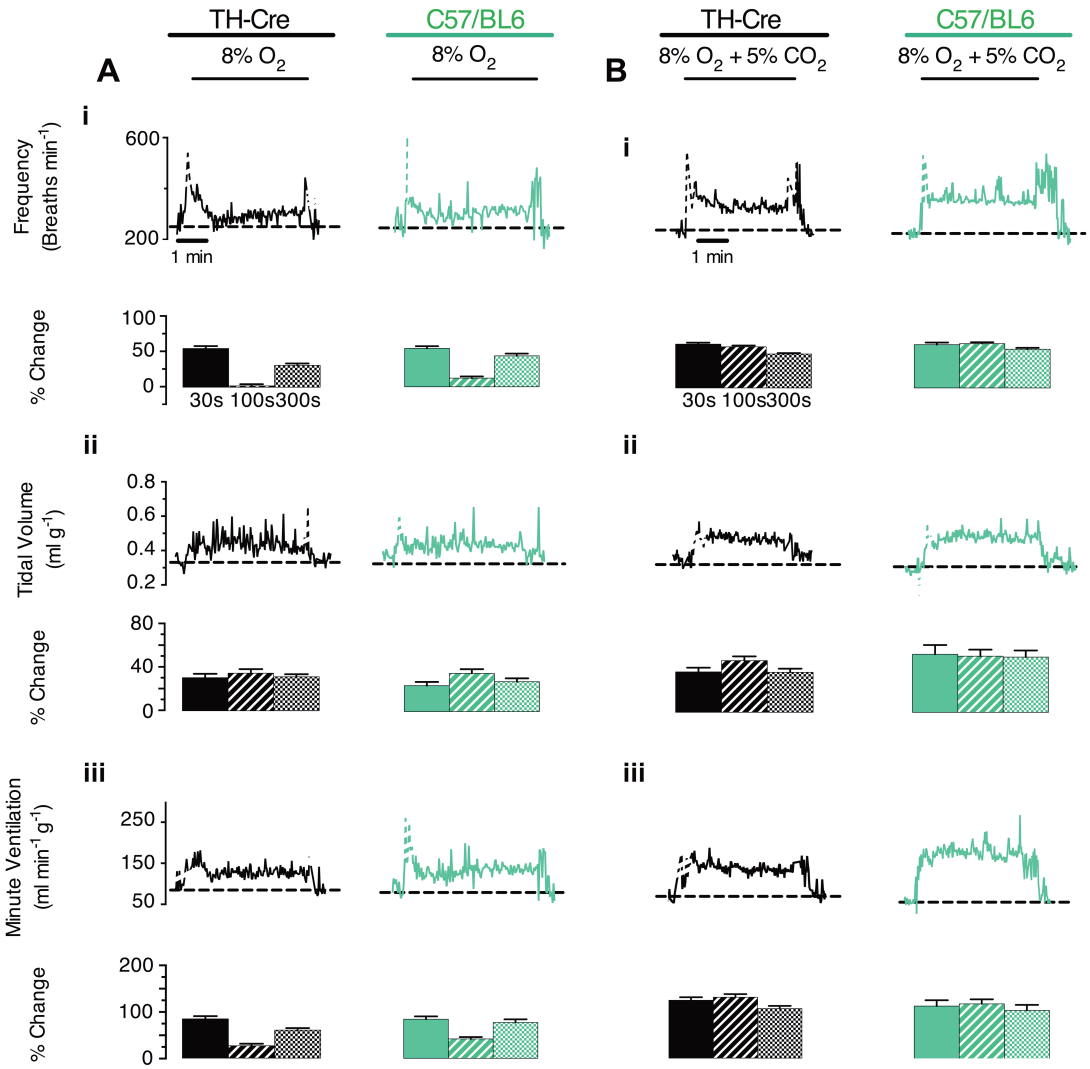

Supplementary Figure 3B: the mean ventilatory response to hypoxia is comparable between TH-Cre and C57/Bl6 mice. This importantly demonstrates that the introduction of Cre recombinase into tyrosine hydroxylase expressing cells has no underlying effect on the ventilatory response to hypoxia. This is also apparent during hypoxia with hypercapnia.

Appendix 3C

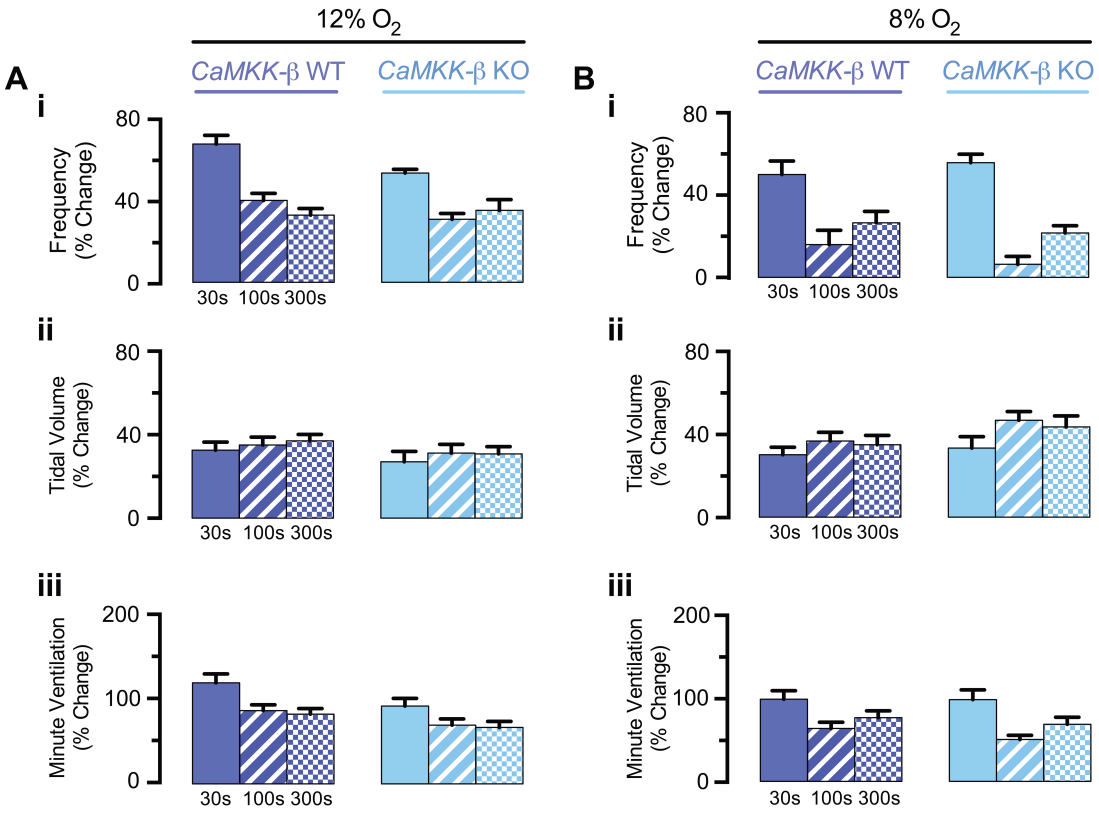

Supplementary Figure 3C: The mean ventilatory response to hypoxia is unaffected following global deletion of CaMKK-β. The CaMKK-β wild-type (CaMKK-β WT) and global knockouts (CaMKK-β KO) were generously provided Dr. David Carling.

Appendix 3D

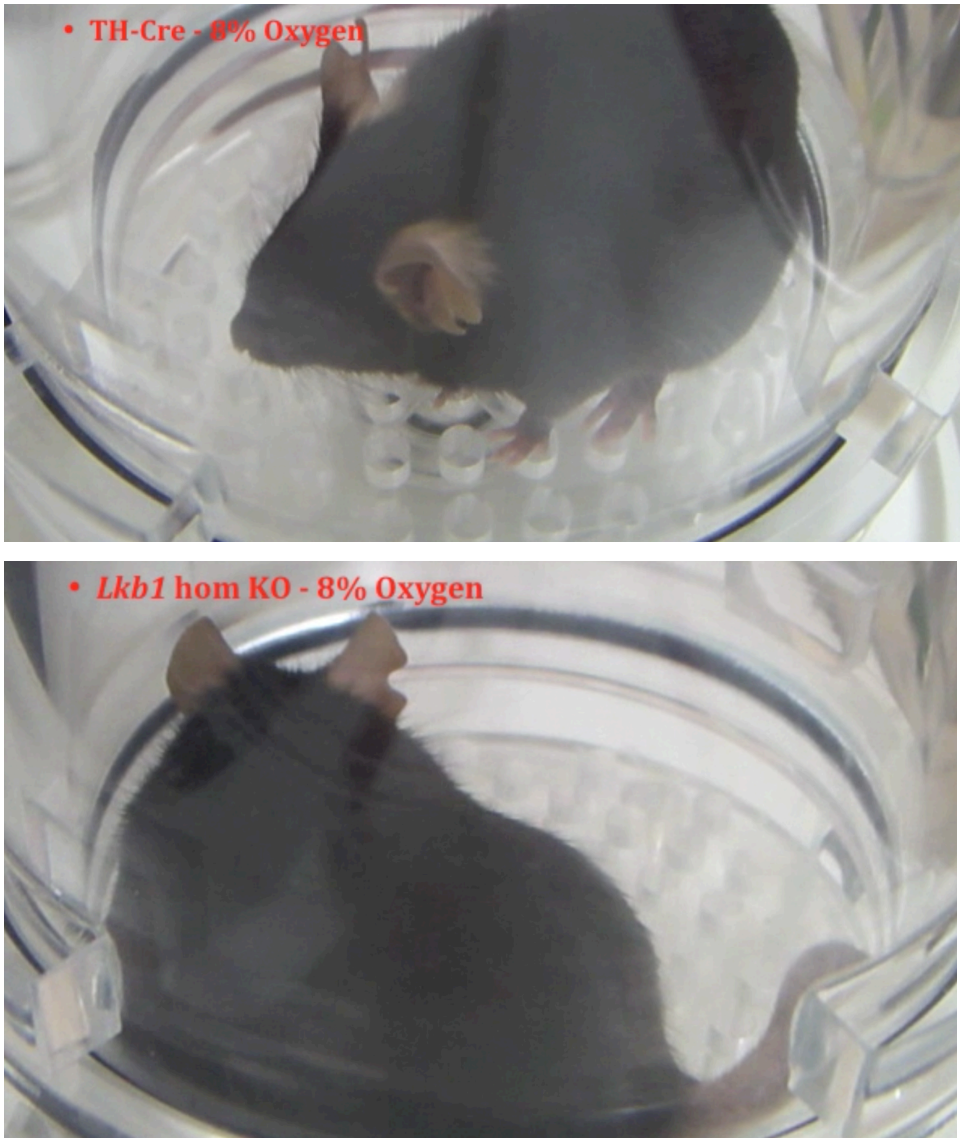

Supplementary Figure 3D: Still images of TH-Cre and *Lkb1* knockout mice during 8% O_2. Unlike TH-Cre, *Lkb1* knockokuts would normally lie down and barely move.

Chapter Four:
The role of AMPK in the ventilatory response to hypoxia and hypercapnia

4.1 Introduction

Studies from the previous chapter demonstrated that LKB1 is essential for respiratory adaptation during hypoxia. However, the hypomorphic nature of these mice makes it difficult to deduce the specific effects of complete *Lkb1* deletion in catecholaminergic cells as, although significantly less severe than the *Lkb1* knockouts, *Lkb1* floxed mice also exhibit mild breathing irregularities. Also, the effect of LKB1 deletion on respiratory adaptation to acute hypoxia does not exclusively indicate a downstream role for AMPK, as hypothesised, since LKB1 is also known to modulate cell function by activating AMPK-related kinases (AMPK-RKs). Therefore, further studies are required to determine if LKB1 mediates respiratory adaptation during hypoxia via AMPK activation.

4.1.1 AMPK and its related kinases

Studies of the human kinome have identified 12 AMPK related kinases (NUAK1, NUAK2, BRSK1, BRSK2, QIK, QSK, SIK, MARK1, MARK2, MARK3, MARK4, and MELK) (Manning et al., 2002; Lizcano et al., 2004). A series of alternative upstream kinases have been found to regulate each AMPK-RK subfamily. For example, MARKK/TAO1 (thousand and one amino acids) activates MARK1-4 (Hutchison et al., 1998) while SIK1 is also regulated by protein kinase A (PKA) upon adrenocorticotropic hormone (ACTH) stimulation (Takemori et al., 2002). Nevertheless, apart from MELK, LKB1 has been found to constitutively phosphorylate the AMPK-RKs at a site equivalent to AMPK's Thr-172 (Lizcano et al., 2004). This raises the possibility that LKB1 could mediate respiratory adjustments during hypoxia through AMPK-RKs. However, only AMPK activation by LKB1 is determined by metabolic status; by allosteric activation and/or the protection from dephosphorylation by phosphatases. No direct evidence has been provided in support of the possibility that the regulation of AMPK-RK activity also involves dephosphorylation by phosphatases. Furthermore, AICAR, which activates AMPK following its conversion into the AMP mimetic ZMP, does not activate any of the AMPK-RKs (Lizcano et al., 2004). This indicates that the AMPK-RKs are regulated differently than AMPK and unlikely to be

activated in response to increases in the ADP:ATP and AMP:ATP ratios during metabolic stress, such as hypoxia.

4.1.2 Expression and function of the AMPK-related kinases

4.1.2.1 MARKs and BRSKs

Of the 12 AMPK-RKs, MAP/microtubule affinity-regulating kinases 1 and 4 (MARK1 and MARK4) and brain-specific kinases 1 and 2 (BRSK1 and BRSK2) are mostly expressed in the brain; although low expression of these kinases were found in the testis (MARK4 and BRSK 1/2) and pancreas (BRSK 1/2) (Jeon et al., 2005; Moroni et al., 2006). Therefore these kinases could be expressed in central catecholaminergic cells and be relevant to my investigation. BRSK1 and BRSK 2 have been found to establish neuronal polarity and axon specification in an LKB1-dependent manner (Bright et al., 2008). Similarly, MARK1 and MARK4 also play a role in mediating neuronal polarity. However, additional functions have also been identified for each isoform of MARK (Jeon et al., 2005; Moroni et al., 2006).

MARK1 is thought to be involved in regulating synaptic plasticity as its activity increases in response to brain-derived neurotrophic factor (BDNF) and depolarisation of neuronal cells (Jeon et al., 2005). Also, unlike AMPK which protects against neuronal cell death, up-regulation of MARK4 expression decreases cell viability and promotes cell death in response to cerebral ischaemia (Schneider et al., 2004). That MARK4 is regulated by a fall in O_2-supply may be significant, but like HIF, its action would likely be over minutes and hours rather than seconds.

MARK4 has also been found to control cell cycle and is highly expressed in a variety of cancer cells, i.e. hepatocellular carcinomas and human gliomas (Kato et al., 2001; Beghini et al., 2003). The other two isoforms of MARK, namely MARK2 and MARK3, are ubiquitously expressed with no major sites of relatively high expression levels (Hurov et al., 2007; C. Y. Peng et al., 1998).

Like MARK1/4, MARK2/3 also have a role in establishing cell polarity. However, studies in mice lacking MARK2 have indicated that this isoform is also involved in fertility, learning and memory, growth, and the immune system (Hurov et al., 2007; Segu et al., 2008; Bessone et al., 1999). MARK2 has also been implicated in the regulation of metabolism as knockout mice are hypermetabolic and exhibit a variety of metabolic disorders, which include adiposity, insulin hypersensitivity, increased glucose uptake, and resistance to weight gain during a high-fat diet (Hurov et al., 2007). However, the mechanism by which MARK2 regulates metabolism remains to be fully identified, although prenatal growth retardation observed in these mice indicates a possible role during embryonic and postnatal growth (Hurov et al., 2007). Once again, however, MARK2 activity is determined by changes in expression rather than by changes in LKB1-dependent activation.

4.1.2.2 SIKs

The major site of expression for the salt-inducible kinase 1 (SIK1) is the adrenal gland, within the cortex and not the catecholaminergic medulla (Okamoto et al., 2004), and has been suggested to be important during the early stages of ACTH stimulation as it regulates steroidogenic gene expression (Takemori et al., 2002; Z. Wang et al., 1999). SIK1 is also required to maintain cell volume and composition in response to increases in intracellular sodium (Sjöström et al., 2007). SIK2 and SIK3 are ubiquitously expressed, however, SIK2's major site of expression is within adipose tissue. SIK2 inhibits CREB-mediated gene expression and, similar to AMPK, mediates insulin signaling in adipose tissue (Horike et al., 2003). Studies in *Drosophila* have indicated that SIK3 plays an important role in cell proliferation and mitosis and knockouts exhibit spindle and chromosome abnormalities (Bettencourt-Dias et al., 2004). At present no studies indicated modulation of SIK be metabolic stress, nor any broad role of SIK in regulating cellular metabolic homeostasis.

4.1.2.3 NUAKs

NUAK1 is ubiquitously expressed and reported to be associated with tumour progression and metastasis. NUAK1 has also been found to protect tumour cells from cell death during nutrient starvation (Suzuki et al., 2003; 2004). The NUAK2 isoform is also ubiquitously expressed, though expression levels are dependent on the tissue type; NUAK2 is present in the thymus, kidney, stomach, spleen, with higher expression levels in the skin, testis, ovary, liver, and largest expression levels in the adrenal gland (separate expression levels within cortex and medulla has yet to be examined) and brain tissue (Lefebvre and Rosen, 2005). That NUAK2 is present in the brain raises the possibility that it might contribute to the regulation of neuronal function. Moreover, studies have suggested that NUAK2 activity is regulated by glucose deprivation, increased AMP (and thus metabolic status), salt stress, and oxidative stress caused by H_2O_2 (Lefebvre and Rosen, 2005). However, as mentioned previously, AICAR does not activate NUAK2. Furthermore, alternative AMPK activators, namely phenformin and metformin, either fail to activate or suppress NUAK2 activity, respectively (Lizcano et al., 2004; Lefebvre and Rosen, 2005). Hence, this suggests that AMPK and NUAK2 activity are differentially regulated and that NUAK2 is unlikely to be modulated in response to acute hypoxia in specialised oxygen-sensing cells as the ADP:ATP and AMP:ATP ratios increase.

4.1.3 Aims

Given the above, further studies are required to determine if, as hypothesised, the LKB1-AMPK signaling pathway regulates the activity of specialised oxygen-sensing cells in order to confer appropriate ventilatory adaptation during hypoxia. The current chapter therefore addresses the specific role of AMPK in this process by assessing the effects of dual deletion of *AMPK α1* and *α2* catalytic subunits in catecholaminergic cells (as described in Chapter 2) on respiratory adaptation to hypoxia (and/or hypercapnia). Unlike the *Lkb1* floxed mice, the *AMPK α1* and *α2* double floxed mice are not hypomorphic and the *AMPK α1* and *α2* double knockouts are specifically deficient in

AMPK activity in catecholaminergic cells. Also in these mice, the effects of AMPK deletion can be examined without affecting activities of AMPK-RKs as LKB1 is still present. Finally, the dual deletion of AMPK catalytic subunits does not only prevent activation by LKB1, but also, eliminates possible allosteric activation by AMP during metabolic stress which may have still occurred in the *Lkb1* knockouts. As a result, these *AMPK α1* and *α2* double knockouts may not only clarify the role of AMPK in respiratory adaptation to hypoxia, but may exhibit a more severe phenotype that may have been masked by alternative modes of activation of AMPK in the *Lkb1* knockouts.

4.2 Results

4.2.1 The effects of *AMPK* deletion on the ventilatory response to hypoxia

Under normoxia, baseline readings of body temperature, venous blood gas composition, blood pH, breathing frequency, tidal volume and minute ventilation of mice lacking both *AMPK α1* and *α2* catalytic subunits were consistent with those measures taken form control mice, including *AMPK α1* and *α2* floxed mice (which, unlike the *Lkb1* floxed mice, are not hypomorphic), TH-Cre mice and C57/Bl6 mice (as discussed in Chapter 2: Table 2.1 and Figure 2.12). Moreover, there was no significant difference in weight gain with age, between 2 and 12 months (Chapter 2: Figure 2.8). However, conditional deletion of both isoforms of the AMPK catalytic α-subunit in catecholaminergic cells, driven by Cre-expression under the control of a tyrosine hydroxylase (TH) promoter, resulted in irregular breathing and precipitated apnoeas during hypoxia.

4.2.1.1 *AMPK* deletion increases the frequency and duration of apnoeas in a PO_2-dependent manner

Ventilatory records obtained using unrestrained whole-body plethysmography revealed that the conditional deletion of both *AMPK α1* and *α2* catalytic subunits in catecholaminergic cells of mice precipitated frequent and prolonged apnoeas during hypoxia. Moreover, both the frequency and duration of apnoeic events appeared to increase in a manner inversely related to PO_2. As before, apnoeas were identified as a cessation of breathing for a duration that is at least equivalent to the duration of two regular breaths (i.e. two respiratory cycles have been missed) (Y.-J. Peng et al., 2011; Nakamura and Kuwaki, 2004; Voituron et al., 2009), which equated to a cessation ≥500ms in our experimental mice.

Figure 4.1A shows the ventilatory activity of TH-Cre, *AMPK α1* and *α2* double floxed, and *AMPK α1* and *α2* double knockout mice during normoxia (21% O_2), mild hypoxia (12% O_2), and severe hypoxia (8% O_2) and the calculated means ± SEM for the apnoeic index (apnoeas/min), apnoea duration, and apnoea duration

index (product of the apnoeic index and duration) under each condition. Similar to outcomes previously described for TH-Cre mice in Chapter 3, the increase in the number of apnoeas appeared only mildly PO_2-dependent in the *AMPK α1* and *α2* floxed mice. This is demonstrated by the measured increase in the mean apnoeic index from 0.32 ± 0.09 apnoeas min^{-1} (n = 31 from 6 mice) during 12% O_2 to 1.8 ± 0.32 apnoeas min^{-1} (n = 12 from 4 mice) during 8% O_2 ($p < 0.001$, by one-way ANOVA). The mean duration of apnoeas in the *AMPK α1* and *α2* floxed mice also appeared mildly PO_2-dependent, with an increase from 419 ± 58ms to 709 ± 17ms ($p < 0.001$, by one-way ANOVA) during 12% and 8% O_2, respectively (Figure 4.1 – Panel B and table 4.1). In contrast, in the *AMPK α1* and *α2* double knockout mice both the frequency and duration of apnoeas increased more markedly than for either TH-Cre or *AMPK α1* and *α2* floxed mice, and in a manner that was clearly PO_2-dependent. This is shown in Figure 4.1 – Panel B (and summarised in table 3.1) which provides a cross comparison of the mean apnoeic index, which measured 1.3 ± 0.3 min^{-1} at 12% O_2 (n = 29 exposures from 6 mice, $p < 0.01$ with *AMPK α1* and *α2* floxed mice) and 14 ± 2 min^{-1} at 8% O_2 (n = 19 exposures from 5 mice, $p < 0.0001$) and apnoea duration which increased from 630 ± 57m at 12% O_2 ($p < 0.05$ when compared to TH-Cre and *AMPK α1* and *α2* floxed mice) to 953 ± 40ms at 8% O_2 ($p < 0.0001$ when compared to TH-Cre and *AMPK α1* and *α2* floxed mice).

Overall, this translates to a PO_2-dependent increase in the apnoea duration index which when compared to either TH-Cre mice (12% O_2: 0.3 ± 0.1; 8% O_2: 0.7 ± 0.1) or *AMPK α1* and *α2* floxed mice (12% O_2: 0.2 ± 0.1; 8% O_2: 1.3 ± 0.2), was significantly greater for *AMPK α1* and *α2* double knockouts (12% O_2: 1 ± 0.3, $p < 0.05$ versus TH-Cre and *AMPK α1* and *α2* floxed mice; 8% O_2: 13.8 ± 2.2, $p < 0.0001$ versus TH-Cre and *AMPK α1* and *α2* floxed mice) (Figure 4.1 – Panel Biii). Furthermore, whereas the PO_2-dependency of the apnoea duration index in TH-Cre mice was primarily driven by the PO_2-dependent nature of the apnoeic index (as the mean apnoea duration remained comparable at 12% O_2 and 8% O_2), in the *AMPK α1*

and *α2* floxed the increase was driven by a PO_2-dependent increases in both the apnoeic index and apnoea duration (Table 3.1).

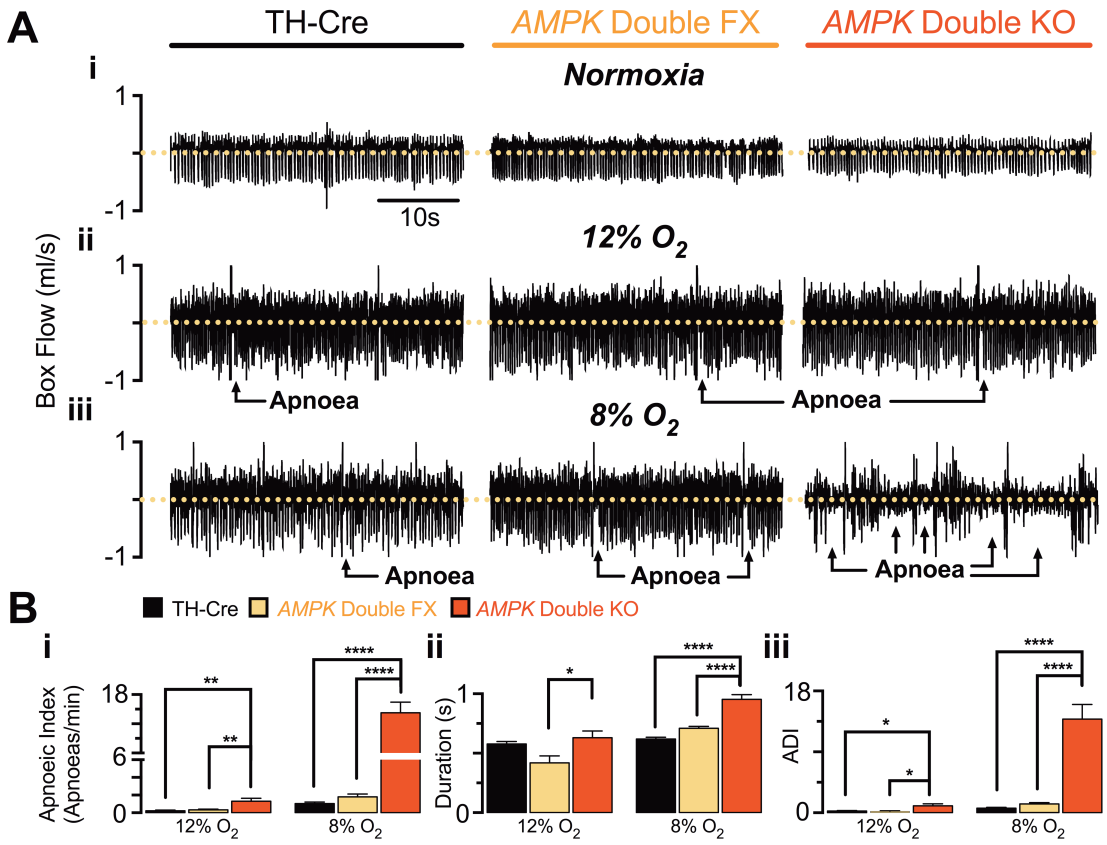

Figure 4.1: Conditional deletion of *AMPK* in catecholaminergic cells precipitates apnoeas in a PO_2-dependent manner. (A) Records of ventilatory activity from TH-Cre (*left panel*), *AMPK α1* and *α2* double floxed (*AMPK* Double FX, *middle panel*) and *AMPK α1* and *α2* double knockout mice (*AMPK* Double KO, *right panel*) during **(i)** normoxia (21% O_2 + 0.05% CO_2), **(ii)** mild hypoxia (12% O_2 + 0.05% CO_2) and **(iii)** severe hypoxia (8% O_2 + 0.05% CO_2). **(B)** Mean ± SEM for **(i)** apnoeic index (AI, apnoeas per minute), **(ii)** apnoea duration (s) and **(iii)** the apnoea-duration index (TH-Cre - 12% O_2: n = 19, 8% O_2: n = 24, black; *AMPK* Double FX - 12% O_2: n = 31, 8% O_2: n = 12, yellow; *AMPK* Double KO - 12% O_2: n = 29, 8% O_2: n = 19, red). * = $p < 0.05$, ** = $p < 0.01$, **** = $p < 0.0001$. Significance tested by one-way ANOVA with Bonferroni multiple comparisons.

Table 4.1: The effects of *AMPK* deletion on the frequency and duration of apnoeas during hypoxia.

	TH-Cre			AMPK Double Floxed			*AMPK* Double Knockout			Related Figure
	21% O_2	12% O_2	8% O_2	21% O_2	12% O_2	8% O_2	21% O_2	12% O_2	8% O_2	
Apnoeic Index (Apnoeas/min)	NA	0.2 ± 0.1 n = 19	1.0 ± 0.2 n = 24	NA	0.3 ± 0.1 n = 31	1.8 ± 0.3 n = 12	NA	1.3 ± 0.3 n = 29	14 ± 0.2 n = 19	4.1 Panel Bi
Apnoea Duration (ms)	NA	587 ± 21 n = 19	620 ± 21 n = 24	NA	419 ± 58 n = 31	709 ± 17 n = 12	NA	630 ± 57 n = 29	953 ± 40 n = 19	4.1 Panel Bii
Apnoea Duration Index	NA	0.3 ± 0.1 n = 19	0.7 ± 0.1 n = 24	NA	0.2 ± 0.1 n = 31	1.3 ± 0.3 n = 12	NA	1.0 ± 0.3 n = 29	14 ± 2.0 n = 19	4.1 Panel Biii

NA = not applicable

Breathing irregularities of *AMPK α1* and *α2* double knockout mice appeared even more complex when examined on an expanded time scale as illustrated in Figure 4.2. Under mild hypoxia, apnoeas appeared only slightly prolonged in *AMPK α1* and *α2* double knockout mice (maximum apnoea was ~1s) when compared to the control TH-Cre and *AMPK α1* and *α2* floxed mice (maximum was ~830ms). Also, the apnoeas observed in both control TH-Cre and *AMPK α1* and *α2* floxed mice as well as *AMPK α1* and *α2* double knockout mice were often preceded by a sigh, which was identified as an exaggerated breath with an inspiratory and expiratory amplitude, i.e. tidal volume, measuring at least twice as large as the amplitudes of the three previous breaths (Voituron et al., 2009). However, under severe hypoxia the apnoeas were not only more frequent and prolonged, with a maximum apnoea duration of ~6s in *AMPK α1* and *α2* double knockout mice (~ 900ms in TH-Cre and *AMPK α1* and *α2* floxed mice) but the ventilatory pattern also varied extensively. Periodic breathing was occasionally evident as prolonged post-sigh apnoeas would occur at regular intervals of ~0.1Hz (as shown in Figure 4.2 – Panel Biii, *upper panel* and on an expanded time-course in Appendix 4A). Unlike the *Lkb1* knockouts, such periodic breathing was not associated with Cheyne-Stokes-like breathing, which is characterised by a sinusoidal ventilatory pattern that cycles from progressively deeper and faster breathes to a gradual decreases in frequency and tidal volume which ultimately reaches an apnoeic event (Eckert et al., 2007).

Nevertheless, other forms of disordered breathing were identified in *AMPK α1* and *α2* double knockout mice during 8% O_2, which included non-rhythmic periods of hypoventilation with prolonged apnoeas that either preceded a sigh or occurred spontaneously (Figure 4.2 – Panel Biii, *lower panel*).

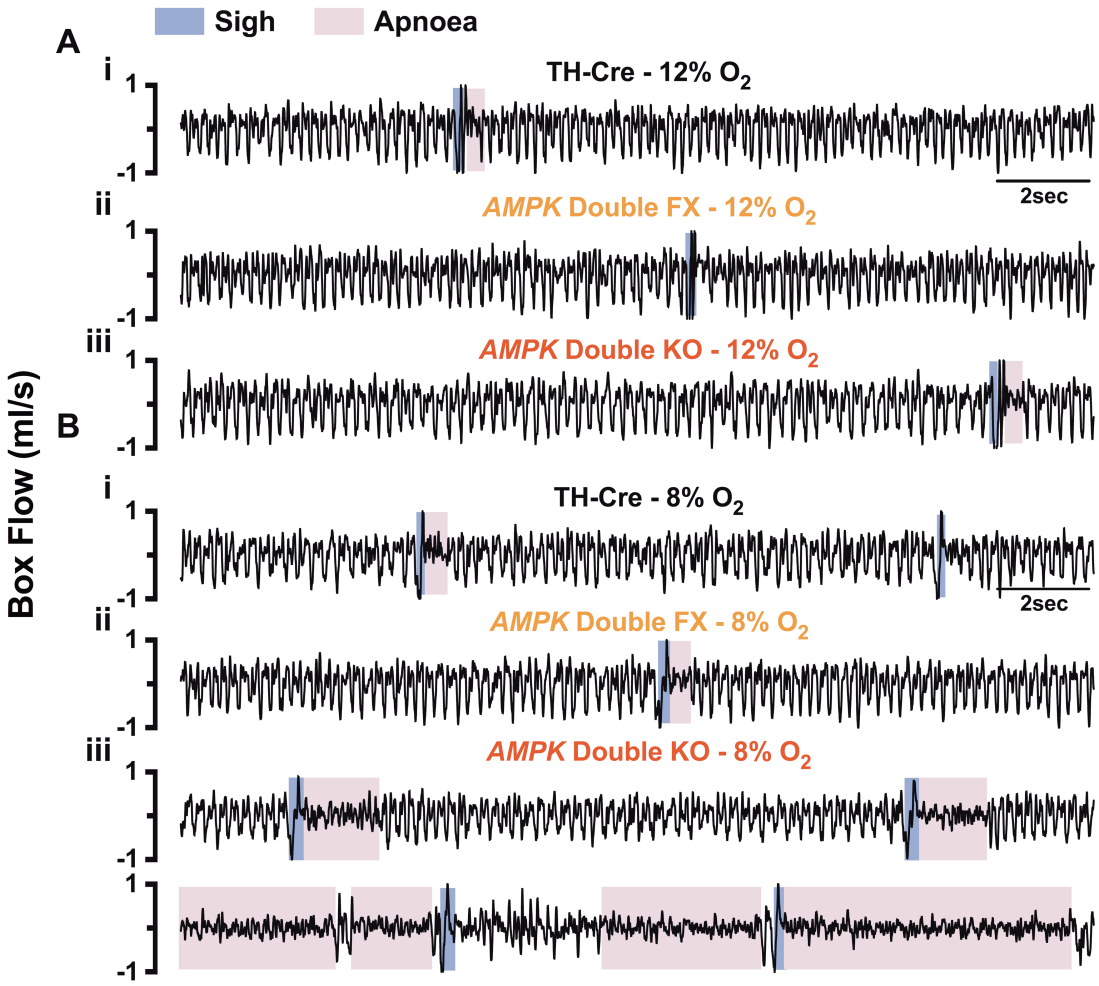

Figure 4.2: Conditional deletion of *AMPK* in catecholaminergic cells precipitates abnormalities in ventilatory pattern that includes apnoeas and hypoventilation in a manner that is PO_2-dependent. Typical ventilatory records on an expanded time scale during **(A)** mild hypoxia (12% O_2) and **(B)** severe hypoxia (8% O_2) from **(i)** TH-Cre**, (ii)** *AMPK* $\alpha 1$ and $\alpha 2$ double floxed mice (*AMPK* Double FX), and **(iii)** *AMPK* $\alpha 1$ and $\alpha 2$ double knockout mice (*AMPK* Double KO). **(Biii)** Different *AMPK* Double KO mice during severe hypoxia (8% O_2), which exhibit post-sigh apnoeas (*upper and lower panel*) as well as periods of hypoventilation with spontaneous and post-sigh apnoeas (*lower panel*).

Further analysis, with the support of Dr. Paolo Puggioni, indicate that central rather than obstructive apnoeas are induced by *AMPK α1* and *α2* deletion in catecholaminergic cells. As described in chapter 3, central apnoeas are characterised by the lack of central drive to breath and a lack of respiratory effort during the cessation of breathing. In contrast, obstructive apnoea results from an obstruction of the airway and is associated with ongoing respiratory efforts during the period over which ventilation ceases (Eckert et al., 2007). Computational video-analysis of thoracic movement was studied in parallel with measurements of inspiration and expiration by plethysmography and revealed that thoracic movement in TH-Cre mice continuously oscillated in parallel with inspiratory and expiratory events from corresponding ventilatory records obtained during 8% O_2 (Figure 4.3 - Panel A). This was also apparent in the *AMPK α1* and *α2* double knockouts as thoracic movement oscillated correspondingly with inspiratory and expiratory events, with robust movements also recorded during exaggerated breaths, e.g. sighs (Figure 4.3 – Panel B, *purple*). However, during apnoeic events there was little or no evidence of thoracic activity and accordingly a lack of respiratory effort (Figure 4.3 – Panel B, *pink*). Hence, the deletion of *AMPK* function in catecholaminergic cells appears to precipitate central and not obstructive apnoeas.

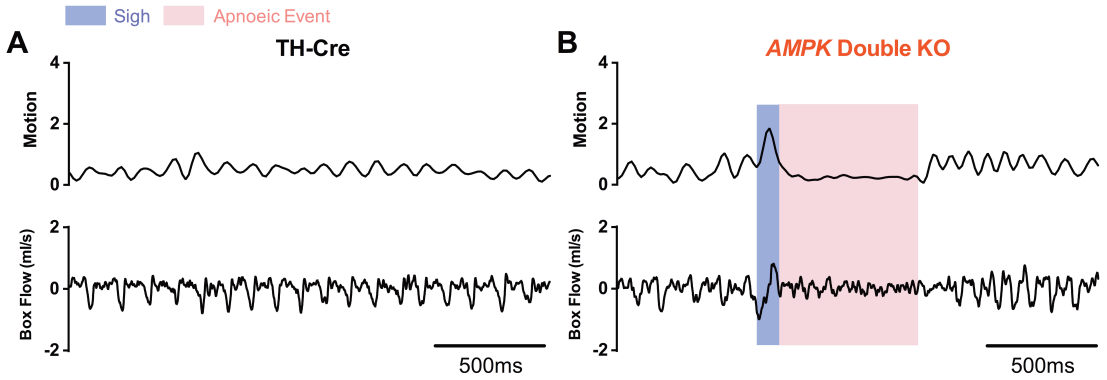

Figure 4.3: Computational video analysis of thoracic movement during ventilation. Computational video analysis of thoracic movement (*upper panel*) with corresponding ventilatory traces obtained using unrestrained whole body plethysmography (8% O_2 + 0.05% CO_2, *lower panel*) in a **(A)** TH-Cre and **(B)** *AMPK α1* and *α2* double knockout mouse (*AMPK* double KO). Sighs are highlighted in purple; apnoeas highlighted in pink

4.2.1.2 Poincaré analysis reveals the PO_2-dependence of disordered breathing in AMPK *α1* and *α2* knockout mice

Whether considering the periods of hypoventilation, post-sigh apnoeas, or spontaneous apnoeas, deletion of *AMPK α1* and *α2* catalytic subunits in catecholaminergic cells led to breathing irregularities that increased in severity from mild to severe hypoxia. This was confirmed by plotting the inter-breath intervals (BBn) versus the subsequent inter-breath interval (BBn+1) to generate Poincaré plots. Example Poincaré plots of 500 breaths from a single exposure period are shown in Figure 4.4, which compares the breathing regularity of TH-Cre, *AMPK* α1 and α2 floxed, and *AMPK α1* and *α2* double knockout mouse during normoxia (21% O_2), mild hypoxia (12% O_2), and severe hypoxia (8% O_2).

Clearly the variability in the inter-breath interval is comparable across all three genotypes under normoxic conditions (Figure 4.4 – Panel A). However, as previously described in Chapter 3, a marginal increase in breathing irregularity is observed in TH-Cre mice in a manner inversely related to PO_2 levels. This was also observed in the *AMPK α1* and *α2* floxed mice and is entirely consistent, as noted above, with previous studies on wild-type C57/BL6 mice (Stettner et al., 2008). In marked contrast *AMPK α1* and *α2* double knockout mice exhibited not only marked but clearly PO_2-dependent increases in breathing irregularities (Figure 4.4 – Panels A-C, *lower panels*). From these plots, long inter-breath intervals were apparent in *AMPK α1* and *α2* double knockout mice, ranging from 0.5s to ~4s. Strikingly, the number of interbreath intervals within this range increased markedly during 8% O_2. This suggests that the loss of *AMPK* function in catecholaminergic cells leads to marked increases in inter-breath interval and thus precipitates hypoventilation.

Clearly, the increase in breathing irregularity in *AMPK α1* and *α2* double knockout mice increased in a manner proportional to the severity of hypoxia, and was markedly greater than that observed in either control TH-Cre or *AMPK α1* and *α2* floxed mice. This fact was confirmed by comparison of the variability of inter-breath interval by comparison of the standard deviation (SD) of the BBn and BBn+1, as shown in Figure 4.4 (Panels A-C, *lower panels*). Consistent with the observations made of the

Poincaré plots, a marginal and comparable PO_2-dependent increase was observed in both TH-Cre and *AMPK α1* and *α2* floxed mice during 12% O_2 (TH-Cre: 47 ± 5ms, n = 20 exposures from 5 mice; *AMPK α1* and *α2* floxed: 59 ± 3ms, n = 31 exposures from 6 mice) and 8% O_2 (TH-Cre: 65 ± 5ms, n = 24 exposures from 5 mice; *AMPK α1* and *α2* floxed: 59 ± 3ms, n = 12 exposures from 4 mice). In marked contrast, *AMPK α1* and *α2* double knockout mice exhibited a large SD, which significantly increased in a PO_2-dependent manner from 12% O_2 to 8% O_2 ($p < 0.0001$), but also to levels significantly greater than the controls during 12% O_2 (78 ± 5 ms, n = 29 exposures from 5 mice, $p < 0.001$ versus *AMPK α1* and *α2* floxed, $p < 0.0001$ versus TH-Cre) and 8% O_2 (238 ± 23ms, n = 19 exposures from 5 mice, $p < 0.0001$ versus *AMPK α1* and *α2* floxed and TH-Cre mice)(Figure 4.4, *lower panels*).

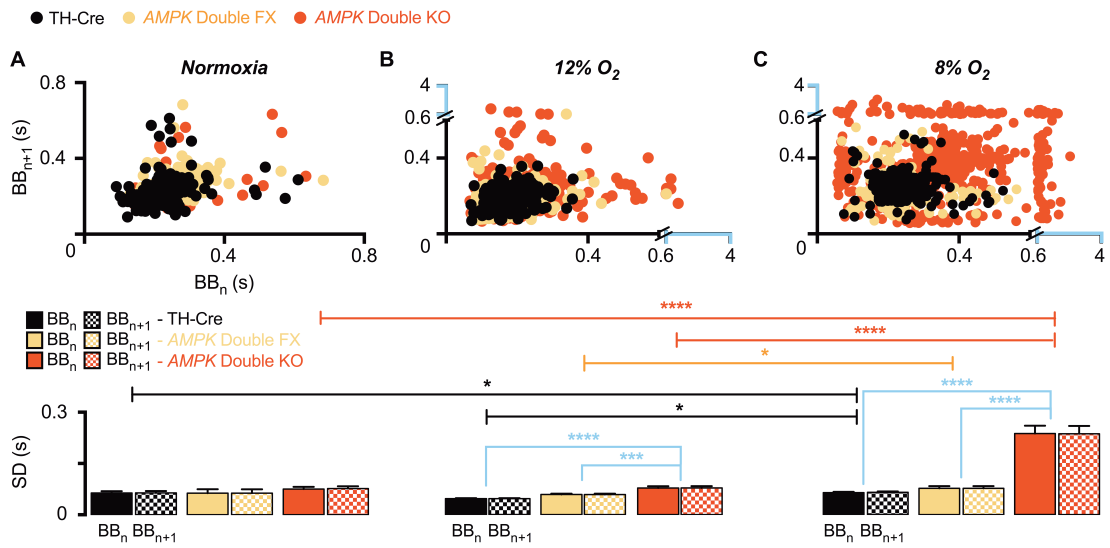

Figure 4.4: Conditional deletion of *AMPK* in catecholaminergic cells affects the regularity of breathing in a PO_2-dependent manner. *Upper panels* show Poincaré plots of the inter-breath interval (BB_n) versus subsequent interval (BB_{n+1}) of TH-Cre (black), *AMPK α1* and *α2* double floxed (*AMPK* Double FX, yellow) and *AMPK α1* and *α2* double knockout mice (*AMPK* Double KO, red) during **(A)** normoxia (21% O_2 + 0.05% CO_2), **(B)** mild hypoxia (12% O_2 + 0.05% CO_2), and **(C)** severe hypoxia (8% O_2 + 0.05% CO_2). The corresponding *lower panels*, show the mean ± SEM for the standard deviation (SD) of BB_n and BB_{n+1} of each genotype under normoxia (TH-Cre: n = 25, N = 5 mice; *AMPK* double FX: n = 8, N = 4 mice; *AMPK* double KO: n = 15, N = 5 mice), mild hypoxia (TH-Cre: n = 20, N = 5 mice; *AMPK* Double FX: n = 31, N = 6 mice; *AMPK* Double KO: n = 29, N = 5 mice) and severe hypoxia (TH-Cre: n = 24, N = 5 mice; *AMPK* Double FX: n = 12, N = 4 mice; *AMPK* Double KO: n = 19, N = 5 mice). * = $p < 0.05$, *** = $p < 0.001$, and **** = $p < 0.0001$. Significance tested by one-way ANOVA with Bonferroni multiple comparisons.

4.2.1.3 Deletion of AMPK activity in catecholaminergic cells attenuates the hypoxic increase in breathing frequency, tidal volume, and minute ventilation

The deletion of both *AMPK α1* and *α2* catalytic subunits in catecholaminergic cells markedly attenuated the average increase in ventilation during mild and severe hypoxia. Figure 4.5 shows example records for the change in frequency, tidal volume, and minute ventilation (2s sampling period) over the 5min exposure to 12% O_2 and 8% O_2 in both *AMPK α1* and *α2* floxed and *AMPK α1* and *α2* double knockout mice. By contrast to the robust increases in these parameters observed in *AMPK α1* and *α2* floxed mice, all measures of ventilatory activity were markedly attenuated in *AMPK α1* and *α2* double knockouts. Moreover, as might be expected given the above, these effects were PO_2-dependent.

Breathing frequency As illustrated by the example records, when compared to control *AMPK α1* and *α2* floxed mice, the *AMPK α1* and *α2* double knockouts exhibited an attenuation of ventilatory response to hypoxia across 3 different time points during 12% O_2. Initially, the breathing frequency in control *AMPK α1* and *α2* floxed mice increased by 59 ± 2% at 30s following the onset of 12% O_2 (n = 30 exposures from 5 mice), before decreasing to 38 ± 2% at 100s due to respiratory depression (Bissonnette, 2000). Thereafter, respiratory frequency in the *AMPK α1* and *α2* floxed mice was maintained at 31 ± 1% at the end of the hypoxic exposure (300s, Figure 4.6). In marked contrast, in *AMPK α1* and *α2* double knockouts the initial increase in breathing frequency after 30s was significantly less at 32 ± 3% relative to normoxia (n = 30 exposures from 5 mice, $p < 0.0001$). Strikingly, respiratory depression, assessed after 100s, resulted in a further decrease in breathing frequency that was also significantly attenuated at 5 ± 2% when compared to *AMPK α1* and *α2* floxed mice ($p < 0.0001$). Thereafter, the percentage change in breathing frequency remained significantly attenuated at 2 ± 1% of that observed under normoxia ($p < 0.0001$) at the end of the 5min exposure to 12% O_2 (Figure 4.6 – Panel Ai and Table 3.2).

During severe hypoxia, 8% O_2, the impact of *AMPK* deletion on the average ventilatory response was greater still (Figure 4.6 – Panel Bi). Similar to 12% O_2, here it was notable that there was an initial robust increase in breathing frequency at 30s in

AMPK α1 and *α2* floxed mice by 46 ± 5% relative to normoxia (n = 13 exposures from 5 mice) before reducing to 21 ± 4% due to respiratory depression; this is profoundly lower than the decrease observed at 12% O_2 due to respiratory depression (38 ± 2% at 100s). Nevertheless, the percentage change in breathing frequency relative to normoxia recovered to 28 ± 4% by the end of the hypoxia exposure (300s) (Table 3.2).

A significant decrease relative to controls was observed in the *AMPK α1* and *α2* double knockouts across all three time points during 8% O_2. Consistent with the PO_2-dependent increases in apnoea-duration index and interbreath interval, the degree to which *AMPK* deletion attenuated the ventilatory response to hypoxia was found to be inversely relate to PO_2. At 30s following the onset of 8% O_2, the percentage change in frequency increased by only 11 ± 3% relative to that observed during normoxia (n = 26 exposures from 5 mice, $p < 0.0001$). Strikingly, respiratory depression, assessed in *AMPK α1* and *α2* double knockout mice at 100s, resulted in a further decrease in breathing frequency that resulted in marked hypoventilation of -12 ± 2% relative to normoxia ($p < 0.0001$). Thereafter, the percentage change in breathing frequency relative to normoxia remained below normoxic levels throughout the remainder of the 5min exposure, measuring -10 ± 2% after 300s; significantly lower when compared to *AMPK α1* and *α2* floxed mice ($p < 0.0001$, Figure 4.6 – Panel Bi). This suggests that *AMPK α1* and *α2* double knockouts mice are able to increase breathing frequency initially during hypoxia, even though significantly attenuated at 30s when compared to controls. However mice lacking AMPK are unable to sustain this increase in breathing frequency for the remainder of the 5min exposure.

Tidal Volume In marked contrast to the time-dependent changes in breathing frequency, hypoxia induced a sustained increase in mean tidal volume in *AMPK α1* and *α2* floxed mice throughout the 5min exposure to 12% O_2 (30s: 23 ± 3%; 100s: 31 ± 3%; 300s: 23 ± 3%) and 8% O_2 (30s: 48 ± 9%; 100s: 41 ± 6%; 300s: 37 ± 6%) (Figure 4.6 – Panel Aii). Interestingly, the increase in tidal volume in AMPK *α1* and *α2* double knockouts increased to a sustainable level that was comparable to controls under 12% O_2 (30s: 22 ± 5%, 100s: 29 ± 3%, 300s: 21 ± 3%) but was significantly attenuated throughout the 5min exposure to 8% O_2 (30s: 13 ± 6%, $p < 0.001$; 100s: 12 ± 6%, $p <$

0.0001; 300s: 2 ± 7%, $p < 0.001$) (Figure 4.6 – Panel A,Bii and Table 3.3). Hence, deletion of *AMPK α1* and *α2* in catecholaminergic cells results in a PO_2-dependent attenuation in tidal volume between 12% O_2 and 8% O_2.

Minute Ventilation Adjustments in minute ventilation were robust in *AMPK α1* and *α2* floxed mice throughout the 5min exposure to 12% O_2 (30s: 96 ± 6, 100s: 79 ± 5, 300s: 59 ± 4%) and 8% O_2 (30s: 106 ± 6, 100s: 72 ± 11; 300s: 72 ± 8%) (Figure 4.6 – Panel A,Biii). As would be expected given the above, however, the deletion of *AMPK α1* and *α2* catalytic subunits in catecholaminergic cells led to a significant attenuation of minute ventilation during hypoxia. Furthermore, the degree of attenuation increased in severity from 12% O_2 (30s: 65 ± 5%, $p < 0.0001$; 100s: 35 ± 4, $p < 0.0001$; 300s: 22 ± 4, $p < 0.0001$) to 8% O_2 (30s: 36 ± 5%, $p < 0.0001$; 100s: 7 ± 5, $p < 0.0001$; 300s: -4 ± 5, $p < 0.0001$) (Figure 4.6 – Panel A,Biii and Table 3.4).

Collectively, these data strongly suggests that, like outcomes for *Lkb1* knockout mice (Chapter 3), AMPK is required for the modulation by hypoxia of oxygen-sensing catecholaminergic cells and thereby underpins the ventilatory response to hypoxia. That aside it was also notable that *AMPK α1* and *α2* double knockout mice would lie down and barely move during all exposures to 8% O_2, but not 12% O_2, and this was never observed for control TH-Cre and *AMPK α1* and *α2* floxed mice. Therefore, it is possible that these mice adjust behaviours in order to reduce O_2 requirements when unable to compensate for a fall in O_2 supply by increased ventilation (Appendix 4B).

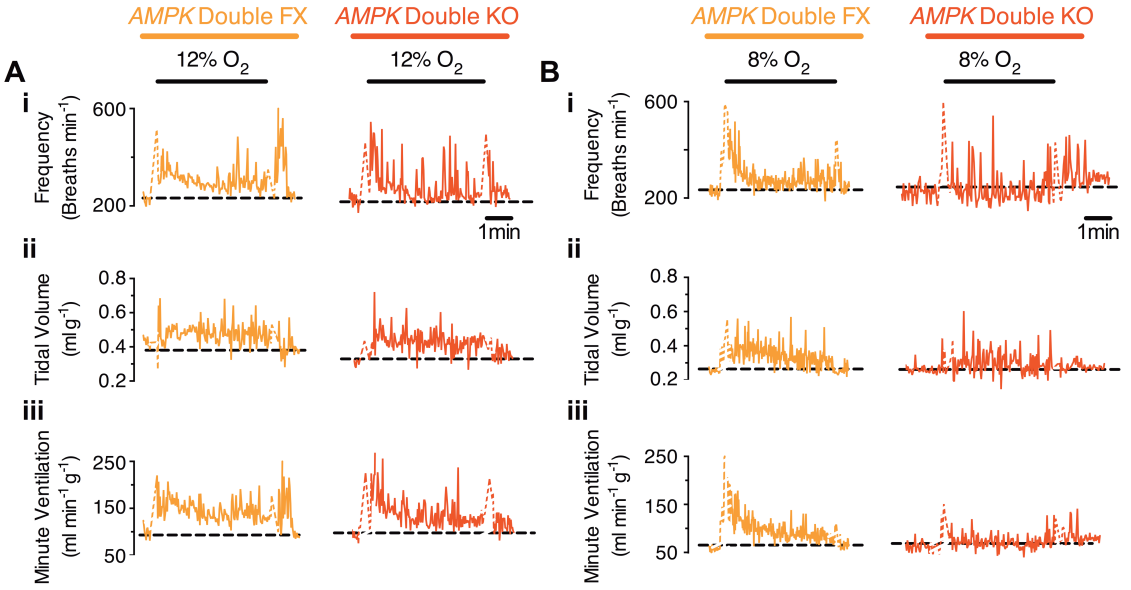

Figure 4.5: Conditional deletion of *AMPK* in catecholaminergic cells attenuates the hypoxic ventilatory response in a manner that is PO_2-dependent. The effect over a 5min period of exposure to **(A)** mild hypoxia (12% O_2) and **(B)** severe hypoxia (8% O_2) on **(i)** breathing frequency (min^{-1}), **(ii)** tidal volume (ml g^{-1}) and **(iii)** minute ventilation (ml min^{-1} g^{-1}) in *AMPK α1* and *α2* double floxed (*AMPK* double FX, orange) and *AMPK α1* and *α2* double knockout mice (*AMPK* double KO, red) with 2s sampling periods. Dashed black line indicating basal level, white line breaks indicate artefact of gas exchange.

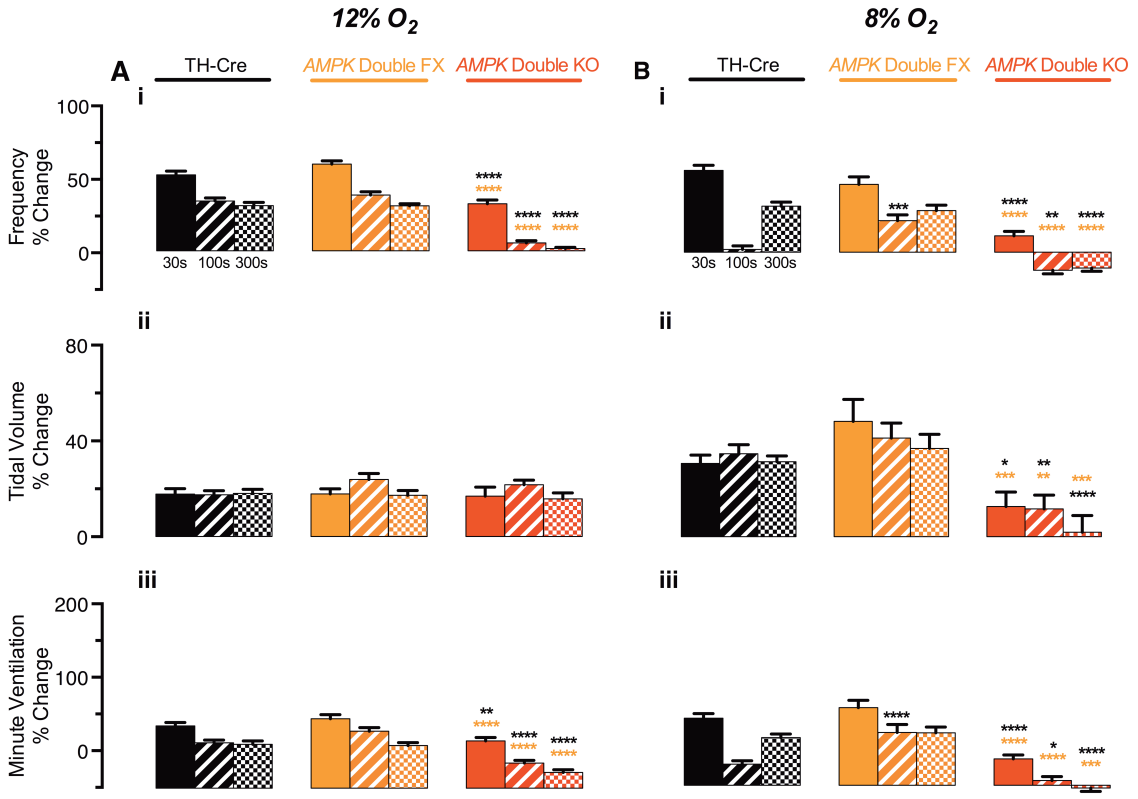

Figure 4.6: The mean ventilatory response to hypoxia is attenuated in *AMPK α1* and *α2* double knockout mice. Mean ± SEM for percent change during **(A)** mild hypoxia (12% O_2) and **(B)** severe hypoxia (8% O_2) in **(i)** breathing frequency (min^{-1}), **(ii)** tidal volume (ml g^{-1}) and **(iii)** minute ventilation (ml min^{-1} g^{-1}) at 3 time points of the 5min hypoxic exposure in TH-Cre (12% O_2: n = 25 exposures; 8% O_2: n = 37 exposures; N = 4 mice, black), *AMPK α1* and *α2* double floxed (*AMPK* Double FX; 12% O_2: n = 30 exposures; 8% O_2: n = 13 exposures, N = 5 mice, orange), and *AMPK α1* and *α2* double knockout mice (*AMPK* Double KO 12% O_2: n = 30 exposures; 8% O_2: n = 26 exposures, N = 5 mice, red). * = $p < 0.05$, ** = $p < 0.01$, *** = $p < 0.001$, **** = $p < 0.0001$. Significance tested by one-way ANOVA with Bonferroni multiple comparisons.

Table 4.2: Mean percentage change in breathing frequency during hypoxia

	Breathing Frequency (% Change)						Related Figure
	12% O_2			8% O_2			
	30s	100s	300s	30s	100s	300s	
TH-Cre	51 ± 3	34 ± 2	31 ± 2	55 ± 3	2 ± 2	31 ± 3	4.6 A,B (i)
	n = 25 exposures from 5 mice			n = 37 exposures from 5 mice			
AMPK Double Floxed	59 ± 2	38 ± 2	31 ± 1	46 ± 5	21 ± 4	28 ± 4	
	n = 30 exposures from 5 mice			n = 13 exposures from 5 mice			
AMPK Double Knockouts	32 ± 3	5 ± 2	2 ± 1	11 ± 3	-12 ± 2	-10 ± 2	
	n = 30 exposures from 5 mice			n = 26 exposures from 5 mice			

Table 4.3: Mean percentage change in tidal volume during hypoxia

	Tidal Volume (% Change)						Related Figure
	12% O_2			8% O_2			
	30s	100s	300s	30s	100s	300s	
TH-Cre	23 ± 3	23 ± 2	24 ± 2	31 ± 4	35 ± 4	31 ± 2	4.6 A,B (ii)
	n = 25 exposures from 5 mice			n = 37 exposures from 5 mice			
AMPK Double Floxed	23 ± 3	31 ± 3	23 ± 3	48 ± 9	41 ± 6	37 ± 6	
	n = 30 exposures from 5 mice			n = 13 exposures from 5 mice			
AMPK Double Knockouts	22 ± 5	29 ± 3	21 ± 3	13 ± 6	12 ± 6	2 ± 7	
	n = 30 exposures from 5 mice			n = 26 exposures from 5 mice			

Table 4.4: Mean percentage change in minute ventilation during hypoxia

	Minute Ventilation (% Change)						Related Figure
	12% O_2			8% O_2			
	30s	100s	300s	30s	100s	300s	
TH-Cre	86 ± 5	63 ± 4	61 ± 5	92 ± 6	29 ± 5	65 ± 5	4.6 A,B (iii)
	n = 25 exposures from 5 mice			n = 37 exposures from 5 mice			
AMPK Double Floxed	96 ± 6	79 ± 5	59 ± 4	106 ± 6	72 ± 11	72 ± 8	
	n = 30 exposures from 5 mice			n = 13 exposures from 5 mice			
AMPK Double Knockouts	65 ± 5	35 ± 4	22 ± 4	36 ± 5	7 ± 5	-4 ± 5	
	n = 30 exposures from 5 mice			n = 26 exposures from 5 mice			

4.2.1.3a The effects of *AMPK* deletion on the breathing frequency response during hypoxia is driven by changes to the durations of the inspiration and expiration

Given the above it seemed likely that further insight might be obtained from analyses of inspiration time, expiration time, and total breath duration, as this would allow us to determine whether or not the inspiratory and/or expiratory phases of ventilation are compromised in the *AMPK α1* and *α2* double knockout mice. Figures 4.7 and 4.8 show example and averaged (mean ± SEM) records, respectively, of the ratiometric change (Hypoxia/Normoxia) in inspiration time (Ti), expiration time (Te), and total breath time (*To*) during 12% O_2 and 8% O_2 in *AMPK α1* and *α2* double floxed and knockout mice.

Inspiration time (Ti) Upon exposure to 12% O_2 and 8% O_2, *AMPK α1* and *α2* floxed mice exhibited a time-dependent change in Ti (Figure 4.8 – Panel A). This involved a reduction in Ti duration relative to normoxia at the start of the 5min exposure, at 30s following the onset of hypoxia, before a gradual prolongation of Ti is observed that plateaus by 2min and remains stable for the remainder of the 5min exposure. This is demonstrated by the measured mean ± SEM of Ti at 30s as well as the overall mean ± SEM of Ti during the final 2min of the hypoxic exposure between 3 and 5min (using the formula for error of propagation). In the *AMPK α1* and *α2* floxed mice, the mean ± SEM of Ti at 30s markedly fell to 0.78 ± 0.04 (n = 7 exposures from 5 mice) during 12% O_2 and 0.74 ± 0.06 (n = 10 exposures from 5 mice) during 8% O_2; this therefore equates to a faster inspiration phase in response to mild and severe hypoxia when compared to normoxia. Thereafter, Ti progressively lengthened until Ti under hypoxia was similar in duration to Ti under normoxia (hence approaching a ratio of 1). This is indicated by the overall mean ratio observed during the plateau observed during the final 2min of the hypoxic exposure, which was 1.1 ± 0.01 during 12% O_2 and 1.09 ± 0.02 during 8% O_2.

In the *AMPK α1* and *α2* double knockouts, a time-dependent change in Ti was also observed during hypoxia (Figure 4.8 – Panel A). Once more, an initial shortening of Ti duration was observed relative to normoxia at the start of the exposure to 12% O_2

and 8% O_2. Relative to the control *AMPK α1* and *α2* floxed mice, this reduction in inspiration time at 30s was comparable as it fell to 0.80 ± 0.04 (n = 6 exposures from 6 mice) during 12% O_2 and 0.89 ± 0.05 (n = 10 exposures from 5 mice, $p < 0.0001$) at 8% O_2. A PO_2-dependent lengthening of Ti duration was also observed in the *AMPK α1* and *α2* double knockouts to a level that recovered to Ti during normoxia at 12% O_2 (1.01 ± 0.03) and to a level that exceeded Ti during normoxia at 8% O_2 (1.19 ± 0.04); this was also significantly longer than the mean Ti observed in *AMPK α1* and *α2* floxed mice during the final 2min of the hypoxic exposure at 12% O_2 ($p < 0.01$) and 8% O_2 ($p < 0.0001$).

Therefore, in response to hypoxia both control *AMPK α1* and *α2* floxed mice and *AMPK α1* and *α2* double knockouts similarly exhibit an initial shortening of inspiration time relative to normoxia. Moreover, while inspiration time of *AMPK α1* and *α2* floxed mice recovers back to values equivalent to those observed under normoxia during 12% O_2 and 8% O_2, in the *AMPK α1* and *α2* double knockouts this only occurs at 12% O_2 as under 8% O_2 inspiration duration overshoots the inspiration time observed under normoxia.

Expiration Time (Te) Unlike Ti, Te of control *AMPK α1* and *α2* floxed mice decreased relative to normoxia in a manner that was maintained throughout the 5min exposure to 12% O_2 and 8% O_2. Therefore, these mice exhibited a shortening of expiration time during hypoxia (Figure 4.8 – Panel B). Reductions in Te exhibited time-dependent characteristics but, similar to Ti, plateaued by 2min of the hypoxic exposure. Overall, this is demonstrated by the marked reduction in mean Te relative to normoxia at 30s during 12% O_2 (0.54 ± 0.07) and 8% O_2 (0.59 ± 0.10). Thereafter, mean ratio of Te lengthened slightly but remained markedly shorter than Te of normoxia during the final 2 minutes of 12% O_2 (0.73 ± 0.03) and 8% O_2 (0.90 ± 0.03).

AMPK α1 and *α2* double knockouts also exhibited a time-dependent change in Te during 12% O_2 and 8% O_2. Again, an initial shortening of Te was observed at 30s at the start of the hypoxic exposure to 12% O_2 and 8% O_2. Relative to the control *AMPK α1* and *α2* floxed mice, this reduction in expiration time at 30s was comparable during 12% O_2 as it fell to 0.57 ± 0.10 but markedly less during 8% O_2 as it only fell to 0.80 ±

0.07. Thereafter, Te duration prolonged in the *AMPK α1* and *α2* double knockouts from 3-5min to a level that was shorter than normoxic Te at 12% O_2 (0.65 ± 0.02) and to a level that was slightly longer than normoxic Te during 8% O_2 (1.09 ± 0.06). Nevertheless, while the mean Te observed in *AMPK α1* and *α2* floxed mice during the final 2min was not significantly different relative to control *AMPK α1* and *α2* floxed mice under 12% O_2, the difference reached significance using an unpaired student's t-test under 8% O_2 ($p < 0.01$).

Therefore, in response to 12% O_2 both control *AMPK α1* and *α2* floxed mice and *AMPK α1* and *α2* double knockouts similarly exhibit an initial shortening of expiration time relative to normoxia. However, under 8% O_2 the shortening of Te at 30s is less severe in the *AMPK α1* and *α2* double knockouts relative to the *AMPK α1* and *α2* floxed mice. Moreover, while expiration time of *AMPK α1* and *α2* floxed mice lengthens slightly it remains more rapid than that observed under normoxia during the final 2min of 12% O_2 and 8% O_2 exposures. By contrast, in the *AMPK α1* and *α2* double knockouts Te lengthens to values more rapid than that observed during normoxia under 12% O_2 but lengthens to values slightly longer than that observed under normoxia during 8% O_2.

Total Breath Duration (To) In controls, outcomes for Ti and Te translated into reductions in *To* during 12% O_2 and 8% O_2 relative to hypoxia; consistent with observed increases in breathing frequency (Section 4.2.1.3). Initially *To*, relative to normoxia, fell at 30s to 0.59 ± 0.06 during 12% O_2 and 0.63 ± 0.08 during 8% O_2, before slightly lengthening to 0.81 ± 0.03 and 0.96 ± 0.02, respectively, during the final 2min of the hypoxic exposure. This is primarily driven by reductions in the duration of the expiratory phase as Te decreases relative to normoxia throughout the 5min hypoxic exposures while Ti plateaus at levels comparable with Ti under normoxia. By contrast, average reductions in *To* during hypoxia are attenuated by *AMPK α1* and *α2* deletion in a time and PO_2-dependent manner. Relative to control *AMPK α1* and *α2* floxed mice, *To* of *AMPK α1* and *α2* double knockouts similarly fell to 0.59 ± 0.06 at 30s following the onset of 12% O_2, but only fell to 0.82 ± 0.05 during 8% O_2 (though not significantly different). Thereafter, *To* prolonged but remained more rapid than *To* during normoxia from 3-5min under 12% O_2 (0.74 ± 0.02), which was enhanced compared to controls

although not significantly different. , In contrast, Te during was longer than normoxic levels at 8% O_2 from 3-5min (1.12 ± 0.05) and was significantly longer than Te maintained from 3-5 min in control *AMPK α1* and *α2* floxed mice ($p < 0.01$).

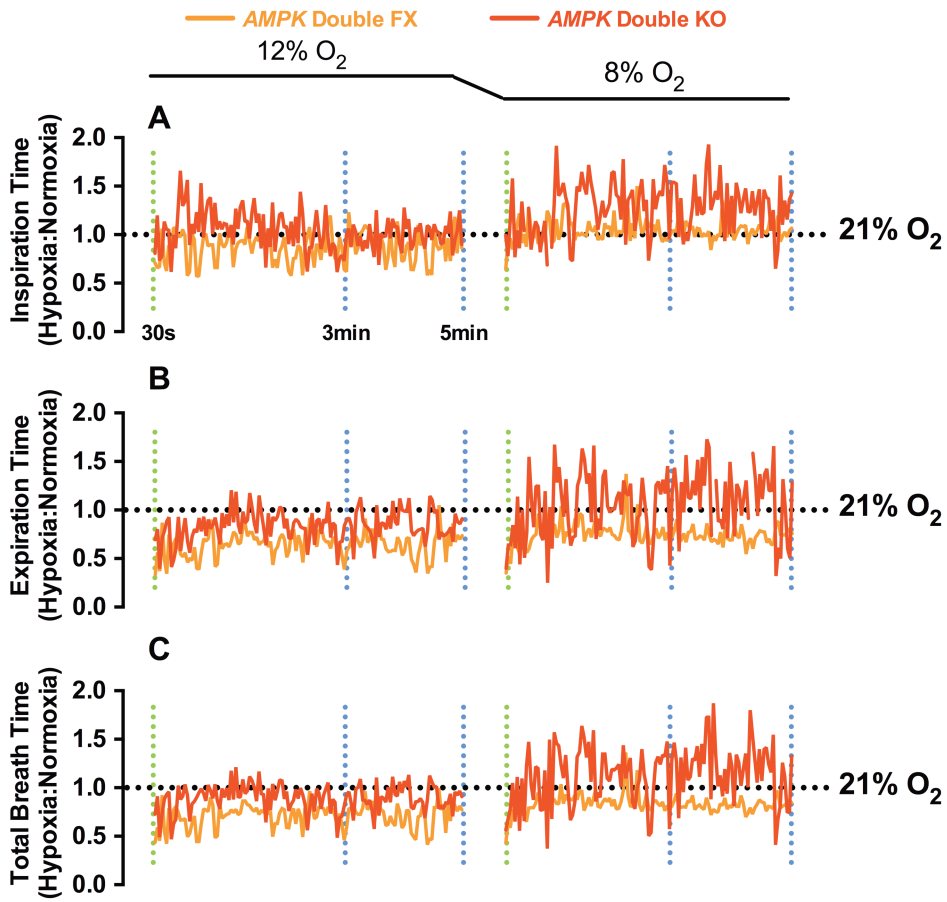

Figure 4.7: The effect of *AMPK* deletion on the duration of inspiration, expiration and total breath duration during hypoxia. Example records of the ratiometric changes (relative to normoxia as indicated by dotted line at 1.0, 21% O_2) in the duration (s) of **(A)** inspiration (Ti), **(B)** expiration (Te) and **(C)** total breath (To) over a 5min exposure with 2s sampling periods during mild hypoxia (12% O_2, *left panels*) and **(B)** severe hypoxia (8% O_2, *right panels*) in *AMPK α1* and *α2* double floxed (*AMPK* Double FX, orange) and *AMPK α1* and *α2* double knockout (*AMPK* Double KO, red) mice. 30s following the onset of hypoxia indicated by green vertical dotted line; 3-5min indicated by blue vertical dotted lines.

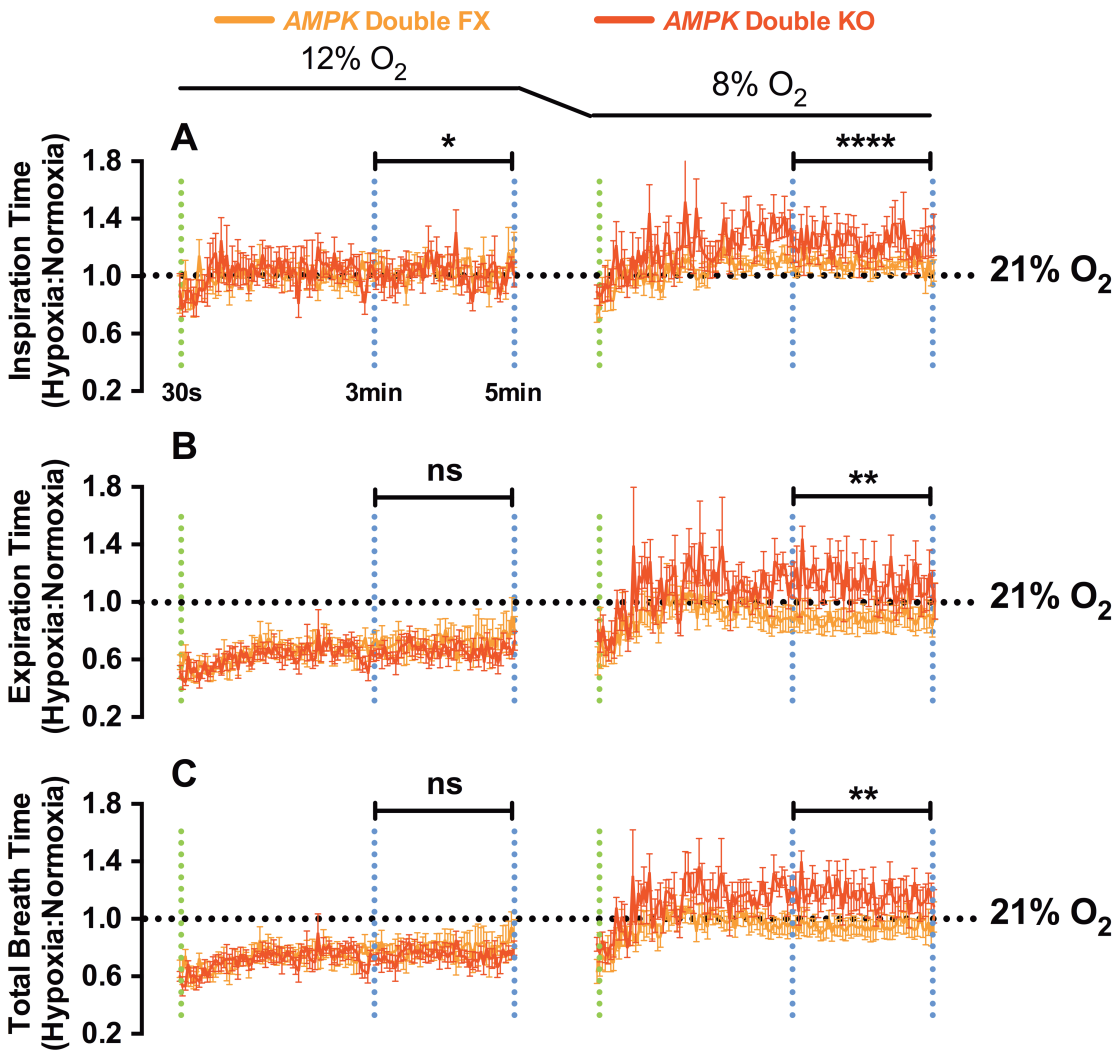

Figure 4.8: The effect of *AMPK* deletion on the mean duration of inspiration, expiration and total breath duration during hypoxia. Mean ± SEM of the ratiometric changes (relative to normoxia as indicated by dotted line at 1.0, 21% O_2) in the duration (s) of **(A)** inspiration (Ti), **(B)** expiration (Te) and **(C)** total breath (To) over a 5min exposure with 2s sampling periods during mild hypoxia (12% O_2, *left panels*) and **(B)** severe hypoxia (8% O_2, *right panels*) in *AMPK α1* and *α2* double floxed (*AMPK* Double FX, orange) and *AMPK α1* and *α2* double knockout (*AMPK* Double KO, red) mice (*AMPK* Double FX - 12% O_2: n = 7 exposures, 8% O_2: n = 10 exposures, N = 5 mice; *AMPK* Double KO - 12% O_2: n = 6 exposures, 8% O_2: n = 10 exposures, N = 6 mice). ns = not significant, * = $p < 0.05$, ** = $p < 0.01$, **** = $p < 0.0001$. Unpaired student's t-test was used to test for significance at 30s following the onset of hypoxia (indicated by green vertical dotted line) and from 3-5min (as indicated by blue vertical dotted lines).

4.2.1.3b The effects of *AMPK* deletion on tidal volume during hypoxia are driven by changes to the duration of inspiration and expiration

When analysing tidal volume during hypoxia, *AMPK α1* and *α2* double knockouts exhibited a marginal increase relative to normoxia during 12% O_2 and 8% O_2, which was significantly lower than the increases for *AMPK α1* and *α2* floxed mice (Section 4.2.1.3). There are two possible explanations for this phenomenon: (1) an increase in the volume of air moved per unit time, or (2) prolonged total breath time relative to normoxia. To determine the relative contribution of these two processes, a different method of ratiometric analysis was performed. Here tidal volume was divided by inspiration (Tv/Ti), expiration (Tv/Te), and total breath time (Tv/To). Figures 4.9 and 4.10 show example and averaged (mean ± SEM) records against time for each of the ratiometric indices relative to values observed during normoxia.

Tv/Ti In both *AMPK α1* and *α2* floxed and double knockout mice, time-dependent changes in Tv/Ti were observed. During 12% O_2, Tv/Ti increased at 30s to 1.53 ± 0.11 in *AMPK α1* and *α2* floxed mice and comparably to 1.45 ± 0.15 in the *AMPK α1* and *α2* double knockouts. In contrast, a robust increase was observed at 30s during 8% O_2 to 1.81 ± 0.23 in *AMPK α1* and *α2* floxed mice while being markedly less at 1.28 ± 0.08 in *AMPK α1* and *α2* double knockouts. Thereafter, Tv/Ti gradually decreases in both control and knockouts until plateauing by 2min and remaining stable for the remainder of the 5min exposure to 12% O_2 and 8% O_2. This is indicated by the mean ± SEM of the overall Tv/Ti from 3-5min, which in the *AMPK α1* and *α2* floxed mice is 1.27 ± 0.05 during 12% O_2 and 1.13 ± 0.03 during 8% O_2. The time-dependent reduction in Tv/Ti for the *AMPK α1* and *α2* double knockouts was comparable at 12% O_2 as it fell to 1.23 ± 0.05, but significantly less during 8% O_2 as Tv/Ti fell to 0.93 ± 0.04 ($p < 0.001$). Therefore, at 8% O_2, Tv/Ti in the *AMPK α1* and *α2* double knockout mice decreases to a level even less than Tv/Ti during normoxia, thereby suggesting the volume of air moved per unit time of inspiration reduces, i.e. during shallow breaths.

Tv/Te A time-dependent change was also observed in Tv/Te in both *AMPK α1* and *α2* floxed and *AMPK α1* and *α2* double knockout mice during hypoxia. Under 12% O_2, the initial increase at 30s was comparable at 2.72 ± 0.84 in *AMPK α1* and *α2* floxed

mice and 2.26 ± 0.35 in the *AMPK α1* and *α2* double knockouts. However, Figure 4.10B shows that the initial increase at 30s following the onset of 8% O_2 was significantly greater in controls as it reached 2.65 ± 0.60 in the *AMPK α1* and *α2* floxed mice while in the *AMPK α1* and *α2* double knockouts Tv/Te only increased to 1.55 ± 0.18 ($p < 0.05$). Thereafter, Tv/Te gradually decreases in both control and knockouts until stabilising by 2min for the remainder of the 5min exposure. In *AMPK α1* and *α2* floxed mice this decrease was marginal as Tv/Te remained greater relative to normoxic levels as the ratio only fell to 2.05 ± 0.15 during 12% O_2 and 1.40 ± 0.05 during 8% O_2. However, in the *AMPK α1* and *α2* double knockouts, the average Tv/Te during the final 2min decreased further in a PO_2-dependent manner and to levels markedly less than the *AMPK α1* and *α2* floxed mice; the ratio reached 1.96 ± 0.07 (not significantly different) and 1.09 ± 0.06 ($p < 0.001$) during 12% O_2 and 8% O_2, respectively.

Tv/To Overall, the above translated into a time-dependent attenuation of Tv/To during hypoxia in *AMPK α1* and *α2* double knockout mice relative to changes observed in control *AMPK α1* and *α2* floxed mice. At the start of the exposure to 12% O_2 and 8% O_2, Tv/To increased at 30s to 2.23 ± 0.49 and 2.29 ± 0.43, respectively, in the control *AMPK α1* and *α2* floxed mice. Subsequently, Tv/To decreased in a PO_2-dependent manner in the controls as demonstrated by the measured mean ± SEM of Tv/To between 3-5min, which reached 1.76 ± 0.10 during 12% O_2 and 1.29 ± 0.04 during 8% O_2. In *AMPK α1* and *α2* double knockouts, an increase in Tv/To was also observed at 30s during 12% O_2 and 8% O_2. However, while the increase was comparable to controls at 12% O_2 (1.96 ± 0.26) a significant attenuation in Tv/To was observed in the *AMPK α1* and *α2* double knockouts at the start of the exposure to 8% O_2 (1.41 ± 0.12, $p < 0.05$). A pronounced fall in Tv/To was observed thereafter as average Tv/To during the final 2min of the 12% O_2 and 8% O_2 hypoxic exposure fell to 1.68 ± 0.05 (not significantly different) and 1.00 ± 0.04 ($p < 0.0001$), respectively. Given that inspiration time is significantly longer in the *AMPK α1* and *α2* double knockouts compared to controls, this suggests that the increase in tidal volume relative to control mice during 8% O_2 results from a prolongation of breath duration and not a compensatory increase in the volume of air moved per unit time.

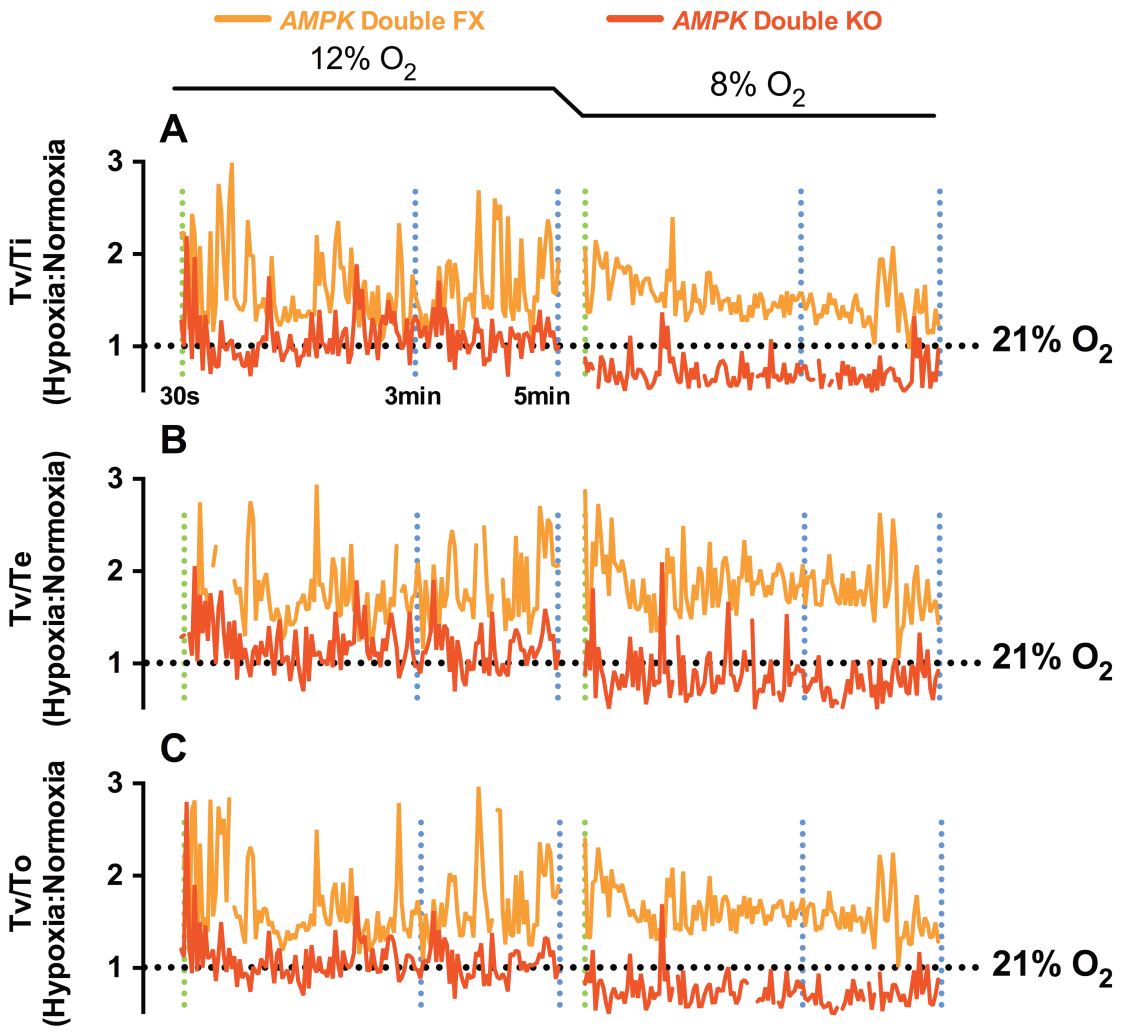

Figure 4.9: The effects of *AMPK* deletion on the tidal volume relative to the inspiration, expiration, and total breath duration during hypoxia. Example records of the ratiometric changes (relative to normoxia as indicated by dotted line at 1.0, 21% O_2) in tidal volume (TV) response relative to the duration of **(A)** inspiration (Tv/Ti), **(B)** expiration (Tv/Te), and **(C)** total breath duration (Tv/To) over a 5min exposure during mild hypoxia (12% O_2, *left panels*) and severe hypoxia (8% O_2, *right panels*) in *AMPK α1* and *α2* double floxed (*AMPK* Double FX, orange) and *AMPK α1* and *α2* double knockout (*AMPK* Double KO, red) mice. 30s following the onset of hypoxia is indicated by green vertical dotted line; 3-5min indicated by blue vertical dotted lines.

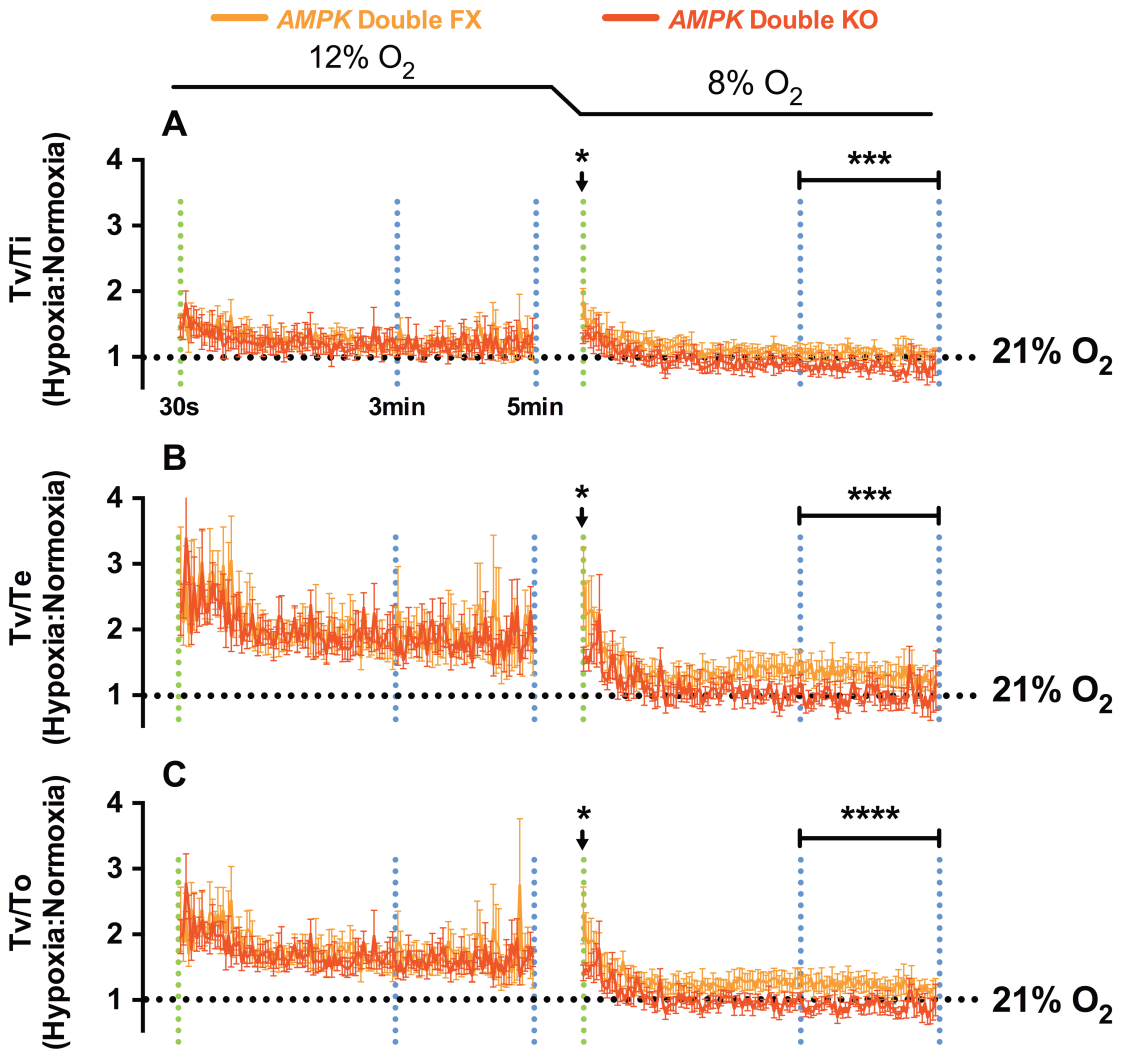

Figure 4.10: The effects of *AMPK* deletion on the mean tidal volume response relative to the inspiration, expiration, and total breath duration during hypoxia. Mean ± SEM of the ratiometric changes (relative to normoxia as indicated by dotted line at 1.0, 21% O_2) in tidal volume (Tv) response relative to the duration of **(A)** inspiration (Tv/Ti), **(B)** expiration (Tv/Te), and **(C)** total breath duration (Tv/To) over a 5min exposure during mild hypoxia (12% O_2, *left panels*) and severe hypoxia (8% O_2, *right panels*) in *AMPK α1* and *α2* double floxed (*AMPK* Double FX, orange) and *AMPK α1* and *α2* double knockout (*AMPK* Double KO, red) mice. (*AMPK* Double FX - 12% O_2: n = 7 exposures, 8% O_2: n = 10 exposures, N = 5 mice; *AMPK* Double KO - 12% O_2: n = 6 exposures, 8% O_2: n = 10 exposures, N = 6 mice). * = $p < 0.05$, ** = $p < 0.01$, **** = $p < 0.0001$. Unpaired student's t-test was used to test for significance at 30s following the onset of hypoxia (indicated by green vertical dotted line) and from 3-5min (as indicated by blue vertical dotted lines).

4.2.2 The effects of *AMPK α1*- and *α2*-subunit deletion in catecholaminergic cells on the ventilatory response to hypoxia is reversed by co-exposure to hypercapnia

4.2.2.1 Hypercapnia reverses the effects of *AMPK* deletion on breathing frequency and duration of apnoeas during hypoxia

Unlike the profound effects observed during severe hypoxia (8% O_2), *AMPK* deletion in catecholaminergic cells had no effect on the ventilatory response to hypercapnia (5% CO_2). Moreover, exposure of mice to hypercapnia with hypoxia (8% O_2 + 5% CO_2) reversed entirely the disordered breathing precipitated in these mice by 8% O_2 alone.

Figure 4.11A shows the ventilatory activity from *AMPK α1* and *α2* floxed mice and *AMPK α1* and *α2* double knockout mice during 8% O_2 alone, 8% O_2 + 5% CO_2 and 5% CO_2 alone. Surprisingly, the inclusion of 5% CO_2 to 8% O_2 reversed entirely the disordered breathing observed in the *AMPK α1* and *α2* double knockouts, such that exposure to 8% O_2 + 5% CO_2 elicited a marked increase in all measured indices of ventilation and was comparable with the response to 5% CO_2 alone, and with no evidence of apnoeas or periods of hypoventilation (Figure 4.11 – Panel Aii). This is further highlighted by cross-comparison of the mean ± SEM of the apnoeic index, apnoea duration, and apnoea duration index (Figure 4.11 – Panel B) as well as examining the ventilatory activity on an expanded time course in Figure 4.12.

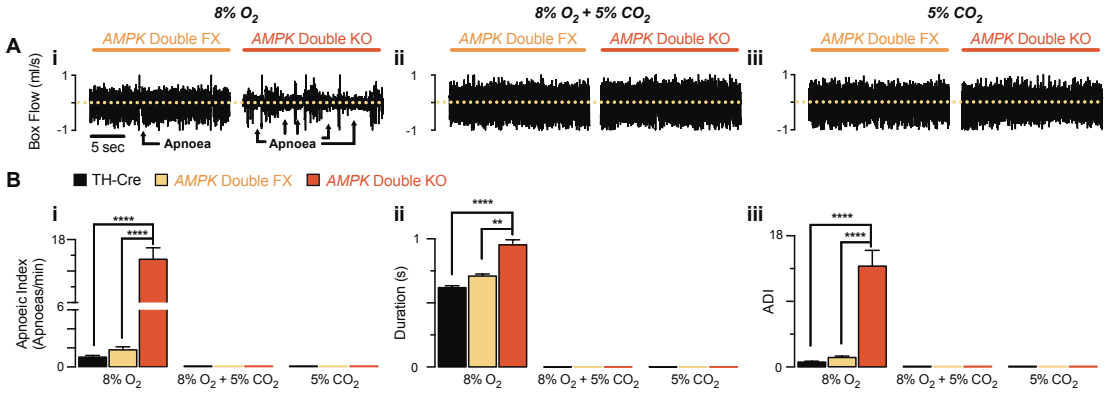

Figure 4.11: Conditional deletion of *AMPK* as no effect on the ventilatory pattern during hypercapnia even with the inclusion of severe hypoxia. (A) Records of ventilatory activity during **(i)** severe hypoxia (8% O_2 + 0.05% CO2), **(ii)** severe hypoxia with hypercapnia (8% O_2 + 5% CO_2), and **(iii)** hypercapnia alone (21% O_2 + 5% CO_2) in *AMPK α1* and *α2* double floxed (AMPK Double Fx) and *AMPK α1* and *α2* double knockout (AMPK double KO) mice. **(B)** Mean ± SEM for **(i)** apnoeic index (AI, apnoeas per minute), **(ii)** apnoea duration (s) and **(iii)** the apnoea-duration index during severe hypoxia (8% O_2 - TH-Cre: n = 24, black; *AMPK* Double FX: n = 12, yellow; *AMPK* Double KO: n = 22, red) and their reversal with the inclusion hypercapnia (8% O_2 + 5% CO_2 - TH-Cre: n = 17; *AMPK* Double FX: n = 20; *AMPK* Double KO: n = 29) or hypercapnia alone (5% CO_2 - TH-Cre: n = 20; *AMPK* Double FX: n = 20; *AMPK* Double KO: n = 20). ** = $p < 0.01$, **** = $p < 0.0001$. Significance tested by one-way ANOVA with Bonferroni multiple comparisons.

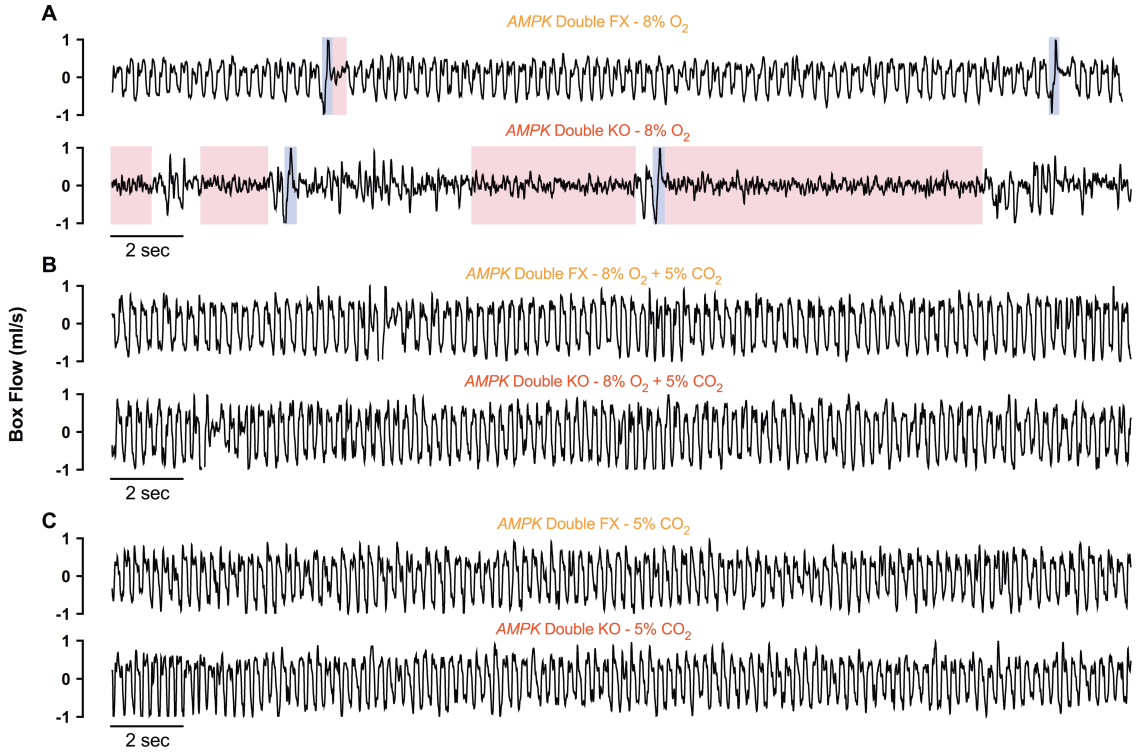

Figure 4.12: Co-exposure of hypercapnia with severe hypoxia reverses the effects of conditional *AMPK* deletion on the ventilatory activity during hypoxia alone. Typical ventilatory records on an expanded time scale from *AMPK α1* and *α2* double floxed (*AMPK* Double FX, *upper panel)* and *AMPK α1* and *α2* double knockout mice (*AMPK* Double KO, *lower panel*) during **(A)** severe hypoxia (8% O_2 + 0.05% CO_2), **(B)** severe hypoxia with hypercapnia (8% O_2 + 5% CO_2), and **(C)** hypercapnia alone (21% O_2 + 5% CO_2).

4.2.2.2 Poincaré analysis reveals that PO_2-dependent disordered breathing in *AMPK α1* and *α2* double knockout mice is reversed by hypercapnia

That the inclusion of 5% CO_2 reversed the irregularity of breathing evoked by hypoxia in *AMPK α1* and *α2* double knockout mice was confirmed by Poincaré plots of inter-breath interval (BBn) versus subsequent inter-breath interval (BBn+1). These are shown in Figure 4.13, which compares the breathing regularity of control *AMPK α1* and *α2* floxed mice with *AMPK α1* and *α2* double knockouts during 8% O_2 alone, 8% O_2 + 5% CO_2, and 5% CO_2 alone. These clearly show that significant increases in the irregularity of breathing observed at 8% O_2 in the *AMPK α1* and *α2* double knockouts are reversed by co-exposure to 8% O_2 + 5% CO_2, and are not observed in the presence of 5% CO_2 alone. In fact, the regularity of breathing was restored to levels comparable to that observed in the control *AMPK α1* and *α2* floxed mice under the same conditions (Figure 4.13 – Panel A-C, *upper panels*). This is consistent with the findings mentioned above, which demonstrate that apnoeas induced by hypoxia are no longer observed with combined exposure to a hypoxic + hypercapnic stimulus.

This is confirmed by comparing the SD of inter-breath intervals of control *AMPK α1* and *α2* floxed mice with the *AMPK α1* and *α2* double knockouts mice. This is illustrated in Figure 4.13 which shows that the SD for *AMPK α1* and *α2* floxed mice is reduced from 77 ± 6ms at 8% O_2 (n = 12 exposures from 4 mice) to 24 ± 1ms (n = 20 exposures from 5 mice) and 33 ± 2ms (n = 20 exposures from 5 mice) under 8% O_2 + 5% CO_2 and 5% CO_2 alone, respectively. By contrast, although the exposure of *AMPK α1* and *α2* double knockouts to 8% O_2 increased the SD to 238 ± 23ms (n = 19 exposures from 5 mice), the SD decreased to levels comparable to the *AMPK α1* and *α2* floxed mice as it reached 27 ± 1ms (n = 29 exposures from 5 mice) with 8% O_2 + 5% CO_2 and similarly to 37 ± 2ms (n = 20 exposures from 5 mice) under 5% CO_2 alone.

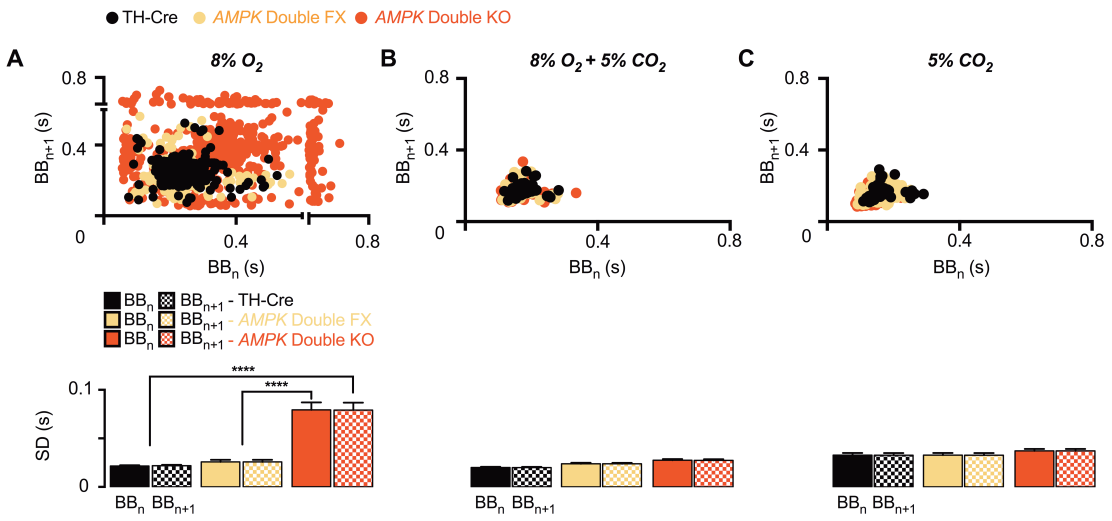

Figure 4.13: Conditional deletion of *AMPK* as no effect on the regularity of breathing during hypercapnia even with the inclusion of severe hypoxia. (A-C) *Upper panels* show poincaré plots of the inter-breath interval (BBn) versus subsequent interval (BBn+1) of TH-Cre (black), *AMPK α1* and *α2* double floxed (*AMPK* double FX, yellow), and *AMPK α1* and *α2* double knockout (*AMPK* double KO, red) mice during **(A)** severe hypoxia (8% O_2 + 0.05% CO_2), **(B)** severe hypoxia with hypercapnia (8% O_2 + 5% O_2), and **(C)** hypercapnia alone (21% O_2 + 5% CO_2). The corresponding *lower panels*, show the mean ± SEM for the standard deviation (SD) of BBn and BBn+1 for each genotype during 8% O_2 (TH-Cre: n = 20 exposures from 5 mice; *AMPK* double FX: n = 12 exposures from 4 mice; *AMPK* double KO: n = 19 exposures from 5 mice), 8% O_2 + 5% CO_2 (TH-Cre: n = 17, N = 5 mice; *AMPK* double FX: n = 20, N = 5 mice; *AMPK* double KO: n = 29, N = 5 mice) and 5% CO_2 (TH-Cre: n = 20, N = 5 mice; *AMPK* double FX: n = 20, N = 5 mice; *AMPK* double KO: n = 20, N = 5 mice). **** = $p < 0.0001$. Significance tested by one-way ANOVA with Bonferroni multiple comparisons.

4.2.2.3 Hypercapnia overcomes the effects of *AMPK* deletion on the hypoxic ventilatory response

Next, the impact of 5% CO_2, in the presence and absence of 8% O_2, on frequency, tidal volume, and minute ventilation was assessed. Figure 4.14 shows example records for the change in the frequency, tidal volume, and minute ventilation (2s sampling period) over the 5min exposure of mice to 8% O_2, 8% O_2 + 5% CO_2 and 5% CO_2.

Breathing Frequency In control *AMPK α1* and *α2* floxed mice, a robust increase in breathing frequency was observed and was sustained throughout the 5min exposure to 8% O_2 + 5% CO_2 (30s: 75 ± 2%; 100s: 64 ± 2%; 300s: 55 ± 2%; n = 20 from 5 mice) and 5% CO_2 (30s: 64 ± 3%; 100s: 68 ± 2%; 300s: 67 ± 3%; n = 20 from 5 mice). A robust and sustained increase in breathing frequency was also observed in *AMPK α1* and *α2* double knockouts that, unlike the *Lkb1* knockouts (as described in Chapter 3), reached a comparable magnitude to that of *AMPK α1* and *α2* floxed mice throughout the 5min exposure to 8% O_2 + 5% CO_2 (30s: 66 ± 4%; 100s: 59 ± 2%; 300s: 53 ± 2%; n = 22 from 5 mice) and similarly to 5% CO_2 alone (30s: 58 ± 3%; 100s: 63 ± 2%; 300s: 60 ± 2%; n = 23 from 5 mice). This demonstrates that *AMPK* deletion attenuates the increase in breathing frequency in response to hypoxia but not hypercapnia, even when mice are co-exposed to hypoxia with hypercapnia.

Tidal Volume Tidal volume modulation in response to 8% O_2 + 5% CO_2 and 5% CO_2 alone were time-dependent in both *AMPK α1* and *α2* floxed and *AMPK α1* and *α2* double knockout mice. Initially in *AMPK α1* and *α2* floxed mice at 30s following the induction of 8% O_2 + 5% CO_2, tidal volume increased to 52 ± 5% CO_2 of that observed under normoxia + normocapnia and peaked at 85 ± 5% after 100s, before declining slightly to 78 ± 4% at 300s. By contrast, upon exposure to 5% CO_2 alone, tidal volume increased by 42 ± 4% at 30s relative to normoxia + normocapnia, before increasing to a stable level of 68 ± 4% after 100s which was maintained for the remainder of the exposure period (300s, 63 ± 8%). A robust and sustained increase in tidal volume was also observed in *AMPK α1* and *α2* double knockouts that reached a comparable magnitude to that of *AMPK α1* and *α2* floxed mice throughout the 5min exposure to 8%

O_2 + 5% CO_2 (30s: 42 ± 4%; 100s: 76 ± 4%; 300s: 71 ± 4%) and similarly to 5% CO_2 alone (30s: 40 ± 4%; 100s: 66 ± 5%; 300s: 68 ± 5%).

Minute Ventilation Minute Ventilation increased markedly in control *AMPK α1* and *α2* floxed mice throughout the 5min exposure to 8% O_2 + 5% CO_2. After 30s, minute ventilation increased by 161 ± 10% relative to normoxia + normocapnia and then peaked at 200 ± 9% after 100s before declining slightly to 174 ± 7% at 300s. This was marginally greater than the response to 5% CO_2 alone, which triggered an increase to 133 ± 10% after 30s, before peaking at 179 ± 5% after 100s in a manner that was sustained for the remainder of the 5min exposure (300s: 179 ± 8%). Unlike the *Lkb1* knockouts, the deletion of *AMPK α1* and *α2* double knockouts in catecholaminergic cells had no affect on minute ventilation throughout the 5min exposure to 8% O_2 + 5% CO_2 (30s: 132 ± 9%; 100s: 176 ± 7%; 300s: 160 ± 8%) and 5% CO_2 alone (30s: 119 ± 8%; 100s: 167 ± 10%; 300s: 168 ± 10%).

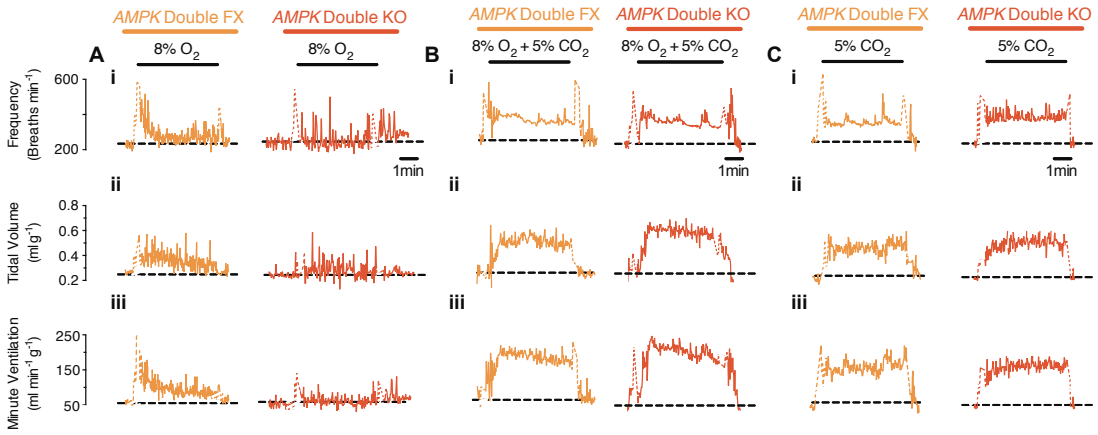

Figure 4.14: Conditional deletion of *AMPK* has no affect on the mean ventilatory response to hypercapnia even with the inclusion of severe hypoxia. Example records of the effect over a 5min period of exposure to **(A)** severe hypoxia (8% O_2 + 0.05% CO_2) **(B)** severe hypoxia with hypercapnia (8% O_2 + 5% CO_2), and **(C)** hypercapnia alone (5% CO_2) on **(i)** breathing frequency (min^{-1}), **(ii)** tidal volume (ml g^{-1}) and **(iii)** minute ventilation (ml min^{-1} g^{-1}) in *AMPK α1* and *α2* double floxed (*AMPK* double FX, orange) and *AMPK α1* and *α2* double knockout mice (*AMPK* double KO, red) with 2s sampling periods. Dashed black lines indicate baseline levels, white line breaks indicate artefact of gas exchange.

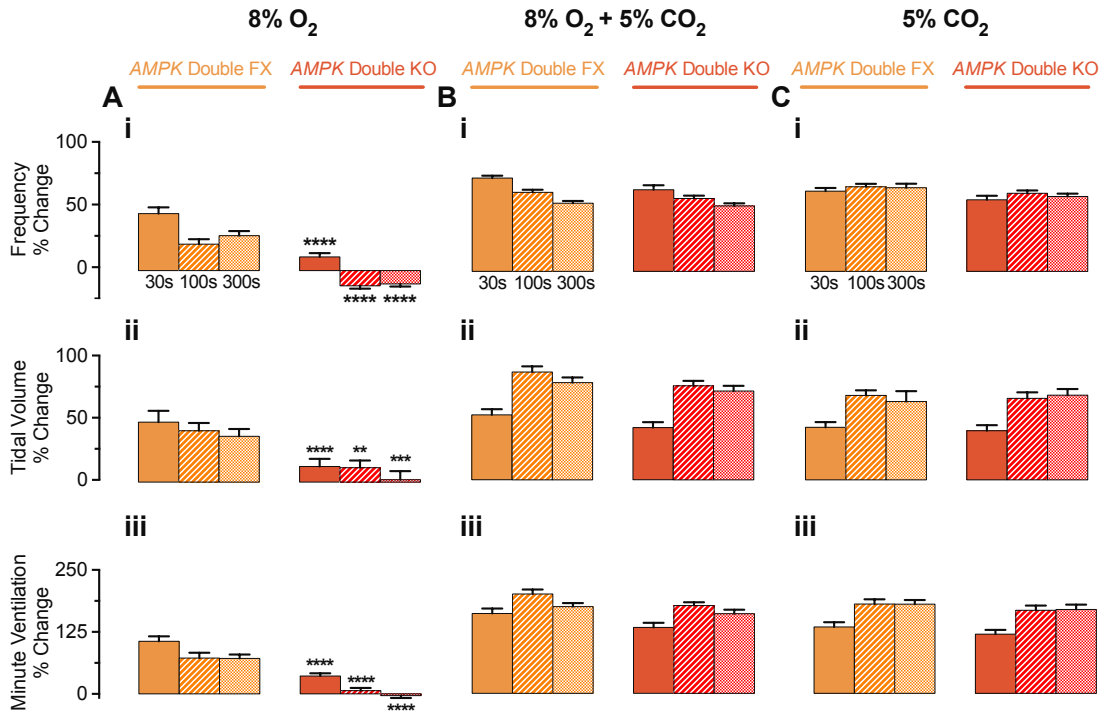

Figure 4.15: The effects of deletion of *AMPK* on the mean hypoxic ventilatory response are reversed with the inclusion of hypercapnia. Mean ± SEM for percent change during **(A)** severe hypoxia (8% O_2 + 0.05% CO_2), **(B)** hypercapnia with severe hypoxia (8% O_2 + 5% CO_2), and **(C)** hypercapnia alone (21% O_2 + 5% CO_2) in **(i)** breathing frequency (min^{-1}), **(ii)** tidal volume (ml g^{-1}) and **(iii)** minute ventilation (ml min^{-1} g^{-1}) at 3 time points during the 5min hypoxic exposure in *AMPK α1* and *α2* double floxed (*AMPK* Double FX - 8% O_2 : n = 13 from 5 mice; 8% O_2 + 5% CO_2: n = 20 exposures from 5 mice; 5% CO_2: n = 20 exposures from 5 mice, orange), and *AMPK α1* and *α2* double knockout mice (*AMPK* Double KO – 8% O_2: n = 26 from 5 mice; 5% CO_2: n = 23 exposures from 5 mice; 8% O_2 + 5% CO_2: n = 22 exposures from 5 mice, red). ** = $p < 0.01$, *** = $p < 0.001$, **** = $p < 0.0001$. Significance tested by one-way ANOVA with Bonferroni multiple comparisons.

4.2.2.3a Hypercapnia overcomes the effects of *AMPK* deletion on the durations of inspiration and expiration during hypoxia

Given the above it seemed likely that further insight might be obtained from analyses of inspiration time, expiration time, and total breath duration, as this would allow us to determine whether the inspiratory and/or expiratory phases of ventilation are reversed in *AMPK α1* and *α2* double knockouts in the presence of a hypercapnic stimulus. Figures 4.16 and 4.17 display example and average records, respectively, of the changes to the duration of inspiration (Ti), expiration (Te), and total breath duration (*To*) relative to normoxia + normocapnia during 8% O_2, 8% O_2 + 5% CO_2, and 5% CO_2 alone in control *AMPK α1* and *α2* double floxed and *AMPK α1* and *α2* double knockout mice.

Inspiration Time (Ti) Similar to that observed during 8% O_2 alone, a time-dependent response was observed for Ti in *AMPK α1* and *α2* floxed and *AMPK α1* and *α2* double knockout mice with 8% O_2 + 5% CO_2 and 5% CO_2 alone. This involved an initial reduction in Ti relative to normoxia + normocapnia at 30s before gradually increasing until plateauing by 2min and remained stable for the rest of the 5min exposure. This is demonstrated by the measured mean ± SEM of the ratio of Ti relative to normoxia at 30s and the overall mean ± SEM (using the formula for error of propagation) of Ti ratio during the final 2min of the hypercapnia ± hypoxia exposure between 3 and 5min. In the control *AMPK α1* and *α2* floxed mice, Ti hardly decreases relative to normoxia as Ti ratio only reaches 0.98 ± 0.07 (n = 9 from 5 mice) upon being exposed to 8% O_2 + 5% CO_2 at 30s. Thereafter progressive prolongation leads to an overshoot above durations observed during normoxia + normocapnia, with Ti reaching 1.20 ± 0.02 during the final 2min of the exposure. Under 5% CO_2 alone, control *AMPK α1* and *α2* floxed mice exhibited a greater reduction in Ti at 30s with a ratio of 0.85 ± 0.09 (n = 7 from 4 mice). A progressive prolongation of Ti occurred thereafter, but unlike in the presence of hypercapnia + hypoxia, Ti recovered to levels equivalent to that observed during normoxia + normocapnia for the final 2min of the exposure to 5% CO_2 (1.0 ± 0.03). This suggests that under 8% O_2 + 5% CO_2, the duration of the inspiratory phase of respiration increases with time of exposure until exceeding the duration

observed during normoxia + normocapnia. In contrast, under 5% CO_2 alone Ti recovers to durations similar to those observed during normoxia.

In the *AMPK α1* and *α2* double knockout mice, a time-dependent change in Ti was also observed during 8% O_2 + 5% CO_2 and 5% CO_2 alone. Once more, the ratio of Ti initially decreased at 30s to 0.90 ± 0.05 during 8% O_2 ± 5% CO_2, which was a reduction comparable to that observed in *AMPK α1* and *α2* floxed mice at 30s. Subsequently, Ti for the *AMPK α1* and *α2* double knockouts increased with time to 1.21 ± 0.02 during the final 2min, which is a magnitude that exceeds normoxic + normocapnic values but is comparable to that observed for *AMPK α1* and *α2* floxed mice. In contrast, in response to 5% CO_2 Ti was similar relative to normoxia + normocapnia at 30s (0.97 ± 0.36), but prolonged relative to that observed in the controls (though not significantly different using an unpaired student's t-test). Furthermore, by the final 2min of the exposure to 5% CO_2, Ti levels remained near that maintained during normoxia + normocapnia at 0.93 ± 0.03, which was comparable to Ti observed in the control *AMPK α1* and *α2* floxed mice from 3-5min under 5% CO_2.

Expiration Time (Te) A robust and sustained reduction in Te relative to normoxia was evident in both *AMPK α1* and *α2* floxed mice and *AMPK α1* and *α2* double knockout mice during 8% O_2 + 5% CO_2 and 5% CO_2 alone. In the *AMPK α1* and *α2* floxed mice, the expiratory phase significantly shortened at 30s following the onset of 8% O_2 + 5% CO_2 and 5% CO_2 as indicated by the mean ± SEM of Te at 30s, which was 0.58 ± 0.05 and 0.45 ± 0.06, respectively. Thereafter, Te remained relatively stable at 0.52 ± 0.01 and 0.50 ± 0.01, respectively, during the final 2min of the exposures to 8% O_2 and 5% CO_2, respectively.

In the *AMPK α1* and *α2* double knockout mice, the changes in expiratory durations relative to normoxia in response to 8% O_2 + 5% CO_2 and 5% CO_2 alone were comparable to the changes made in the control *AMPK α1* and *α2* floxed mice at 30s. This is demonstrated by the relative reduction in Te at 30s to 0.72 ± 0.16 during 8% O_2 + 5% CO_2 and 0.44 ± 0.10 during 5% CO_2. However, the relative reduction of Te thereafter appeared more enhanced in the *AMPK α1* and *α2* double knockouts when compared to *AMPK α1* and *α2* floxed mice as it maintained at 0.43 ± 0.01 and 0.47 ±

0.02 during the final 2 minutes of the 8% O_2 + 5% CO_2 and 5% CO_2 exposure, respectively. However, this did not reach statistical significance when compared to controls using an unpaired student's t-test.

Total Breath Duration (To) In controls, and similarly in the *AMPK α1* and *α2* double knockouts, outcomes for Ti and Te translated into robust reductions in *To* throughout the 5min exposure to 8% O_2 + 5% CO_2 and 5% CO_2 alone; consistent with observed increases in the breathing frequency (Section 4.2.2.3). Initially, *To* of *AMPK α1* and *α2* floxed mice, fell at 30s relative to normoxia + normocapnia to 0.69 ± 0.05 during 8% O_2 + 5% CO_2 and 0.55 ± 0.07 during 5% CO_2. Subsequently, *To* gradually increased slightly to 0.71 ± 0.01 and 0.63 ± 0.02 during the final 2min of the exposures to 8% O_2 + 5% CO_2 and 5% CO_2 alone, respectively. Similarly in the *AMPK α1* and *α2* double knockouts, *To* shortened at 30s to 0.76 ± 0.13 during 8% O_2 + 5% CO_2 and 0.57 ± 0.15 during 5% CO_2 before reaching 0.61 ± 0.01 and 0.58 ± 0.02, respectively, during the final 2min of the exposure.

Therefore, AMPK-dependent modulation of catecholaminergic cells is necessary during hypoxia and not hypercapnia to appropriately adjust the durations of the inspiratory and expiratory phases to accommodate an increase in breathing frequency.

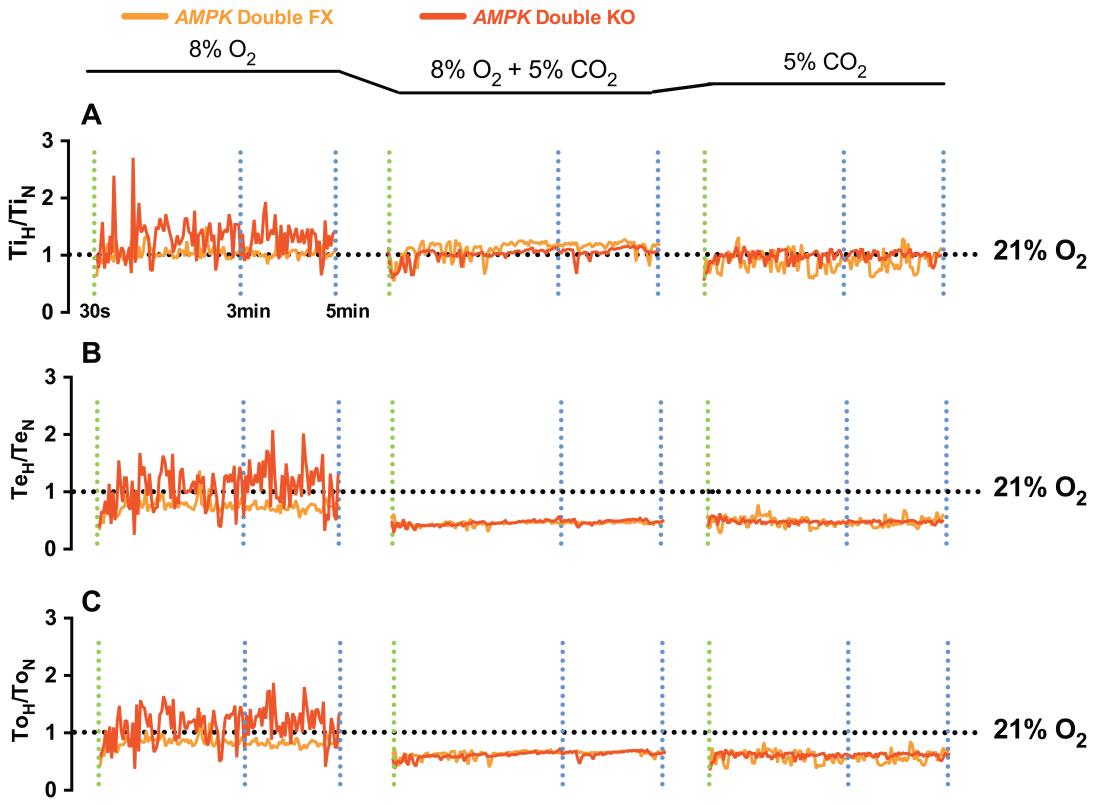

Figure 4.16: Hypercapnia reverses the effects of *AMPK* deletion on the durations of inspiration, expiration and total breath during hypoxia. Example records of the ratiometric changes (relative to normoxia as indicated by dotted line at 1.0, 21% O_2) in the duration (s) of **(A)** inspiration (Ti), **(B)** expiration (Te) and **(C)** total breath (To) over a 5min exposure with 2s sampling periods during severe hypoxia (8% O_2 + 0.05% CO_2), severe hypoxia with hypercapnia (8% O_2 + 5% CO_2), and hypercapnia alone (21% O_2 + 5% CO_2,) in *AMPK α1* and *α2* double floxed (*AMPK* Double FX, orange) and *AMPK α1* and *α2* double knockout (*AMPK* Double KO, red) mice. 30s following the onset of hypoxia and/or hypercapnia indicated by green vertical dotted line; 3-5min indicated by blue vertical dotted lines.

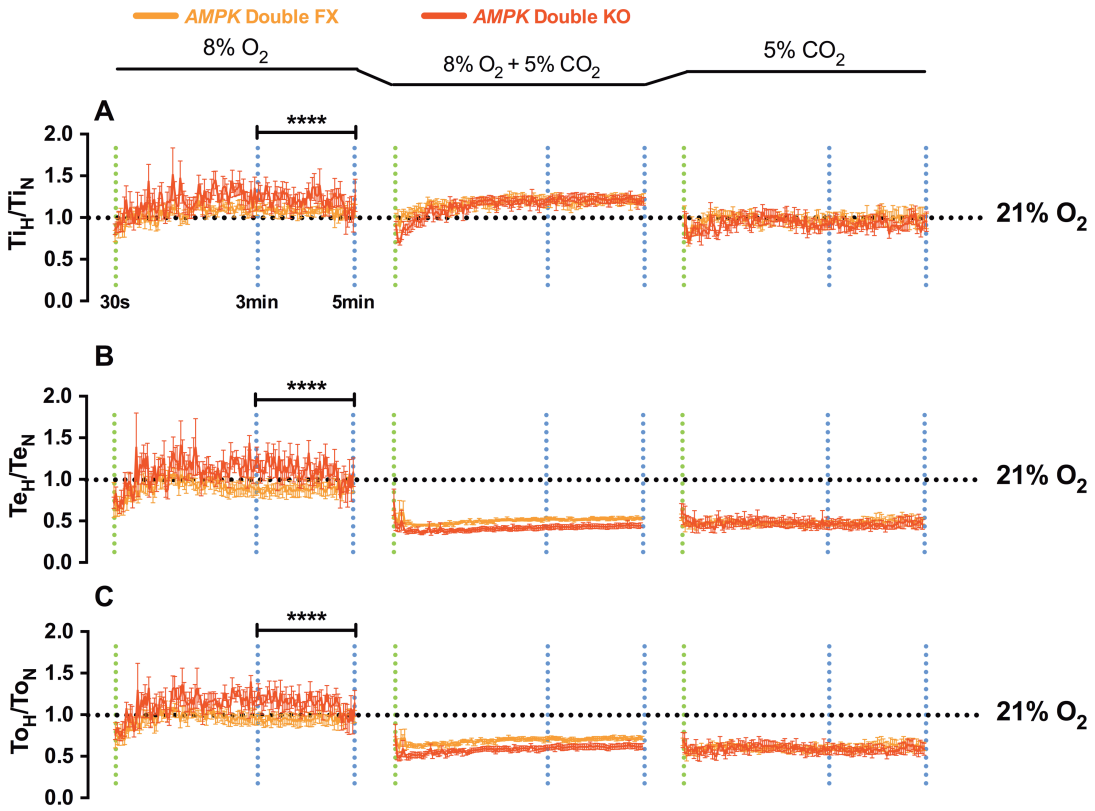

Figure 4.17: Hypercapnia reverses the effects of *AMPK* deletion on the mean duration of inspiration, expiration and total breath duration during severe hypoxia. Mean ± SEM of the ratiometric changes (relative to normoxia as indicated by , line at 1.0, 21% O_2) in the duration (s) of **(A)** inspiration (Ti), **(B)** expiration (Te) and **(C)** total breath over a 5min exposure with 2s sampling periods during severe hypoxia (8% O_2 + 0.05% CO_2, *left panels*), hypercapnia with severe hypoxia (8% CO_2 + 5% CO_2, *middle panels*), and hypercapnia alone (21% O_2 + 5% CO_2, *right panels*) in *AMPK α1* and *α2* double floxed (*AMPK* Double FX, orange) and *AMPK α1* and *α2* double knockout (*AMPK* Double KO, red) mice. (*AMPK* Double FX - 8% O_2: n = 10 exposures from 5 mice, 8% O_2 + 5% CO_2: n = 10 exposures from 5 mice, 5% CO_2: n = 7 exposures from 4 mice; *AMPK* Double KO - 8% O_2: n = 10 exposures from 5 mice, 8% O_2 + 5% CO_2: n = 10 exposures from 5 mice, 5% CO_2: n = 7 exposures from 4 mice). **** = $p < 0.0001$. Unpaired student's t-test was used to test for significance at 30s following the onset of hypoxia and/or hypercapnia (indicated by green vertical dotted line) and from 3-5min (as indicated by blue vertical dotted lines).

4.3 Discussion

4.3.1 Summary of findings

Chapter 4 shows that AMPK-dependent pathways are critical for appropriate modulation of ventilation in response to hypoxia. The loss of both $\alpha 1$ and $\alpha 2$ catalytic subunits of *AMPK* in catecholaminergic cells precipitates irregular breathing patterns during hypoxia and attenuates the ventilatory response. These irregular breathing patterns included periods of hypoventilation with spontaneous and post-sigh apnoeas, which resulted from failure of central respiratory drive rather than airway obstruction. By contrast, AMPK deletion had no effect on the ventilatory response to hypercapnia, and all respiratory defects observed during hypoxia were reversed upon exposure of mice to hypoxia with hypercapnia. Therefore, AMPK deletion in catecholaminergic cells specifically compromises respiratory adjustments during hypoxia and its activity is therefore key to the appropriate regulation of ventilation in response to hypoxia, and to the maintenance of oxygen supply and energy homeostasis at the whole-body level.

4.3.2 The increase in ventilation in response to hypoxia requires AMPK activity in catecholaminergic cells

Importantly, dual deletion of *AMPK* $\alpha 1$ and $\alpha 2$ catalytic subunits in catecholaminergic cells had no effect on normoxic ventilation. Also, the *AMPK* $\alpha 1$ and $\alpha 2$ double knockouts were still able to trigger a complete ventilatory response to hypercapnia. In contrast, increases in minute ventilation during hypoxia were seriously compromised in the *AMPK* $\alpha 1$ and $\alpha 2$ double knockouts and in a PO_2-dependent manner. This thereby suggests that the blunted ventilatory response to hypoxia is secondary to a primary abnormality of respiratory modulation by oxygen-sensing catecholaminergic cells. These outcomes argue strongly in support of the view that catecholaminergic neurons deliver increased drive to breath during hypoxia, and that *AMPK* deletion removes the capacity of these neurons to deliver increased drive during

hypoxia in a manner that is independent of any impairment of the respiratory apparatus/muscles.

As previously described in Chapter 3, several studies have demonstrated that the ventilatory response to hypoxia is biphasic in mice. The initial rapid increase in ventilation in response to acute hypoxia, designated as the augmentation phase, has been proposed to be driven by afferent input to the respiratory centres in the brainstem following the rapid activation of the carotid body to acute hypoxia (Ramirez, Quellmalz, et al., 1998; Bissonnette, 2000). Subsequently, respiratory depression occurs and is thought to be due to the depressive effects of hypoxia and a resultant, time-dependent reduction in carotid body and central respiratory neurons due to declining metabolic rate. However, the biphasic nature of the hypoxic ventilatory response is retained *in vitro i*n rhythmically active preparations from which input from peripheral chemoreceptors are removed(Ramirez, Schwarzacher, et al., 1998).

The *AMPK α1* and *α2* double knockouts similarly exhibit a biphasic ventilatory response to hypoxia with an initial augmentation phase that peaks within 30s following the onset of hypoxia, before the onset of respiratory depression which peaks at 100s. However, the augmentation phase appears significantly attenuated and the depressive phase more severe than controls during exposure to both 12% and 8% O_2. Yet, though attenuated, the *AMPK α1* and *α2* double knockouts still exhibit an initial increase in both breathing frequency and tidal volume at 30s, albeit markedly reduced relative to control mice. Thereafter breathing frequency progressively declines during the depressive phase to the point at which the mice enter hypoventilation relative to normoxia; breathing frequency decreases to near baseline levels under 12% O_2 (5 ± 2%) and markedly below baseline levels under 8% O_2 (-12 ± 2%). This suggests that peripheral and/or central chemoreceptors are still able to trigger a ventilatory response to hypoxia during the augmentation phase, which in addition to being attenuated, is insufficient to maintain an appropriate ventilatory response during hypoxia.

The respiratory central pattern generators (rCPGs) receive inputs from peripheral and central chemoreceptors and accordingly adjust ventilation to meet metabolic demands. This is accomplished by coordinating rhythmic patterns of motor activity for:

(1) the respiratory pump (diaphragm, thorax, and abdomen), (2) lung inflation and deflation, and (3) upper airway muscles to control airflow (Euler, 1983; Guyenet, 2005; Solomon et al., 2000). During hypoxia, these coordinated rhythmic movements are appropriately adjusted by the rCPGs, based on signals from peripheral and central oxygen-sensing cells, to drive an increase in rhythmic ventilatory movements, and hence ventilation, to protect against metabolic stress and maintain physiological PO_2 and PCO_2 at the whole-body level (Euler, 1983). Given *AMPK α1* and *α2* double knockouts are not able to sustain an increase in ventilation and that they exhibit severely disordered breathing suggests that the ventilatory response to hypoxia, and coordination of the appropriate ventilatory response through the rCPGs, requires AMPK-dependent modulation of a group of catecholaminergic cells that represent the bodies primary oxygen-sensors and whose role it is to maintain oxygen, and hence energy homeostasis at the whole-body level.

4.3.3 The modulation of the inspiratory and expiratory phases of breathing during hypoxia requires AMPK activity in catecholaminergic cells

Interestingly, the augmentation of the depressive phase of ventilation in *AMPK* knockout mice appears to result from an attenuation of increases in breathing frequency and tidal volume in a PO_2-dependent manner (Figure 4.8 and 4.10). This is apparent from studies on the duration of inspiration (*Ti*), expiration (*Te*), and total breath duration (*To*) as well as the change in tidal volume (*Tv*) relative to *Ti* (*Tv*/*Ti*), *Te* (*Tv*/*Te*), and *To* (*Tv*/*To*) during hypoxia.

To significantly increases as a result of marked prolongation of Te and Ti. This suggests that during the depressive phase of the ventilatory response to hypoxia. It seems likely, therefore, that the rCPGs are unable to appropriately modulate the inspiratory and expiratory phases of respiration in the manner required to promote an increase in ventilation in response to hypoxia. However, this is unlikely to be a result of defects in the rCPGs themselves, but perhaps more likely a result from inadequate signalling from either the afferent inputs from peripheral chemoreceptors or inputs from central catecholaminergic chemoreceptors to the rCPGs during hypoxia. This is apparent

as rhythmic breathing is completely restored and breathing irregularities resolved when the *AMPK α1* and *α2* double knockouts are exposed to both a hypoxic and hypercapnic stimulus.

4.3.4 AMPK-dependent modulation of catecholaminergic cells is necessary to protect against hypoventilation and apnoeas during hypoxia

Given the blunted ventilatory response to hypoxia described above, perhaps it is not surprising that the deletion of *AMPK α1* and *α2* in catecholaminergic cells precipitates the number and duration of apnoeas during hypoxia. The increase was PO_2-dependent as the apnoea duration index significantly increased from 12% O_2 to 8% O_2. Similar to the *Lkb1* knockouts in chapter 3, this strongly suggests that pO_2 levels play a prominent role in determining the apnoeic threshold, which cannot therefore be solely governed by PCO_2 (Dempsey, 2005), since the apnoea duration index increased in a PO_2-dependent manner even though there was a continuous supply of normocapnia (0.05% CO_2) *and* the mice paradoxically hypoventilated, i.e. they did not blow off CO_2 excessively as did controls. Taken together, this strongly indicates that while PO_2 decreases during hypoxia in the *AMPK* knockouts, PCO_2 probably does not and may be increased relative to controls and even eupneic PCO_2. Also, as mentioned previously, this is supported by studies demonstrating that: (1) supplying PO_2 can resolve or eliminate the occurrence of periodic breathing and apnoeas (Lahiri, 1983), (2) that mice with blunted hypoxic ventilatory responses are more susceptible to breathing irregularities and apnoeas (Adachi, 2006), and (3) hypoxia has the capacity to alter the degree of hypocapnia required to trigger apnoeas (Xie et al., 2001).

The *AMPK α1* and *α2* double knockouts exhibited extended periods of hypoventilation with post-sigh and spontaneous apnoeas. It is worth noting that the periods of hypoventilation occasionally appeared arrhythmic and quite ataxic-like (Figure 4.2). This is quite similar to the respiratory phenotype manifested with Rett syndrome, which has been shown to be associated with the progressive degeneration of the catecholaminergic neuromodulatory systems, namely noradrenergic, in the brain (Ide et al., 2005). This includes the noradrenergic A6 neurons of the locus coeruleus as well

as the hypoxia-sensitive noradrenergic A1 and A2 groups which also receive inputs from the carotid body (Viemari et al., 2005; Ide et al., 2005; King et al., 2012). A reduction in the adrenergic C1 and C2 neurons has also been implicated with Rett syndrome (Viemari et al., 2005). Given that *AMPK* deletion has been targeted to all catecholaminergic neurons and that *AMPK α1* and *α2* double knockout mice consequently exhibit breathing irregularities similar to those manifested with Rett syndrome, thereby provides strong support of the view that the central catecholaminergic cells are crucial to the ventilatory response during hypoxia, that they protect against hypoventilation and apnoea and that their capacity to do so is dependent on AMPK.

4.3.5 The ventilatory response to hypoxia is more severely affected by *AMPK* deletion in catecholaminergic cells than by the deletion of *Lkb1*

The *AMPK α1* and *α2* double knockouts exhibited a similar but significantly more severe ventilatory phenotype than the *Lkb1* knockouts during hypoxia (as described in Chapter 3). Due to the PO_2-dependency of respiratory depression during hypoxia in these mice, this is more apparent under 8% O_2 as:

- *AMPK α1* and *α2* double knockouts exhibited a significantly greater apnoea duration index (13.8 ± 2.2) than the *Lkb1* knockouts (5.4 ± 0.6), with the maximum apnoea duration being ~6s in the *AMPK α1* and *α2* double knockouts and ~4s in the *Lkb1* knockouts.
- *AMPK* deletion has more profound effects on the variability in inter-breath interval, as illustrated by the Poincaré plots. The standard deviation of inter-breath interval in the *Lkb1* knockouts was 153 ± 6ms while in the *AMPK α1* and *α2* double knockouts this was significantly greater at 238 ± 23ms.
- Even though both knockout mice exhibited extended periods of hypoventilation with post-sigh and spontaneous apnoeas, the periods of hypoventilation in the *Lkb1* knockouts maintained rhythmicity while in the *AMPK α1* and *α2* double knockouts these periods occasionally appeared to be non-rhythmic and almost ataxic-like. Again, this suggests that AMPK activity may help protect or

maintain rhythmicity generated by rCPGs by maintaining increased inputs from the catecholaminergic oxygen-sensing cells in response to hypoxia. This may not have occurred or may have not been picked up in the *Lkb1* knockouts as AMP can still activate AMPK allosterically during metabolic stress, even following *Lkb1* deletion, which may in its own right be sufficient to protect or maintain enough hypoxic respiratory drive to insure rhythmicity is maintained by the rCPGs during hypoxia.

The fact that both knockout mice exhibit a similar phenotype crucially demonstrates that the effects observed in the *Lkb1* knockouts in Chapter 3 are neither a result of: (1) the hypomorphic expression of LKB1 in non-catecholaminergic cells, nor (2) a result of reduced activities of the LKB1-dependent AMPK-related kinases. Moreover, the less severe phenotype observed in the *Lkb1* knockouts may be a result of the ability of AMPK to still be activated up to 10-fold by AMP during metabolic stress and may thus still be able to provide a degree of hypoxia-response coupling. Taken together, these findings strongly suggest that the LKB1-AMPK signaling pathway is required in catecholaminergic cells to mediate an appropriate ventilatory response to hypoxia.

However, differences in the pattern of ventilatory abnormalities between the *AMPK α1* and *α2* double knockouts and *Lkb1* knockouts were also apparent during hypoxia:

- Cheyne-Stokes-like breathing was only present in the *Lkb1* knockouts. This perhaps is consistent with the suggestion above that, unlike the *AMPK α1* and *α2* double knockouts, the rCPGs in the *Lkb1* knockouts can maintain rhythmic ventilation as Cheyne-Stokes-like breathing would require continuous and well coordinated adjustments of rhythmic breathing by the rCPGs to generate its characteristic crescendo-decrescendo breathing pattern (See General discussion - Chapter 6).
- During the augmentation phase of the ventilatory response to hypoxia, *AMPK α1* and *α2* double knockouts are able to increase breathing frequency, though attenuated when compared to controls, while increases in breathing frequency is almost completely ablated in the *Lkb1* knockouts. This may be down to a combination of things: (1) the general hypomorphic status of the *Lkb1* knockouts

in addition to the specific deletion of *Lkb1* in catecholaminergic cells; (2) *AMPK* deletion can be acutely compensated for by one of its related kinases during the augmentation phase, which is unlikely to occur upon the deletion of the upstream kinase *Lkb1*; or (3) the possibility that amongst the catecholaminergic cells, *Lkb1* deletion may have tissue/cell-specific actions that are not observed following the deletion of *AMPK* and vice versa (see General Discussion in Chapter 6).

4.3.6 Conclusion

In conclusion, the LKB1-AMPK signalling pathway is required in catecholaminergic cells for the modulation of ventilation during hypoxia. The catecholaminergic circuit involved possibly includes the primary peripheral chemoreceptor, namely the carotid body, as well as the oxygen-sensitive central chemoreceptors in the brainstem, both of which project to the rCPGs. This supports the hypothesis that AMPK-dependent signalling has been adapted to regulate oxygen supply, and thus energy supply at the whole-body level. Defects in AMPK activity may therefore compromise the ability to appropriately modulate respiration during hypoxic stress that occurs during sleep or at high-altitudes. The findings of the current chapter may also offer an explanation for the high comorbidity observed with metabolic syndrome-related disorders and sleep-disordered breathing, with the former disorder already associated with AMPK (Ruderman et al., 2013). This perhaps appears more noteworthy when noting that the AMPK activator, metformin, which is used for the management of type 2 diabetes within the metabolic syndrome was previously and unexpectedly found to be an efficient treatment for sleep apnoea (S. Wiwanitkit and V. Wiwanitkit, 2012).

APPENDIX

Appendix 4A

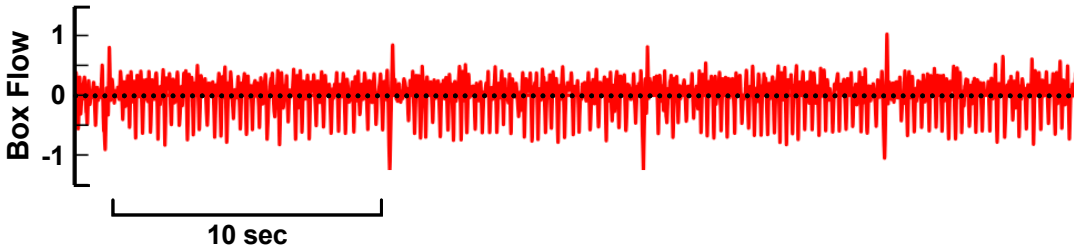

Supplementary Figure 4A: Periodic breathing observed during 8% O_2 in *AMPK* $\alpha 1$ and $\alpha 2$ double knockouts with post-sigh apnoeas occurring at regular intervals of ~0.1Hz.

Appendix 4B

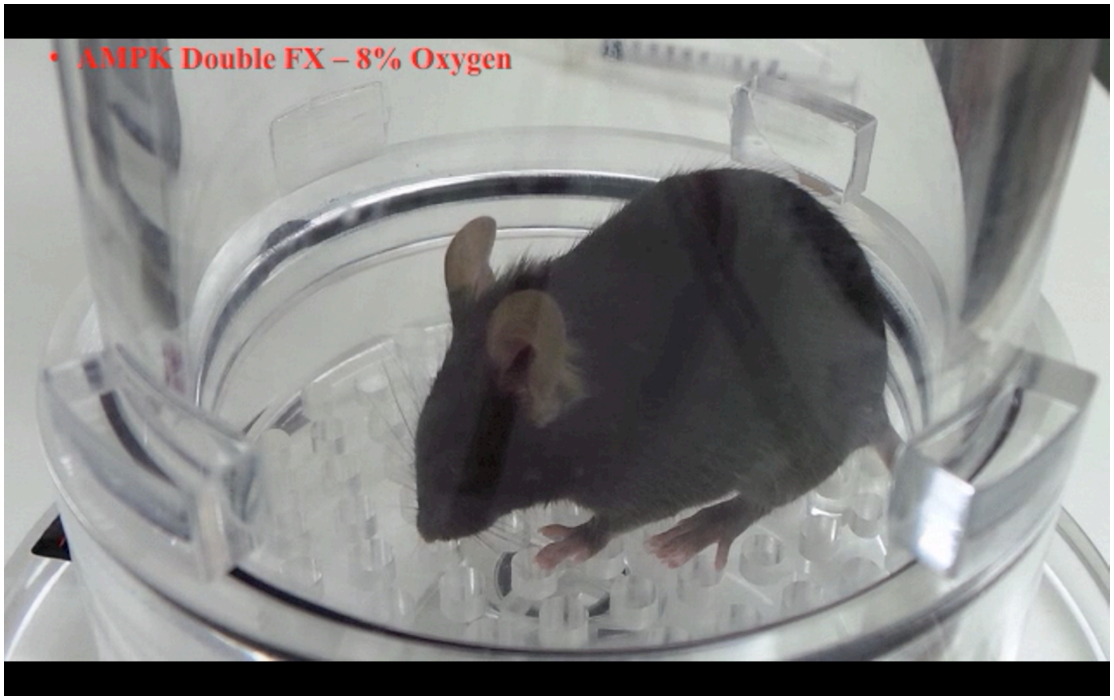

Supplementary Figure 4B: Still images of *AMPK α1* and *α2* double floxed and knockout mice during 8% O_2. Unlike the control floxed mice, *AMPK α1* and *α2* double knockouts would normally lie down and barely move.

Chapter Five:

AMPK α1-containing heterotrimers are of primary importance to respiratory adjustments during hypoxia with α2-containing heterotrimers only able to partially compensate for its loss in catecholaminergic cells

5.1 Introduction

5.1.1 Overview

Studies from the previous chapter have demonstrated that AMPK activity is required for appropriate respiratory modulation during hypoxia. The findings from chapter 4 are crucial as, unlike the *Lkb1* knockouts, the *AMPK α1* and *α2* double knockout mice are not hypomorphic and are not deficient in AMPK-related kinase activity. Therefore, all outcomes resulted from the loss of AMPK activation in catecholaminergic cells. Also, the *AMPK α1* and *α2* double knockouts exhibit hypoxia-induced disordered breathing and an attenuated hypoxic ventilatory response that appears even more severe than *Lkb1* knockouts. This strongly suggests that the effects observed in the *Lkb1* knockouts did not result from their non-specific hypomorphic nature or the additional attenuation of AMPK-RK activities in these mice, but likely from the loss of the LKB1-AMPK signaling pathway within a common cell-type or circuit, i.e. catecholaminergic and/or oxygen-sensing.

Nevertheless, certain AMPK-dependent cellular functions have exhibited redundancy with respect to the α1 and α2 catalytic subunits. For instance, during contraction of skeletal muscle, α1 and α2 isoforms can compensate for each other to maintain normal glucose uptake (Jørgensen et al., 2004). In contrast, however, studies have indicated that redundancy does not exist between the α1 and α2 isoforms of AMPK with respect to its role in promoting myogenesis, with the α1-isoform of the catalytic subunit being of primary importance (Fu et al., 2013). Taken together, this raises the possibility that either (1) a single AMPK α-subunit isoform is of primary importance for appropriate modulation of the ventilatory response during hypoxia, or (2) redundancy or compensation exists between the AMPK α1 and α2 catalytic subunits.

5.1.2 Aims

The aim of the current chapter is to determine whether a single α-subunit isoform is of primary importance for the ventilatory response to hypoxia or whether redundancy exists between the α1 and α2 catalytic subunits. This involved examining the ventilatory

response to hypoxia following the single deletion of the *α1* and *α2* isoforms of the AMPK catalytic subunits in catecholaminergic cells using single *AMPK α1* knockouts and *AMPK α2* knockouts, respectively. The outcomes from the single knockouts will also be compared to the dual deletion of *AMPK α1* and *α2* (as described in Chapter 4) in order to determine the degree of redundancy or compensation that may occur in between the α1 and α2 catalytic subunits.

5.2 Results

5.2.1 The effects of single deletion of *AMPK α1-* and *α2-subunits* on the ventilatory response to hypoxia

Under normoxia, baseline readings for body temperature, venous blood gas composition, blood pH, breathing frequency, tidal volume and minute ventilation of mice lacking either the *AMPK α1* or *α2* catalytic subunits in catecholaminergic cells were consistent with those measures taken from control mice, including *AMPK α1* and *α2* double floxed mice, TH-Cre mice and C57/Bl6 mice (as discussed in Chapter 2: Table 2.1; Figure 2.12). Moreover, there was no significant difference in weight gain with age, between 2 and 12 months (Chapter 2: Figure 2.8). However, deletion of the AMPK *α1-subunit* in catecholaminergic cells resulted in disordered breathing during severe hypoxia (8% O_2) and precipitated apnoeas, which was not apparent following the deletion of *AMPK α2-subunit*. Yet, the breathing irregularities during hypoxia appeared even more severe with dual deletion of *AMPK α1* and *α2* than with single deletion of *AMPK α1*. Taken together, this suggests that the activity of α1-containing AMPK heterotrimers is of primary importance to respiratory adjustments during hypoxia with α2-containing heterotrimers only able to partially compensate for its loss in catecholaminergic cells

5.2.1.1 Deletion of the *AMPK* catalytic α1-subunit increases the frequency and duration of apnoeas during hypoxia

Ventilatory traces obtained using unrestrained whole body plethysmography revealed that conditional deletion of the *AMPK α1* subunit, but not the *AMPK α2* subunit, induced more frequent and prolonged apnoeas when compared to control, *AMPK α1* and *α2* double floxed mice. As mentioned in chapters 3 and 4, apnoeas were identified as a cessation of breathing for a duration that is at least equivalent to the duration of two regular breaths (i.e. two respiratory cycles have been missed)

(Y.-J. Peng et al., 2011; Nakamura and Kuwaki, 2004; Voituron et al., 2009), which equated to a cessation ≥500ms in our experimental mice.

Figure 5.1A shows example ventilatory traces of *AMPK α1* and *α2* double floxed, *AMPK α2* knockout, *AMPK α1* knockout, and *AMPK α1* and *α2* double knockout mice during 8% O_2 and the calculated means ± SEM for the apnoeic index (apnoeas/min), apnoea duration, and apnoea duration index (product of the apnoeic index and duration) for each of the four genotypes. As described in Chapter 4, and consistent with studies on C57/Bl6 mice (Stettner et al., 2008), 8% O_2 induced brief and infrequent apnoeas in control *AMPK α1* and *α2* floxed mice. Outcomes for mice in which *AMPK α2* had been deleted from all catecholaminergic cells were comparable to the control *AMPK α1* and *α2* floxed mice. In marked contrast, the ventilatory response to hypoxia was greatly suppressed in *AMPK α1* knockouts, which presented severely disordered breathing and apnoeas (Figure 5.1 –Panel Aii). This is evident from the mean apnoeic index of 10.0 ± 1.4 min^{-1} (n = 19 exposures from 6 mice, $p < 0.0001$) in the *AMPK α1* knockouts, which was far greater than that observed in either *AMPK α1* and *α2* floxed mice (1.8 ± 0.3 min^{-1}, n = 12 exposures from 4 mice) or *AMPK α2* knockouts (2.0 ± 0.4 min^{-1}, n = 16 exposures from 5 mice). Similarly, the mean duration of apnoeas during 8% O_2 measured in *AMPK α1* knockouts (967 ± 90ms $p < 0.0001$) was greater than for either the *AMPK α1* and *α2* floxed mice (709 ± 17ms) or *AMPK α2* knockouts (686 ± 35ms). Overall, this translated to an apnoea duration index that was comparable between *AMPK α1* and *α2* floxed mice (1.3 ± 0.2) and *AMPK α2* knockouts (1.5 ± 0.3), and profoundly greater in the *AMPK α1* knockouts at 9 ± 1.6 ($p < 0.0001$)

Importantly, however, the apnoea duration index for the *AMPK α1* knockouts during hypoxia was not as severe as that observed in the *AMPK α1* and *α2* double knockouts (Figure 5.1 – Panel B). Taken together, this suggests that that although the *α2* subunit is not of primary importance to respiratory modulation during hypoxia, it appears to have the capacity to partially compensate for a loss of AMPK *α1* in catecholaminergic cells to protect against an increase in apnoea frequency.

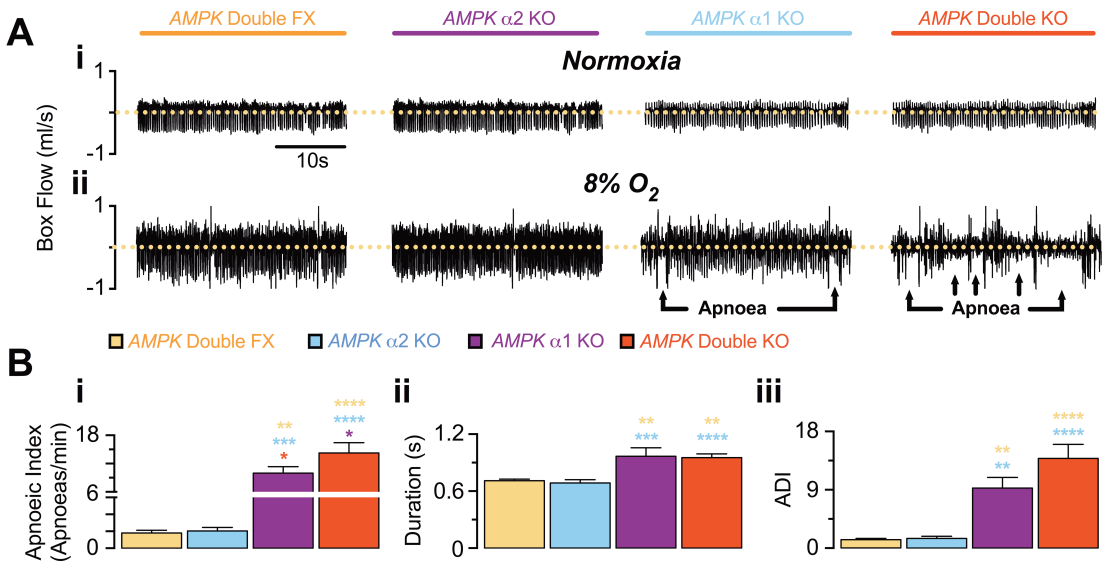

Figure 5.1: The effects of single and dual deletion of the *AMPK* catalytic *α1*- and *α2-subunits* on apnoea frequency and duration. (A) Records of ventilatory activity from *AMPK α1* and *α2* floxed mice (*AMPK* Double FX), *AMPK* α_2*-subunit* knockout (*AMPK* α2 KO), *AMPK* α_1*-subunit* knockout (*AMPK* α1 KO), and *AMPK α1* and *α2* double knockouts (*AMPK* Double KO) during **(i)** normoxia (21% O_2) and **(ii)** severe hypoxia (8% O_2). **(B)** Mean ± SEM for **(i)** apnoeic index (AI, apnoeas per minute), **(ii)** apnoea duration (s) and **(iii)** the apnoea-duration index. (*AMPK* Double FX: n = 12 from 4 mice; *AMPK* α2 KO: n = 16 from 5 mice; *AMPK* α1 KO: n = 19 from 6 mice; *AMPK* Double KO: n = 19 exposures from 5 mice). * = $p < 0.05$, ** = $p < 0.01$, *** = $p < 0.001$, **** = $p < 0.0001$. Significance tested by one-way ANOVA with Bonferroni multiple comparisons.

Breathing irregularities of *AMPK α1* knockout mice appeared even more complex when examined on an expanded time scale as illustrated in Figure 5.2. Under 8% O_2, the apnoeas observed in control *AMPK α1* and *α2* floxed mice and *AMPK α2* knockouts were brief and infrequent and often preceded by a sigh (an exaggerated breath with an inspiratory and expiratory amplitude, i.e. tidal volume, at least twice as large as the inspiratory and expiratory amplitude of the three previous breaths (Voituron et al., 2009) (Figure 5.2 – Panels A and B). However, deletion of the *AMPK α1* subunit resulted in not only more frequent and prolonged apnoeas, but also a ventilatory pattern that varied extensively. Furthermore, and similar to the *AMPK α1* and *α2* double knockouts but not *Lkb1* knockouts, periodic breathing was apparent in the *AMPK α1* knockouts with no appearance of Cheyne-Stokes-like breathing (Figure 5.2 – Panel C). Nevertheless, other forms of disordered breathing were identified in the *AMPK α1* knockouts during 8% O_2, which included periods of hypoventilation with prolonged apnoeas that occurred either spontaneously or following a sigh (Figure 5.2 – Panel C, *lower panel*). Although similar ventilatory abnormalities were induced by hypoxia in *AMPK α1* and *α2* double knockout, the severity of appeared marginally greater in the *AMPK α1* and *α2* double knockouts relative to the *AMPK α1* knockouts (Figure 5.2 – Panel D).

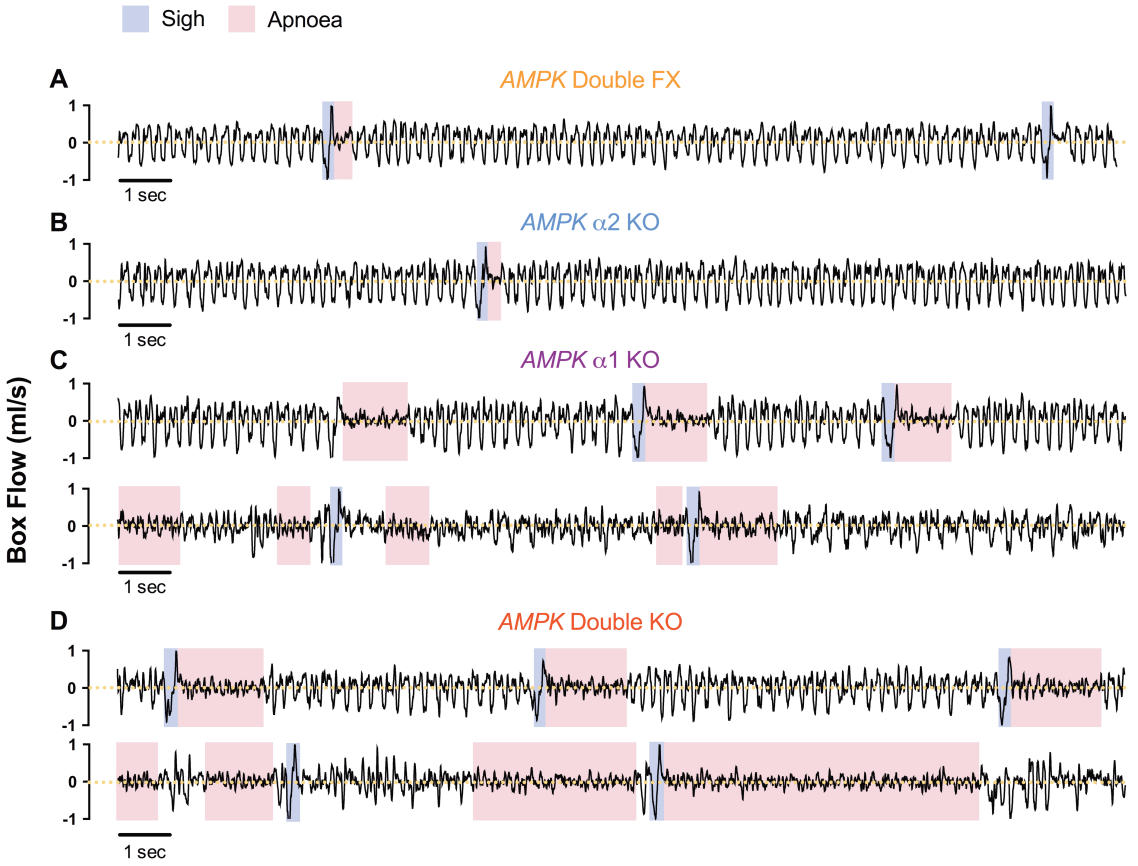

Figure 5.2: The effects of single and dual deletion of *AMPK α1-* and *α2-subunits* on the ventilatory pattern during hypoxia. Typical ventilatory records on an expanded time scale during severe hypoxia (8% O_2) from **(A)** *AMPK α1* and *α2* floxed mice (*AMPK* Double FX), **(B)** *AMPK α2-subunit* knockout (*AMPK* α2 KO), **(C)** *AMPK α1-subunit* knockout (*AMPK α1* KO), and **(D)** *AMPK α1* and *α2* double knockout mice (*AMPK* Double KO).

5.2.1.2 Poincaré analysis reveals that the deletion of the *AMPK α1 subunit* but not *α2 subunit* triggers disordered breathing during hypoxia

Whether considering the periods of hypoventilation, post-sigh apnoeas, or spontaneous apnoeas, the deletion of the *AMPK α1* subunit in catecholaminergic neurones led to marked breathing irregularities during severe hypoxia, while the deletion of the alternative catalytic subunit, *AMPK α2*, had no discernable effects during exposure to 8% O_2. This is confirmed in Figure 5.3 which compares Poincaré plots of the inter-breath intervals (BBn) versus the subsequent inter-breath interval (BBn+1) from a single hypoxic exposure period for *AMPK α1* and *α2* double floxed mice, *AMPK α2* knockouts, *AMPK α1* knockouts, and *AMPK α1* and *α2* double knockouts during normoxia (Panel Ai) and 8% O_2 (Panel Bi).

Clearly the variability in the interbreath interval is comparable across all four genotypes under normoxic conditions (21% O_2). In control *AMPK α1* and *α2* floxed mice, and similarly in *AMPK α2* knockout mice, there is a marginal increase in breathing irregularity upon switching form 21% O_2 to 8% O_2, which did not reach significance by one-way ANOVA. In marked contrast, *AMPK α1* knockout mice exhibited marked increases in breathing irregularities (Figure 5.3 – Panel Bi, *middle panel*). From these plots, long interbreath intervals were apparent in the *AMPK α1* knockouts, ranging from 0.5s to ~2s; this suggests that loss of *AMPK α1* activity in catecholaminergic cells leads to marked increases in inter-breath interval during hypoxic stress and thus precipitates hypoventilation. Strikingly, the irregularity and peak duration of interbreath interval (~3-4s) was even more severe in the *AMPK α1* and *α2* double knockout mice, consistent with the higher apnoeic index.

These observations were confirmed by comparison of the variability by standard deviation (SD) of BBn and BBn+1 (as shown in Figure 5.3 A,Bii). In the *AMPK α1* and *α2* double floxed mice, SD increased only marginally, from 63 ± 12ms during normoxia (n = 8 from 4 mice) to 77 ± 6ms during 8% O_2 (n = 12 from 4 mice). Likewise, the SD in *AMPK α2* knockout mice increased marginally from 57 ± 14ms under normoxic conditions (n = 6 from 4 mice) to 72 ± 8ms during severe hypoxia (n = 16 from 5 mice).

It is striking, therefore, that deletion of the *AMPK α1-subunit* in catecholaminergic cells increased the SD of BBn and BBn+1 from 73 ± 13ms (n = 10 exposures from 5 mice) during normoxia to 167 ± 24ms under severe hypoxia (n = 19 from 6 mice; $p < 0.01$ when compared to either *AMPK α1* and *α2* floxed mice or *AMPK α2* knockouts). Additionally, as would be expected given the above, the SD was yet greater for *AMPK α1* and *α2* double knockouts during severe hypoxia, at 238 ± 23ms (n = 19 from 5 mice; $p < 0.05$, compared to AMPK *α1* knockouts) from 76 ± 7ms (n = 15 from 5 mice) under normoxia (Figure 5.3 Bii).

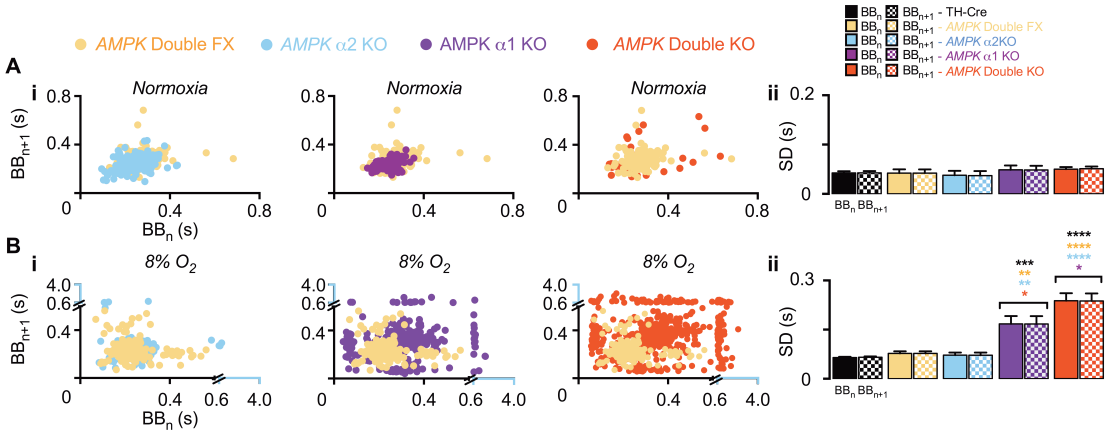

Figure 5.3: The effects of single and dual deletion of the *AMPK α1*- and *α2-subunits* on the regularity of breathing. Poincaré plots of the inter-breath interval (BB_n) versus subsequent interval (BB_{n+1}) in *AMPK α1* and *α2* double floxed (*AMPK* Double FX, yellow), *AMPK α2-subunit* knockout (*AMPK α*2 KO, blue), *AMPK α1-subunit* knockout (*AMPK α*1 KO, purple), and *AMPK α1* and *α2* double knockout mice (*AMPK* Double KO, red) during **(Ai)** normoxia (21% O_2) and **(Bi)** severe hypoxia (8% O_2). The corresponding mean ± SEM for the standard deviation (SD) of BB_n and BB_{n+1} for each genotype under **(Aii)** normoxia (*AMPK* Double FX: n = 8; *AMPK α*2 KO: n = 6; *AMPK α*1 KO: n = 10; and *AMPK* Double KO: n = 15) and **(Bii)** 8% O_2 (*AMPK* Double FX: n = 12; *AMPK α*2 KO: n = 16; *AMPK α*1 KO: n = 19; *AMPK* Double KO: n = 19). * = $p < 0.05$, ** = $p < 0.01$, *** = $p < 0.001$, and **** = $p < 0.0001$. Significance tested by one-way ANOVA with Bonferroni multiple comparisons.

5.2.1 3 The effects of single deletion of the *AMPK α1-* and *α2-subunit* on the hypoxic increase in breathing frequency, tidal volume, and minute ventilation

The dual deletion of both *α1* and *α2* catalytic subunits of *AMPK* in catecholaminergic cells markedly attenuated the average increase in ventilation during severe hypoxia in a time-dependent manner, as previously described in Chapter 4. Outcomes for this chapter further demonstrate that the *AMPK* α1 subunit is of primary importance for the maintenance of the ventilatory response during 8% O_2. Figure 5.4 shows example records for the change in breathing frequency, tidal volume, and minute ventilation (2s sampling period) over the 5min exposure to 8% O_2 in *AMPK α1* and *α2* double floxed, *AMPK α2* knockout, *AMPK α1* knockout, and *AMPK α1* and *α2* double knockout mice. Similar to the control *AMPK α1* and *α2* double floxed mice, *AMPK α2* knockouts exhibited a robust increase in all parameters studied. However, the deletion of the *AMPK α1* subunit markedly attenuated all measures of ventilatory activity as observed in *AMPK α1* and *α2* double knockouts.

Breathing Frequency As illustrated by the example records (Figure 5.4 – Panel A), when compared to *AMPK α1* and *α2* floxed mice, 8% O_2 triggered a robust mean increase in breathing frequency in the *AMPK α2* knockout mice, while *AMPK α1* knockout mice exhibited a marked attenuation across 3 different time points of the 5min exposure (Figure 5.5 – Panel A). In the control *AMPK α1* and *α2* double floxed mice, breathing frequency initially increased relative to normoxia by 46 ± 5% (n = 13 from 5 mice) at 30s before decreasing to 21 ± 4% at 100s due to respiratory depression (Bissonnette, 2000). Thereafter, the breathing frequency in the *AMPK α1* and *α2* floxed mice was maintained at 28 ± 4% at the end of the hypoxic exposure (300s). The increases in percentage change of breathing frequency relative to normoxia was similar in the *AMPK α2* knockout mice throughout the 5min exposure to 8% O_2 (30s: 47 ± 4%; 100s: 16 ± 3%; 300s: 23 ± 5%, n = 18 from 5 mice). By contrast, the initial increase at 30s was significantly less at 23 ± 3% in *AMPK α1* knockout mice (n = 28 from 6 mice) when compared to control *AMPK α1* and *α2* double floxed mice ($p < 0.0001$) and *AMPK α2* knockout mice ($p < 0.001$), but was not quite as severe as the attenuation

observed in the *AMPK α1* and *α2* double knockouts (11 ± 3%; n = 26 from 6 mice). Nevertheless, it is important to note that unlike the *Lkb1* knockouts that do not generate an increase in breathing frequency at 30s during 8% O_2, an increased frequency was observed in the *AMPK α1* knockouts. Thereafter breathing frequency decreased further to -11 ± 2% at 100s in the *AMPK α1* knockouts as a result of respiratory depression, leading to marked hypoventilation relative to normoxia: this decrease was significantly less than control *AMPK α1* and *α2* double floxed mice ($p < 0.0001$) and *AMPK α2* knockout mice ($p < 0.001$) but comparable to that observed in the *AMPK α1* and *α2* double knockouts (-12 ± 2%). By the end of the 5min exposure, the percentage change in the frequency of breathing remained below baseline levels in the *AMPK α1* knockout mice at -7 ± 2% compared to -10 ± 2% for *AMPK α1* and *α2* double knockout (Figure. 5.5 – Panel Ai).

Tidal Volume Hypoxia induced a sustained increase in mean tidal volume (Figure 5.5 – Panel B) in control *AMPK α1* and *α2* floxed mice throughout the 5min exposure to 8% O_2 (30s: 48 ± 9%; 100s: 41 ± 6%; 300s: 37 ± 6%; n = 13 from 5 mice). Surprisingly, although not significant, the increase in tidal volume was slightly attenuated by deletion of the *AMPK α2-subunit* in catecholaminergic cells (30s: 27 ± 4%; 100s: 32 ± 5%; 300s: 21 ± 3%; n = 18 from 5 mice). This was also apparent following the deletion of the *AMPK α1-subunit* throughout the 5min hypoxic exposure, though the decrease at 30s was more severe and significantly less than the control *AMPK α1* and *α2* floxed mice (30s: 18 ± 4%, $p < 0.01$; 100s: 29 ± 5%; 300s: 19 ± 4%; n = 28 from 6 mice). By contrast, however, the increase in tidal volume was more severely attenuated throughout the 5min exposure following the dual deletion of *AMPK α1-* and *α2-subunits* when compared to either the single AMPK *α1* or *AMPK α2* knockouts (30s: 13 ± 6%, 100s: 12 ± 6%, 300s: 2 ± 7%; n = 26 exposures from 5 mice).

Minute Ventilation Adjustments in minute ventilation (Figure 5.5 – Panel C) were robust throughout the 5min exposure period to 8% O_2 in *AMPK α1* and *α2* floxed mice (30s: 106 ± 6%; 100s: 72 ± 11%; 300s: 72 ± 8%; n = 13 from 5 mice). Also, as would be expected given the above, deletion of *AMPK α2* in catecholaminergic cells led

to marginal reductions in minute ventilation during hypoxia (30s: 86 ± 8%; 100s: 52 ± 7%; 300s: 52 ± 6%; n = 18 from 5 mice), although not statistically significant when compared to the *AMPK α1* and *α2* floxed mice. However conditional deletion of the *AMPK α1* subunit in catecholaminergic cells led to a marked attenuation of increases in minute ventilation (30s: 46 ± 7%; 100s: 13 ± 5%; 300s: 10 ± 5%; n = 28 from 6 mice) and was significantly less than the *AMPK α1* and *α2* double floxed mice ($p < 0.0001$) and *AMPK α2* knockout mice ($p < 0.001$). Nevertheless, although significantly attenuated, the *AMPK α1* knockouts still manage to maintain a marginal increase in minute ventilation for the duration of hypoxia, unlike mice lacking both *AMPK α1* and *α2* catalytic subunits which reach hypoventilation by 300s (30s: 36 ± 5%, 100s: 6 ± 5%, 300s: -4 ± 5%; n = 26 exposures from 5 mice).

Collectively, these data strongly suggests that redundancy does not exist between the AMPK *α1*- and AMPK *α2*-subunits with respect to mediating the appropriate ventilatory response to hypoxia. Given the degree of attenuation observed following its conditional deletion in TH-expressing cells, the α1-isoform of the AMPK catalytic subunit appears to play a dominant role in allowing the catecholaminergic oxygen-sensitive cells to drive the ventilatory response to hypoxia,. Nevertheless, although the deletion of the alternative α2-isoform has no significant affects on the ventilatory response to hypoxia, α2-containing AMPK heterotrimers appear to partially compensate for the loss of *AMPK α1* as the effects of dual deletion of *AMPK α1* and *α2-subunits* is more severe than with *AMPK α1* deletion alone.

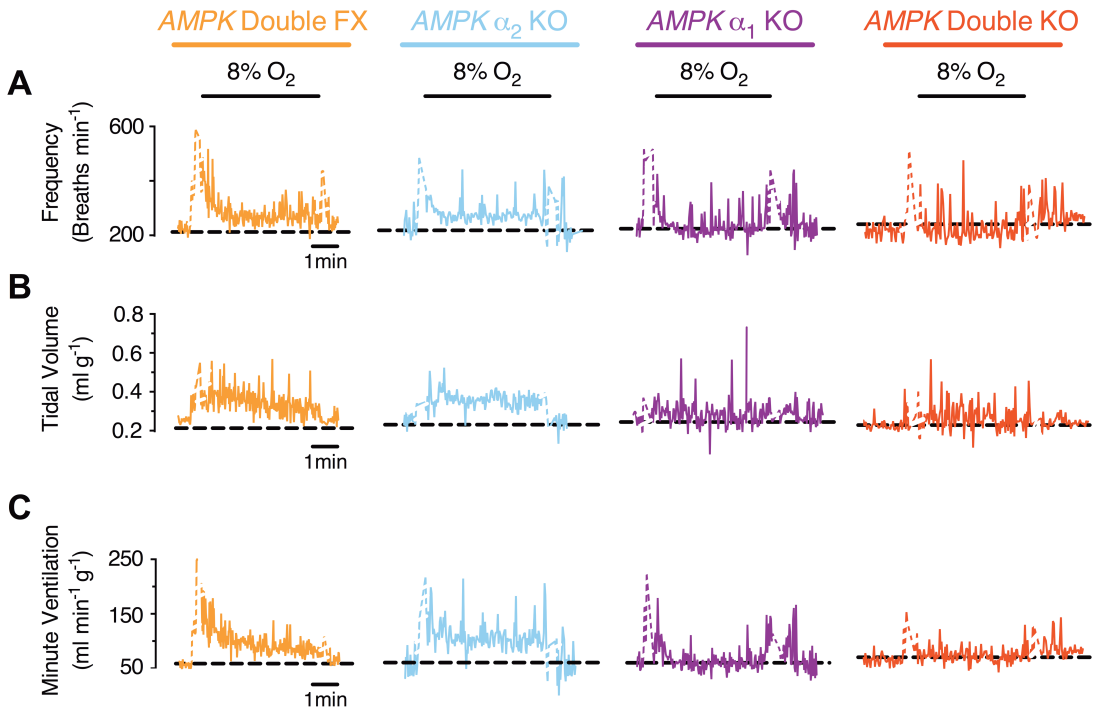

Figure 5.4: The effects of single or dual deletion of *AMPK α1-* and *α2-subunits* on the ventilatory response to hypoxia. The effect over a 5min period of exposure to severe hypoxia (8% O_2) on **(A)** breathing frequency (min^{-1}), **(B)** tidal volume (ml g^{-1}) and **(C)** minute ventilation (ml min^{-1} g^{-1}) in *AMPK α1* and *α2* double floxed (*AMPK* Double FX, orange), *AMPK α2-subunit* knockout (*AMPK* α2 KO, blue), *AMPK α1-subunit* knockout (*AMPK* α1 KO, purple), and *AMPK α1* and *α2* double knockout mice (*AMPK* Double KO, red) with 2s sampling periods. Dashed black line indicating basal level, white line breaks indicate artefact of gas exchange.

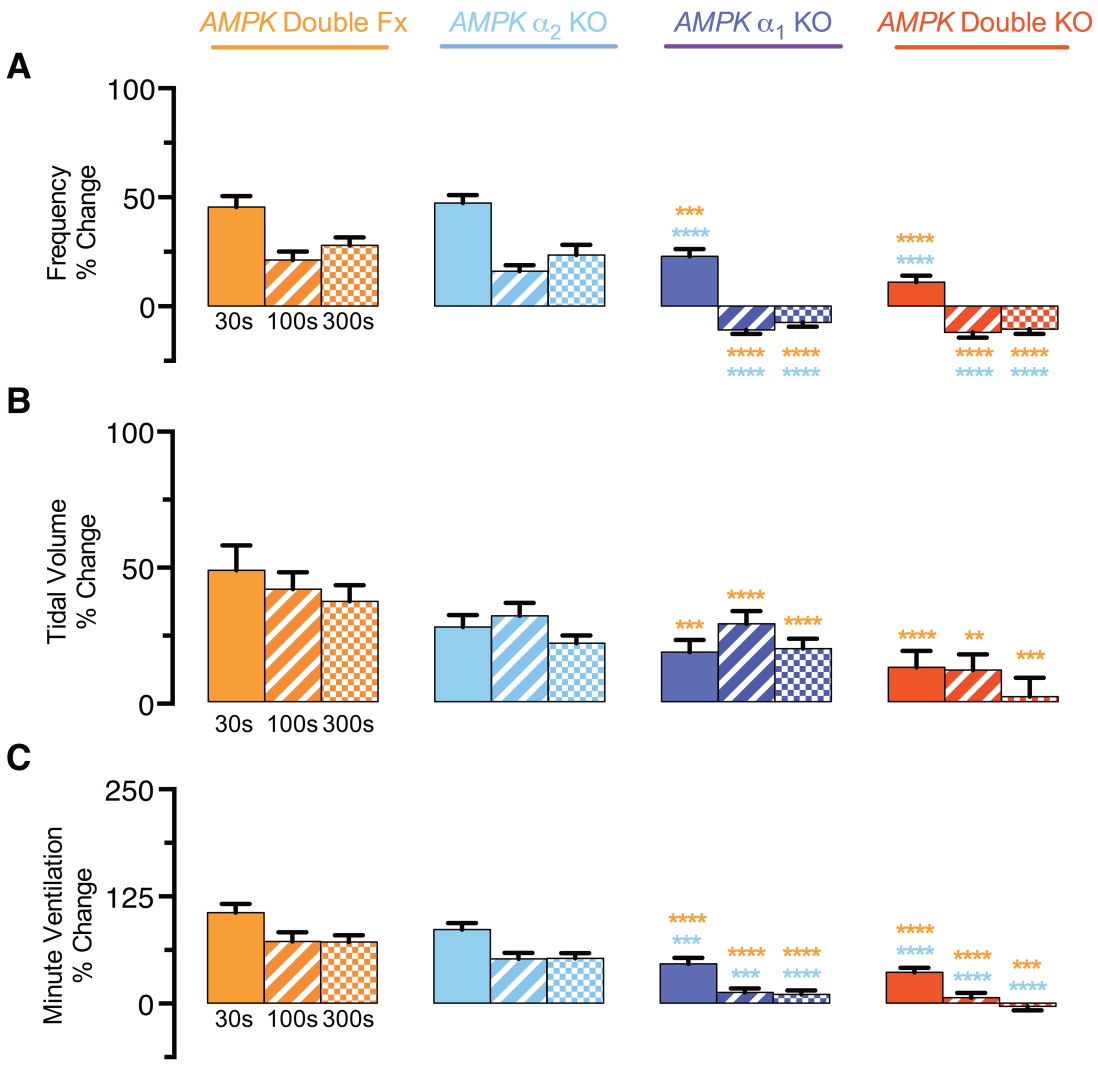

Figure 5.5: The effects of single or dual deletion of *AMPK α1*- and *α2-subunit* on the mean ventilatory response to hypoxia. Mean ± SEM for percent change during severe hypoxia (8% O_2) in **(A)** breathing frequency (min^{-1}), **(B)** tidal volume (ml g^{-1}) and **(C)** minute ventilation (ml min^{-1} g^{-1}) of mice at 3 time points during the 5min hypoxic exposure in *AMPK* α1 and α2 double floxed (*AMPK* double FX, n = 13 exposures, N = 5 mice, orange), *AMPK α2-subunit* knockout (*AMPK α*2 KO, n = 18 exposures, N = 5 mice, blue), *AMPK α1-subunit* knockout (*AMPK α*1 KO, n = 28 exposures, N = 6 mice, purple), and *AMPK α1* and *α2* double knockout mice (*AMPK* Double KO, n = 26 exposures, N = 6 mice, red).** = $p < 0.01$, *** = $p < 0.001$, **** = $p < 0.0001$. Significance tested by one-way ANOVA with Bonferroni multiple comparisons.

5.2.3.1a The effects of single deletion of *AMPK α1*- and *α2 -subunit* on the ventilatory response to hypoxia results in part from changes in the durations of inspiration and expiration

Given the above it seemed likely that further insight might be obtained from analyses of inspiration time, expiration time, and total breath duration, as this would allow us to determine whether or not the inspiratory and/or expiratory phases of ventilation is compromised in AMPK *α1* knockouts as was observed in the *AMPK α1* and *α2* double knockout mice in Chapter 4. Figures 5.6 and 5.7 show example and averaged (mean ± SEM) records, respectively, of the changes during 8% O_2 in inspiration time (Ti), expiration time (Te), and total breath time (To) relative to normoxia (Hypoxia/Normoxia) in control *AMPK α1* and *α2* double floxed, *AMPK* α2 knockout, *AMPK α1* knockout, and *AMPK α1* and *α2* double knockout mice.

Inspiration Time (Ti) As described in Chapter 4, upon exposure to 8% O_2, *AMPK α1* and *α2* floxed mice initially exhibited a time-dependent change in Ti. This involved a reduction in Ti duration relative to normoxia at 30s following the onset of 8% O_2 before recovering thereafter back towards levels observed during normoxia by 2min and plateauing for the remainder of the 5min exposure. In the *AMPK α2* knockouts, a time-dependent change in Ti was also observed. However, these mice exhibited subtle differences relative to control, as the degree of lengthening of Ti from 2min onwards appears to exceed that observed in floxed mice (Figure 5.7 – Panel A). This is demonstrated by the measured mean ± SEM of Ti at 30s as well as the overall mean ± SEM of Ti during the final 2min of the hypoxic exposure from 3-5min. In the *AMPK* α1 and α2 floxed mice, the mean ± SEM of Ti at 30s of 8% O_2 (relative to Ti maintained during normoxia) fell to 0.74 ± 0.06 (n = 5 exposures from 5 mice). Thereafter, Ti progressively lengthened until Ti under hypoxia was similar in duration to Ti under normoxia (hence approaching a ratio of 1) as the overall mean ratio from 3-5min was 1.09 ± 0.02 during 8% O_2 (using the formula for error of propagation). In the *AMPK α2* knockouts, the mean ± SEM of Ti at 30s markedly fell to 0.86 ± 0.05 (n = 13 from 5 mice) upon the start of the exposure to 8% O_2. This equates to a faster inspiration phase in response to hypoxia and at a level comparable with controls.

Thereafter, Ti progressively lengthened in a time-dependent manner in the *AMPK α2* knockouts until Ti under hypoxia exceeded Ti maintained under normoxia, as indicated by the measured mean ratio observed during the final 2min (1.16 ± 0.03). Although not significantly different using a one-way ANOVA, this was slightly longer than Ti of the control *AMPK α1* and *α2* floxed mice.

In the *AMPK α1* knockouts, a time-dependent change in Ti was also observed during hypoxia, which mirrored the changes observed in the *AMPK α2* knockouts. Once more, an initial shortening of Ti was observed relative to normoxia upon exposure to 8% O_2. The reduction in Ti at 30s was again comparable to controls, falling to 0.80 ± 0.06 (n = 11 from 5 mice). Subsequently, Ti increased relative to normoxia in the *AMPK α1* knockouts and reached 1.16 ± 0.03 during the final 2min of the exposure. This is comparable to the prolongation of Ti observed in the *AMPK α2* knockouts and slightly greater than controls (although not statistically significant).

The effects of the dual deletion of *AMPK α1* and *α2* subunits on the appropriate modulation of Ti during hypoxia was similar to the effects following the single deletion of either *AMPK α1* or *AMPK α2*. This is demonstrated by the lengthening of Ti from 3-5min, which reached 1.19 ± 0.02 (n = 10 from 5 mice, Figure 5.7 – Panel A).

Expiration Time Unlike Ti, in the *AMPK α1* and *α2* double floxed mice, Te decreased relative to normoxia at 30s and from 3-5min following the onset of 8% O_2, as described in Chapter 4. This is demonstrated by the marked reduction in mean Te relative to normoxia at 30s (0.59 ± 0.10) before the mean ratio of Te slightly lengthened to 0.90 ± 0.03 during the final 2 minutes. Surprisingly, the AMPK *α2* knockouts exhibiting a shortening in Te that was even greater than control *AMPK α1* and *α2* double floxed mice and was maintained throughout the 5min exposure to 8% O_2, declining to 0.55 ± 0.05 at 30s before recovering only marginally to 0.75 ± 0.03 during the final 2min (Figure 5.7 – Panel B). By contrast, reductions in Te at 30s were markedly smaller, although not significantly, in the *AMPK α1* knockouts, (0.84 ± 0.15). Thereafter, Te lengthened to levels greater than normoxic levels (1.26 ± 0.08),

and to levels significantly greater than either the controls ($p < 0.0001$) or *AMPK* $\alpha 2$ knockouts ($p < 0.0001$). These changes in Te in the *AMPK* $\alpha 1$ knockouts were comparable to those observed in *AMPK* $\alpha 1$ and $\alpha 2$ double knockouts (Figure 5.7 – Panel B).

Total Breath Duration (To) Figure 5.7C shows that upon exposure to hypoxia *To* of *AMPK* $\alpha 1$ and $\alpha 2$ floxed mice fell to 0.63 ± 0.08 at 30s following the onset of 8% O_2, before lengthening to 0.96 ± 0.02 during the final 2min of the exposure. In *AMPK* $\alpha 2$ knockouts *To* initially fell to 0.63 ± 0.04 at 30s, which was comparable to controls, but did not lengthen to the same degree from 3-5min (0.86 ± 0.01). These reductions in *To* were primarily driven by a shortening of the expiratory phase (Te, see above), as initial shortening of Ti in the *AMPK* $\alpha 2$ knockouts was smaller and lengthened over time to levels greater than those observed during normoxia. It is also notable, however, that reductions in Te and *To* were greater than controls following the deletion of the *AMPK* $\alpha 2$*-subunit* in catecholaminergic cells. A possible explanation is that, following the deletion of *AMPK* $\alpha 2$*-subunit* in catecholaminergic cells, the reciprocal inhibition between the inspiratory and expiratory neurons to control the ventilatory pattern has been altered in a manner that promotes the disinhibition of expiratory neurons.

In marked contrast, in the *AMPK* $\alpha 1$ knockouts, *To* initially fell to only 0.82 ± 0.11 at 30s before lengthening to levels that exceeded normoxia over the final 2min (1.23 ± 0.06) of the exposure and to levels significantly greater than the controls ($p < 0.0001$) and *AMPK* $\alpha 2$ knockouts ($p < 0.0001$). This is consistent with the observed changes in the average breathing frequency for *AMPK* $\alpha 1$ knockouts, which was attenuated at the start of the exposure to hypoxia before mice entered hypoventilation thereafter (Section 5.2.3).

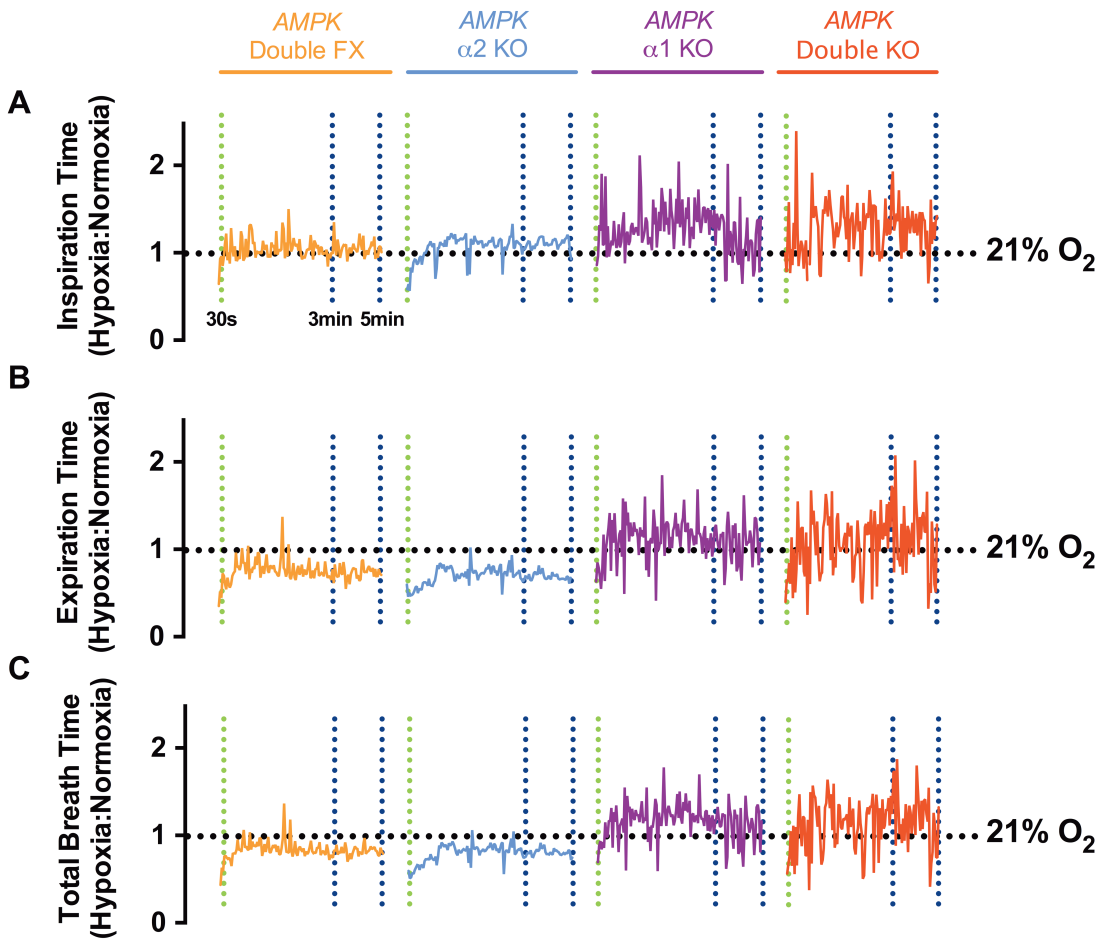

Figure 5.6: The effects of single or dual deletion of *AMPK α1-* and *α2-subunits* on the durations of inspiration, expiration time, and total breath during hypoxia. Example records of the ratiometric changes (relative to normoxia as indicated by dotted line at 1.0, 21% O_2) of the durations of **(A)** inspiration (Ti), **(B)** expiration (Te) and **(C)** total breath (To) over a 5min exposure with 2s sampling periods during severe hypoxia (8% O_2) in *AMPK α1* and *α2* double floxed (*AMPK* Double FX, orange), *AMPK α2-subunit* knockout (*AMPK* α2 KO, blue), *AMPK α1-subunit* knockout (*AMPK* α1 KO, purple), and *AMPK α1* and *α2* double knockout mice (*AMPK* Double KO, red). 30s indicated by the vertical dotted green line; 3-5min indicated by the vertical dotted blue lines.

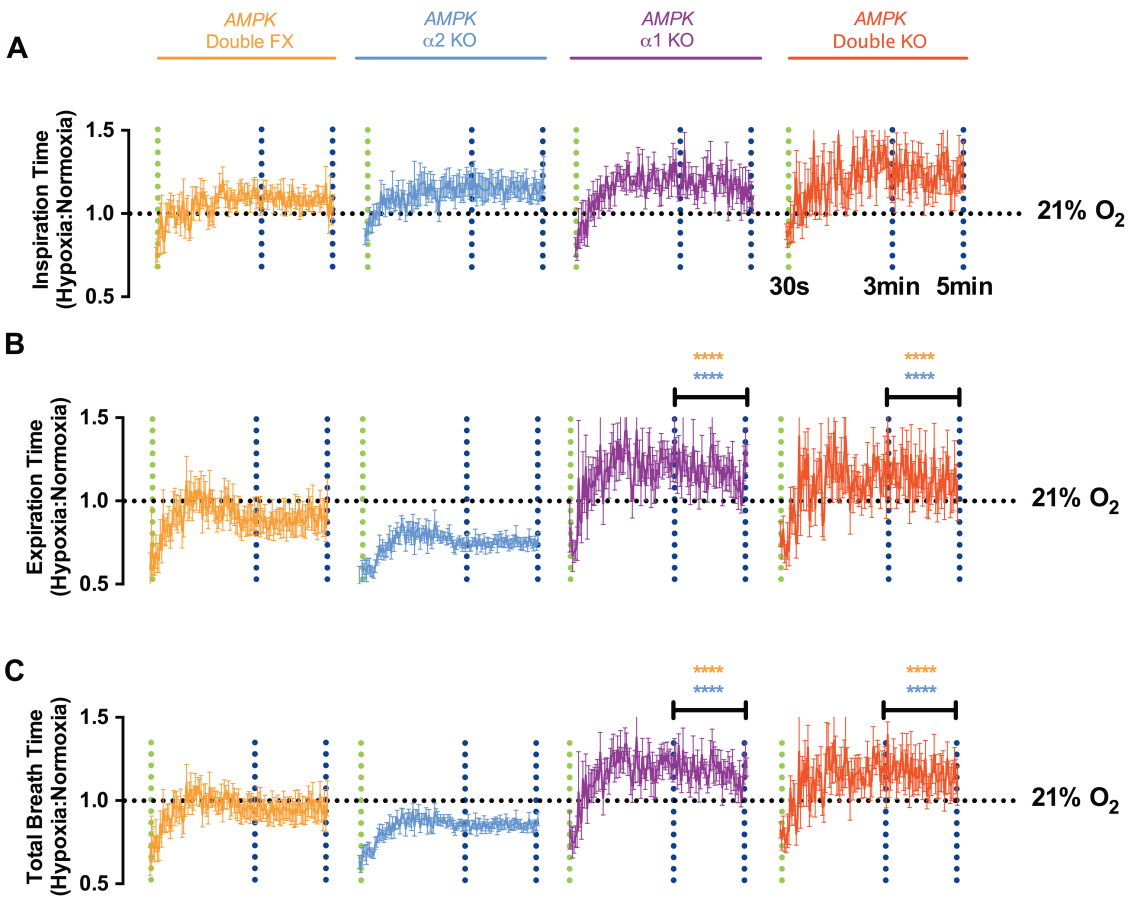

Figure 5.7: The effects of single or dual deletion of *AMPK α1-* and *α2-subunits* on the mean durations of inspiration, expiration and total breath during hypoxia. Mean ± SEM of the ratiometric changes (relative to normoxia as indicated by dotted line at 1.0) in the durations of **(A)** inspiration (Ti), **(B)** expiration (Te) and **(C)** total breath over a 5min exposure with 2s sampling periods during severe hypoxia (8% O_2) in *AMPK α1* and *α2* double floxed (*AMPK* Double FX, n = 10 exposures from 5 mice, orange), *AMPK α2-subunit* knockout (*AMPK α2* KO, n = 13 exposures from 5 mice, blue), *AMPK α1-subunit* knockout (*AMPK α1* KO, 11 exposures from 5 mice, purple), and *AMPK α1* and *α2* double knockout mice (*AMPK* Double KO, n = 10 exposures from 5 mice, red) mice. * = $p < 0.05$, ** = $p < 0.01$, *** = $p < 0.001$, **** = $p < 0.0001$. One-way ANOVA with Bonferonni multiple comparisons post-hoc test was used to test for significance at 30s following the onset of hypoxia (indicated by green vertical dotted line) and from 3-5min (as indicated by blue vertical dotted lines).

5.2.3.2b The effects of *AMPK* α1 deletion on tidal volume during hypoxia is driven by changes to the durations of the inspiration and expiration

When analysing the mean increase in tidal volume during severe hypoxia, the *AMPK α2* knockouts and *AMPK α1* knockouts exhibited an increase relative to normoxia, which was less when compared to *AMPK α1* and *α2* floxed mice, although not significantly different. Moreover, the effects of single deletion of *AMPK α1* and *AMPK α2* in catecholaminergic cells on the increase in tidal volume were less severe than the effects following the dual deletion of *AMPK α1* and *α2* (Section 5.2.3). As mentioned in Chapter 3 and 4, there are two possible explanations for the changes in tidal volume in response to hypoxia: (1) an increase in the volume of air moved per unit time, or (2) prolonged total breath time relative to normoxia. To determine the relative contribution of these two processes, ratiometric analysis was performed examining changes in tidal volume relative to inspiration duration (Tv/Ti), expiration duration (Tv/Te), and total breath duration (Tv/To). Figures 5.8 and 5.9 show example and averaged (mean ± SEM) records, respectively, against time for each of the ratiometric indices relative to values observed during normoxia in *AMPK α1* and *α2* double floxed, *AMPK α2* knockout, *AMPK α1* knockout, and *AMPK α1* and *α2* double knockout mice.

Tv/Ti Figure 5.9A shows the outcome of analyses for Tv/Ti. For *AMPK α1* and *α2* double floxed, a time-dependent change in Tv/Ti was observed (as previously described in Chapter 4). This involved an initial increase to 1.81 ± 0.23 at 30s before slightly decreasing to 1.13 ± 0.03 from 3-5min (n = 10 exposures from 10 mice). The time-dependent change in Tv/Ti in *AMPK α2* knockout mice was marginally less than control mice as Tv/Ti initially increased to 1.44 ± 0.09 at 30s before decreasing to an averaged 1.09 ± 0.03 during the final 2min, although this did not reach significance using a one-way ANOVA. However, the decrease of Tv/Ti was even greater following deletion of the *AMPK α1* subunit. At 30s, Tv/Ti only reached to 1.34 ± 0.15 and thereafter significantly decreased to 0.96 ± 0.03 between 3-5 min, which was significantly less than controls ($p < 0.01$) and *AMPK α2* knockouts ($p < 0.05$). Still, this

was not as severe as the attenuation observed in the *AMPK α1* and *α2* double knockouts as Tv/Ti only increased to 1.28 ± 0.08 at 30s before decreasing to 0.92 ± 0.02 ($p < 0.01$ versus control *AMPK α1* and *α2* floxed mice and *AMPK α2* knockouts) . Nevertheless, that Tv/Ti decreased below 1.0 in both the *AMPK α1* knockouts and *AMPK α1* and *α2* double knockouts demonstrates that even though the duration of inspiration is prolonged relative to normoxia, the volume of air movement per unit time of inspiration is slower.

Tv/Te A time-dependent change in Tv/Te was also observed in *AMPK α1* and *α2* floxed mice, *AMPK α2* knockouts, *AMPK α1* knockouts, and *AMPK α1* and *α2* double knockouts (Figure 5.9 – Panel B). In the *AMPK α1* and *α2* floxed mice, Tv/Te increased at the start of the hypoxic exposure to 2.65 ± 0.60 at 30s. Thereafter, a time-dependent decrease in Tv/Te occurred until stabilising by 2min for the remainder of the 5min exposure at a value of 1.40 ± 0.05 between 3-5min. Here, the deletion of *AMPK α2*-subunit in catecholaminergic cells had no identifiable effect during 8% O_2 as Tv/Te initially increased to 2.44 ± 0.27 at 30s. However, the decrease observed thereafter in the *AMPK α2* knockouts to 1.65 ± 0.02 between 3-5 min was less than the decrease observed in the control *AMPK α1* and *α2* floxed mice ($p < 0.01$, Figure 5.9 – Panel B). This is likely a result of an increased rate of air movement in the *AMPK α2* knockouts, as they exhibit a more rapid expiratory phase than controls.

By contrast, the deletion of the alternative *AMPK α1-subunit* in catecholaminergic cells had profound effects on the changes to Tv/Te, relative to both control and the *AMPK α2* knockouts, as 8% O_2 only increased Tv/Te to 1.59 ± 0.28 at 30s (although not statistically significant when compared to *AMPK α1* and *α2* double floxed mice and *AMPK α2* knockouts) before significantly decreasing until returning back to that observed under normoxia from 3-5min (1.00 ± 0.04, $p < 0.0001$ when compared to *AMPK α1* and *α2* double floxed mice and *AMPK α2* knockouts). However, the attenuation observed appeared comparable to the *AMPK α1* and *α2* double knockouts, which exhibit an initial increase to 1.55 ± 0.18 at 30s before falling to 1.07 ± 0.02 during the final 2min of the exposure (Figure 5.9 – Panel B).

Tv/To Overall, the above translated into a time-dependent change in Tv/To in response to hypoxia in all 4 genotypes (Figure 5.9 – Panel C). At the start of the exposure to 8% O_2, Tv/To of *AMPK α1* and *α2* floxed mice and *AMPK α2* knockouts similarly increased at 30s to 2.29 ± 0.43 and 1.93 ± 0.21, respectively. Subsequently, Tv/To decreased during 3-5min to 1.29 ± 0.02 in the controls and 1.33 ± 0.01 in the *AMPK α2* knockouts. However, in marked contrast, the deletion of the *AMPK α1 subunit* led to marked attenuation of the increase Tv/To during 8% O_2, which only rose to only 1.47 ± 0.22 at 30s (although not significantly significant) before declining to 0.97 ± 0.01 during 3-5 min ($p < 0.0001$ when compared to control *AMPK α1* and *α2* floxed mice and *AMPK* α2 knockouts). The inhibitory effects resulting from *AMPK α1-subunit* deletion were equally severe as the effects observed by dual deletion of *AMPK α1* and *α2* (30s: 1.41 ± 0.12, 3-5min: 1.00 ± 0.01).

These findings suggest that expiration time and thus Tv/Te are primarily influenced by *AMPK α1* deletion, given that deletion of both *α1* and *α2* subunits has no greater effect and that mice lacking the α2-subunit alone are comparable to controls. That Tv/To mirrored the outcome for Tv/Te, suggests that the effects of AMPK deletion on expiration time are the dominant factor when considering total breath time. These cross comparisons do, however, raise the possibility that AMPK subunits may contribute differently to the activity of different subpopulations of respiratory catecholaminergic neurons, and may perhaps modulate different aspects of respiratory function.

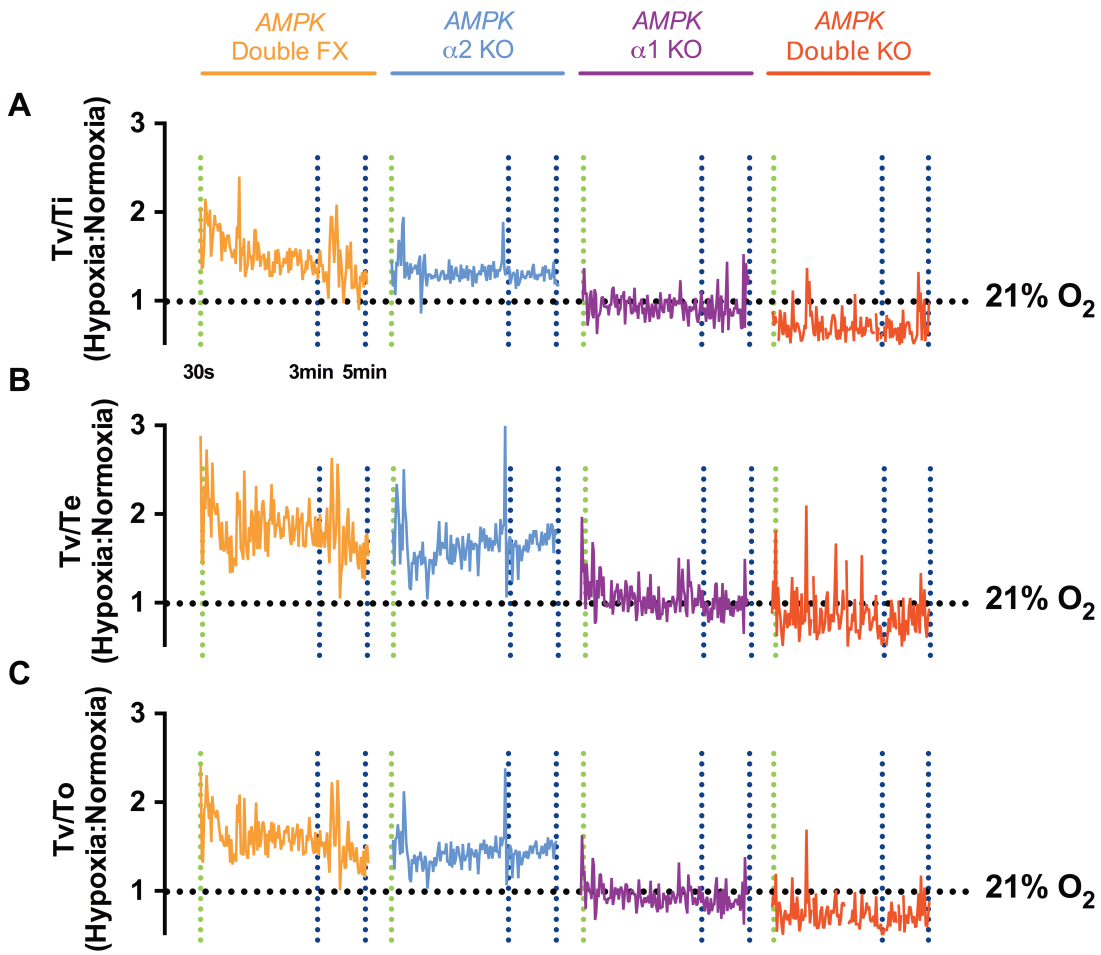

Figure 5.8: The effects of single or dual deletion of *AMPK α1*- and *α2-subunits* on tidal volume during hypoxia is driven by changes to the inspiration, expiration, and total breath duration. Example records of the ratiometric changes (relative to normoxia as indicated by dotted line at 1.0, 21% O_2) in tidal volume (Tv) relative to the durations of **(A)** inspiration (Tv/Ti), **(B)** expiration (Tv/Te), and **(C)** total breath duration (Tv/To) over a 5min exposure during severe hypoxia (8% O_2) in *AMPK α1* and *α2* double floxed (*AMPK* Double FX, orange), *AMPK* α_2*-subunit* knockout (*AMPK* α2 KO, blue), *AMPK* α_1*-subunit* knockout (*AMPK* α1 KO, purple), and *AMPK α1* and *α2* double knockout (*AMPK* Double KO, red) mice. 30s indicated by the vertical dotted green line; 3-5min indicated by the vertical dotted blue lines.

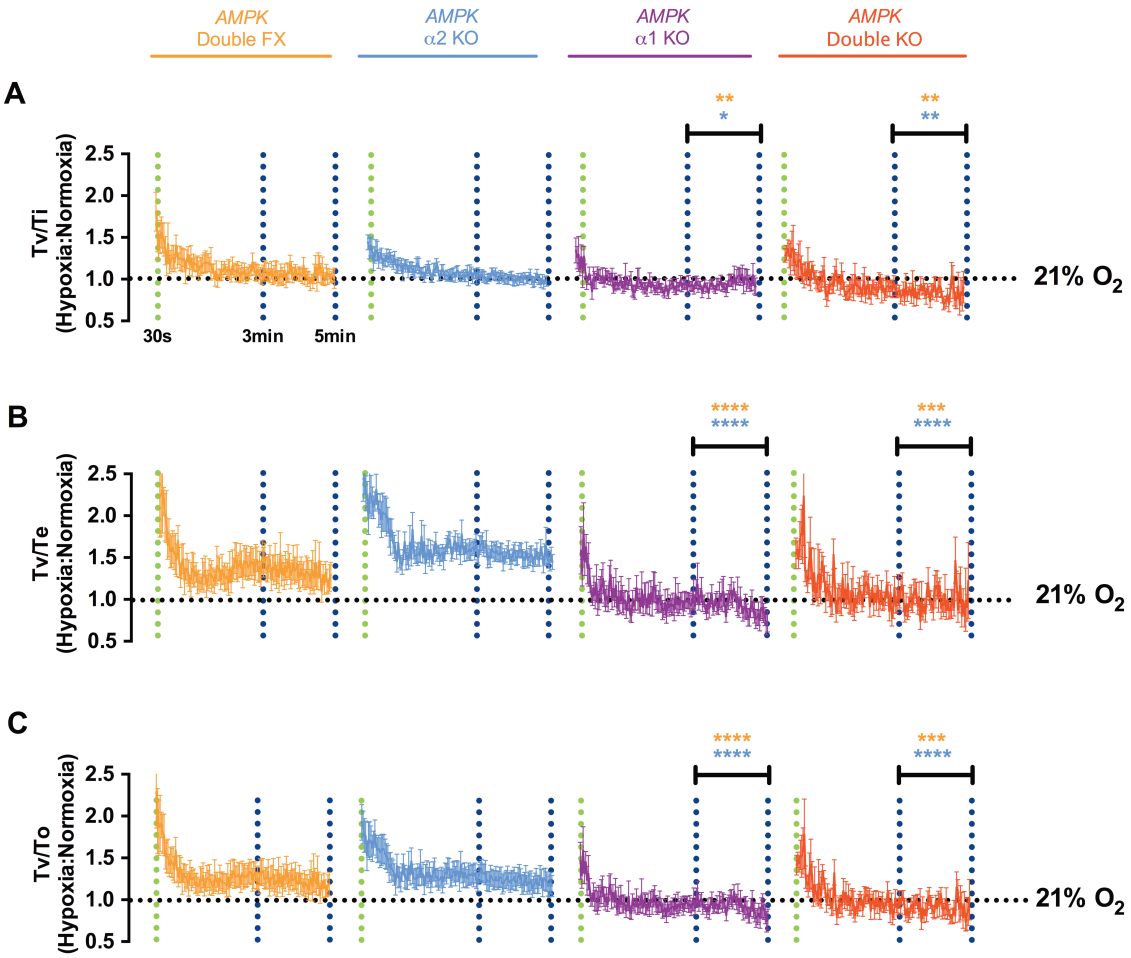

Figure 5.9: The effects of single or dual deletion of *AMPK α1-* and *α2-subunits* on the average hypoxic change in tidal volume relative to the durations of inspiration, expiration, and total breath durations. Example records of the ratiometric changes (relative to normoxia as indicated by dotted line at 1.0, 21% O_2) in tidal volume (Tv) relative to the duration of **(A)** inspiration (Tv/Ti), **(B)** expiration (Tv/Te), and **(C)** total breath duration (Tv/To) over a 5min exposure during severe hypoxia (8% O_2) in *AMPK α1* and *α2* double floxed (*AMPK* Double FX, n = 10 exposures from 5 mice, orange), *AMPK α2-subunit* knockout (*AMPK α2* KO, n = 13 exposures from 5 mice, blue), *AMPK α1-subunit* knockout (*AMPK α1* KO, 11 exposures from 5 mice, purple), and *AMPK α1* and *α2* double knockout mice (*AMPK* Double KO, n = 10 exposures from 5 mice, red) mice. * = $p < 0.05$, ** = $p < 0.01$, *** = $p < 0.001$, **** = $p < 0.0001$. One-way ANOVA with Bonferonni multiple comparisons post-hoc test was used to test for significance at 30s following the onset of hypoxia (indicated by green vertical dotted line) and from 3-5min (as indicated by blue vertical dotted lines).

5.3 Discussion

5.3.1 Summary of findings

The AMPK α1 and α2 subunits have distinct contributions to the ventilatory response to hypoxia, with the former being of primary importance. The deletion of *AMPK α2* had little discernable effects on the regularity of breathing during hypoxia, suggesting that AMPK α1 can sufficiently compensate for its loss in catecholaminergic cells to protect against hypoventilation and apnoeas. In contrast, the loss of *AMPK α1* activity exhibited a marked attenuation in the ventilatory response to hypoxia and significant increases in breathing irregularities, including spontaneous and post-sigh apnoeas and periods of marked hypoventilation. Nevertheless, the effects of dual deletion of *AMPK α1* and *α2* on the appropriate modulation of ventilation during hypoxia was greater still than the *AMPK α1* knockouts. This was confirmed by:

- Comparison of the apnoeic index under 8% O_2 (Figure 5.1 – Pane Bi): this markedly increased in the *AMPK α1* knockouts (10 ± 1.4 min^{-1}) but was greater still in the *AMPK α1* and *α2* double knockouts (14 ± 2 min^{-1})
- Comparison of the standard deviation of the inter-breath interval under 8% O_2 (Figure 5.3 - Biii): this increased to 167 ± 24ms in single *AMPK α1* knockouts and strikingly greater to 238 ± 23ms in the *AMPK α1* and *α2* double knockouts.
- Comparison of minute ventilation under 8% O_2 (Figure 5.5 - Panel C): although markedly attenuated, a marginal increase in minute ventilation was maintained in the *AMPK α1* knockouts by the end of the 5min exposure (30s = 46 ± 7%; 100s = 13 ± 5%; 300s = 10 ± 5%) while the attenuation was greater still for *AMPK α1* and *α2* double knockouts and not sustained by the end of the hypoxic exposure (30s = 36 ± 5%, 100s = 6 ± 5%, 300s = -4 ± 5%).

This thereby suggests that α2-containing AMPK heterotrimers can partially compensate for the loss of *AMPK α1* in catecholaminergic cells to protect against disordered breathing during hypoxia. Nevertheless, further studies on the durations of the inspiratory and expiratory phases of respiration and the rate of air movement at each

phase indicates that each isoform of the AMPK catalytic α-subunit may have distinct contributions to the modulation of ventilation during hypoxia. Namely, the expiration duration, and thus Tv/Te, were primarily influenced by *AMPK α1* deletion (with not greater effect following dual deletion of *AMPK α1* and *α2*) but not in mice lacking the α2-subunit alone (which were comparable to controls).

5.3.2 The α1 and α2 isoforms of AMPK contribute differently to the ventilatory response to hypoxia

Unlike the redundancy between AMPK α1 and AMPK α2 with respect to maintaining glucose uptake during contraction of skeletal muscle (Jørgensen et al., 2004), each isoform of the catalytic subunit contribute differently to the ventilatory response to hypoxia. The differential contributions of AMPK α1 and α2 to the ventilatory response to hypoxia may be down to a combination of things:

1. AMPK α1- and α2-containing heterotrimers may have different downstream targets in respiratory catecholaminergic cells that may translate to differential capacities to mediate hypoxic chemotransduction, subsequent cell activation, and ultimately the ventilatory response to hypoxia. As mentioned earlier, previous studies have demonstrated AMPK's ability to directly regulate ion channels as necessarily occurs in specialised oxygen-sensing cells to promote depolarization and cell activation during hypoxia (Ikematsu et al., 2011; Ross et al., 2011; Wyatt et al., 2007). Hence, given the primary importance observed in the present chapter for the AMPK α1 subunit in the ventilatory response to hypoxia, this raises the possibility that the α1-containing AMPK heterotrimers, rather than α2-containing heterotrimers, are able to mediate hypoxic chemotransduction in catecholaminergic cells by appropriately targeting ion channels in response to hypoxia. However, this perhaps is unlikely, or not the dominating reason as to why *AMPK* α1 and α2 have different contributions to the ventilatory response to hypoxia. The reason is that α2-containing AMPK heterotrimers have been found to directly target ion channels (Ikematsu et al., 2011; Ross et al., 2011), which

perhaps explains how AMPK α2 can partially compensate for the loss of AMPK α1 in catecholaminergic cells.

2. Expression levels of AMPK α1 may be considerably higher than α2 in oxygen-sensing catecholaminergic cells. Hence, when the α1-subunit is deleted, it has a more severe effect on hypoxic chemotransduction and, ultimately, the ventilatory response to hypoxia than when deleting the α2-subunit. Perhaps in support of this, the specialised oxygen-sensing pulmonary smooth muscle cells, though not catecholaminergic, have a higher expression level of AMPK α1 leading to suggestions that the α1-containing AMPK heterotrimers mediate hypoxia-response coupling (Evans et al., 2006). However, this does not necessarily mean that all catecholaminergic cells that function to modulate ventilation in response to hypoxia have higher expression or reliance of the AMPK α1-isoform over the α2-isoform. Instead, AMPK subunits may be differentially expressed or involved within subpopulations of respiratory catecholaminergic neurons, i.e inspiratory versus expiratory neurons, and thus contribute differentially to the ventilatory response to hypoxia. This could be the reason that the duration of the expiratory phase, and thus Tv/Te, are primarily influenced by *AMPK α1* deletion and not *AMPK α2*.
3. Another possibility is that α1 and α2 are differentially localised or compartmentalised within the cell thereby mediating different sensitivities and responsiveness to the same stimuli. This would consequently designate different cellular functions and ultimately different influences on the ventilatory response to hypoxia. This has been elegantly demonstrated with respect to AMPK's ability to regulate the Kv2.1 channel depending on the mode of activation (Ikematsu et al., 2011). In these studies, activation of AMPK by the Ca^{2+} ionophore, ionomycin, (presumably by Ca^{2+}/CaMKKβ-dependent phosphorylation of Thr-172 (Hawley et al., 2005) did not lead to phosphorylation of Kv2.1. In contrast, activation of AMPK in a Ca^{2+}-independent manner, by A769662, phosphorylated Kv2.1 at two separate sites. This led to the suggestion that there are distinct pools

of AMPK heterotrimers subcellularly that are compartmentalised and accordingly differentially sensitive and responsive to certain stimuli. This perhaps may be mediated by the a-kinase anchoring proteins (AKAPS), which have been found to compartmentalise AMPK, thereby regulating its cellular function (Y. Zhang et al., 2013). Taken together, this highlights the possibility that AMPK α1 and α2 are differentially compartmentalised subunit, with AMPK α1 fittingly localised in oxygen-sensing cells to appropriately couple hypoxia to ion channel regulation during hypoxia to promote cell activation, and ultimately the ventilatory response to hypoxia. Perhaps in support of this are studies in skeletal muscle that demonstrated that AMPK α2 is predominantly localised in the nucleus while α1 is localised to the cytoplasm and cell membrane (Salt *et al*., 1998; McGee *et al.*, 2003).

5.3.3 Conclusion

In conclusion, AMPK α1 containing heterotrimers are of primary importance to the ventilatory response to hypoxia with AMPK α2 only able to partially compensate for its loss in catecholaminergic cells. This may be a result of a difference in downstream targets, expression levels and/or localisation of the two isoforms within catecholaminergic oxygen-sensing cells in a manner that gives AMPK α1 the capacity to appropriately mediate the hypoxic response. This perhaps appears more noteworthy when considering that the AMPK α1 gene, *PRKAA1*, has been associated with long-term adaptation to hypoxia at high-altitude (Moore, 2011); in addition to its ability to reestablish ATP levels during metabolic stress, AMPK is able to regulate protein synthesis by inhibiting the mTOR pathway. Accordingly, AMPK demonstrates great versatility with respect to its capacity to mediate an appropriate ventilatory response to metabolic stress, in this instance acute hypoxia, to maintain oxygen and energy supply at the whole-body level but may also play a role ubiquitously in the alternative O_2-sensing pathway involved with the slow modulation of gene expression to adapt to chronic reductions in arterial PO_2.

Chapter Six:
General Discussion

6.1 Summary of findings

Ventilatory drive is mediated by respiratory central pattern generators (rCPGs), which are continuously modulated by specialised peripheral and central chemoreceptors to adjust ventilatory patterns according to changes in arterial PO_2, PCO_2, and pH levels. With respect to PO_2, catecholaminergic oxygen-sensing cells within the carotid body and brainstem are vital as they are able to sense reductions in oxygen-supply and accordingly trigger an increase in ventilation. However, the molecular mechanism within the oxygen-sensing cells by which respiratory adjustments are made during acute hypoxia remains controversial. The aims of this thesis were to examine the possible role for the LKB1-AMPK signalling pathway, which is central to cellular adaptations to metabolic stress, in mediating the appropriate modulation of ventilation during hypoxia.

As described in Chapter 2, this first involved the development of transgenic mice in which *Lkb1* or *AMPK* were conditionally deleted in catecholaminergic cells by driving Cre expression through a tyrosine-hydroxylase-specific promoter region; global knockout of *Lkb1* (Sakamoto, 2006) or *AMPK* activity (Viollet et al., 2009) are embryonic lethal. Importantly, the ventilatory phenotypes of control and knockout mice were indistinguishable under normoxic conditions. In contrast, as described in chapter 3 to 4, the conditional deletion of *Lkb1* and *AMPK* α1 and α2 activity in catecholaminergic cells precipitates irregular breathing patterns during hypoxia in a PO_2-dependent manner. It also resulted in a significant attenuation of the increase in minute ventilation that necessarily occurs during hypoxia to maintain oxygen levels; interestingly, this was driven by the inability of the knockout mice to appropriately modulate the durations of inspiration and expiration to promote an overall reduction in total breath duration, and thus an increase in breathing frequency. Nevertheless, all ventilatory abnormalities observed during hypoxia were resolved in both the *Lkb1* and *AMPK α1* and *α2* double knockouts when exposed to hypoxia with hypercapnia.

As described in chapter 5, the use of single *AMPK* α1 and α2 knockout mice allowed me to further examine the differential contributions of the *AMPK* α1 and α2 isoforms to the ventilatory response to hypoxia. This revealed that each isoform

distinctly contributes to the hypoxic ventilatory response, with the AMPK α1 isoform being of primary importance. The deletion of *AMPK α2* had little discernable effects on the regularity of breathing during hypoxia, suggesting that AMPK α1 can sufficiently compensate for its loss in catecholaminergic cells to protect against hypoventilation and apnoeas. In contrast, the loss of *AMPK α1* activity exhibited a marked attenuation in the ventilatory response to hypoxia and significant increases in breathing irregularities, including spontaneous and post-sigh apnoeas and periods of marked hypoventilation. Nevertheless, the effects of dual deletion of *AMPK α1* and *α2* on the appropriate modulation of ventilation during hypoxia was greater still than the *AMPK α1* knockouts. This thereby suggests that α2-containing AMPK heterotrimers can partially compensate for the loss of *AMPK α1* in catecholaminergic cells to protect against disordered breathing during hypoxia.

In this chapter, I will further discuss how the results in this thesis adds to current understanding of the molecular mechanisms involved in mediating the ventilatory response to hypoxia and the prospects for further research in this area.

6.2 Discussion

6.2.1 The importance of the LKB1-AMPK signalling pathway within oxygen-sensing cells and ultimately the ventilatory response to hypoxia

As discussed in chapter 4, the hypoxia-induced ventilatory abnormalities were similar between *Lkb1* and *AMPK α1* and *α2* double knockouts, with both mice exhibiting prolonged periods of hypoventilation with spontaneous and post-sigh apnoeas. Yet the ventilatory phenotype appeared more severe in the *AMPK α1* and *α2* double knockouts. This, linked with the recognised role for LKB1 as the essential upstream kinase required for full activation of AMPK in response to metabolic stress (Hawley et al., 2003), strongly suggests that the LKB1-AMPK signalling pathway is required in catecholaminergic oxygen-sensing cells to mediate hypoxic chemotransduction, subsequent cell activation, and thus the appropriate ventilatory response to hypoxia.

Previous *in vitro* studies have provided evidence in support of the view that AMPK has the capacity to mediate hypoxia-response coupling in specialised oxygen-sensing cells. These included pharmacological and electrophysiological studies that demonstrated the ability of AMPK to directly regulate ion channels (Ross et al., 2011; Wyatt et al., 2007) and to activate the oxygen-sensing type I cells of the carotid body (CB1 cells) (Wyatt et al., 2007), as necessarily occurs during hypoxia. However, these studies fall short from demonstrating (1) whether AMPK-dependent modulation of oxygen-sensing cells is sufficient or required to trigger the ventilatory response to hypoxia at the whole-body level, and (2) if this is dependent on the primary upstream kinase LKB1, which is necessary to couple metabolic stress to AMPK activation.

Hence, the findings of chapters 4 and 5 provide support and further demonstrate, for the first time, the requirement of AMPK activity within catecholaminergic cells for respiratory adjustments during hypoxia. Studies in chapter 3 further suggests that this is likely mediated by LKB1-dependent phosphorylation, and hence activation, of AMPK during hypoxic stress (with preliminary studies indicating that the alternative upstream kinase CaMKK-B is not required). Accordingly, the LKB1-AMPK signalling pathway may maintain energy levels not only at a cellular level but also the whole-body level by regulating the ventilatory response to changes in O_2-supply.

However, as mentioned in chapter 3, both mitochondrial reactive oxygen species (mROS) and increases in the ADP:ATP and AMP:ATP ratios have been suggested to drive LKB1-dependent activation of AMPK during hypoxia (Emerling et al., 2009). However, while the hypoxic inhibition of ATP-synthesis has been identified as the primary event that triggers the hypoxic chemotransduction pathway in specialised oxygen-sensing cells (Wyatt and Buckler, 2004; Buckler and Turner, 2013), studies in cells that do not function to monitor and maintain oxygen-supply have demonstrated that hypoxia activates AMPK in an LKB1-dependent manner via increases in mitochondrial reactive oxygen species (mROS) and not AMP (Emerling et al., 2009). Also, several studies have provided evidence that strongly opposes such an AMP-independent and mROS-dependent activation of AMPK during hypoxia; the use of AMP-insensitive AMPK heterotrimers have shown that H_2O_2 can no longer activate AMPK directly and

that H_2O_2 promotes AMPK activation in an LKB1-dependent manner by inhibiting mitochondrial function and subsequently increasing the AMP:ATP ratio (Hawley et al., 2010; Auciello et al., 2014). Therefore, if H_2O_2 or mROS were to effect AMPK activation during hypoxia, this would likely involve the facilitation of mitochondrial inhibition (Evans et al., 2011; Auciello et al., 2014). Although this strongly indicates that direct activation of AMPK by mROS during hypoxia, in an AMP-independent manner, is highly unlikely the studies from this thesis does not provide any evidence in support or against the possible roles of mROS and/or AMP in mediating LKB1-dependent activation of AMPK during hypoxia.

6.2.2 The differential effects of *Lkb1* and *AMPK* deletion on the ventilatory response to hypoxia

On the whole, the effects of conditional *Lkb1* and *AMPK* deletion in catecholaminergic cells resulted in similar ventilatory abnormalities (i.e. PO_2-dependent increases in apnoea duration index with spontaneous and post-sigh apnoeas and a blunted ventilatory response) strongly suggests that the LKB1-AMPK signalling pathway is required within the catecholaminergic oxygen-sensing network to mediate the appropriate modulation of ventilation required during hypoxia to maintain oxygen, and thus energy supply. However, a few differences in the ventilatory abnormalities between the *Lkb1* and *AMPK α1* and *α2* double knockouts were also apparent. These differences included: (1) the augmentation phase of the ventilatory response to hypoxia, which is more robust in the *AMPK α1* and *α2* double knockouts than in the *Lkb1* knockouts, (2) Cheyne-Stokes-like breathing, which was exhibited in the *Lkb1* knockouts but not the *AMPK α1* and *α2* double knockouts, (3) the marginal attenuation of breathing frequency in response to hypercapnia in the *Lkb1* knockouts but not *AMPK α1* and *α2* double knockouts.

As described in chapters 3 and 4, the augmentation phase of the ventilatory response to hypoxia is the rapid increase in ventilation following the onset of hypoxia. This has been proposed to be predominantly driven by afferent input to the respiratory centres in the brainstem following the rapid hypoxic activation of the carotid bodies. Furthermore, Cheyne-Stokes-like breathing is characterised by a sinusoidal ventilatory

pattern that cycles from progressively deeper and faster breathes to a gradual decrease in frequency and tidal volume until ultimately reaching an apnoeic event. This has been associated with increased chemosensitivity of peripheral and/or central chemoreceptors (Eckert et al., 2007). Accordingly, it seems likely that the differences observed are driven by differential effects on the chemosensitivity of certain catecholaminergic cells following *Lkb1* and *AMPK* deletion. Further studies on peripheral and central chemoreceptors are required to deduce whether this is indeed the case. This may include *in vitro* studies looking at the functional integrity of carotid bodies dissected from the *Lkb1* knockouts and *AMPK α1* and *α2* double knockouts during hypoxia and/or the effects of their deletion on the activation of central catecholaminergic neurons during hypoxia.

6.2.3. The role of LKB1 and AMPK in carotid body type I cells

Given that the carotid bodies are believed to be the primary arterial chemoreceptors that drive the entire ventilatory response to hypoxia, one may be tempted to conclude based on the findings of this thesis that the LKB1-AMPK signalling pathway is predominantly required within the type I cells to mediate an appropriate ventilatory response to hypoxia. However, it is understandably excessive to draw such a conclusion solely based on the ventilatory studies performed in this thesis, not least because other peripheral and/or central catecholaminergic neurons may have also been affected and consequently contributed to the overall phenotype. This perhaps is highlighted by the similarities observed between the ventilatory abnormalities exhibited following *Lkb1* and *AMPK* deletion in catecholaminergic cells with those manifested with Rett syndrome, which is associated with the degeneration of central catecholaminergic cells as further discussed below (and as described in chapters 3 and 4).

In vitro studies on the carotid body were in fact performed by the University of Birmingham (under subcontract) and confirm that *Lkb1* and *AMPK* deletion have differential effects on the chemosensitivity of the carotid body. Consistent with the view that the carotid body type 1 cells (CB1 cells) mediates and drive the ventilatory response to hypoxia, activation of the carotid body and afferent fibre discharge during hypoxia is

significantly attenuated following *Lkb1* deletion (Appendix 6A). However, surprisingly and in marked contrast, despite a significantly attenuated hypoxic ventilatory response, *AMPK* deletion does not inhibit carotid body activation and afferent fibre discharge during hypoxia. This was also demonstrated by experiments performed by the University of Birmingham, which showed that reductions in PO_2 raised chemoafferent discharge exponentially in the carotid bodies of *AMPK* double knockouts (Appendix 6B). This quite significantly indicates that a functional carotid body does not act as the primary driver for increases in ventilation in response to hypoxia. Hence, the blunted hypoxic ventilatory response in the *AMPK* double knockout mice is likely a result of a primary abnormality of an additional or alternative primary catecholaminergic oxygen-sensing cell-type(s). However, the possible identity of these catecholaminergic cells and whether they have an integrative and/or effector function in the central modulation/coordination of ventilation during hypoxia is something that will require more detailed studies.

Nevertheless, the differential effects of *Lkb1* and *AMPK* deletion on carotid body type I cells provides an explanation as to why the differences listed above were exhibited between the *Lkb1* knockouts and *AMPK* double knockouts:

1. The augmentation phase of the ventilatory response to hypoxia: the retained chemosensitivity of the carotid bodies in the *AMPK* double knockouts may have led to the more robust increase in breathing frequency observed, and hence minute ventilation, relative to the *Lkb1* knockouts which contain carotid bodies that have lost their oxygen-sensing ability (though the ventilatory response was significantly attenuated in both knockout mice when compared to controls). This may be surprising as it opposes the widely accepted view that the carotid body drives the entire ventilatory response to hypoxia (Dahan et al., 2008; C. A. Smith et al., 2010), as despite a fully functional carotid body, the *AMPK* double knockouts are unable to trigger a complete ventilatory response to hypoxia during the augmentation phase and are also unable to maintain the ventilatory response and paradoxically hypoventilate, thereafter. Nevertheless, the attenuated increase observed in the *AMPK* double knockouts during the augmentation phase may therefore be driven by

increased afferent inputs from the carotid body via direct projections to the rCPGs, with the larger portion of the ventilatory response attenuated due to possible effects of *AMPK* deletion on central oxygen-sensing cells that also provide input to the rCPGs in response to hypoxia, i.e. neurons of the NTS (Figure 6.1, King et al., 2012; Song et al., 2011). This perhaps is supported by evidence suggesting that central catecholaminergic neurons are crucial for appropriate modulation of ventilation during hypoxia (Roux et al., 2010; 2000; King et al., 2012; Teppema et al., 1997). However, to determine whether there is an alternative primary oxygen-sensing chemoreceptor besides the carotid body or whether the relay circuit between the carotid body and rCPGs has been disrupted in the knockout mice will require more detailed studies and will be discussed further below.

Taken together, this suggests that the similar ventilatory abnormalities observed in the *Lkb1* and *AMPK α1* and *α2* double knockouts is not a result of their effects/requirements in the carotid body type I cells, but a common catecholaminergic oxygen-sensing cell/tissue located elsewhere. One candidate may be the aortic bodies, however this seems unlikely as these peripheral chemoreceptors have a subordinate role during hypoxia, usually following the chronic absence of a functional carotid body (Lahiri et al., 1981). Hence, the aortic bodies are unlikely to be affected in the *AMPK α1* and *α2* double knockouts as the functional integrity of the carotid bodies are fully retained. Another possible candidate that perhaps seems more likely are the central oxygen-sensing catecholaminergic neurons that have been implicated with breathing irregularities (as discussed below) but also their ability to adapt and mediate the entire hypoxic ventilatory response in the absence of peripheral input from the carotid body (Viemari et al., 2005; Soulage et al., 2005; Roux et al., 2000).

2. Cheyne-Stokes like breathing (CSB) exhibited in the *Lkb1* knockouts: One primary cause of CSB appears to be ventilatory instability due to oscillating feedback within the respiratory network resulting from an augmented chemoreflex gain or prolonged feedback delay (Naughton et al., 1993; Hall et al., 1996; Quaranta et al., 1997; Solin

et al., 2000). The overall gain of the respiratory system, i.e. its loop gain, is the product of the gains from passive components, namely the plant, and the controller. The lungs, circulation and metabolising tissues compromise the plant while the controller compromises two chemoreflex inputs, peripheral and central chemoreceptors, that have one output → ventilation. Accordingly, it is unlikely that every instance of CSB has the same cause. However, many cases of CSB has been associated with increased controller gain, mainly as a result of an enhanced hypercapnic ventilatory response and an increase in central chemoreceptor chemoreflex gain (Topor et al., 2007; Cherniack and Longobardo, 2006). A negative interaction between peripheral and brainstem chemoreceptors has also been identified previously (Day and R. J. A. Wilson, 2009; 2008). Taken together, CSB manifested in the *Lkb1* knockouts, but not *AMPK α1* and *α2* double knockouts, may be a result of increased controller gain within the respiratory network as central CO_2-sensing is enhanced consequent to the carotid body losing responsiveness to PO_2 and possibly PCO_2.

3. The marginal attenuation at the start of the hypercapnic ventilatory response in *Lkb1* knockouts: Peripheral chemoreceptors, and primarily the carotid bodies, contribute to approximately 20-40% of the entire ventilatory response to hypercapnia, with central chemoreceptors providing the remaining 60-80% of ventilatory drive (Cunningham, 1986; Dahan, 1990; Fatemian, 2003). Furthermore, peripheral chemoreceptors drive the fast component of the ventilatory response to PCO_2, as central chemoreflex has a delayed response to blood gas perturbations (C. A. Smith et al., 2006; Day and R. J. A. Wilson, 2009). Nevertheless, carotid body activation by hypercapnia has been found to be PO_2-dependent (Pepper et al., 1995). All together, this is in agreement with the observations made in the *Lkb1* knockouts, as the ventilatory response to hypercapnia was only marginally attenuated for the first 100s of the exposure by ~20-30% before peaking to levels comparable to controls thereafter (Chapter 3, Figure 3.14, p. 119). Hence, the difference between the hypercapnic ventilatory response in the *Lkb1* and *AMPK α1* and *α2* double knockouts is likely a result of the differential effect following their deletion on the

oxygen-sensitivity of the carotid body, and accordingly, its PO_2-dependent hypercapnia sensitivity.

Taken together, the LKB1-AMPK signalling pathway is key to respiratory adaptations during hypoxia and thereby protects against apnoeas by regulating oxygen-sensing catecholaminergic cells other than the type I cells of the carotid body, with the central catecholaminergic neurons being the primary candidates. Future studies examining the effects of *Lkb1* and *AMPK* deletion on brainstem catecholaminergic neurons during hypoxia may therefore provide further insight and ratify whether the common ventilatory abnormalities observed in the knockout mice is a result of their requirement centrally, and accordingly identify a primary oxygen-sensing chemoreceptor that is required to mediate an appropriate ventilatory response to hypoxia.

However, something worth addressing is why *Lkb1* but not *AMPK* deletion attenuates the chemosensitivity of the CB1 cells. A possibility is that following *AMPK* deletion, LKB1 is still able to activate one or a few AMPK-related kinases that have the capacity to compensate for the loss of AMPK activity and mediate hypoxic chemotransduction and CB1 cell activation. Whereas with *Lkb1* deletion, neither AMPK nor its related kinases are able to mediate hypoxic chemotransduction as the cells are deficient of the primary upstream kinase. Further studies comparing the expression and activity levels of the AMPK-related kinases in the carotid body type I cells of *Lkb1* knockouts and *AMPK α1* and *α2* double knockouts may clarify this possibility. If up-regulation of any AMPK-related kinases is detected in the *Lkb1* knockout carotid bodies, further knockdown experiments using sh-RNA targeting these AMPK-related kinases can be applied to the CB1 cells of *AMPK α1* and *α2* double knockouts to observe whether the cells are still able to compensate for the loss of AMPK, and hence respond to hypoxia. Another possibility is that AMPK is simply not required for mediating the hypoxic chemotransduction pathway in the carotid body, despite the fact it appropriately inhibits ion channels, namely the BK_{Ca} (Ross et al., 2011), and promotes carotid body cell activation (Ross et al., 2011; Wyatt et al., 2007). Therefore, further studies are required to determine the purpose or role of AMPK's capacity to inhibit hypoxia-sensitive K^+ channels during activation of the CB1 cells.

6.2.4 The role of LKB1 and AMPK in central catecholaminergic cells

6.2.4.1 Identification of respiratory diseases and the insight they offered on the importance of central catecholaminergic cells to the regulation of the respiratory network

6.2.4.1a Ondine's curse – congenital central hypoventilation syndrome

Congenital central hypoventilation syndrome (CCHS) is a lethal respiratory disorder that results in hypoventilation and central respiratory apnoeas during sleep, which can ultimately lead to respiratory arrest and death (Goridis et al., 2010). Furthermore, during both wakefulness and sleep, respiratory stimulation by hypoxia and hypercapnia is significantly attenuated in CCHS patients (Spengler et al., 2001). The idiopathic form of CCHS was first described in 1962, by Severinghaus and Mitchell (Severinghaus, 1962). Both had initially chosen the eponym, Ondine's curse, to describe the symptoms manifested in three patients who had undergone high cervical and brainstem surgery. The three adult patients were able to breathe normally during wakefulness but exhibited hypoventilation and severe central apnoeas during sleep and required mechanical ventilation to avoid respiratory arrest (Severinghaus, 1962). However, hypoventilation has also been observed during wakefulness in severe cases of CCHS (Paton et al., 1989). It was not until 1970, that the first case of CCHS was reported in an infant by Mellins *et al*. (Mellins et al., 1970).

PHOX2B and congenital central hypoventilation syndrome

A staggering 96% of patients with CCHS carry a mutation in the homeobox gene *PHOX2B,* which has been found to be the main cause of CCHS (Amiel et al., 2009; Weese-Mayer et al., 2006). *PHOX2B* is situated within chromosome 4p12 and is highly conserved with 314 amino acids and a 20 poly-alanine tract. Sequence analysis further indicated that the most frequent mutation in *PHOX2B* present in CCHS patients involved a heterozygous expansion of 5-7 alanine residues to the 20 poly-alanine tract (Amiel et al., 2009; Dubreuil et al., 2008). Transgenic mice have been developed in attempt to model the most common form of human CCHS; these

mice had 7 alanine residues introduced to the *PHOX2B* gene. Homozygous pups were embryonic lethal (Pattyn et al., 1999) while heterozygous pups (*Phox2b*$^{+/27Ala}$) died shorty after birth due to respiratory failure (Dubreuil et al., 2008). Nevertheless, neonatal *Phox2b*$^{+/27Ala}$ mice have been extensively used as models of human CCHS to identify the function and expression patterns of *PHOX2B* and how they are defected in the disease state.

Expression of *PHOX2B*

Studies in rats revealed that *PHOX2B* is abundantly expressed in the rostral end of the VRC within the brainstem, namely within the chemosensitive glutamatergic, but non-catecholaminergic, neurons of the RTN (Abbott et al., 2011; Stornetta et al., 2006). Caudally, *PHOX2B* expression was significantly less and, interestingly, was not observed within the respiratory central pattern generators (CPGs). Nevertheless, expression has also been located within catecholaminergic cells that are essential for respiratory reflexes. Peripherally, it has been located within the specialised oxygen-sensing type I cells of the carotid body (CB1 cells) as well as the petrosal ganglion, which the CB is innervated by (Dauger et al., 2003). The expression of *PHOX2B* continues along the relay pathway from peripheral chemoreceptors, that is from the carotid body, to central medullary catecholaminergic neurons that modulate respiration based on chemical drive (Stornetta et al., 2006); the medullary catecholaminergic neurons include the noradrenergic A1/A2 and adrenergic C1/C2 clusters and is further described in section 1.4 (Erickson and Millhorn, 1994; Teppema et al., 1997; Roux et al., 2003).

Function of *PHOX2B*

The expression pattern of *PHOX2B* as described above correlates with the chain of interconnected catecholaminergic neurons involved in the integration of information sent from both peripheral and central chemoreceptors to the rCPGs to modulate respiration based on chemical drive. Further studies have demonstrated that *PHOX2B* expression is required for the development of the catecholaminergic

network mentioned above, including the carotid body, petrosal ganglion and the central catecholaminergic neurons, and has been associated with the respiratory defects manifested with CCHS (Qian et al., 2001; Pattyn, 2000; Dauger et al., 2003). All together, the expression and requirement of *PHOX2B* in the chemosensory circuit and not within the rCPGs themselves is consistent with the respiratory abnormalities observed in most CCHS patients. That is, normal rhythmic breathing is maintained during wakefulness but impaired during sleep and sustained periods of hypoxia and/or hypercapnia (Stornetta et al., 2006; Paton et al., 1989).

CCHS and breathing irregularities

As briefly mentioned above, human or rodent models carrying a heterozygous mutation to *PHOX2B* manifest breathing irregularities, particularly hypoventilation and central apnoeas, that predominately appear during sleep or as a consequence to a chemical drive to breathe, i.e. hypoxia or hypercapnia (Spengler et al., 2001). Therefore, chemoreceptor modulation of respiration is defective with CCHS. Nevertheless, the respiratory defects are not accompanied by underlying defects in respiratory muscles or the cardiovascular system (Mellins et al., 1970). All together, this highlights the importance of *PHOX2B*, and accordingly the development of the catecholaminergic chemosensitive circuit, to appropriately modulate ventilation based on changes in the chemical drive to breathe.

6.2.4.1b Rett syndrome

Rett Syndrome was first described in 1966 by a paediatrician, Dr. Andreas Rett, who noticed that a certain number of his female patients manifested similar abnormal behaviours along with similar clinical histories. However, it was not until 1983 that this neurodevelopmental disorder became increasingly recognised when further studied and published by Dr. Hagberg (B. Hagberg et al., 1983). Hagberg had identified that approximately 1 in 10,000 girls were affected by Rett syndrome with patients developing normally until 6-18 months of age, at which point they started manifesting symptoms. These symptoms include autism, seizures, loss of speech, and stereotypic

hand movements (B. Hagberg et al., 1983; B. Hagberg and G. Hagberg, 1997). The Rett patients also experienced a variety of breathing irregularities, which included apnoeas, breath holding, and periods of hyperventilation (B. Hagberg et al., 1983). It has been proposed that such breathing irregularities experienced by some Rett patients has been the cause of subsequent sudden infant death syndrome (Kerr et al., 1997).

MECP2 and the development of Rett syndrome

Various mutations have been linked with Rett syndrome but most variants possess overlapping symptoms. In 1985, a congenital variant of Rett syndrome was first described which resulted from a mutation within the *FOXG1* gene. Symptoms of such a mutation include impaired motor development, stereotypic hand movements, and decreased muscle tone (Ariani et al., 2008; Mencarelli et al., 2010). Even though some of these symptoms overlap with classic Rett syndrome, carriers of this congenital variant do not develop normally until 6-18 months.

Exclusion mapping studies involving families with a long history of Rett syndrome has identified that the locus of classic Rett syndrome is mapped to the X chromosome on chromosome 28 (Xq28) (Curtis et al., 1993). Further genetic analysis of the locus revealed mutations in the gene that encodes for methyl-CpG-binding protein 2 (*MECP2*) (Zoghbi et al., 1999). Approximately 70-90% of classic Rett syndrome cases present a loss of function mutation in the *MECP2* gene (Shahbazian and Zoghbi, 2001).

Function of MECP2

MECP2 was initially described as a transcriptional repressor that was attracted to methylated CpG sites of the genome. Methylated cytosine is usually positioned at the start of a gene; the area where transcription factors bind to regulate gene expression (Jones et al., 1998; Nan et al., 1996; 1998; Skene et al., 2010). During gene expression, chromatin necessarily unfolds the DNA to an “open-state” which is sustained by the acetylation of histones. MECP2 targets the CpG sites at the start of the gene via its methyl-binding domain and recruits a co-repressor complex

(Sin3A and HDAC1&2), which subsequently reverses the acetylation of histones and compresses the chromatin. This causes the DNA to fold back into its helical form thereby restricting the binding of the transcriptional machinery, and in effect silencing gene expression (Nan et al., 1998; Amir and Zoghbi, 2000). In contrast, studies on hypothalamic RNA from *MECP2* knockout mice have suggested that MECP2 can act as a transcriptional activator as some genes were down regulated in its absence (Chahrour et al., 2008). It was suggested that as MECP2 binds to the CpG site, and rather than recruiting a co-repressor complex, it instead recruits a co-activator complex (CREB-1) that releases histones and unfolds chromatin, such that DNA is unfolded and exposed; this gives the transcriptional machinery access to the promoter region thereby rendering the gene active (Skene et al., 2010).

Rett syndrome and catecholaminergic neurons

Studies performed on brains of Rett patients and *MECP2* knockouts mice display a decrease in catecholaminergic content (Zoghbi et al., 1985; Riederer et al., 1985). Male heterozygote *MECP2* knockout mice (MECP2$^{-/y}$) exhibit comparable levels of bioamines when compared to wild-type mice at birth. However, *MECP2*$^{-/y}$ mice exhibit a gradual reduction in noradrenaline content at P14 before further decreasing at P28 (Ide et al., 2005), thereby suggesting that the progression of the respiratory irregularities correlates with the degeneration of catecholaminergic neuromodulatory systems in the brain. Nevertheless, additional reductions in serotonin levels, which was identified from P28 onwards, may also contribute to the respiratory abnormalities exhibited thereafter (Ide et al., 2005). However, this may be as a consequence of reduced catecholaminergic content as numerous noradrenergic inputs to serotonergic neurons have been identified (Peyron et al., 1996), which have been shown to regulate central serotonin activity (Linnér et al., 2004).

Studies have further shown that deficits in catecholaminergic content in *MECP2*$^{-/y}$ mice may be a result of reductions in the expression of tyrosine hydroxylase (TH) and dopamine beta-hydroxylase (DBH) (X. Zhang et al., 2010);

both enzymes are required for catecholamine synthesis. TH acts as the first and rate-limiting enzyme during catecholamine biosynthesis (Karobath, 1971), hence any reduction in TH expression will subsequently have an effect on catecholaminergic content. With that, studies in *MECP2*$^{-/y}$ mice have used TH as a marker for catecholaminergic cells to observe the effects of *MECP2* loss on catecholamine content. These studies showed that within the central catecholaminergic neurons of the locus coereleus, ventral A1/C1 and dorsal A2/C2 neurons, all of which are chemosensitive, there was a marked reduction in the number of TH-positive neurons in *MECP2*$^{-/y}$ mice (Roux et al., 2010; Viemari et al., 2005; Biancardi et al., 2008; King et al., 2012; Roux et al., 2000) All together, this highlights the importance of central catecholaminergic cells for modulating ventilation and, thus, protecting against breathing irregularities.

Rett syndrome and respiratory irregularities

The respiratory phenotype manifested by Rett patients commonly includes an increased apnoeic index (apnoea frequency), severely unstable breathing pattern, breath holding, variable breath durations, and periods of hyperventilation (Weese-Mayer et al., 2006). Similar to findings made in humans, studies in mice have indicated that respiratory abnormalities are due to developmental defects in the brainstem (Julu et al., 2001). The central respiratory networks of *MECP2* knockout mice display fewer connections between neurons and an irregular rhythmic pattern that is often interrupted due to spontaneous and prolonged calcium increases (Spitzer, 2002; Mironov et al., 2009). Calcium signals are a vital factor in neuronal development and their frequency and duration can promote either elongation or retraction of neuronal process. For instance, introducing a hypoxic stimulus to inspiratory neurons of neonatal mice results in an increase in calcium transients, which subsequently leads to the retraction of neuronal processes (Mironov and Langohr, 2005). Rett patients exhibit apnoeas, and the frequency and duration of these apnoeic events increase in severity with the progression of the disease. Such an increase in the apnoeic index and duration causes the respiratory network to

become hypoxic, which may subsequently result in an increase in calcium transients and retraction of neuronal processes. Therefore, as the disease progresses, more and more neuronal connections are retracted and respiratory network becomes defective and unstable.

6.2.4.2 Similarities between the breathing irregularities in the *LKB1* and *AMPK* double knockouts and Rett syndrome

As observed with Rett syndrome and cases of CCHS, the *Lkb1* and *AMPK α1* and *α2* double knockouts similarly exhibit periods of hypoventilation with PO_2-dependent increases in the frequency of post-sigh and spontaneous apnoeas. As mentioned above, the breathing irregularities exhibited with CCHS is associated with failed developed of the catecholaminergic network, including the carotid body, petrosal ganglion and the central catecholaminergic neurons. Rett syndrome has been strongly associated with the progressive degeneration of central catecholaminergic neuromodulatory systems, including the ventrolateral A1/C1 and dorsomedial A2/C2 neurons in the brainstem. It is notable therefore that A1/C1 and A2/C2 catecholaminergic neurons have also been proposed as the primary central catecholaminergic neurons that send signals to the rCPGs during hypoxia, in a manner dependent on afferent input from the carotid body to protect against metabolic stress and maintain physiological PO_2 and PCO_2 at the whole-body level (D. W. Smith et al., 1995; Soulage et al., 2005; Berquin et al., 2000; King et al., 2012; Li et al., 2008). Thus, given that *Lkb1* and *AMPK* deletion has been targeted to all catecholaminergic neurons and that both knockout mice consequently exhibit breathing irregularities similar to those manifested with Rett syndrome and the degeneration of central catecholaminergic cells irrespective of the hypoxic sensitivity of the carotid body, suggests that the LKB1-AMPK signalling pathway may be crucial within similar neurons, such as the A1/C1 and A2/C2 neurons, to mediate an appropriate ventilatory response during hypoxia.

Furthermore, in *Mecp2*$^{-/y}$ knockout mice, the model for Rett syndrome, respiratory abnormalities significantly improved when treated with desipramine, which specifically targets noradrenaline reuptake and subsequently increases the amount of

noradrenaline available in the synaptic cleft. This thereby mimics the increase in neurotransmitter release from noradrenergic neurons within the NTS. Treatment with desipramine also increased the number of central catecholaminergic neurons, namely the ventrolateral A1/C1 and dorsomedial A2/C2 cell groups (Roux et al., 2007). This therefore supports my view that that the LKB1-AMPK signalling pathway may be crucial within central catecholaminergic cells, such as the A1/C1 and A2/C2 neurons, for activation during hypoxia and subsequent noradrenaline release, to ultimately modulate the ventilatory response.

Recent studies on laser micro-dissected A1, C1, A2, and C2 neurons have demonstrated that AMPK is indeed expressed in all 4 catecholaminergic regions with its activity increasing in response to metabolic stress, namely hypoglycemia (Shrestha et al., 2014). Accordingly, AMPK available in these catecholaminergic neurons may also be of primary importance to mediate an appropriate response to metabolic stress in the form of acute hypoxia, and ultimately an appropriate ventilatory response at the whole-body level. Further studies can be performed to examine such a role for AMPK in the A1/C1 and A2/C2 neurons during hypoxia and will be discussed further below (Section 6.2.3.2).

6.2.4.3 The effects of LKB1 and AMPK deletion on brainstem catecholaminergic neurons during hypoxia

A few techniques can be employed to compare the effects of *Lkb1* and *AMPK* deletion on central catecholaminergic cells during hypoxia. For instance, following exposure to hypoxia, differences in c-FOS expression in catecholaminergic cells can be examined in brainstem slices of control and knockout mice; catecholaminergic cells can be identified using fluorescently tagged antibodies against tyrosine-hydroxylase. Differences or a reduction in c-FOS levels in the catecholaminergic neurons in the brainstem of *Lkb1* and *AMPK α1* and *α2* double knockouts could thereby indicate the locations at which the LKB1-AMPK signalling pathway is required to mediate their appropriate activation during hypoxia. Thereafter, further studies using functional magnetic resonance imaging (fMRI) may also be used to compare the effects of *Lkb1*

and *AMPK* deletion within the identified catecholaminergic regions in the brain during hypoxia *in vivo*. This would provide us with baseline and recovery readings of activity before and after the hypoxic exposure. Hence, the degree of change can be quantified and compared in these regions between control and knockout mice in response to hypoxia.

In fact, I performed preliminary studies using fMRI (with further experiments performed by Professor A Mark Evans, Dr. Sophronia Lewis and analysis conducted by Miss Lara Juričić), and demonstrated that during hypoxia a lower signal change, indicative of reduced activation, was consistently observed in two well-defined dorsal and ventral regions of the brainstem in AMPK *α1* and *α2* double knockouts when compared to control mice (Appendix 6C). Whether the regions identified are comprised of catecholaminergic neurons is something that cannot be deduced from the fMRI studies alone. However, the caudal and ventral regions identified relative to Bregma is consistent with that of the catecholaminergic A2/C2 and A1/C1 neurons, respectively (Appendix 6C). These preliminary fMRI studies on the brainstem therefore suggest that the increases in drive to breathe during hypoxia are primarily determined by AMPK-dependent modulation of central neurons within the brainstem rather than by the carotid body, albeit possibly in an interdependent manner. However, more detailed studies will be required to determine:

1. Whether or not the central AMPK-dependent oxygen-sensors comprise the dorsal A2/C2 neurons of the area postrema and caudal NTS, and/or the ventral A1/C1 neurons; and
2. The mechanism by which continued input and integration of signals from the carotid bodies determines the capacity of these central catecholaminergic efferents to increase respiratory drive from the rCPG.
3. Whether similar effects are observed in the *Lkb1* knockouts, thereby indicating that the similar ventilatory abnormalities observed with the *AMPK α1* and *α2* double knockouts are a result of the LKB1-AMPK signalling pathway being required within the central dorsal and ventral regions of the brainstem.

6.2.5 Key method limitations

6.2.5.1 Barometric method for measuring tidal volume

Although there are key advantages to using unrestrained whole body plethysmography to study the effects of LKB1 and AMPK deletion on the ventilatory response to hypoxia (i.e. avoidance of restraint and anesthesia as mentioned in Chapter 2), this approach also carries limitations. This includes the error generated when measuring tidal volume based on pressure changes in the chamber. As stated in Chapter 2, the plethysmography software uses the formula of Fenn and Drorbaugh to derive tidal volume values, which takes into account the core temperature of the mouse, the chamber temperature, and the corresponding vapor pressures (Drorbaug and Fenn, 1955). According to this formula, the conditioning of inspired air is the sole cause of the increase in pressure observed in the chamber during inspiration while air is being warmed and humidified to core pulmonary values (and vice versa during expiration). Accordingly, one source of error when calculating tidal volume comes from values for alveolar temperature and humidity, which are not directly measured but are estimated and used in computing the calibration constant/algorithm used to calculate tidal volume. Therefore, the absolute values of tidal volume, and hence minute ventilation, may be biased and usually overestimated by errors induced by these estimated parameters. Hence, the significant attenuation of tidal volume observed in the *AMPK a1* and *a2* double knockouts may be even more severe than calculated. Nevertheless, the technique described above to calculate tidal volume has been validated with a systemic error of <7% (Bonora, 2004; Onodera, 1997; Ramanantsoa et al., 2007).

Perhaps the larger source of error with respect to using the barometric method to measure tidal volume comes from the basic assumption mentioned above that the pressure changes in the chamber is primarily due to the conditioning of inspired air. Yet, when the temperature and humidity of the air in the chamber is matched to physiological conditions, the pressure changes are only reduced by two-thirds. This suggests that other parameters also influence the pressure changes in the plethysmography chamber and further studies have demonstrated that breathing frequency and airway resistance are also involved (Enhorning et al., 1998). Although there is no doubt that the lack of LKB1

and AMPK attenuates the tidal volume during hypoxia, it is for the limitations described above that this data should be interpreted with caution.

6.2.5.2 Flow rate of hypoxic and/or hypercapnic gas

During the studies performed in this thesis, the flow rate of the hypoxic and/or hypercapnic gas applied into the chamber was set to 3L/min (as described in chapter 2). Such a high rate was selected to ensure that the gas filled the chamber rapidly so that an immediate and full ventilatory response to the gas can be observed. However, the bias flow for which the air was drawn out of the chamber was set to 1L/min. Clearly this would result in an increased pressure in the chamber that may have dampened the flow rate produced by the ventilating mouse. Hence, this may mean that the apnoeas observed are not as long in duration as observed, as shallow breaths post-apnoea may have not been picked up in the dampened signal. Nevertheless, given that all experimental mice were subjected to the same gas flow rate of 3L/min, and hence all signals were dampened to a similar extent, there is therefore no doubt that the relative increase between the control and knockout mice is significant with respect to the number and duration of apnoeas.

That being said, the ideal protocol would be to match the flow rate of the gas being introduced with the bias flow rate of the gas being removed in the chamber (in this case 1L/min) to avoid dampening the signal. Additionally, this would avoid any difficulties that may arise when exhaling against the increased pressure generated by having a flow rate of 3L/min.

6.2.5.3 Degree of hypoxaemia

Given that the *Lkb1*, *AMPK α1, and AMPK α1* and *α2* knockouts do not respond to the hypoxic challenge, it is possible that the amount of oxygen in the blood is significantly less than controls when stimulated by a hypoxic stimulus. Hence, the hypoxaemia developed in the knockouts is likely to be more severe than that observed in controls. Studies have demonstrated that severe hypoxia and hypoxaemia can result in significant depression of breathing as central inhibition of respiratory neurons during

hypoxia masks the stimulatory input from peripheral chemoreceptors (Sudo and Fukuda, 1997). While there is no doubt about the attenuated response to hypoxia in the knockout mice per se, the severity of the disordered breathing could be, at least partly, attributable to central hypoxic depression, which compounds and exaggerates the phenotype. Hence, it would be beneficial if future studies were aimed to examine whether there is any differences in the arterial oxygen saturation levels (SpO_2) between control and knockout mice. This can be achieved with the use of a tail cuff pulse oximeter. However, it is important to note that unlike the studies performed in this thesis, this would require the animal to be restrained during the hypoxic response.

6.2.5.4 Future studies

To further elucidate the possible LKB1-AMPK dependent roles of the dorsal and/or ventral regions of the brainstem during hypoxia, viral injections can be employed to target/infect these regions and observe their role/requirement in the ventilatory response to hypoxia. This can be accomplished by injecting a fluorescently tagged recombinant Cre-recombinase carrying virus vector into the dorsal and/or ventral regions of the brainstem of *Lkb1* and *AMPK α1* and *α2* floxed mice. Accordingly, *Lkb1* and *AMPK* deletion will only be targeted to the injected region and the mice can be examined for ventilatory abnormalities during hypoxia. Immunofluorescent studies on brain slices can then be performed to identify the precise location of injection and hence whether catecholaminergic neurons have been infected. However, an important thing to consider is that the injections will not selectively target catecholaminergic oxygen-sensing cells and that other non-catecholaminergic infected cells may contribute to the overall phenotype. Hence, a fittingly additional experiment is to inject a recombinant Cre inducible AAV1/2 vector carrying halorhodopsin in the dorsal and/or ventral regions in TH-Cre mice. Accordingly, halorhodopsin will only be present in tyrosine hydroxylase expressing cells, and hence catecholaminergic neurons, in the ventral and/or dorsal regions, i.e. the A1/C1 and A2/C2, respectively. Optogenetics can then be employed to silence these neurons during hypoxia to determine whether they are fundamentally required to drive the ventilatory response to hypoxia.

6.3 Conclusion

In conclusion, the LKB1-AMPK signalling pathway is required in catecholaminergic cells to appropriately modulate ventilation in response to hypoxia and thereby protect against hypoventilation and apnoeas. This requirement appears to lie within the central catecholaminergic neurons within the brainstem, rather than in the carotid body type 1 cells, with the dorsomedial A2/C2 and/or ventrolateral A1/C1 neurons proposed as the primary oxygen-sensing candidates (Figure 6.1). Thus, the LKB1-AMPK signalling pathway is not only important to maintain energy homeostasis at a cellular level, but has also been adapted to regulate oxygen, and thus energy supply, at the whole-body level. AMPK activity may therefore compromise the ability to appropriately modulate respiration during hypoxic stress that occurs during sleep or at high-altitudes and may provide a therapeutic target. Additionally, the findings of this thesis may also offer an explanation for the high comorbidity observed with metabolic syndrome-related disorders and sleep-disordered breathing, with the former disorder already associated with AMPK (Ruderman et al., 2013). This perhaps appears more noteworthy when noting that the AMPK activator, metformin, which is used for the management of type 2 diabetes within the metabolic syndrome, was previously and unexpectedly found to be an efficient treatment for sleep apnoea (S. Wiwanitkit and V. Wiwanitkit, 2012; 2011).

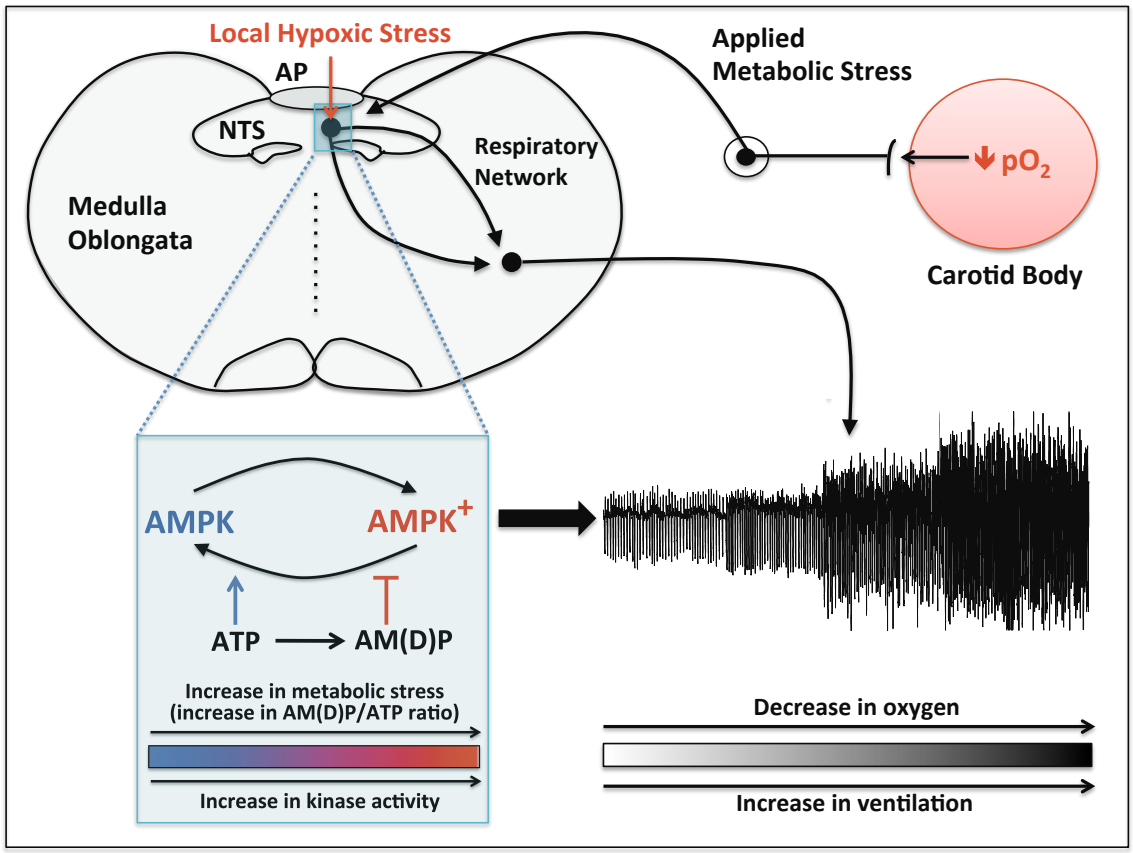

Figure 6.1: Proposed role for the LKB1-AMPK signalling pathway in central catecholaminergic neurons in the brainstem and not carotid body. Lkb1/AMPK dependent modulation of the central catecholaminergic neurons, possibly the dorsomedial A2/C2 and ventrolateral A1/C1 neurons of the brainstem, during hypoxia increases ventilatory drive via their modulatory input to the respiratory central pattern generators.

Appendix 6A

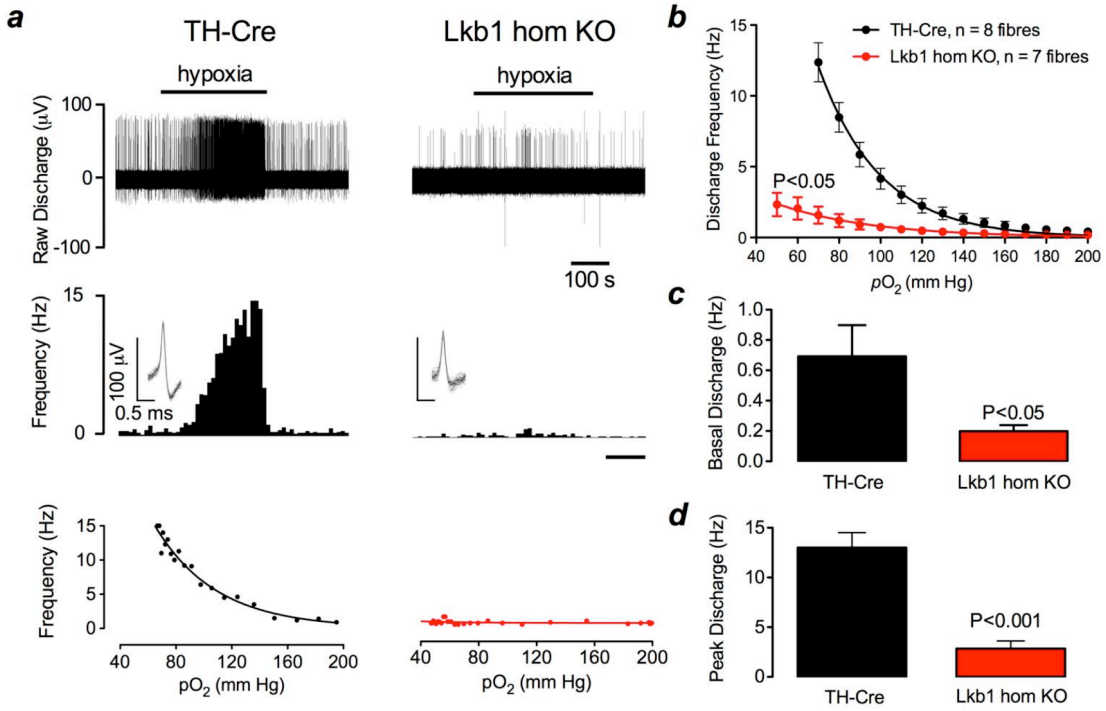

Supplementary figure 6A: *Lkb1* deletion markedly inhibits the response of the carotid body to hypoxia. *Upper panel* shows extracellular recordings of single fibre chemoafferent discharge vs PO_2 for control (TH-Cre) and *Lkb1* homozygous knockout (*Lkb1* hom KO). *Middle panels*, frequency-time histograms (inset, single fibre discriminations). *Lower panels*, frequency-PO_2 response curves. **(b)** Mean discharge frequency vs PO_2 response curves from ≥5 mice (7-8 carotid body fibres); 2 factor ANOVA with Bonferroni Dunn post hoc analysis. **(c)** Mean basal single fibre discharge frequency and (**d**) Mean peak single fibre discharge frequency during hypoxia; Statistical significance by single factor ANOVA with Bonferroni Dunn post hoc analysis. **Experiments performed by collaborators at the University of Birmingham under subcontract (intellectual property rests with A Mark Evans and the University of Edinburgh)

Appendix 6B

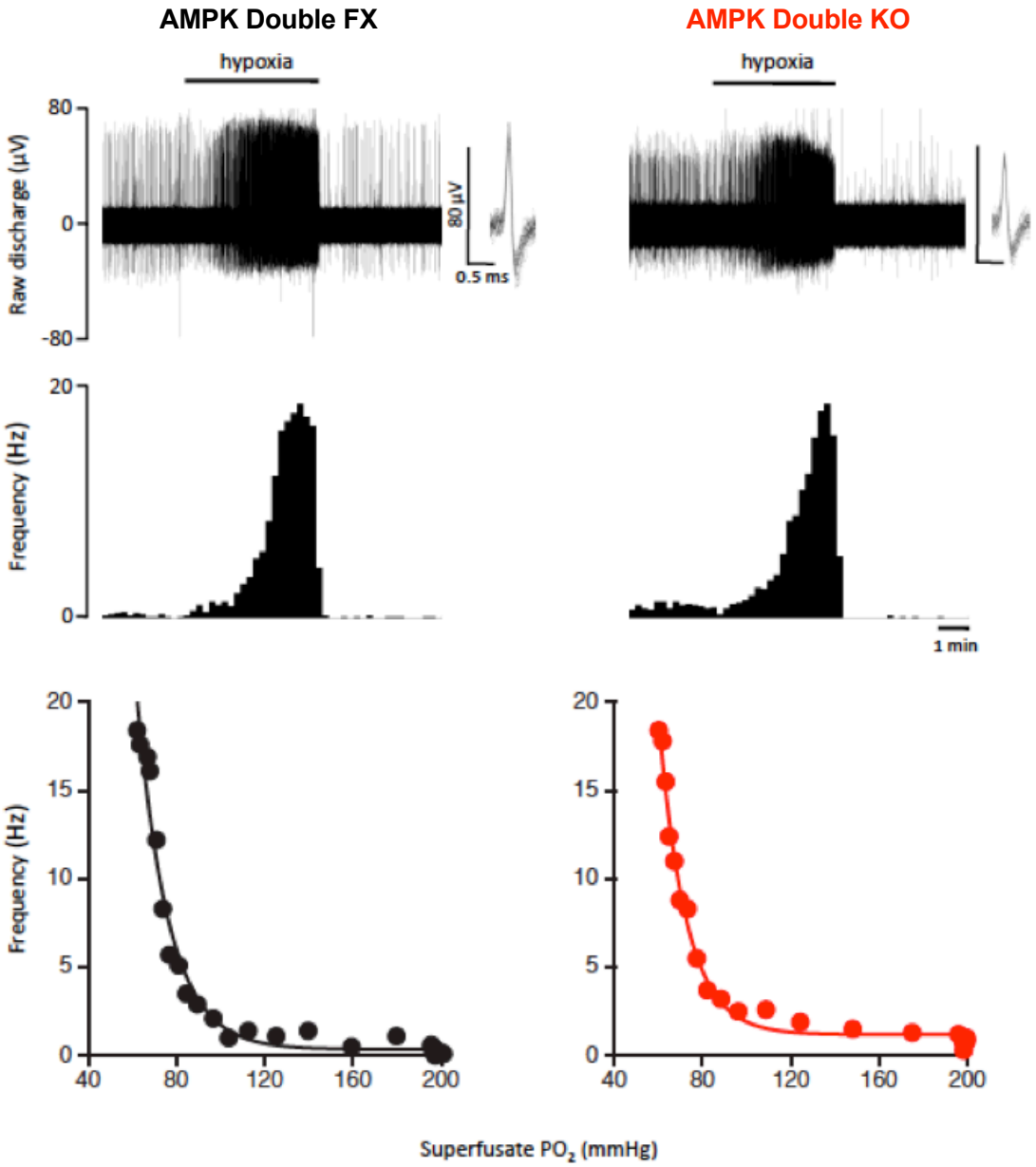

Supplementary figure 6B: *AMPK* deletion does not inhibit carotid body activation by hypoxia. *Upper panels* show extracellular recordings of single fibre chemoafferent discharge vs PO_2 for *AMPK-α1 and -α2 double floxed (AMPK Double FX*) and *AMPK-α1* and -α2 double knockouts (*AMPK* double KO); inset, single fibre discriminations. *Middle*,frequency-time histograms. *Lower*, frequency-PO_2 response curves **Experiments performed by collaborators at the University of Birmingham under subcontract (intellectual property rests with A Mark Evans and the University of Edinburgh)

Appendix 6C

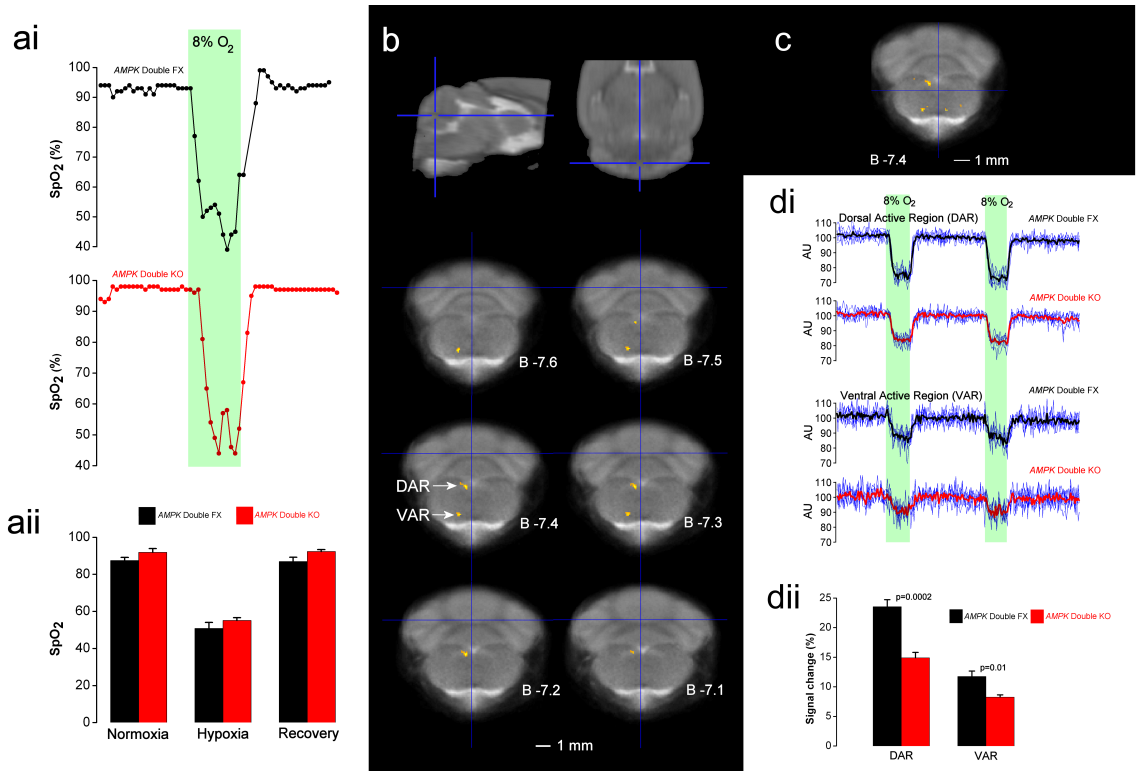

Supplementary figure 6C: Functional MRI demonstrates that *AMPK* deletion inhibits activation by hypoxia of dorsal and ventral regions of the brainstem. (ai) oxygen saturation versus time in *AMPK*-α1 and -α2 double floxed (*AMPK* Double FX) and *AMPK*- α 1 and - α 2 double knockouts (*AMPK* Double KO) during 2min exposure to hypoxia (8% O_2). **(aii)** mean ± SEM. oxygen saturation during normoxia, hypoxia and recovery. **(b)** Dorsal (DAR) and ventral (VAR) active regions of brainstem that exhibited significantly lower signal change ($p<0.005$) during hypoxia. (**c**) Removing cluster threshold reveals bilateral, right-sided symmetry for VAR only. Numbers denote position (mm) with respect to Bregma, scale bar 1 mm. **(di)** Signal time courses for detected regions in blue for each individual mouse, overlaid on mean signal for *AMPK* Double FX (black line) and *AMPK* Double KO (red line). **(dii)** mean±s.e.m. percentage signal changes for DAR and VAR during hypoxia. **Preliminary studies were performed by myself. Further experiments were conducted with Professor A Mark Evans and Dr. Sophronia Lewis. Analysis performed by Ms. Lara Juricic. **Intellectual property rests with A Mark Evans and the University of Edinburgh.

Bibliography

Abbott, S. B. G. et al. (2009) Photostimulation of retrotrapezoid nucleus phox2b-expressing neurons in vivo produces long-lasting activation of breathing in rats. *The Journal of neuroscience : the official journal of the Society for Neuroscience*. [Online] 29 (18), 5806–5819.

Abbott, S. B. G. et al. (2011) Phox2b-expressing neurons of the parafacial region regulate breathing rate, inspiration, and expiration in conscious rats. *The Journal of neuroscience : the official journal of the Society for Neuroscience*. [Online] 31 (45), 16410–16422.

Adachi, T. et al. (2004) Hypoxemia and blunted hypoxic ventilatory responses in mice lacking heme oxygenase-2. *Biochemical and biophysical research communications*. [Online] 320 (2), 514–522.

Alheid, G. F. & McCrimmon, D. R. (2008) The chemical neuroanatomy of breathing. *Respiratory physiology & neurobiology*. [Online] 164 (1-2), 3–11.

Alheid, G. F. et al. (2011) Caudal nuclei of the rat nucleus of the solitary tract differentially innervate respiratory compartments within the ventrolateral medulla. *Neuroscience*. [Online] 190207–227. [online]. Available from: http://www.ncbi.nlm.nih.gov/pmc/articles/PMC3169098/pdf/nihms303775.pdf.

Amiel, J. et al. (2009) PHOX2B in respiratory control: lessons from congenital central hypoventilation syndrome and its mouse models. *Respiratory physiology & neurobiology*. [Online] 168 (1-2), 125–132.

Amir, R. E. & Zoghbi, H. Y. (2000) Rett syndrome: methyl-CpG-binding protein 2 mutations and phenotype-genotype correlations. *American journal of medical genetics*. 97 (2), 147–152.

Anon (1930) *Sinus carotidien et refléxes respiratoires. II. Influences respiratoires réflexes de l'acidose, de l'alcalose, de l'anhydride carbonique, de l'ion hydrogéne et de l'anoxémie: sinus carotidiens et échanges respiratoires dans les poumons et au dela poumons*. 39400–408.

Ariani, F. et al. (2008) FOXG1 is responsible for the congenital variant of Rett syndrome. *American journal of human genetics*. [Online] 83 (1), 89–93.

Auciello, F. R. et al. (2014) Oxidative stress activates AMPK in cultured cells primarily by increasing cellular AMP and/or ADP. *FEBS letters*. [Online]

Baena-González, E. et al. (2007) A central integrator of transcription networks in plant stress and energy signalling. *Nature*. [Online] 448 (7156), 938–942.

Beghini, A. et al. (2003) The neural progenitor-restricted isoform of the MARK4 gene in 19q13.2 is upregulated in human gliomas and overexpressed in a subset of glioblastoma cell lines. *Oncogene*. [Online] 22 (17), 2581–2591.

Berquin, P. et al. (2000) Brainstem and hypothalamic areas involved in respiratory chemoreflexes: a Fos study in adult rats. *Brain research*. [Online] 857 (1-2), 30–40.

Bert, P. (1868) Changements de Pression de l'air dam la poitrine pendant les deux temps de l'acte Respiratoire. *C R Sot Biol.* 22–23.

Bessone, S. et al. (1999) EMK protein kinase-null mice: dwarfism and hypofertility associated with alterations in the somatotrope and prolactin pathways. *Developmental biology*. [Online] 214 (1), 87–101.

Bettencourt-Dias, M. et al. (2004) Genome-wide survey of protein kinases required for cell cycle progression. *Nature*. [Online] 432 (7020), 980–987.

Biancardi, V. et al. (2008) Locus coeruleus noradrenergic neurons and CO2 drive to breathing. *Pflügers Archiv : European journal of physiology*. [Online] 455 (6), 1119–1128.

Bianchi, A. L. et al. (1995) Central control of breathing in mammals: neuronal circuitry, membrane properties, and neurotransmitters. *Physiological reviews*. 75 (1), 1–45.

Biscoe, T. J. & Duchen, M. R. (1990) Responses of type I cells dissociated from the rabbit carotid body to hypoxia. *The Journal of physiology*. 42839–59.

Biscoe, T. J. et al. (1989) Measurements of intracellular Ca2+ in dissociated type I cells of the rabbit carotid body. *The Journal of physiology*. 416421–434.

Bissonnette, J. M. (2000) Mechanisms regulating hypoxic respiratory depression during fetal and postnatal life. *American journal of physiology. Regulatory, integrative and comparative physiology*. 278 (6), R1391–R1400.

Bissonnette, J. M. & Knopp, S. J. (2001) Developmental changes in the hypoxic ventilatory response in C57BL/6 mice. *Respiration physiology*. 128 (2), 179–186.

Bright, N. J. et al. (2008) Investigating the Regulation of Brain-specific Kinases 1 and 2 by Phosphorylation. *Journal of Biological Chemistry*.

Brown, K. A. et al. (2008) La pléthysmographie inductive respiratoire automatisée pour évaluer la respiration chez les nourrissons présentant un risque d'apnée postopératoire. *Canadian Journal of Anesthesia/Journal canadien d'anesthésie*. [Online] 55 (11), 739–747.

Buckler, K. J. & Turner, P. J. (2013) Oxygen sensitivity of mitochondrial function in rat

arterial chemoreceptor cells. *The Journal of physiology*. [Online] 591 (Pt 14), 3549–3563.

Buttigieg, J. et al. (2008) Functional mitochondria are required for O2 but not CO2 sensing in immortalized adrenomedullary chromaffin cells. *American journal of physiology. Cell physiology*. [Online] 294 (4), C945–C956.

Carlson, M. (1999) Glucose repression in yeast. *Current Opinion in Microbiology*. [Online] 2 (2), 202–207. [online]. Available from: http://web.sls.hw.ac.uk/teaching/Derek_J/mol2_1/further_reading/Sugar%20metabolism/files/glucose_repression.pdf.

Carlson, M. et al. (1981) Mutants of yeast defective in sucrose utilization. *Genetics*. 98 (1), 25–40.

Chahrour, M. et al. (2008) MeCP2, a key contributor to neurological disease, activates and represses transcription. *Science (New York, N.Y.)*. [Online] 320 (5880), 1224–1229.

Chandel, N. S. (2010) Mitochondrial complex III: an essential component of universal oxygen sensing machinery? *Respiratory physiology & neurobiology*. [Online] 174 (3), 175–181.

Chapin, J. L. (1954) Ventilatory response of the unrestrained and unanesthetized hamster to CO2. *The American journal of physiology*. 179 (1), 146–148.

Chen, R. Z. et al. (2001) Deficiency of methyl-CpG binding protein-2 in CNS neurons results in a Rett-like phenotype in mice. *Nature genetics*. [Online] 27 (3), 327–331.

Cherniack, N. S. & Longobardo, G. S. (2006) Mathematical models of periodic breathing and their usefulness in understanding cardiovascular and respiratory disorders. *Experimental physiology*. [Online] 91 (2), 295–305.

Cohen, M. I. (1971) Switching of the respiratory phases and evoked phrenic responses produced by rostral pontine electrical stimulation. *The Journal of physiology*. 217 (1), 133–158.

Crute, B. E. et al. (1998) Functional domains of the alpha1 catalytic subunit of the AMP-activated protein kinase. *The Journal of biological chemistry*. 273 (52), 35347–35354.

Curtis, A. R. et al. (1993) X chromosome linkage studies in familial Rett syndrome. *Human genetics*. 90 (5), 551–555.

Dahan, A. et al. (2008) Plasticity in the brain: influence of bilateral carotid body resection (bCBR) on central CO2 sensitivity. *Advances in experimental medicine*

and biology. [Online] 605312–316.

Dauger, S. et al. (2003) Phox2b controls the development of peripheral chemoreceptors and afferent visceral pathways. *Development*. [Online] 130 (26), 6635–6642.

Davies, S. P. et al. (1995) 5′-AMP inhibits dephosphorylation, as well as promoting phosphorylation, of the AMP-activated protein kinase. Studies using bacterially expressed human protein phosphatase-2Cα and native bovine protein phosphatase-2Ac. *FEBS letters*.

Day, T. A. & Wilson, R. J. A. (2009) A negative interaction between brainstem and peripheral respiratory chemoreceptors modulates peripheral chemoreflex magnitude. *The Journal of physiology*. [Online] 587 (Pt 4), 883–896.

Day, T. A. & Wilson, R. J. A. (2008) A negative interaction between central and peripheral respiratory chemoreceptors may underlie sleep-induced respiratory instability: a novel hypothesis. *Advances in experimental medicine and biology*. [Online] 605447–451.

Dempsey, J. A. (2005) Crossing the apnoeic threshold: causes and consequences. Experimental physiology 90 (1) 13–24.

Derenne, J. P. et al. (1995) History of diaphragm physiology: the achievements of Galen. *European Respiratory ...*.

Doi, A. & Ramirez, J.-M. (2010) State-dependent interactions between excitatory neuromodulators in the neuronal control of breathing. *The Journal of neuroscience : the official journal of the Society for Neuroscience*. [Online] 30 (24), 8251–8262.

Donnelly, D. F. (2005) Development of carotid body/petrosal ganglion response to hypoxia. *Respiratory physiology & neurobiology*.

Drorbaug, J. E. & Fenn, W. O. (1955) A BAROMETRIC METHOD FOR MEASURING VENTILATION IN NEWBORN INFANTS. *Pediatrics*.

Dubreuil, V. et al. (2008) A human mutation in Phox2b causes lack of CO2 chemosensitivity, fatal central apnea, and specific loss of parafacial neurons. *Proceedings of the National Academy of Sciences*. [Online] 105 (3), 1067–1072.

Dubreuil, V. et al. (2009) Breathing with Phox2b. *Philosophical transactions of the Royal Society of London. Series B, Biological sciences*. [Online] 364 (1529), 2477–2483.

Duchen, M. R. & Biscoe, T. J. (1992a) Mitochondrial function in type I cells isolated from rabbit arterial chemoreceptors. *The Journal of physiology*.

Duchen, M. R. & Biscoe, T. J. (1992b) Relative mitochondrial membrane potential and [Ca2+]i in type I cells isolated from the rabbit carotid body. *The Journal of physiology*.

Dutschmann, M. & Herbert, H. (2006) The Kölliker-Fuse nucleus gates the postinspiratory phase of the respiratory cycle to control inspiratory off-switch and upper airway resistance in rat - Dutschmann - 2006 - European Journal of Neuroscience - Wiley Online Library. *European Journal of Neuroscience*.

Eckert, D. J. et al. (2007) Central Sleep ApneaPathophysiology and Treatment. *CHEST Journal*. [Online] 131 (2), 595–607.

Eden, G. J. & Hanson, M. A. (1987) Maturation of the respiratory response to acute hypoxia in the newborn rat. *The Journal of physiology*. 3921–9.

Emerling, B. M. et al. (2009) Hypoxic activation of AMPK is dependent on mitochondrial ROS but independent of an increase in AMP/ATP ratio. *Free radical biology & medicine*. [Online] 46 (10), 1386–1391.

Enhorning, G. et al. (1998) Whole-body plethysmography, does it measure tidal volume of small animals? *Canadian journal of physiology and pharmacology*. 76 (10-11), 945–951.

Erecinska, M. & Wilson, D. F. (1981) *Erecinska and Wilson (1981) Inhibitors of mitochondrial functions*.

Erickson, J. T. & Millhorn, D. E. (1994) Hypoxia and electrical stimulation of the carotid sinus nerve induce fos-like immunoreactivity within catecholaminergic and serotoninergic neurons of the rat brainstem. *The Journal of Comparative Neurology*. [Online] 348 (2), 161–182.

Euler, von, C. (1983) On the central pattern generator for the basic breathing rhythmicity. *Journal of applied physiology: respiratory, environmental and exercise physiology*. 55 (6), 1647–1659.

Evans, A. M. et al. (2006) AMP-activated protein kinase couples mitochondrial inhibition by hypoxia to cell-specific Ca2+ signalling mechanisms in oxygen-sensing cells. *Novartis Foundation symposium*. 272234–52–discussion252–8–274–9.

Evans, A. M. et al. (2011) Hypoxic pulmonary vasoconstriction: mechanisms of oxygen-sensing. *Current opinion in anaesthesiology*. [Online] 24 (1), 13–20. [online]. Available from: http://www.ncbi.nlm.nih.gov/pmc/articles/PMC3154643/pdf/ukmss-35828.pdf.

Feil, R. et al. (1997) Regulation of Cre recombinase activity by mutated estrogen

receptor ligand-binding domains. *Biochemical and biophysical research communications*. [Online] 237 (3), 752–757.

Feldman, J. L. & Del Negro, C. A. (2006) Looking for inspiration: new perspectives on respiratory rhythm. *Nature reviews. Neuroscience*. [Online] 7 (3), 232–242.

Feldman, J. L. & Smith, J. C. (1989) Cellular mechanisms underlying modulation of breathing pattern in mammals. *Annals of the New York Academy of Sciences*. 563114–130.

Galen et al. (1984) *Galen on respiration and the arteries*.

Goridis, C. et al. (2010) Phox2b, congenital central hypoventilation syndrome and the control of respiration. *Seminars in Cell & Developmental Biology*. [Online] 21 (8), 814–822.

Gourine, A. V. (2005) On the peripheral and central chemoreception and control of breathing: an emerging role of ATP. *The Journal of physiology*. [Online] 568 (Pt 3), 715–724.

Grainge, C. (2004) Breath of life: the evolution of oxygen therapy. *Journal of the Royal Society of Medicine*. [Online] 97 (10), 489–493.

Gray, P. A. et al. (1999) Modulation of respiratory frequency by peptidergic input to rhythmogenic neurons in the preBötzinger complex. *Science (New York, N.Y.)*. 286 (5444), 1566–1568.

Gray, P. A. et al. (2001) Normal breathing requires preBötzinger complex neurokinin-1 receptor-expressing neurons. *Nature neuroscience*. [Online] 4 (9), 927–930.

Gu, H. et al. (1994) Deletion of a DNA polymerase beta gene segment in T cells using cell type-specific gene targeting. *Science (New York, N.Y.)*. 265 (5168), 103–106. [online]. Available from: http://www.bio.davidson.edu/molecular/restricted/01TTarget/1994_cre.pdf.

Guyenet, P. G. (2005) Regulation of Ventral Surface Chemoreceptors by the Central Respiratory Pattern Generator. *The Journal of neuroscience : the official journal of the Society for Neuroscience*. [Online] 25 (39), 8938–8947.

Guyenet, P. G. & Mulkey, D. K. (2010) Retrotrapezoid nucleus and parafacial respiratory group. *Respiratory physiology & neurobiology*. [Online] 173 (3), 244–255.

Guyenet, P. G. et al. (2013) C1 neurons: the body's EMTs. *American journal of physiology. Regulatory, integrative and comparative physiology*. [Online] 305 (3), R187–R204.

Guyenet, P. G. et al. (2010) Central CO2 chemoreception and integrated neural mechanisms of cardiovascular and respiratory control. *Journal of Applied …*.

Guyenet, P. G. et al. (1993) Central respiratory control of A5 and A6 pontine noradrenergic neurons. *The American journal of physiology*. 264 (6 Pt 2), R1035–R1044.

Hagberg, B. & Hagberg, G. (1997) Rett syndrome: epidemiology and geographical variability. *European child & adolescent psychiatry*. 6 Suppl 15–7.

Hagberg, B. et al. (1983) A progressive syndrome of autism, dementia, ataxia, and loss of purposeful hand use in girls: Rett's syndrome: report of 35 cases. *Annals of Neurology*. [Online] 14 (4), 471–479.

Hall, B. et al. (2009) Overview: generation of gene knockout mice. *Current protocols in cell biology / editorial board, Juan S. Bonifacino ... [et al.]*. [Online] Chapter 19Unit19.1219.12.1–Unit19.1219.12.17. [online]. Available from: http://www.ncbi.nlm.nih.gov/pmc/articles/PMC2782548/.

Hardie, D. G. (2007) AMP-activated/SNF1 protein kinases: conserved guardians of cellular energy. *Nature Reviews Molecular Cell Biology*. [Online] 8 (10), 774–785.

Hardie, D. G. & Ashford, M. L. J. (2014) AMPK: regulating energy balance at the cellular and whole body levels. *Physiology (Bethesda, Md.)*. [Online] 29 (2), 99–107.

Hawley, S. A. et al. (2005) Calmodulin-dependent protein kinase kinase-β is an alternative upstream kinase for AMP-activated protein kinase. *Cell metabolism*. [Online] 2 (1), 9–19.

Hawley, S. A. et al. (1996) Characterization of the AMP-activated protein kinase kinase from rat liver and identification of threonine 172 as the major site at which it phosphorylates AMP-activated protein kinase. *The Journal of biological chemistry*. 271 (44), 27879–27887.

Hawley, S. A. et al. (2003) Complexes between the LKB1 tumor suppressor, STRAD alpha/beta and MO25 alpha/beta are upstream kinases in the AMP-activated protein kinase cascade. *Journal of biology*. [Online] 2 (4), 28.

Hawley, S. A. et al. (2010) Use of cells expressing gamma subunit variants to identify diverse mechanisms of AMPK activation. *Cell metabolism*. [Online] 11 (6), 554–565.

Hedbacker, K. & Carlson, M. (2008) SNF1/AMPK pathways in yeast. *Frontiers in bioscience : a journal and virtual library*. 132408–2420. [online]. Available from: http://www.ncbi.nlm.nih.gov/pmc/articles/PMC2685184/pdf/nihms89520.pdf.

Heymans, C. et al. (1931) Heymans: Sur la regulation reflexe de la circulation... - Google Scholar. *Arch Int Pharmacodyn Ther*.

Hilaire, G. et al. (1989) Possible modulation of the medullary respiratory rhythm generator by the noradrenergic A5 area: an in vitro study in the newborn rat. *Brain research*. 485 (2), 325–332.

Hooke, R. (1667) *An Account of an Experiment Made by M. Hook, of Preserving Animals Alive by Blowing Through Their Lungs with Bellows*.

Horike, N. et al. (2003) Adipose-specific expression, phosphorylation of Ser794 in insulin receptor substrate-1, and activation in diabetic animals of salt-inducible kinase-2. *The Journal of biological chemistry*. [Online] 278 (20), 18440–18447.

Hurov, J. B. et al. (2007) Loss of the Par-1b/MARK2 polarity kinase leads to increased metabolic rate, decreased adiposity, and insulin hypersensitivity in vivo. *Proceedings of the National Academy of Sciences of the United States of America*. [Online] 104 (13), 5680–5685.

Hutchison, M. et al. (1998) Isolation of TAO1, a protein kinase that activates MEKs in stress-activated protein kinase cascades. *The Journal of biological chemistry*. 273 (44), 28625–28632.

Ide, S. et al. (2005) Defect in normal developmental increase of the brain biogenic amine concentrations in the mecp2-null mouse. *Neuroscience letters*. [Online] 386 (1), 14–17.

Ikematsu, N. et al. (2011) Phosphorylation of the voltage-gated potassium channel Kv2.1 by AMP-activated protein kinase regulates membrane excitability. *Proceedings of the National Academy of Sciences of the United States of America*. [Online] 108 (44), 18132–18137.

Iredale, J. P. (1999) Demystified ... gene knockouts. *Molecular pathology : MP*. 52 (3), 111–116.

Iseli, T. J. et al. (2005) AMP-activated protein kinase beta subunit tethers alpha and gamma subunits via its C-terminal sequence (186-270). *The Journal of biological chemistry*. [Online] 280 (14), 13395–13400.

Iyer, N. V. et al. (1998) Cellular and developmental control of O2 homeostasis by hypoxia-inducible factor 1 alpha. *Genes & development*. 12 (2), 149–162.

Janczewski, W. A. & Feldman, J. L. (2006) Distinct rhythm generators for inspiration and expiration in the juvenile rat. *The Journal of physiology*. [Online] 570 (Pt 2), 407–420.

Jeon, S. et al. (2005) Microtubule affinity-regulating kinase 1 (MARK1) is activated by electroconvulsive shock in the rat hippocampus. *Journal of neurochemistry*. [Online] 95 (6), 1608–1618.

Jiang, C. & Haddad, G. G. (1994) A direct mechanism for sensing low oxygen levels by central neurons. *Proceedings of the National Academy of Sciences of the United States of America*. 91 (15), 7198–7201.

Jones, P. L. et al. (1998) Methylated DNA and MeCP2 recruit histone deacetylase to repress transcription. *Nature genetics*. [Online] 19 (2), 187–191.

Julu, P. O. et al. (2001) Characterisation of breathing and associated central autonomic dysfunction in the Rett disorder. *Archives of disease in childhood*. 85 (1), 29–37.

Jørgensen, S. B. et al. (2004) Knockout of the 2 but Not 1 5'-AMP-activated Protein Kinase Isoform Abolishes 5-Aminoimidazole-4-carboxamide-1- -4-ribofuranosidebut Not Contraction-induced Glucose Uptake in Skeletal Muscle. *Journal of Biological Chemistry*. [Online] 279 (2), 1070–1079.

Karamanou, M. & Androutsos, G. (2013) *Antoine-Laurent de Lavoisier (1743-1794) and the birth of respiratory physiology.* Vol. 68. [Online].

Karobath, M. (1971) Catecholamines and the Hydroxylation of Tyrosine in Synaptosomes Isolated from Rat Brain. *Proceedings of the National Academy of ….*

Kato, T. et al. (2001) Isolation of a Novel Human Gene, MARKLI, Homologous to MARK3 and Its Involvement in Hepatocellular Carcinogenesis. *Neoplasia*. [Online] 3 (1), 4–9.

Kerr, A. M. et al. (1997) Rett syndrome: analysis of deaths in the British survey. *European child & adolescent psychiatry*. 6 Suppl 171–74.

King, T. L. et al. (2012) Hypoxia activates nucleus tractus solitarii neurons projecting to the paraventricular nucleus of the hypothalamus. *American journal of physiology. Regulatory, integrative and comparative physiology*. [Online] 302 (10), R1219–R1232.

Lahiri, S. et al. (1981) Comparison of aortic and carotid chemoreceptor responses to hypercapnia and hypoxia. *Journal of applied physiology: respiratory, environmental and exercise physiology*. 51 (1), 55–61.

Lahiri, S. et al. (1983) Dependence of high altitude sleep apnea on ventilatory sensitivity to hypoxia. *Respiration physiology*. 52 (3), 281–301.

Lakso, M. et al. (1992) Targeted oncogene activation by site-specific recombination in transgenic mice. *Proceedings of the National Academy of Sciences of the United*

States of America. 89 (14), 6232–6236.

Lantier, L. et al. (2014) AMPK controls exercise endurance, mitochondrial oxidative capacity, and skeletal muscle integrity. *FASEB journal : official publication of the Federation of American Societies for Experimental Biology*. [Online] 28 (7), 3211–3224.

Lefebvre, D. L. & Rosen, C. F. (2005) Regulation of SNARK activity in response to cellular stresses. *Biochimica et biophysica acta*. [Online] 1724 (1-2), 71–85.

Li, A. et al. (2008) 'Brainstem Catecholaminergic Neurons Modulate both Respiratory and Cardiovascular Function', in *Integration in Respiratory Control*. Advances in Experimental Medicine and Biology. [Online]. New York, NY: Springer New York. pp. 371–376.

Lindeberg, J. et al. (2004) Transgenic expression of Cre recombinase from the tyrosine hydroxylase locus. *Genesis (New York, N.Y. : 2000)*. [Online] 40 (2), 67–73.

Linnér, L. et al. (2004) Selective noradrenaline reuptake inhibition enhances serotonergic neuronal activity and transmitter release in the rat forebrain. *Journal of neural transmission (Vienna, Austria : 1996)*. [Online] 111 (2), 127–139.

Liu, H. et al. (1999) O2 deprivation inhibits Ca2+-activated K+ channels via cytosolic factors in mice neocortical neurons. *The Journal of clinical investigation*. [Online] 104 (5), 577–588.

Lizcano, J. M. et al. (2004) LKB1 is a master kinase that activates 13 kinases of the AMPK subfamily, including MARK/PAR-1. *The EMBO journal*. [Online] 23 (4), 833–843.

Maina, J. N. (2002) Structure, function and evolution of the gas exchangers: comparative perspectives. *Journal of anatomy*. 201 (4), 281–304.

Malpighius, M. (1686) *Opera omnia*.

Manning, G. et al. (2002) The protein kinase complement of the human genome. *Science (New York, N.Y.)*. [Online] 298 (5600), 1912–1934.

McBride, A. et al. (2009) The glycogen-binding domain on the AMPK beta subunit allows the kinase to act as a glycogen sensor. *Cell metabolism*. [Online] 9 (1), 23–34.

McCrimmon, D. R. et al. (2004) Converging functional and anatomical evidence for novel brainstem respiratory compartments in the rat. *Advances in experimental medicine and biology*. 551101–105.

McKay, L. C. et al. (2005) Sleep-disordered breathing after targeted ablation of preBötzinger complex neurons. *Nature neuroscience*. [Online] 8 (9), 1142–1144.

Mellins, R. B. et al. (1970) Failure of automatic control of ventilation (Ondine's curse). Report of an infant born with this syndrome and review of the literature. *Medicine*. 49 (6), 487–504.

Mencarelli, M. A. et al. (2010) Novel FOXG1 mutations associated with the congenital variant of Rett syndrome. *Journal of medical genetics*. [Online] 47 (1), 49–53.

Mifflin, S. W. (1992) Arterial chemoreceptor input to nucleus tractus solitarius. *The American journal of physiology*. 263 (2 Pt 2), R368–R375.

Mills, E. & Jöbsis, F. F. (1972) Mitochondrial respiratory chain of carotid body and chemoreceptor response to changes in oxygen tension. *Journal of neurophysiology*. 35 (4), 405–428.

Mironov, S. L. & Langohr, K. (2005) Mechanisms of Na+ and Ca2+ influx into respiratory neurons during hypoxia. *Neuropharmacology*. [Online] 48 (7), 1056–1065.

Mironov, S. L. et al. (2009) Remodelling of the respiratory network in a mouse model of Rett syndrome depends on brain-derived neurotrophic factor regulated slow calcium buffering. *The Journal of physiology*. [Online] 587 (Pt 11), 2473–2485.

Moroni, R. F. et al. (2006) Distinct expression pattern of microtubule-associated protein/microtubule affinity-regulating kinase 4 in differentiated neurons. *Neuroscience*. [Online] 143 (1), 83–94.

Motto, A. L. et al. (2004) Detection of movement artifacts in respiratory inductance plethysmography: performance analysis of a Neyman-Pearson energy-based detector. *Conference proceedings : ... Annual International Conference of the IEEE Engineering in Medicine and Biology Society. IEEE Engineering in Medicine and Biology Society. Conference*. [Online] 149–52.

Mörschel, M. & Dutschmann, M. (2009) Pontine respiratory activity involved in inspiratory/expiratory phase transition. *Philosophical transactions of the Royal Society of London. Series B, Biological sciences*. [Online] 364 (1529), 2517–2526.

Mulkey, D. K. et al. (2004) Respiratory control by ventral surface chemoreceptor neurons in rats. *Nature neuroscience*. [Online] 7 (12), 1360–1369.

Mulligan, E. et al. (1981) Carotid body O2 chemoreception and mitochondrial oxidative phosphorylation. *Journal of applied physiology: respiratory, environmental and exercise physiology*. 51 (2), 438–446.

Nagy, A. (2000) Cre recombinase: the universal reagent for genome tailoring. *Genesis (New York, N.Y. : 2000)*. 26 (2), 99–109.

Nakamura, A. & Kuwaki, T. (2004) Sleep apnea in mice: a useful animal model for study of SIDS? *Pathophysiology*. [online]. Available from: http://www.google.co.uk/url?sa=t&rct=j&q=&esrc=s&source=web&cd=1&ved=0CCoQFjAA&url=http%3A%2F%2Fwww.researchgate.net%2Fpublication%2F8944828_Sleep_apnea_in_mice_a_useful_animal_model_for_study_of_SIDS%2Ffile%2F9c96052a718be3a9c4.pdf&ei=sJTvUs-OGuHK0QWO04GgBw&usg=AFQjCNF_Pcc62e5W5vFq0ktjoIVCqEr8Qg&bvm=bv.60444564,d.bGE.

Nan, X. et al. (1996) DNA methylation specifies chromosomal localization of MeCP2. *Molecular and Cellular Biology*. 16 (1), 414–421.

Nan, X. et al. (1998) Transcriptional repression by the methyl-CpG-binding protein MeCP2 involves a histone deacetylase complex. *Nature*. [Online] 393 (6683), 386–389.

Nguyen, M. V. C. et al. (2012) MeCP2 Is Critical for Maintaining Mature Neuronal Networks and Global Brain Anatomy during Late Stages of Postnatal Brain Development and in the Mature Adult Brain. *The Journal of neuroscience : the official journal of the Society for Neuroscience*. [Online] 32 (29), 10021–10034.

Okamoto, M. et al. (2004) Salt-inducible kinase in steroidogenesis and adipogenesis. *Trends in endocrinology and metabolism: TEM*. 15 (1), 21–26.

Onimaru, H. & Homma, I. (2003) A novel functional neuron group for respiratory rhythm generation in the ventral medulla. *The Journal of neuroscience : the official journal of the Society for Neuroscience*. 23 (4), 1478–1486.

Orban, P. C. et al. (1992) Tissue- and site-specific DNA recombination in transgenic mice. *Proceedings of the National Academy of Sciences of the United States of America*. 89 (15), 6861–6865.

Paton, J. Y. et al. (1989) Hypoxic and hypercapnic ventilatory responses in awake children with congenital central hypoventilation syndrome. *The American review of respiratory disease*. [Online] 140 (2), 368–372.

Pattyn, A. (2000) Specification of the Central Noradrenergic Phenotype by the Homeobox Gene Phox2b. *Molecular and Cellular Neuroscience*. [Online] 15 (3), 235–243.

Pattyn, A. et al. (1999) The homeobox gene Phox2b is essential for the development of autonomic neural crest derivatives. *Nature*. [Online] 399 (6734), 366–370.

Peng, C. Y. et al. (1998) C-TAK1 protein kinase phosphorylates human Cdc25C on serine 216 and promotes 14-3-3 protein binding. *Cell growth & differentiation : the molecular biology journal of the American Association for Cancer Research*. 9 (3), 197–208.

Peng, Y.-J. et al. (2011) Hypoxia-inducible factor 2α (HIF-2α) heterozygous-null mice exhibit exaggerated carotid body sensitivity to hypoxia, breathing instability, and hypertension. *Proceedings of the ...*.

Peyron, C. et al. (1996) Lower brainstem catecholamine afferents to the rat dorsal raphe nucleus. *The Journal of Comparative Neurology*. [Online] 364 (3), 402–413.

Peyronnet, J. et al. (2003) Prenatal hypoxia and early postnatal maturation of the chemoafferent pathway. *Advances in experimental medicine and biology*. 536525–533.

Polekhina, G. et al. (2003) AMPK beta subunit targets metabolic stress sensing to glycogen. *Current biology : CB*. 13 (10), 867–871.

Priestley, J. & DFRS, L. L. (1775) *Experiments And Observations On Different Kinds Of Air - Joseph Priestley, LL.D.F.R.S. - Google Books*.

Qian, Y. et al. (2001) Formation of brainstem (nor)adrenergic centers and first-order relay visceral sensory neurons is dependent on homeodomain protein Rnx/Tlx3. ... *& development*.

Ramanantsoa, N. et al. (2007) Effects of temperature on ventilatory response to hypercapnia in newborn mice heterozygous for transcription factor Phox2b. *American journal of physiology. Regulatory, integrative and comparative physiology*. [Online] 293 (5), R2027–R2035.

Ramirez, J. M., Quellmalz, U. J., et al. (1998) The hypoxic response of neurones within the in vitro mammalian respiratory network. *The Journal of physiology*. 507 (Pt 2)571–582.

Ramirez, J. M., Schwarzacher, S. W., et al. (1998) Selective lesioning of the cat pre-Bötzinger complex in vivo eliminates breathing but not gasping. *The Journal of ...*.

Rekling, J. C. & Feldman, J. L. (1998) PREBÖTZINGER COMPLEX AND PACEMAKER NEURONS: Hypothesized Site and Kernel for Respiratory Rhythm Generation. *Annual Review of Physiology*. [Online] 60 (1), 385–405.

Richter, D. W. (1996) 'Neural Regulation of Respiration: Rhythmogenesis and Afferent Control', in *Comprehensive human physiology*. [Online]. Berlin, Heidelberg: Springer Berlin Heidelberg. pp. 2079–2095.

Riederer, P. et al. (1985) Neurochemical aspects of the Rett syndrome. *Brain & development*. 7 (3), 351–360.

Robertson, J. M. & Walsh-Weller, J. (1998) 'An Introduction to PCR Primer Design and Optimization of Amplification Reactions', in *Forensic DNA profiling protocols*. [Online]. New Jersey: Humana Press. pp. 121–154.

Robinson, D. M. et al. (2000) Development of the ventilatory response to hypoxia in Swiss CD-1 mice. *Journal of applied physiology (Bethesda, Md. : 1985)*. 88 (5), 1907–1914.

Ross, F. A. et al. (2011) Selective expression in carotid body type I cells of a single splice variant of the large conductance calcium- and voltage-activated potassium channel confers regulation by AMP-activated protein kinase. *The Journal of biological chemistry*. [Online] 286 (14), 11929–11936.

Roux, J. C. et al. (2003) Neurochemical development of the brainstem catecholaminergic cell groups in rat. *Journal of neural transmission (Vienna, Austria : 1996)*. [Online] 110 (1), 51–65.

Roux, J. C. et al. (2000) Ventilatory and central neurochemical reorganisation of O2 chemoreflex after carotid sinus nerve transection in rat. *The Journal of physiology*. 522 Pt 3493–501.

Roux, J.-C. et al. (2010) Progressive noradrenergic deficits in the locus coeruleus of Mecp2 deficient mice. *Journal of Neuroscience Research*. [Online] 88 (7), 1500–1509.

Roux, J.-C. et al. (2007) Treatment with desipramine improves breathing and survival in a mouse model for Rett syndrome. *European Journal of Neuroscience*. [Online] 25 (7), 1915–1922.

Ruderman, N. B. et al. (2013) AMPK, insulin resistance, and the metabolic syndrome. *The Journal of clinical investigation*. [Online] 123 (7), 2764–2772.

Sakamoto, K. (2006) Deficiency of LKB1 in heart prevents ischemia-mediated activation of AMPK 2 but not AMPK 1. *AJP: Endocrinology and Metabolism*. [Online] 290 (5), E780–E788.

Sakamoto, K. et al. (2005) Deficiency of LKB1 in skeletal muscle prevents AMPK activation and glucose uptake during contraction. *The EMBO journal*. [Online] 24 (10), 1810–1820.

Sauer, B. & Henderson, N. (1989) Cre-stimulated recombination at loxP-containing DNA sequences placed into the mammalian genome. *Nucleic acids research*. 17 (1), 147–161.

Sauer, B. & Henderson, N. (1988) Site-specific DNA recombination in mammalian cells by the Cre recombinase of bacteriophage P1. *Proceedings of the National Academy of Sciences of the United States of America*. 85 (14), 5166–5170.

Schneider, A. et al. (2004) Identification of regulated genes during permanent focal cerebral ischaemia: characterization of the protein kinase 9b5/MARKL1/MARK4. *Journal of neurochemistry*. 88 (5), 1114–1126.

Segu, L. et al. (2008) Impairment of spatial learning and memory in ELKL Motif Kinase1 (EMK1/MARK2) knockout mice. *Neurobiology of aging*. [Online] 29 (2), 231–240.

Seidler, F. J. & Slotkin, T. A. (1985) Adrenomedullary function in the neonatal rat: responses to acute hypoxia. *The Journal of physiology*. 3581–16.

Severinghaus, J. W. (1962) Ondine's curse ; failure of respiratory center automaticity while awake. *Clin Res*. 10122.

Shahbazian, M. D. & Zoghbi, H. Y. (2001) Molecular genetics of Rett syndrome and clinical spectrum of MECP2 mutations. *Current opinion in neurology*. 14 (2), 171–176.

Shahbazian, M. D. et al. (2002) Insight into Rett syndrome: MeCP2 levels display tissue- and cell-specific differences and correlate with neuronal maturation. *Human molecular ….*

Shectman, J. (2003) *Groundbreaking Scientific Experiments, Inventions, and Discoveries of the 18th Century*. Penn State Press.

Shrestha, P. K. et al. (2014) Hindbrain medulla catecholamine cell group involvement in lactate-sensitive hypoglycemia-associated patterns of hypothalamic norepinephrine and epinephrine activity. *Neuroscience*. [Online] 27820–30.

Siegel, R. E. (1968) *Galen's System of Physiology and Medicine*.

Sjöström, M. et al. (2007) SIK1 is part of a cell sodium-sensing network that regulates active sodium transport through a calcium-dependent process. *Proceedings of the National Academy of Sciences of the United States of America*. [Online] 104 (43), 16922–16927.

Skene, P. J. et al. (2010) Neuronal MeCP2 is expressed at near histone-octamer levels and globally alters the chromatin state. *Molecular cell*. [Online] 37 (4), 457–468.

Slotkin, T. A. & Seidler, F. J. (1988) Adrenomedullary catecholamine release in the fetus and newborn: secretory mechanisms and their role in stress and survival. *Journal of developmental physiology*. 10 (1), 1–16.

Smith, C. A. et al. (2010) An interdependent model of central/peripheral chemoreception: evidence and implications for ventilatory control. *Respiratory physiology & neurobiology*. [Online] 173 (3), 288–297.

Smith, C. A. et al. (2006) Response time and sensitivity of the ventilatory response to CO2 in unanesthetized intact dogs: central vs. peripheral chemoreceptors. *Journal of applied physiology (Bethesda, Md. : 1985)*. [Online] 100 (1), 13–19.

Smith, D. W. et al. (1995) Role of ventrolateral medulla catecholamine cells in hypothalamic neuroendocrine cell responses to systemic hypoxia. *The Journal of neuroscience : the official journal of the Society for Neuroscience*. 15 (12), 7979–7988.

Smith, J. C. et al. (2013) Brainstem respiratory networks: building blocks and microcircuits. *Trends in Neurosciences*. [Online] 36 (3), 152–162.

Solomon, I. C. et al. (2000) Pre-Bötzinger complex functions as a central hypoxia chemosensor for respiration in vivo. *Journal of neurophysiology*. 83 (5), 2854–2868.

Song, G. et al. (2011) Hypoxia-excited neurons in NTS send axonal projections to Kölliker-Fuse/parabrachial complex in dorsolateral pons. *Neuroscience*. [Online] 175145–153.

Soulage, C. et al. (2005) 'Chemosensory Inputs and Neural Remodeling in Carotid Body and Brainstem Catecholaminergic Cells', in *... Genomic Perspectives in ...*. Advances in Experimental Medicine and Biology. [Online]. Boston, MA: Springer US. pp. 53–58.

Spengler, C. M. et al. (2001) Chemoreceptive mechanisms elucidated by studies of congenital central hypoventilation syndrome. *Respiration physiology*. 129 (1-2), 247–255.

Spitzer, N. (2002) Outside and in: development of neuronal excitability. *Current Opinion in Neurobiology*. [Online] 12 (3), 315–323.

Stapleton, D. et al. (1997) AMP-activated protein kinase isoenzyme family: subunit structure and chromosomal location. *FEBS letters*. 409 (3), 452–456.

Stettner, G. M. et al. (2007) Breathing dysfunctions associated with impaired control of postinspiratory activity in Mecp2−/y knockout mice - Stettner - 2007 - The Journal of Physiology - Wiley Online Library. *The Journal of ...*.

Stettner, G. M. et al. (2008) Spontaneous central apneas occur in the C57BL/6J mouse strain. *Respiratory physiology & neurobiology*. [Online] 160 (1), 21–27.

Stornetta, R. L. et al. (2002) A group of glutamatergic interneurons expressing high

levels of both neurokinin-1 receptors and somatostatin identifies the region of the pre-Bötzinger complex. *The Journal of Comparative Neurology*. [Online] 455 (4), 499–512.

Stornetta, R. L. et al. (2006) Expression of Phox2b by brainstem neurons involved in chemosensory integration in the adult rat. *The Journal of neuroscience : the official journal of the Society for Neuroscience*. [Online] 26 (40), 10305–10314.

Sudo, T. & Fukuda, Y. (1997) Metabolism and acid-base status during hypoxic ventilatory depression. *The Japanese journal of physiology*. 47 (6), 531–536.

Suter, M. et al. (2006) Dissecting the Role of 5'-AMP for Allosteric Stimulation, Activation, and Deactivation of AMP-activated Protein Kinase. *Journal of Biological Chemistry*. [Online] 281 (43), 32207–32216.

Suzuki, A. et al. (2003) Identification of a novel protein kinase mediating Akt survival signaling to the ATM protein. *The Journal of biological chemistry*. [Online] 278 (1), 48–53.

Suzuki, A. et al. (2004) IGF-1 phosphorylates AMPK-alpha subunit in ATM-dependent and LKB1-independent manner. *Biochemical and biophysical research communications*. [Online] 324 (3), 986–992.

Takemori, H. et al. (2002) ACTH-induced nucleocytoplasmic translocation of salt-inducible kinase. Implication in the protein kinase A-activated gene transcription in mouse adrenocortical tumor cells. *The Journal of biological chemistry*. [Online] 277 (44), 42334–42343.

Teppema, L. J. & Dahan, A. (2010) The ventilatory response to hypoxia in mammals: mechanisms, measurement, and analysis. *Physiological reviews*. [Online] 90 (2), 675–754.

Teppema, L. J. et al. (1997) Expression of c-fos in the rat brainstem after exposure to hypoxia and to normoxic and hyperoxic hypercapnia. *The Journal of Comparative Neurology*. 388 (2), 169–190.

Thelander, M. et al. (2004) Snf1-related protein kinase 1 is needed for growth in a normal day-night light cycle. *The EMBO journal*. [Online] 23 (8), 1900–1910.

Thoby-Brisson, M. & Ramirez, J. M. (2001) Identification of two types of inspiratory pacemaker neurons in the isolated respiratory neural network of mice. *Journal of neurophysiology*. 86 (1), 104–112.

Thoby-Brisson, M. et al. (2009) Genetic identification of an embryonic parafacial oscillator coupling to the preBötzinger complex. *Nature neuroscience*. [Online] 12 (8), 1028–1035.

Thomas, K. R. & Capecchi, M. R. (1986) Introduction of homologous DNA sequences into mammalian cells induces mutations in the cognate gene. *Nature*. [Online] 324 (6092), 34–38.

Thomas, K. R. & Capecchi, M. R. (1987) Site-directed mutagenesis by gene targeting in mouse embryo-derived stem cells. *Cell*. 51 (3), 503–512.

Thompson, R. J. et al. (2007) A rotenone-sensitive site and H2O2 are key components of hypoxia-sensing in neonatal rat adrenomedullary chromaffin cells. *Neuroscience*. [Online] 145 (1), 130–141.

Topor, Z. L. et al. (2007) Model based analysis of sleep disordered breathing in congestive heart failure. *Respiratory physiology & neurobiology*. [Online] 155 (1), 82–92.

Verna, A. et al. (1975) Loss of chemoreceptive properties of the rabbit carotid body after destruction of the glomus cells. *Brain research*. 100 (1), 13–23.

Viemari, J. C. et al. (2004) Phox2a gene, A6 neurons, and noradrenaline are essential for development of normal respiratory rhythm in mice. *The Journal of neuroscience : the official journal of the Society for Neuroscience*. [Online] 24 (4), 928–937.

Viemari, J.-C. (2008) Noradrenergic modulation of the respiratory neural network. *Respiratory physiology & neurobiology*. [Online] 164 (1-2), 123–130.

Viemari, J.-C. et al. (2005) Mecp2 deficiency disrupts norepinephrine and respiratory systems in mice. *The Journal of neuroscience : the official journal of the Society for Neuroscience*. [Online] 25 (50), 11521–11530.

Viollet, B. et al. (2009) AMPK: Lessons from transgenic and knockout animals. *Frontiers in bioscience (Landmark edition)*. 1419–44. [online]. Available from: http://www.ncbi.nlm.nih.gov/pmc/articles/PMC2666987/.

Voituron, N. et al. (2009) Early breathing defects after moderate hypoxia or hypercapnia in a mouse model of Rett syndrome. *Respiratory physiology & neurobiology*. [Online] 168 (1-2), 109–118.

Wang, G. L. et al. (1995) Hypoxia-inducible factor 1 is a basic-helix-loop-helix-PAS heterodimer regulated by cellular O2 tension. *Proceedings of the National Academy of Sciences of the United States of America*. 92 (12), 5510–5514.

Wang, H. et al. (2002) Depressor and tachypneic responses to chemical stimulation of the ventral respiratory group are reduced by ablation of neurokinin-1 receptor-expressing neurons. *The Journal of neuroscience : the official journal of the Society for Neuroscience*. 22 (9), 3755–3764.

Wang, Z. et al. (1999) Cloning of a novel kinase (SIK) of the SNF1/AMPK family from high salt diet-treated rat adrenal. *FEBS letters*. 453 (1-2), 135–139.

Washburn, C. P. et al. (2003) Cardiorespiratory neurons of the rat ventrolateral medulla contain TASK-1 and TASK-3 channel mRNA. *Respiratory physiology & neurobiology*. 138 (1), 19–35.

Wasicko, M. J. et al. (1999) Resetting and postnatal maturation of oxygen chemosensitivity in rat carotid chemoreceptor cells. *The Journal of physiology*. 514 (Pt 2)493–503.

Weese-Mayer, D. E. et al. (2006) Autonomic nervous system dysregulation: breathing and heart rate perturbation during wakefulness in young girls with Rett syndrome. *Pediatric research*. [Online] 60 (4), 443–449.

Wilson, L. G. (1960) The Transformation of Ancient Concepts of Respiration in the Seventeenth Century. *Isis*. [Online] 51 (2), 161.

Wilson, W. A. et al. (1996) Glucose repression/derepression in budding yeast: SNF1 protein kinase is activated by phosphorylation under derepressing conditions, and this correlates with a high AMP:ATP ratio. *Current Biology*. [Online] 6 (11), 1426–1434.

Wiwanitkit, S. & Wiwanitkit, V. (2011) Metformin and insomnia: an interesting story. *Diabetes & metabolic syndrome*. [Online] 5 (3), 160.

Wiwanitkit, S. & Wiwanitkit, V. (2012) Metformin and sleep disorders. *Indian journal of endocrinology and metabolism*. [Online] 16 Suppl 1S63–S64.

Woods, A. et al. (2005) Ca2+/calmodulin-dependent protein kinase kinase-beta acts upstream of AMP-activated protein kinase in mammalian cells. *Cell metabolism*. [Online] 2 (1), 21–33.

Woods, A. et al. (2003) LKB1 is the upstream kinase in the AMP-activated protein kinase cascade. *Current biology : CB*. 13 (22), 2004–2008.

Wyatt, C. N. & Buckler, K. J. (2004) The effect of mitochondrial inhibitors on membrane currents in isolated neonatal rat carotid body type I cells. *The Journal of physiology*. [Online] 556 (Pt 1), 175–191.

Wyatt, C. N. et al. (2007) AMP-activated protein kinase mediates carotid body excitation by hypoxia. *The Journal of biological chemistry*. [Online] 282 (11), 8092–8098.

Xiao, B. et al. (2007) Structural basis for AMP binding to mammalian AMP-activated protein kinase. *Nature*. [Online] 449 (7161), 496–500.

Xiao, B. et al. (2011) Structure of mammalian AMPK and its regulation by ADP. *Nature*. [Online] 472 (7342), 230–233.

Xie, A. et al. (2001) Effect of hypoxia on the hypopnoeic and apnoeic threshold for CO(2) in sleeping humans. *The Journal of physiology*. 535 (Pt 1), 269–278.

Yuan, G. et al. (2011) Hypoxia-inducible factor 1 mediates increased expression of NADPH oxidase-2 in response to intermittent hypoxia. *Journal of cellular physiology*. [Online] 226 (11), 2925–2933.

Zanella, S. et al. (2006) Possible modulation of the mouse respiratory rhythm generator by A1/C1 neurones. *Respiratory physiology & neurobiology*. [Online] 153 (2), 126–138.

Zeqiraj, E. et al. (2009) Structure of the LKB1-STRAD-MO25 complex reveals an allosteric mechanism of kinase activation. *Science (New York, N.Y.)*. [Online] 326 (5960), 1707–1711.

Zhang, X. et al. (2010) Pontine norepinephrine defects in Mecp2-null mice involve deficient expression of dopamine beta-hydroxylase but not a loss of catecholaminergic neurons. *Biochemical and biophysical research communications*. [Online] 394 (2), 285–290.

Zhang, Y. et al. (2013) A comprehensive analysis of adiponectin QTLs using SNP association, SNP cis-effects on peripheral blood gene expression and gene expression correlation identified novel metabolic syndrome (MetS) genes with potential role in carcinogenesis and systemic inflammation. *BMC medical genomics*. [Online] 614.

Zoghbi, H. Y. et al. (1985) Reduction of biogenic amine levels in the Rett syndrome. *The New England journal of medicine*. [Online] 313 (15), 921–924.

Zoghbi, H. Y. et al. (1999) Rett syndrome is caused by mutations in X-linked MECP2, encoding methyl-CpG-binding protein 2 - Nature Genetics. *Nature genetics*. [Online] 23 (2), 185–188.

Oral Communications

Mahmoud, A. D. (2012), 'LKB1 expression in catecholaminergic cells is required for the ventilatory response of mice to hypoxia but not hypercapnia', *The Physiological Society*. 4th July 2012, Edinburgh, UK

Publications

Review article

Evans, A. M. et al. (2011) Hypoxic pulmonary vasoconstriction: mechanisms of oxygen-sensing. *Current opinion in anaesthesiology*. 24 (1), 13–20.